CENTRO INTERNACIONAL DE ESTUDOS DE DOUTORAMENTO E AVANZADOS DA USC (CIEDUS)

TESE DE DOUTORAMENTO

FLUID SYSTEMS BASED ON IONIC LIQUIDS FOR THE PRETREATMENT OF LIGNOCELLULOSIC BIOMASS

María del Carmen Castro Valiña

ESCOLA DE DOUTORAMENTO INTERNACIONAL
PROGRAMA DE DOUTORAMENTO EN ENXEÑARÍA QUÍMICA E AMBIENTAL

SANTIAGO DE COMPOSTELA

2018

USC
UNIVERSIDADE
DE SANTIAGO
DE COMPOSTELA

DECLARACIÓN DA AUTORA DA TESE

FLUID SYSTEMS BASED ON IONIC LIQUIDS FOR THE PRETREATMENT OF LIGNOCELLULOSIC BIOMASS

Dna. María del Carmen Castro Valiña

Presento a miña tese, seguindo o procedemento adecuado ao Regulamento, e declaro que:

1) A tese abarca os resultados da elaboración do meu traballo.
2) No seu caso, na tese se fai referencia ás colaboracións que tivo este traballo.
3) A tese é a versión definitiva presentada para a súa defensa e coincide coa versión enviada en formato electrónico.
4) A tese non incorre en ningún tipo de plaxio de outros autores nin de traballos presentados por min para a obtención de outros títulos.

Santiago de Compostela, 10 de outubro de 2018

Asdo.: María del Carmen Castro Valiña

USC
UNIVERSIDADE
DE SANTIAGO
DE COMPOSTELA

AUTORIZACIÓN DO DIRECTOR/TITOR DA TESE

FLUID SYSTEMS BASED ON IONIC LIQUIDS FOR THE PRETREATMENT OF LIGNOCELLULOSIC BIOMASS

Dna. Ana María Soto Campos e D. Héctor Rodríguez Martínez

INFORMAN:

Que a presente tese correspóndese co traballo realizado por Dna. María del Carmen Castro Valiña, baixo a dirección de Dna. Ana María Soto Campos e D. Héctor Rodríguez Martínez, e a titorización deste último, e autorizamos a súa presentación, considerando que reúne os requisitos esixidos no Regulamento de Estudos de Doutoramento da USC, e que como directora e director-titor desta non incorre nas causas de abstención establecidas na Lei 40/2015.

Santiago de Compostela, 10 de outubro de 2018

Ana M. Soto Campos

Héctor Rodríguez Martínez

USC
UNIVERSIDADE
DE SANTIAGO
DE COMPOSTELA

To my parents
Antonio and María del Carmen

USC
UNIVERSIDADE
DE SANTIAGO
DE COMPOSTELA

Acknowledgements

I would like to begin these lines by thanking Prof. Ana Soto, co-director of this doctoral thesis, for the opportunity to join the Research Group on Separation Processes and Phase Equilibria that she leads at the University of Santiago de Compostela (USC), and for all her guidance and share of knowledge. I am also indebted to Dr. Héctor Rodríguez, co-director and tutor of the thesis, for all his help and invaluable commitment, that have made this document possible. The work at his side, hand by hand, for almost four years has allowed me to develop as a professional and grow as a scientist; as well as to provide me with a taste for the small details, the rigor, and the work well done. My gratitude is extended to Dr. Eva Rodil, Dr. Óscar Rodríguez and, of course, Prof. Alberto Arce, always concerned about whether everything was going all right.

I would also like to thank my laboratory colleagues, with whom I have shared great moments at different periods during these years. Borja, Iago, Marlen, and Raquel were the best mates I could have had in this scientific adventure. And a special mention to Iria, the lab mate who had to suffer me the most in the worst moments, thank you for always being there. Also, many thanks to Manuel and Oussama, who, during their short stays in the laboratory, made the long work days more enjoyable with their doses of optimism, happiness and friendliness.

Part of the work in this thesis was carried out during a 3-month research stay at the University of Helsinki, in Finland. I am grateful to Prof. Ilkka Kilpeläinen for accepting me as a temporary member of his group during this time. It was a real pleasure for me to work under the supervision of Dr. Alistair King, who was always helpful and answered my questions very kindly. I have to make a mention to my colleagues in the laboratory, Ashley, Arno, Uula, and Niklas, with whom I spent great moments in the laboratory and enjoyed dinners and typical Finnish meals. And, of course, I cannot forget Daniel Rico and Queralt Martínez, who became my family in Helsinki during this period.

My gratitude is extended to the Research Groups on Technologies for the Development of Industrial Bioproducts, led by Dr. Francisco Chenlo and Dr. Ramón Moreira, and on Environmental Biotechnology, led by Prof. Juan Lema, of the Department of Chemical Engineering of the USC; and in particular to some of their members: Santi, Loli, Mar, Mónica... who were kindly assisting me in miscellaneous aspects of the experimental procedures. I am also grateful to Dr. Francisco Guitián and Dr. Álvaro Gil of the Institute of Ceramics of the USC, as well as to the staff of the RIAIDT-USC units who provided support and whose analyses were vital for the development of this thesis. Many thanks for your generosity and kindness.

Almost ending, I would like to thank all my friends in Serbia, Santiago de Compostela, Lugo, and Sarria for their support during all this time. To Román, who, with his optimism and happiness, has brought light at the end of this journey.

And, of course, I want to unreservedly thank my family. To my brother Toni, and specially to my parents María del Carmen and Antonio. This thesis has been possible thanks to them, to their unconditional support. Thank you very much for always being there.

Finally, I would like to acknowledge the Xunta de Galicia for financial support through projects EM2012/042 and GPC2014/026, and the COST Action "Exchange on Ionic Liquids" of the European Union for sponsoring my stay in the University of Helsinki through its scheme of short-term scientific missions.

María Castro

Santiago de Compostela, October 2018

Abstract

Ionic liquids are the basis of a promising technology for the pretreatment of lignocellulosic biomass. With this application in mind, different fluid systems based on ionic liquids were investigated from different perspectives in the present thesis. Initially, pairs of mutually immiscible ionic liquids (where one of them has the capacity to dissolve lignocelluloses) with chloride or acetate as common anion were identified, and their liquid-liquid equilibria were determined and thermodynamically analysed. The binary mixtures of the ionic liquid 1-ethyl-3-methylimidazolium acetate (an archetypical ionic liquid for the dissolution of lignocelluloses) with each of the four lightest alcohols (possible cosolvents or antisolvents with reasonably green credentials) were also examined, both through thermal characterisation and through the determination of selected physical properties (namely density, viscosity, refractive index, and surface tension). All these properties were found to decrease with increasing temperature and/or alcohol concentration. The utilisation of the alcohols as cosolvents of the ionic liquid was found to tune its capacity to dissolve the different major biopolymers in lignocelluloses (cellulose, hemicellulose, and lignin). On the other hand, precipitation of the biopolymers from their solution in the ionic liquid by addition of the alcohol as antisolvent was difficult when using moderate amounts of alcohol, as formation of emulsions and gel-like phases was observed. The mixture of 1-ethyl-3-methylimidazolium acetate and ethanol at relatively low temperatures was tested for the pretreatment of *Eucalyptus globulus* wood particles, leading in some cases to an important degree of fibrillation as well as to crystallinity reduction of the wood, suggesting an effective non-dissolving pretreatment. Similarly, the use of the ionic liquids tetrabutylphosphonium acetate and methyltrioctylphosphonium acetate (which have no capacity in neat to dissolve cellulose or wood) for the pretreatment of *Picea abies* (Norway spruce) wood chips resulted also in significant fibrillation.

USC
UNIVERSIDADE
DE SANTIAGO
DE COMPOSTELA

Contents

USC
UNIVERSIDADE
DE SANTIAGO
DE COMPOSTELA

1. INTRODUCTION

USC
UNIVERSIDADE
DE SANTIAGO
DE COMPOSTELA

1. INTRODUCTION

1.1. Lignocelluloses: renewable feedstock for a sustainable industrial chemical platform

1.1.1. Context

A current trend in the industry is the search for more sustainable processes, less polluting and with less environmental impact. At present, however, substances deriving from a non-renewable source still have a very high specific weight in most processes in the chemical industry, being uses as raw materials or as fuels. This is causing significant environmental problems, such as those related to global warming.

To reverse these effects, a shift towards a new platform of industrial production of materials and chemicals based on renewable raw materials is necessary. The high volume of industrial production, together with the satisfaction of the standards demanded at present by the societies of the developed countries, and increasingly demanded by those of the developing countries, poses a significant challenge. An interesting approach to combine the high production volume and the required standards with the need of a sustainable chemical industry is the use of lignocellulosic biomass as raw material. Nature produces lignocelluloses in a biorenewable way in sufficient quantities to cover the demand of industrial production of the human being (Klemm et al., 1998). In addition, lignocelluloses also present the advantage of a more homogeneous geodistribution, in comparison to the fossil resources that today sustain most of the global productive scheme. And also importantly, it avoids the competition or interaction that other types of biomass would have with the food market (FitzPatrick et al., 2010).

The plant cell walls in lignocellulosic biomass are complex structures mainly composed of three polymers: cellulose, hemicellulose, and lignin (Figure 1.1). The different chemical structures of the biopolymers give an idea of the chemical richness embedded in lignocelluloses, and their versatility to be the basis of an alternative chemical platform for the industrial production of a wide range of chemicals and materials. However, their appropriate exploitation in this regard is conditioned by their

recalcitrant character, which is the result of a natural evolution to resist degradation. With the three major polymers organised into complex non-uniform three-dimensional structures, this recalcitrance of lignocelluloses stems essentially from the crystallinity of cellulose, the hydrophobicity of lignin, and the encapsulation of cellulose by the lignin–hemicellulose matrix (Isikgor and Becer, 2015).

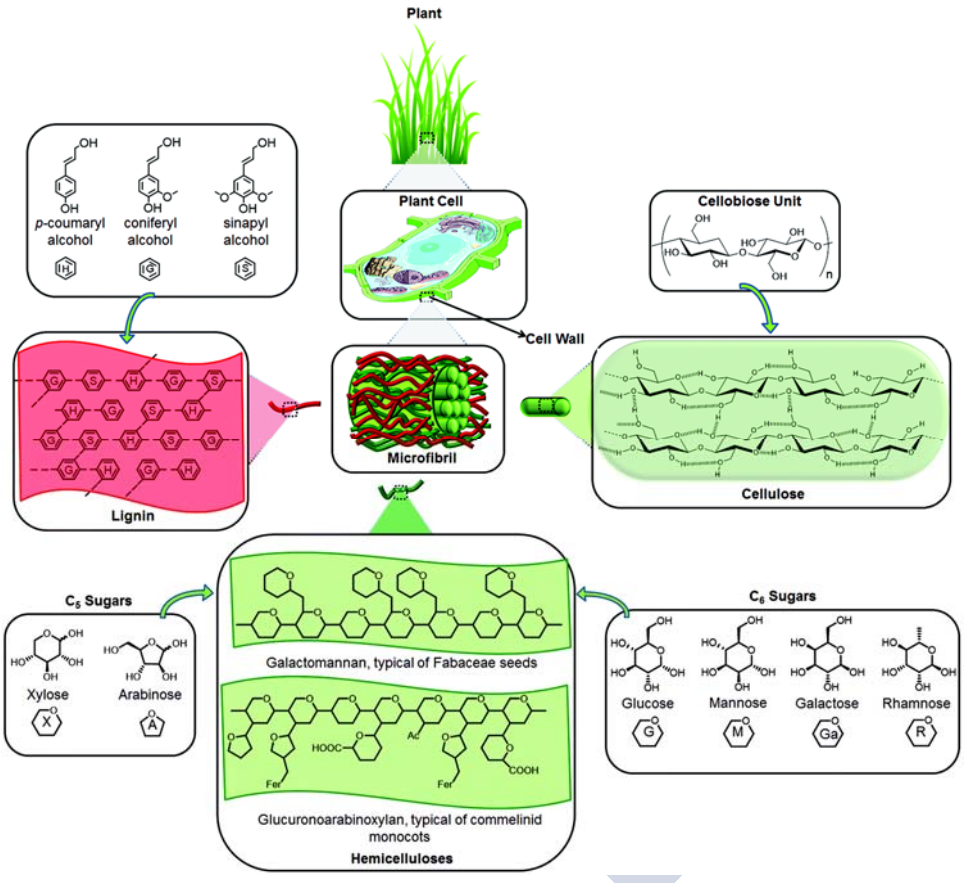

Figure 1.1. Main components and structure of lignocelluloses. Reproduced from Isikgor and Becer (2015) by permission of the Royal Society of Chemistry.

1.1.2. Chemical composition and structural disposition

Chemical composition

The relative composition of cellulose, hemicellulose, and lignin in the cell wall of a plant varies according to its species, tissues, and maturity. Table 1.1 shows some examples

of types of lignocellulosic biomass and their average content in the three biopolymers (Isikgor and Becer, 2015). In general terms, it can be claimed that lignocellulosic biomass consists of 35–50 % cellulose, 20–35 % hemicellulose, and 10–25 % lignin; with proteins, oils, and other organic and inorganic compounds making up the remaining fraction.

Table 1.1. Some types of lignocellulosic biomass and examples of their typical content in cellulose, hemicellulose and lignin (adapted from Isikgor and Becer, 2015).

Lignocellulosic biomass		Cellulose (%)	Hemicellulose (%)	Lignin (%)
Hardwood	Poplar	51-53	26-29	15-16
	Oak	40	36	24
	Eucalyptus	54	18	22
Softwood	Pine	42-50	24-27	20
	Douglas fir	44	11	27
	Spruce	456	23	28
Agricultural waste	Wheat straw	35-39	23-30	12-16
	Barley hull	34	36	14-19
	Barley straw	36-43	24-33	6-10
	Rice straw	29-35	23-26	17-19
	Rice husks	29-36	12-29	15-20
	Oat straw	31-35	20-26	10-15
	Ray straw	36-47	19-25	10-24
	Corn cobs	34-41	32-36	6-16
	Corn stalks	35-40	17-35	7-18
	Sugarcane bagasse	25-45	28-32	15-25
	Sorghum straw	32-35	24-27	15-21
Grasses	Gasses	25-40	25-50	10-30
	Switchgrass	35-40	25-30	15-20

Cellulose is the most abundant biopolymer in Nature, with a basically structural function in vegetables. It is a carbohydrate formed by D-glucopyranose monomers linked together by β-1,4-O-glucosidic bonds (see chemical structure in Figure 1.1 – box labelled as 'Cellobiose Unit'), resulting in the formation of long chains (Klemm et al., 2005; Wyman et al., 2005b). This chemical structure, together with its availability and high production rate (10^{11}–10^{12} tonnes per year), confer a large potential to cellulose as a renewable raw material for a wide variety of products, including building block molecules for further chemical transformations, cellulosic polymers, and biofuels, among others (Klemm et al., 1998).

Cellulose has a strong tendency to aggregate into highly ordered structures. This tendency is due to the formation of intra- and intermolecular hydrogen bonds between the individual chains, which results in the packing of numerous cellulose chains in

crystalline structures known as fibrils (O'Sullivan, 1997). This crystalline structure is very compact since it is composed of a large number of hydrogen bonds at regular intervals (Klemm et al., 1998; Nagarajan et al., 2017). However, disordered amorphous regions together with highly ordered crystalline regions can be identified in the chains (Sjöström, 1993). Techniques such as X-ray diffraction and nuclear magnetic resonance spectroscopy have allowed the identification of four crystalline polymorphs of cellulose (O'Sullivan, 1997; Park et al., 2010):

- Cellulose I: It is the most abundant crystalline structure in Nature, and it is the one usually present in vegetables. There are two subtypes: cellulose I_α (produced by microbes, with a triclinic structure) and cellulose I_β (typically present in higher plants, with a monoclinic structure) (Nagarajan et al., 2017).
- Cellulose II: It is usually obtained from cellulose I via treatments in basic media (mercerisation processes), or through solubilisation and subsequent recrystallisation; although in some specific cases native cellulose II could also be isolated (Kuga et al., 1993; O'Sullivan, 1997; Shibazaki et al, 1998).
- Cellulose III: This is a structure with two known varieties, cellulose III_I and cellulose III_{II}, which are achieved after the ammonia treatment of cellulose I or cellulose II, respectively. It is a reversible transformation.
- Cellulose IV: It is achieved after subjecting cellulose III to a thermal treatment. Cellulose IV_I or cellulose IV_{II} can be obtained according to the starting variety of cellulose III.

A scheme of the interconnection of crystalline structures described is shown in Figure 1.2. It must be noted that the crystal structures cellulose III and cellulose IV are of minor importance, since they are derived from cellulose I or cellulose II, and in addition they also have a lower stability.

A comparison of the spatial configurations of the cellulose I and cellulose II polymorphs is presented in Figure 1.3. The native (biosynthesised) form cellulose I hosts a parallel chain strand arrangement, resulting in a compact structure of recalcitrant character; whereas cellulose II, thermodynamically more stable, presents its chains arranged in an anti-parallel fashion. The latter is a spatial configuration that confers a greater facility to react and, therefore, to be treated as raw material in

industrial processes for its transformation and exploitation. Even greater reactivity is achievable with amorphous cellulose, in which the barriers presented by the crystalline structures are suppressed.

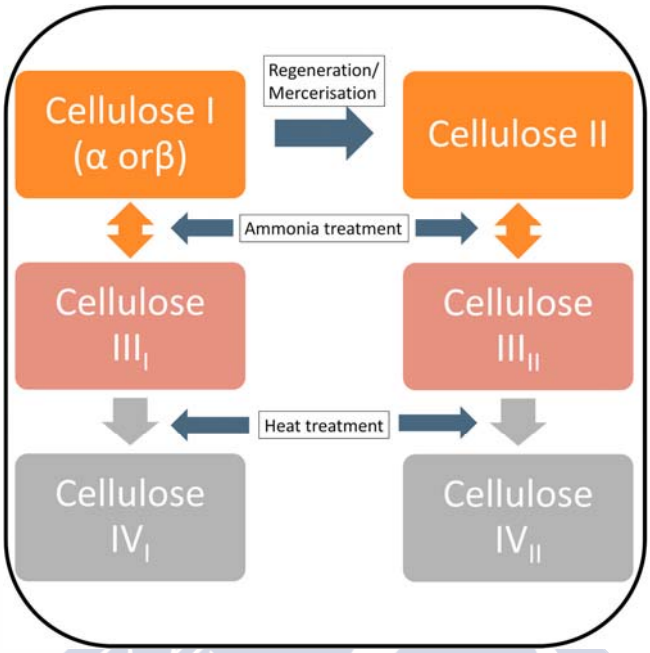

Figure 1.2. Crystalline polymorphs of cellulose. Reproduced form Nagarajan et al. (2017) by permission of Elsevier.

Hemicellulose is a flexible non-cellulosic polysaccharide composed of different sugars forming short and branched chains – see Figure 1.1. The sugars present in hemicellulose can be pentoses (xylose, arabionose) and hexoses (glucose, mannose, galactose), and they may be substituted to some extent with functionalities such as acetyl groups, hexuronic acids (glucuronic acid, methyl glucuronic acid, galacturonic acid) or deoxyhexoses (rhamnose, fucose). The main chain of hemicellulose can consist of a single unit (homopolymer), such as xylan; or of two or more units (heteropolymer), such as glucomannan. The branched nature of hemicellulose makes it amorphous and easier to hydrolyse than cellulose. Its main function is to provide the binding between cellulose and lignin (Sjöström, 1993).

Lignin is a three-dimensional heteroamorphic polymer configured in a tridimensional network formed by monomers of phenylpropane (*p*-coumaryl,

p-coniferyl and *p*-sinapyl alcohols) – see chemical structures of these precursor units in Figure 1.1. The detailed structure of lignin is not exactly known since the methods used for its separation from the wood entail unavoidably its chemical or mechanical degradation (which gives an idea of the difficulty of isolating pure lignin from its native source within the lignocellulosic matrix). Hence, the "real" molecular weight of lignin is not known, although the literature suggests that lignins from hardwoods have a slightly lower molecular weight than those from conifers (Lin and Dence, 1992; Xie and Gathergood, 2013). Moreover, lignins isolated by means of different processes differ in chemical and physical properties. One of the most peculiar characteristics of lignin is that its monomers are linked by different types of covalent bonds that are irregularly distributed along the lignin chain, giving rise to a very complex structure, as can be seen in Figure 1.4.

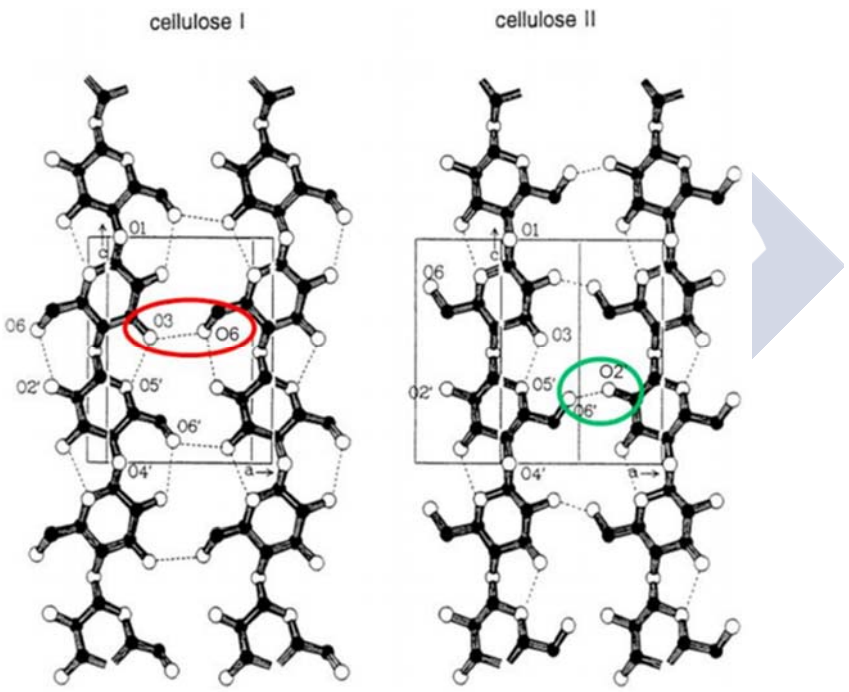

Figure 1.3. Comparison of intramolecular and intermolecular hydrogen bonds in cellulose I and cellulose II. Reproduced from Nagarajan et al. (2017) by permission of Elsevier.

The main purpose of lignin is to provide the plant with rigidity, impermeability, and resistance to the attack by microorganisms and to oxidative stress (Hendriks and

Zeeman, 2009). It is the most recalcitrant component of the plant cell wall, so that the greater the proportion of lignin, the greater the resistance to chemical and enzymatic degradations (Taherzadeh and Karimi, 2008). It can be considered as a "hydrophobic glue" that holds together the different lignocellulosic components.

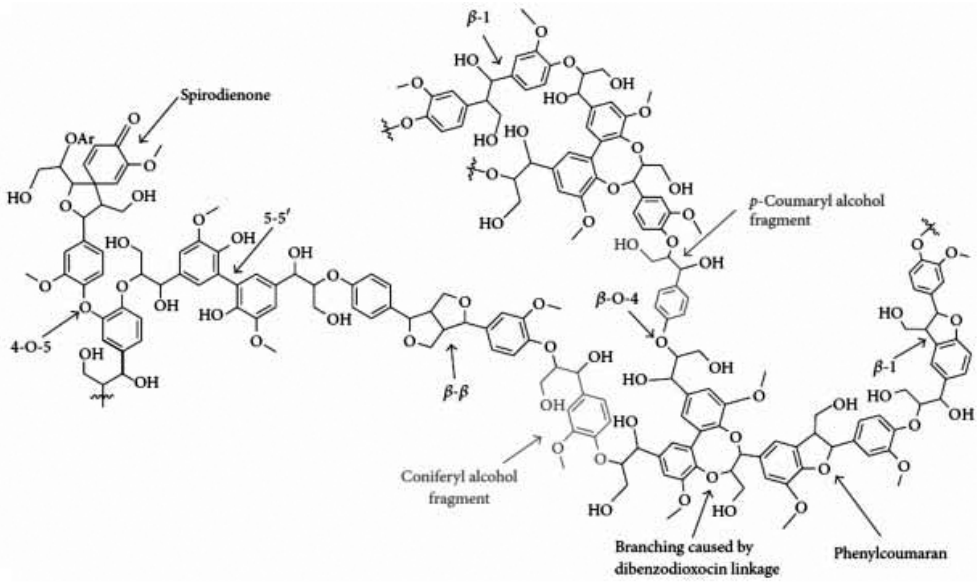

Figure 1.4. Generic molecular structure of softwood lignin highlighting various types of bonds. Reproduced from Zakzeski et al. (2010) by permission of the American Chemical Society.

In addition to cellulose, hemicellulose, and lignin, lignocellulosic biomass contains other components in smaller proportions. Although these components are very different chemically, they can be classified into two categories: extractives and ashes. The extractives refer to a group of organic compounds of low molecular weight (including: terpenes, aliphatic and aromatic acids, alcohols, flavonoids, lignans, tannins, alkaloids, waxes, low molecular weight carbohydrates, etc.), which can be extracted from the biological material using water or organic solvents (Windeisen and Wegener, 2009; Rowell et al., 2013). Their main functions in the plant cell are those of external protection and as a reserve of nutrients. On the other hand, the ashes refer to the inorganic fraction of the material (mainly composed of inorganic salts of potassium, sodium, calcium, magnesium, and silica), which becomes ashes during its combustion.

Structural disposition

The plant cell walls are constituted by a crystalline component and an amorphous component. The crystalline component is composed of cellulose chains, arranged in an orderly manner through the establishment of hydrogen bonding. A number of so arranged chains of cellulose constitutes a microfibril or microfibre; whereas a macrofibril or macrofibre is formed by the grouping of hundreds of microfibrils (Figure 1.5).

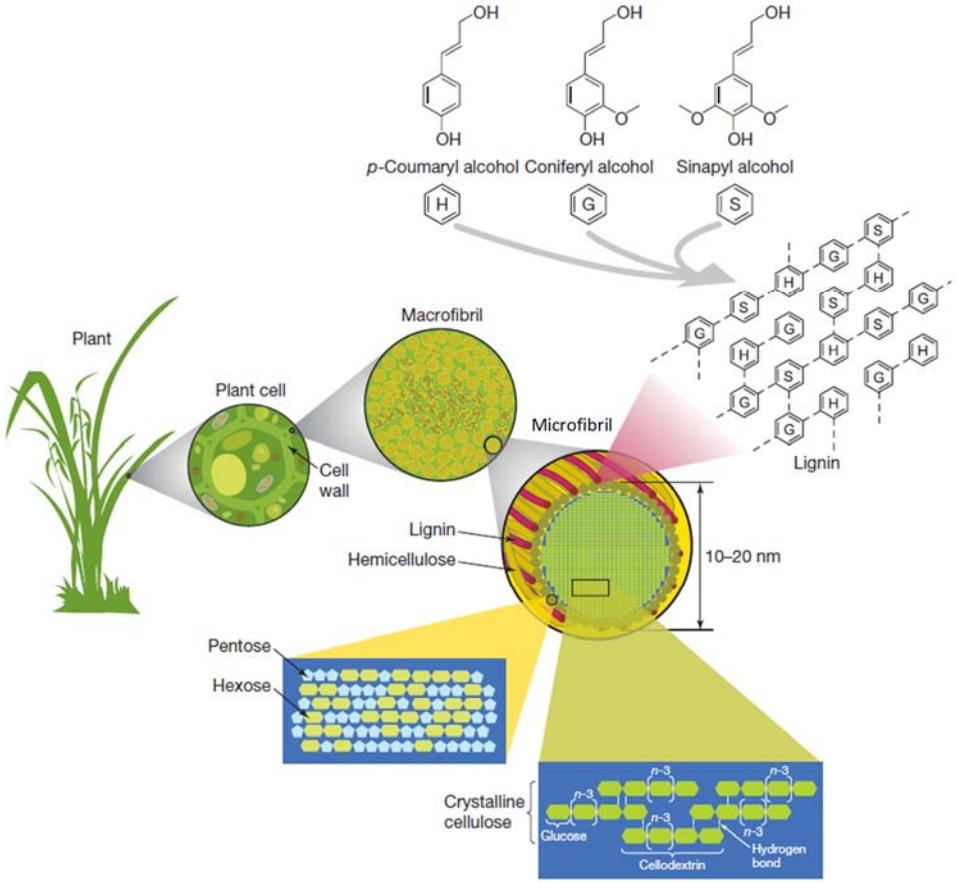

Figure 1.5. Representation of crystalline cellulose microfribrils sheathed by hemicellulose and lignin, and grouped to form a macrofibril which is part of the cell wall of the plant. Reproduced from Rubin (2008) by permission of Springer Nature.

Hemicellulose acts, likely via a non-covalent binding to the surface of the stiff cellulose fibres, as an amorphous matrix, coating these fibres and holding them in place

(Figure 1.6). The substitution with hydrophobic groups in the hemicellulose polysaccharide chains has been suggested to increase the affinity of hemicellulose to lignin (Hansen and Björkman, 1998), establishing in this case not only an entangling but also a covalent cross-linking (Brandt et al., 2013). Thus, a structural cohesion between all three major lignocellulosic polymers is generated.

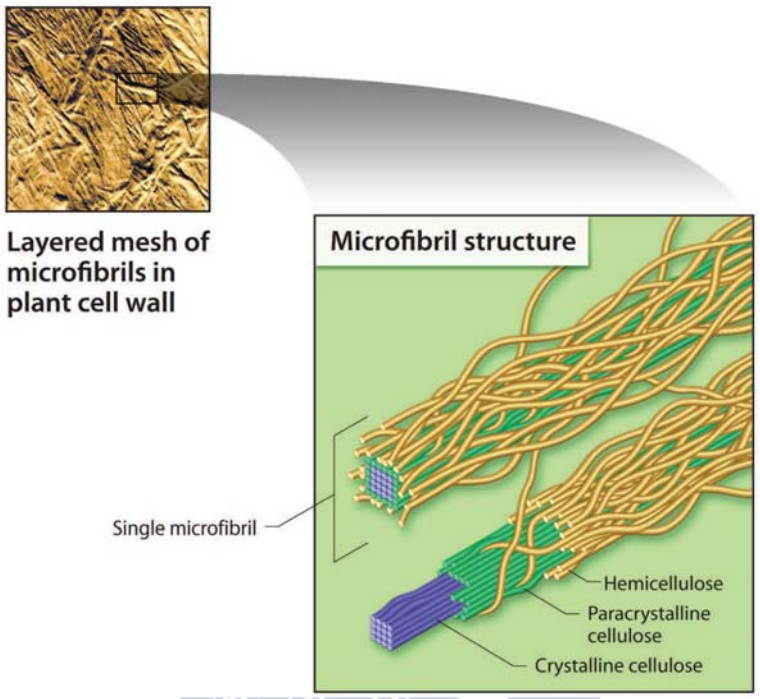

Figure 1.6. Spatial arrangement of cellulose and hemicellulose in the microfibril structure. Image freely available from the Image Gallery Gateway of the U.S. Department of Energy, Office of Biological and Environmental Research at: https://public.ornl.gov/site/gallery/detail.cfm?id=159 (U.S. DOE, 2005).

Beyond the assembly of the three biopolymers into the composite described, lignocellulose is also structured in what is called the ultrastructure (Fujita and Harada, 2000; Hansen and Björkman, 1998). The so-called middle lamella encompasses each cell (in fact it is sometimes alternatively considered as the most outer layer of the cell wall), being shared between the adjacent cells (Figure 1.7). It is virtually free of cellulose (Fengel and Wegener, 1989) and mainly consists of pectins and lignin (Ishii and Shimizu, 2000; Pauly and Keegstra, 2008). During cell growth, cellulose is deposited at the inside of the middle lamella in a disordered state and results in the

primary cell wall; while in mature woody tissue, the middle lamella becomes heavily encrusted with lignin (Brandt et al., 2013). Figure 1.7 also shows a secondary cell wall that may be forming in some plant cells once their growth has stopped, with the purpose of providing further strength, rigidity, and support to the plant (Koch et al., 2004; Speck and Burgert, 2011). It is composed mainly by ordered structures of cellulose fibres, having a different composition than the primary cell wall, and thus building on the heterogeneity (and complexity!) of the structural distribution of lignocelluloses in plants.

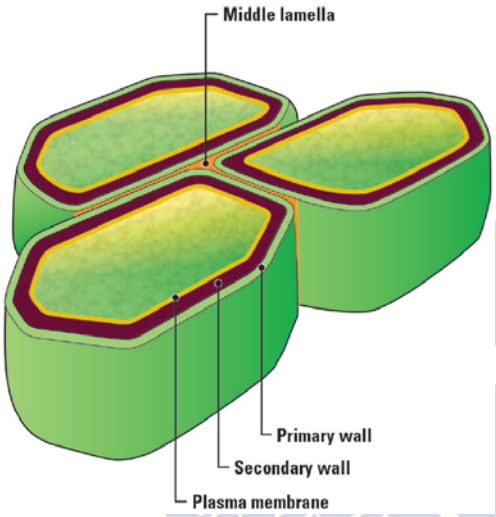

Figure 1.7. Plant cell wall layers and middle lamella. Image freely available from the Image Gallery Gateway of the U.S. Department of Energy, Office of Biological and Environmental Research at: https://public.ornl.gov/site/gallery/detail.cfm?id=249&topic=&citation=&general=middle%20lamella&restsection=all&webid=blank (U.S. DOE, 2007).

1.1.3. Processing of lignocelluloses: the pretreatment

To benefit from the rich chemistry naturally embedded in the constituent biopolymers in a lignocellulose feedstock, their separation or isolation must be somehow accomplished to some extent. To assist in the disengagement of the main biopolymers in the lignocellulosic matrix in the processing of biomass, a so-called pretreatment step is performed. This key step pursues the modification of the lignocellulosic structure

and alteration of the pore size (Kumar et al., 2009; Mosier et al., 2005). The latter may be the result, for example, of reducing the crystallinity of cellulose in the biomass.

Historically the industrial exploitation of lignocellulosic biomass as a resource for the chemical industry has focused on the production of cellulose (Brandt et al., 2013), while belittling the potential contribution of hemicellulose and lignin. As a consequence, the currently most developed industrial processes for the treatment of lignocelluloses are those in the area of pulp and paper production (Ragauskas et al., 2006). In these processes, the pretreatment stage is actually the core stage, in which the fibres are released from the wood matrix by degradation/elimination of the hemicellulose and lignin usually at harsh conditions (Chirat et al., 2012; Klemm et al., 1998; Lin and Dence, 1992). As an archetypical example, about 80 % of the pulp production is carried out by Kraft processes, which consist of the treatment of wood chips or any other lignocellulosic material with aqueous solutions of sodium hydroxide and sodium hydrogen sulfide at temperatures of ca. 400-450 K and pressures of ca. 0.7 MPa. These processes present disadvantages such as pollution and odour problems, high water consumption, and the need of a large production capacity for economic viability (Tan and MacFarlane, 2009); and the only valorisation carried out for most of the lignin is its burning from the pretreating liquor with energy recovery. The technological alternatives to the Kraft pulping, including the sulfite process, organosolv processes, thermomechanical pulping, etc., are also based on the utilisation of harsh operating conditions and the utilisation of aggressive pretreating fluids, resulting in diverse operational difficulties and important polluting emissions.

Beyond the pulp and paper industry, a variety of pretreatment methods have been considered for the processing and woody and other classes of lignocellulosic biomass. Among others, the following are some of the most representative types of pretreatments (Pal et al., 2015; Simmons et al., 2010):

- Mechanical comminution: It is a physical pretreatment consisting on the reduction of the size of the lignocellulosic biomass through chipping, grinding, or milling. It causes a reduction of the crystallinity of the biomass (Jiang et al., 2016), but at the cost of a high energy consumption.
- Dilute acid hydrolysis: Mineral acids such as H_2SO_4 or HCl can be used at relatively low concentrations. It mostly solubilises the hemicelluloses (Wyman et al., 2005a), then enabling the hydrolysis of the

polysaccharides. The amount of inhibitors generated in the hydrolysis of hemicelluloses when using this method is one of its disadvantages, as well as the high temperatures required and the corrosiveness.

- Alkaline hydrolysis: It may imply lower temperatures and pressures than other pretreatment technologies, working just with feedstocks of low lignin content (McMillian, 1994). The most widely used alkali is NaOH, although lime pretreatment is also considered. It also has problems associated with corrosiveness and relatively harsh pH.
- Steam explosion: The biomass is subjected to contact with saturated steam at high pressure, and then the pressure is suddenly decreased, causing a decompression of the material (Martín et al., 2002). It involves high temperatures during short periods of time. Disadvantageously, it performs a quite incomplete destruction of the lignin-carbohydrate matrix and generates inhibitory compounds.
- Ammonia fibre explosion: The biomass is subjected to a treatment with liquid ammonia at elevated temperature and pressure for a certain period of time, and then the pressure is suddenly decreased. Part of the ammonia is consumed during the process (ammonolysis reactions), resulting in the formation of amides (Krishnan et al., 2010).
- Organosolv pretreatment: Lignin and hemicellulose bonds are broken by an organic solvent (e.g. methanol, ethanol, ethylene glycol...) mixed with inorganic acid catalysts (Chum et al., 1998). The low boiling points of the alcohols make them interesting for easy recovery. In general, the recycle of the solvent is a crucial step in determining the economics of the process. The elevated temperatures needed (close to 470 K) are also a disadvantage.
- Biological pretreatment: There are a number of microorganisms with the capacity to degrade biomass, using enzymes such as peroxidases and laccases. This pretreatment can be carried out at relatively mild conditions with low energy input, but its limitations are long residence times, a low efficiency, and possible difficulties with the growth of the culture (Pal et al., 2015).

In spite of this variety, there is a need for the development of better pretreatment methods, as the biomass pretreatment step is known to account for a very relevant portion of the total costs (Simmons et al., 2010).

1.1.4. Towards sustainable biorefinery schemes

According to the International Energy Agency, "biorefinery" is defined as the sustainable processing of biomass for the production of chemical products, biofuels and energy (Cherubini et al., 2009). On the other hand, the U.S. Department of Energy has defined biorefinery as a general concept of a processing plant where the raw material is the biomass that is converted, and from which it is extracted in a wide range of valuable products. Similarly, the American National Renewable Energy Laboratory described biorefinery as a facility that integrates biomass conversion processes and equipment to produce fuels, energy and chemical products from biomass. These concepts are analogous to the petroleum refinery where the hydrocarbons in the crude oil are separated into several components, which can later be used as fuel and as non-combustible products (Figure 1.8). Therefore, the biorefinery seeks the replacement of non-biorenewable sources such as oil by biorenewable sources such as biomass, giving rise to facilities less harmful to the environment in accordance with the principles of green chemistry. (This substitution of oil by biomass in the chemical industry is, however, only a small part of what is pursued with green chemistry.)

In the development of a sustainable biorefinery, the use or generation of chemical products harmful to the environment should be avoided. In this vein, the final goal of the biorefinery, combined with green chemistry, will be the manufacture of "green" chemical products. In addition, any chemical process to be developed should use renewable raw materials, maximising its use and transformation in the final product. During the manufacturing process, energy demands should be minimised, as well as the production and use of toxic chemical compounds. Finally, the end products should ideally be totally environmentally friendly, biodegradable, and easily recyclable, with minimal waste generation (Clark et al., 2009; Manley et al., 2008; Sheldon, 2014).

The traditional emphasis on the production of cellulose in the chemical processing of lignocelluloses, already mentioned in Section 1.1.3, has basically neglected the real potential of hemicellulose and lignin to contribute to the biorefinery paradigm. It is currently acknowledged, however, that the development of viable

biorefinery schemes must take into consideration the valorisation of all three biopolymers (FitzPatrick et al., 2010; Stöcker, 2008; Zakzeski et al., 2010). Figure 1.9 shows an overview of the potential products that could be obtained from cellulose, hemicellulose, and lignin in a lignocellulosic biorefinery according to this integral valorisation.

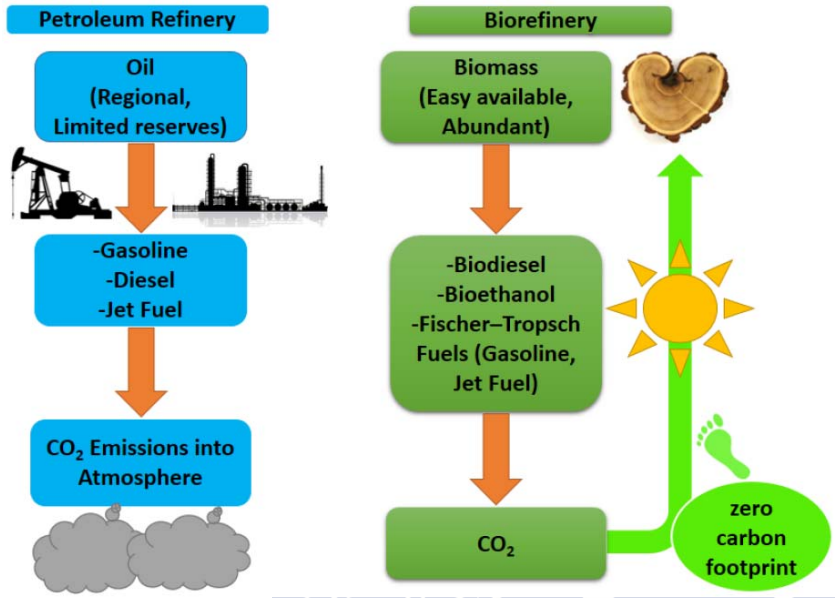

Figure 1.8. Schematic comparison of two fundamental refinery concepts: petroleum refinery and biorefinery. Reproduced from Salan (2017) by permission of MedWin Publishers.

As discussed in Section 1.1.3, the integral utilisation of biomass in this direction implies necessarily the disengagement of the biopolymers interconnected in the lignocellulosic matrix. Unfortunately, the separation of these biopolymers without degrading their chemical structures is highly challenging, likely being a reflection of the intrinsic resistance of the lignocellulosic matrix to its degradation. Inevitably this poses a major economic barrier for the development of a viable lignocellulosic biorefinery (Zhang et al., 2007), as the pretreatment methods developed to date or currently under development present a number of inconveniences and are still far from being satisfactory. An alternative approach, with the potential to lead to a more advantageous performance that the conventional methods, has started to emerge in the last years: the pretreatment of lignocelluloses with fluid systems based on ionic liquids.

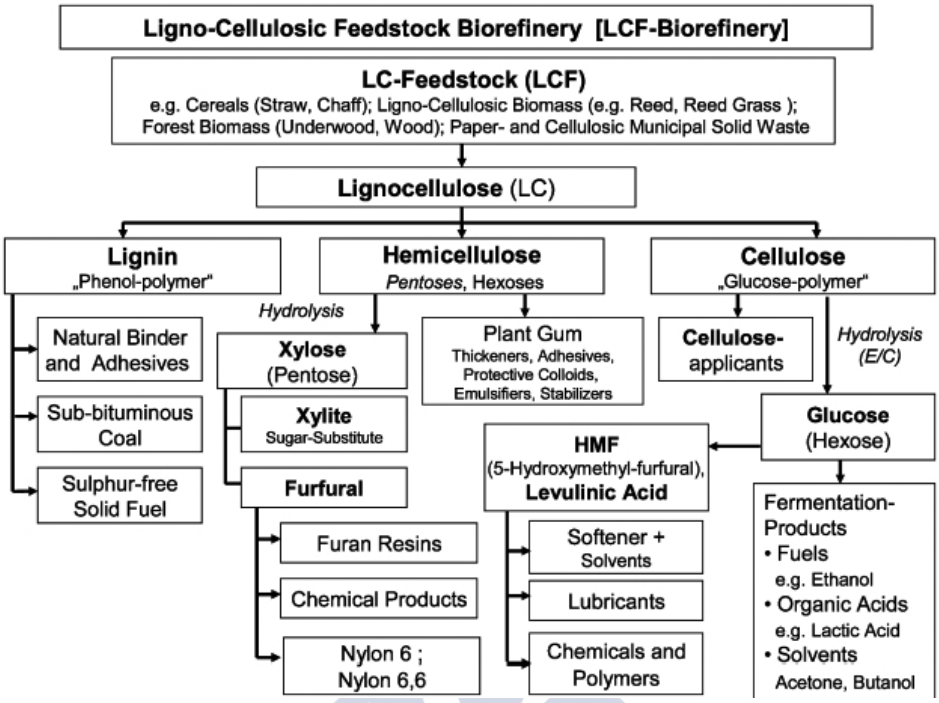

Figure 1.9. Potential scheme of products to be obtained from the different constituent biopolymers of lignocelluloses in a biorefinery. Reproduced from Kamm and Kamm (2004) by permission of Springer Nature.

1.2. Ionic liquids

1.2.1. Context and definition

Ionic liquids are salts that are liquid in their pure state at a low temperature. From a practical point of view, a mark of 373 K maximum for its melting (or glass transition) temperature is usually considered (Freemantle, 2010). For a salt to be liquid at such low temperatures, at least one of its constituent ions must be bulky or with a noticeable asymmetry, so that the charge is delocalised and the packing becomes more difficult, thus lowering the network energy of the crystalline form (Earle and Seddon, 2000).

Although substances that adhere to the current definition of ionic liquid have been known for over a century, it was not until the last years of the 20th century that such substances and their potential were consolidated under a distinctive and attractive tag. These early years of the 21st century have witnessed a sustained

increasing interest in ionic liquids, both in the academic environment and in industry. Figure 1.10 illustrates this growth through the evolution of the number of publications containing the concept 'ionic liquid' since the 1990s.

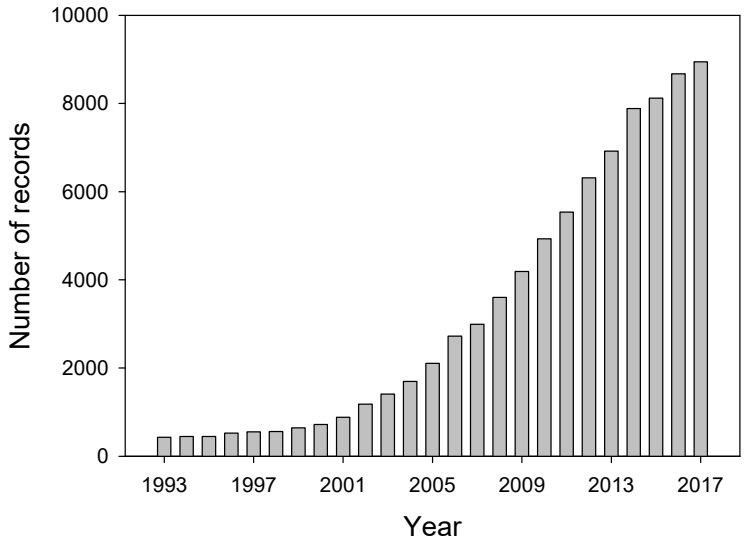

Figure 1.10. Evolution, over the last 25 years, of the annual number of records retrieved by the Web of Science® Core Collection when searching the topic "ionic liquid*". (Search carried out in October 2018.)

1.2.2. Features and properties

The attractiveness of ionic liquids lies in their unique properties. Although it is difficult to generalise properties common to all ionic liquids due to their large number and variety (besides their ionic character and the limit in their melting or glass transition temperature, as imposed by the definition presented in Section 1.2.1), many of them often exhibit appealing sets of properties, including for example the following (Freemantle, 2010):

- Extremely low vapour pressure, essentially negligible under usual pressure and temperature operation conditions.
- Reasonably good thermal and chemical stabilities, leading frequently to a wide range of temperatures in which the ionic liquid is stable in the liquid state.

- Low or negligible flammability.
- Great capacity to solvate a large number of varied compounds.

In addition, the properties of ionic liquids can be 'customised' up to a certain level for a specific purpose, by judicious selection of the cation-anion combination and the design of the chemical structures of the constitutive ions (for example, by modifying the number or length of alkyl substituents) (Stark and Seddon, 2007). This set of properties stimulated the consideration of ionic liquids as alternative 'design' solvents in safer and environmentally friendlier processes (Seddon, 1997). However, the interest generated by ionic liquids and their singular properties goes beyond their use as solvents, and this is attested by the various industrial applications in which they have been gradually introduced (Freemantle, 2010, 2016; Maase, 2008; Plechkova and Seddon, 2008). An overview of their broad spectrum of applications, with a categorisation of their present level of development (from research and development to pilot plant scale, and to a commercialisation status), as evaluated by the German chemical company Iolitec GmbH, is provided in Figure 1.11.

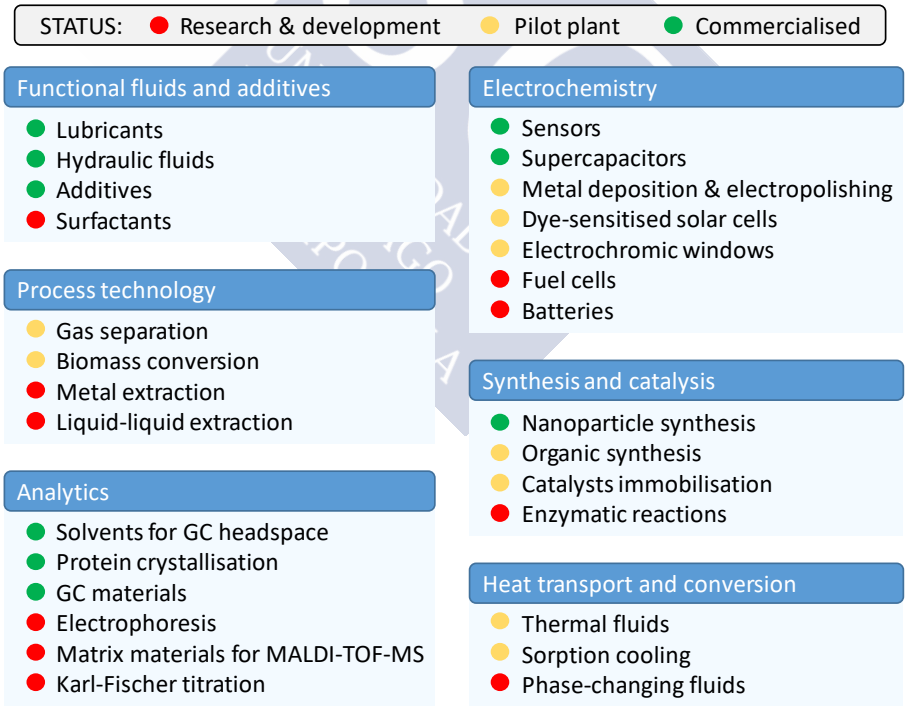

Figure 1.11. Selection of applications of ionic liquids and their development status, according to the company Iolitec GmbH (2017).

1.3. Ionic liquid systems for the pretreatment of lignocellulosic biomass

Swatloski et al. (2002) reported for the first time that some ionic liquids, such as 1-butyl-3-methylimidazolium chloride, could truly dissolve cellulose without derivatising it, in high concentrations, and at relatively mild conditions. This result triggered a very active research on the topic, leading to the discovery of a good number of ionic liquids able to dissolve different types of cellulose at relevant levels (Badgujar and Bhanage, 2015; Mäki-Arvela et al., 2010; Muhammad et al., 2015; Pinkert et al., 2009; Wang et al., 2012). In this dissolution process, the interactions between the anion of the ionic liquid and the hydroxyl groups of cellulose play an important role: an anion with a good hydrogen bonding acceptor ability (such as chloride, acetate...) is a requirement for the ionic liquid to effectively dissolve cellulose. The role of the cation in this mechanism of dissolution is not that clear, although it has to be somehow actively involved. Deeper discussions on this can be found elsewhere (Badgujar and Bhanage, 2015; Wang et al., 2012).

A few years after the ground-breaking discovery of ionic liquids with the capacity to dissolve cellulose, it was also found that lignocellulosic biomass (in particular, wood) could also be dissolved in ionic liquids (Fort et al., 2007, Kilpeläinen et al., 2007), under similarly mild conditions. In general terms, the solubilisation of lignocellulose seems to require similar properties of the ionic liquid than the solubilisation of cellulose (Brandt et al., 2013); so it is not surprising that, broadly speaking, ionic liquids that can dissolve cellulose are also capable of dissolving lignocelluloses (Badgujar and Bhanage, 2015; da Costa Lopes et al., 2013; Hou et al., 2017; Muhammad et al., 2015). Within this group of ionic liquids, there is a predominance of the chloride or acetate anions, mostly combined with dialkyl-substituted imidazolium cations.

The solubility of lignin alone in ionic liquids was also investigated, mostly using various commercially available lignin models (e.g. kraft, alkaline, or organosolv) (Badgujar and Bhanage, 2015; Hou et al., 2017; Mäki-Arvela et al., 2010). It must be noted, however, that their solubilities may not be an adequate reflection of the corresponding behaviour of the lignin within a lignocellulosic material, since both structure and composition can be notably different (Hou et al., 2017). Regarding hemicellulose, it is more easily dissolved that either of the other major biopolymers in

lignocelluloses, and to date no ionic liquids have been reported that can selectively dissolve hemicellulose but cannot dissolve cellulose and lignin (Hou et al., 2017).

Given the negligible volatility of the ionic liquids and of the biopolymers/lignocelluloses, the regeneration of the latter from the ionic liquid solution has been most commonly practiced by addition of (molecular) solvents miscible with the ionic liquid and acting as antisolvents for the dissolved material, thus precipitating it out of the solution (da Costa Lopes et al., 2013; Rodríguez, 2016). The most widely antisolvent used is water, but unfortunately not much attention has been paid to the quantity of antisolvent really needed in an engineering context, nor to the significant energy penalty that may be involved in distilling off the antisolvent from its mixture with the ionic liquid for their recycling to the process (Rodríguez, 2016).

For the case of dissolution of lignocellulosic biomass in ionic liquid, it has been shown that the design of an adequate scheme with the right antisolvents for selective precipitation at several stages can lead to a certain fractionation of the biopolymers (da Costa Lopes et al., 2013; Sun et al., 2009, 2011) – for example a cellulose-enriched material and isolated lignin (Figure 1.12). This is an evidence that ionic liquids can indeed break lignocellulosic bonds that hold the different constituent biopolymers together in the lignocellulosic matrix, without relying mainly in degradation of the lignin, as other pretreatment techniques do. Very interestingly, the crystallinity of cellulose in the regenerated lignocellulosic biomass fractions is lower than in the untreated material, with a change from cellulose I to cellulose II and a loss in fibrillar ordering that results in a higher amorphous component (Brandt et al., 2013); whereas the structures of lignin and hemicellulose remain essentially unaltered after treatment with ionic liquids (Wyman et al., 2009). All these observations would enable a more integral and efficient usage of the lignocellulosic feedstock in a biorefinery scheme (Sun et al., 2011). For example, for the production of biofuels such as bioethanol, enzymes can more efficiently hydrolyse into glucose the amorphous cellulose produced by means of the ionic liquid pretreatment than the highly crystalline cellulose as found in native lignocellulose (Dadi et al., 2007).

Besides the approach based on the solubilisation of the entire lignocellulosic material in the ionic liquid, a second approach in the context of biomass pretreatment emphasises the chemical disruption of the chemical lignocellulose composite without achieving total dissolution in the ionic liquid (Brandt et al., 2013). For instance, the selective (partial) extraction of lignin from the lignocellulosic matrix can be carried out

with some ionic liquids able to dissolve lignin but not cellulose (Brandt et al., 2013; Hou et al., 2017).

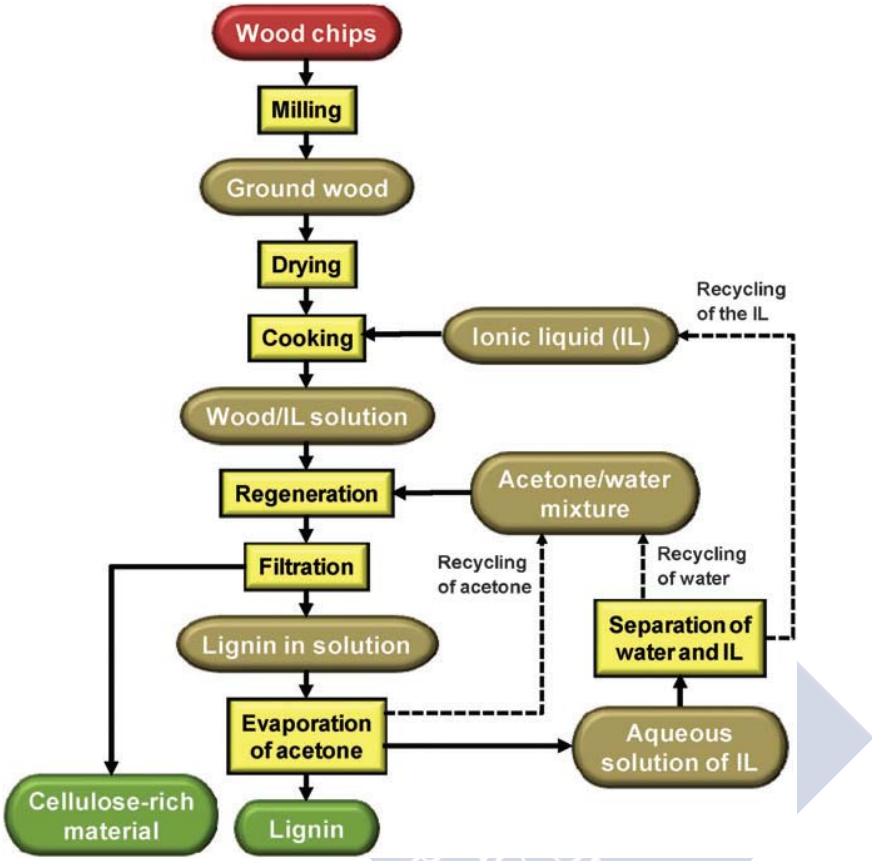

Figure 1.12. Flowchart for a process of dissolution of woody biomass in ionic liquid (IL) and its fractionated regeneration with an antisolvent strategy with water and acetone. Reproduced from Sun et al., 2011 by permission of the Royal Society of Chemistry.

In either of the approaches, the utilisation of solvent systems combining ionic liquids with molecular solvents (e.g. water, acetone, aprotic polar solvents such as dimethylsulfoxide, etc.) has also been tested for a series of varied targets (Hou et al., 2017; Muhammad et al., 2015): the dissolution and processing of cellulose, the extraction of lignin from biomass, or the extraction of hemicellulose from paper-grade pulp, among many others.

With this section providing only a brief and partial glance of what can be found in the very prolific literature on the subject, in light of the above, it can be stated that

ionic liquids offer a basis for an extremely versatile technological platform for the pretreatment of lignocellulosic biomass. This versatility even includes the possibility of combining the ionic liquid technology with the conventional pretreatment methods already in place (Zhang et al., 2017). However, for ionic liquids to actually contribute to the fulfillment of the biorefinery paradigm through any of the multiple process variants investigated, there are still important challenges to be addressed (Brandt et al., 2013; Muhammad et al., 2015; Simmons et al., 2010; Zhang et al., 2017). A first group refers to the ionic liquids themselves: lowering their cost (as they are still comparatively too expensive), improvements in toxicity and biodegradability, or issues on thermal stability in the long term, are matters of concern. And of course, ionic liquids with better performance have to be sought as well, looking for e.g. a better tolerance to water in the system or a satisfactory pretreatment of biomass particles of bigger size (so that the large energy consumption in the preparation of the feedstock for the process can be reduced (Brandt et al., 2013)). Moving to challenges connected with the processing, the efficient recycling of the ionic liquid has been identified as a critical aspect in preliminary technoeconomic analyses (Binder and Raines, 2010; Klein-Marcuschamer et al., 2011). This will require the effective removal of any remaining biomass fractions from the ionic liquid after the antisolvent addition (to avoid the build-up of unwanted pretreatment byproducts that could decrease performance (Simmons et al., 2010)); but also a minimised use of auxiliary substances such as antisolvents, along with a way of removing them from the ionic liquid with a tolerable energy input.

All in all, ionic liquids with their unique properties constitute a very attractive family of substances for biomass processing in a biorefinery context. However, there is a need to overcome key challenges for the development and implementation of commercially viable processes, in which the entire process economy together with environmental and social impacts have to be properly optimised (Zhang et al., 2017). It is therefore a time for fascinating research on this topic!

USC
UNIVERSIDADE
DE SANTIAGO
DE COMPOSTELA

2. OBJECTIVES

USC
UNIVERSIDADE
DE SANTIAGO
DE COMPOSTELA

2. OBJECTIVES

The general objective of this doctoral thesis is the advancement of knowledge on the possibilities and potential of fluid systems based on ionic liquids in the configuration of better process schemes for the improved pretreatment of lignocellulosic biomass. This general objective will be achieved through the development of specific objectives with different perspectives, as detailed below, ranging from a focus on the fundamental science governing the investigated systems to their utilisation in more applied approaches.

A first fluid system of interest will consist on mutually immiscible ionic liquids where one of the ionic liquids has the capacity to dissolve lignocellulosic biomass at relevant levels and the other does not have it. The ideal target will be to find pairs of ionic liquids with full mutual miscibility at a given temperature (at which the lignocellulose-dissolving capacity of the corresponding ionic liquid is not deactivated) and a large mutual immiscibility at a different temperature. In Chapter 3, selected pairs of ionic liquids will be screened for identification of immiscibility regions at practical temperature ranges, and the rigorous determination of the liquid-liquid equilibria of those systems will be carried out.

The investigation of the potential of alcohols as cosolvents or antisolvents of biomass-dissolving ionic liquids in pretreatment schemes constitutes another partial objective. Binary fluid systems resulting from the combination of each of the four lightest alcohols with an archetypical ionic liquid for the dissolution of lignocellulosic biomass will be explored in Chapter 4. A thermal characterisation of these systems will be performed, along with a thorough investigation of some of their key physical properties for the design of processes involving this type of mixtures. In transitioning towards their practical utilisation in process schemes seeking the fractionation of the major biopolymeric components of the biomass, the solubility of representative standards in selected systems will be determined, and some tests for the precipitation of these standards from the ionic liquid solution will be also developed.

Moving to a more applied perspective, a further objective will be to find out whether a fluid system of the type of those explored in Chapter 4 does satisfactorily

pretreat wood under acceptable conditions. In Chapter 5, wood particles of *Eucalyptus globulus* will be directly pretreated with such fluid system, or with the neat ionic liquid, at low temperature. Attention will be paid to a potential reduction in the degree of crystallinity of the wood (mainly due to the cellulose in it), which will improve the reactivity of the cellulose contained in the lignocellulosic matrix in subsequent stages after the pretreatment.

In a similar vein, it is intended to explore the use of ionic liquids with another kind of cation (namely a tetraalkylphosphonium), known to have no capacity for the dissolution of cellulose or wood when in neat. The pretreatment of wood particles of *Picea abies* (Norway spruce) with this fluid system will be investigated in Chapter 6. In approaching the real situation of a scaled-up pretreatment process, industrial chips will be considered in part of the study. The utilisation of cosolvents, as well as different process variables, will be investigated; and their influence will be evaluated through the analysis of fibrillation of the particles and composition of the resulting wood thus pretreated.

3. MUTUALLY IMMISCIBLE IONIC LIQUIDS WITH A COMMON ANION OF BASIC CHARACTER

USC
UNIVERSIDADE
DE SANTIAGO
DE COMPOSTELA

3. MUTUALLY IMMISCIBLE IONIC LIQUIDS WITH A COMMON ANION OF BASIC CHARACTER

3.1. Motivation

The recovery of non-volatile solutes from their solution in ionic liquids cannot be carried out effectively by means of distillation or evaporation techniques, due to the non-volatile character that ionic liquids also possess intrinsically. This is the situation that arises, for example, in biomass pretreatment schemes based on the use of an ionic liquid for the dissolution of the lignocellulosic material. In this case, the approach typically adopted for regeneration of the lignocellulose fractions from the ionic liquid solution is the addition of an antisolvent: a (classical) solvent miscible with the ionic liquid which, at a sufficient concentration in the system, causes the lignocelluloses to precipitate. After the corresponding filtration step, it is necessary to remove the volatile antisolvent from its mixture with the ionic liquid, in order to get the latter in a suitable condition for its recycling to the pretreatment process. This removal of antisolvent is normally carried out through techniques involving its vaporisation, thus introducing a high energy penalty in the process.

An alternative to the use of a volatile solvent in the role of antisolvent could be the use of a second ionic liquid. For such purpose, however, this second ionic liquid should have negligible capacity of dissolving lignocelluloses or some of their main constituents, and should be easily separable from the ionic liquid actually functioning as solvent for the lignocellulose at the core of the pretreatment process. Most ionic liquids meet the first requirement. Regarding the second requirement, an optimal situation would be that in which both ionic liquids would spontaneously phase separate, e.g. upon a switch in temperature, giving rise to two distinct liquid phases. This phenomenon is already known to occur in some pairs of ionic liquids. As an example, 1-ethyl-3-methylimidazolium bis(trifluoromethylsulfonyl)amide and trihexyl(tetradecyl)phosphonium bis(trifluoromethylsulfonyl)amide are miscible in

any proportion above 393 K (a temperature well below their limit of thermal stability (Cao and Mu, 2014; Keating et al., 2011)), but two liquid phases in equilibrium are generated for certain composition ranges below that temperature (Arce et al., 2007): the lower phase rich in the imidazolium ionic liquid and the upper phase rich in the phosphonium ionic liquid.

In the context of a process for the pretreatment of lignocelluloses via dissolution with an ionic liquid, the use as antisolvent of a second ionic liquid showing switchable miscibility with the first one within a workable temperature range would have the benefit of maintaining integrally some of the characteristic advantages of ionic liquids (e.g. negligible vapour pressure) in the global solvent system. Moreover, only sensible heat would be transferred in the process of recovering the biomass-dissolving ionic liquid, as opposed to the much larger latent heat involved in the vaporisation of a classical antisolvent from its mixture with the ionic liquid.

In this regard, this chapter will focus on the exploration of pairs of ionic liquids with the potential to exhibit spontaneous liquid-liquid demixing under certain conditions of temperature and composition, with only one of the members of the pair having a relevant capacity for dissolution of lignocelluloses. On the basis of the rather limited knowledge available to date on mutually immiscible ionic liquids and their liquid-liquid phase behaviour (Arce et al., 2006, 2007), their existence seems to be connected with the combination of ions with sufficiently dissimilar chemical structures. This structural difference may correspond to the cations, while the anion may be common to both ionic liquids. In fact, a common ion helps to reduce the complexity of the systems explored, facilitating the establishment of relations between the structural features of the involved ionic liquids and the produced phase behaviour. Thus, the combination of 1-alkyl-3-methylimidazolium chlorides or acetates (which are known to usually exhibit capacity for dissolution of lignocelluloses (Badgujar and Bhanage, 2015; Brandt et al., 2013)) with tetraalkylphosphonium or tetraalkylammonium ionic liquids with long alkyl substituents and the same anions is explored in this work, with rigorous determination of the liquid-liquid equilibrium in those cases showing any mutual immiscibility. A thermodynamic analysis complements the work, in order to get valuable information for a better understanding of the liquid-liquid equilibria in systems of mixed ionic liquids.

3.2. Theoretical considerations on liquid-liquid equilibrium

3.2.1. General aspects of liquid-liquid equilibrium

"Equilibrium" is defined as a situation in which no change occurs over time, although a real state of equilibrium is never reached, since it would take an infinite time. Therefore, it is considered that a system is in equilibrium when variations occur in very large intervals of time or are so small that their influence is negligible. From the Laws of Thermodynamics, it can be demonstrated that a closed system at constant temperature (T) and constant pressure (P) is in equilibrium when the total Gibbs free energy (G) of the system is minimal with respect to all possible changes at the given temperature and pressure (Smith et al., 2005). This condition can be mathematically expressed as:

$$\left(dG\right)_{P,T} = 0 \tag{3.1}$$

where subscripts P and T indicated constant pressure and temperature respectively. This expression is valid regardless of the number of phases and components in the system, and it can be considered as a criterion or definition of equilibrium. For an open system with a single fluid phase, the Gibbs free energy is related to its independent variables, namely temperature, pressure, and number of moles (n) of each component i, through the following expression:

$$dG = V \cdot dP - S \cdot dT + \sum_i \left(\mu_i \cdot dn_i\right) \tag{3.2}$$

where S and V are respectively the entropy and volume of the system, and μ_i is the chemical potential of component i. If a system with several components and several phases is considered, even if it is a closed system as a whole, each of the different phases is an open system that can exchange mass with the other phases, and Equation 3.2 is of application to each distinct phase:

$$dG = V^{(k)} \cdot dP - S^{(k)} \cdot dT + \sum_i \left(\mu_i{}^{(k)} \cdot dn_i{}^{(k)}\right) \tag{3.3}$$

where superscript k in parentheses refers to a generic phase. The sum of the expressions of Equation 3.3 applied to each of the phases will correspond to the total variation of Gibbs free energy in the system:

$$dG = V \cdot dP - S \cdot dT + \sum_k \sum_i \left(\mu_i^{(k)} \cdot dn_i^{(k)} \right) \tag{3.4}$$

In order to consider the system in equilibrium, thermal and mechanical equilibria are needed, with *T* and *P* being uniform throughout all *m* phases in the entire system:

$$T^{(1)} = T^{(2)} = \cdots = T^{(m)} \tag{3.5}$$

$$P^{(1)} = P^{(2)} = \cdots = P^{(m)} \tag{3.6}$$

Combining Equations 3.1, 3.4, 3.5, and 3.6, the following can be deduced:

$$\mu_i^{(1)} = \mu_i^{(2)} = \cdots = \mu_i^{(m)} \tag{3.7}$$

which constitutes the equilibrium criterion on the basis of the chemical potentials of each component in the mixture, for multiphasic systems with *m* phases. Unfortunately, the chemical potential is a rather abstract concept, not having an immediate equivalent in the physical world. Therefore, it is desirable to express the chemical potential in terms of magnitudes measurable in the laboratory. Thus, in order to facilitate a more practical application of the equilibrium criterion of Equation 3.7, the concept of fugacity is used. Defined by G. N. Lewis, fugacity is a function that satisfies the following equation (Prausnitz et al., 1999):

$$\mu_i - \mu_i^0 = R \cdot T \cdot \ln \frac{f_i}{f_i^0} \tag{3.8}$$

where *R* is the universal gas constant, and superscript 0 indicates a reference state. This reference state and its values of chemical potential (μ_i^0) and fugacity (f_i^0) are arbitrary, although not independent, and as soon as one of them is set the other one is immediately fixed by Equation 3.8.

By means of Equations 3.7 and 3.8, the equilibrium criterion can be expressed now as a function of fugacity, as follows:

$$f_i^{(1)} = f_i^{(2)} = \cdots = f_i^{(m)} \tag{3.9}$$

which is a more suitable expression from a practical point of view, and it is valid as long as all the reference states for all the phases are at the same temperature.

Lewis also defined the activity of a component *i* (a_i) as the ratio between its fugacity and the reference fugacity:

$$a_i = \frac{f_i}{f_i^0} \tag{3.10}$$

which can be interpreted as how 'active' a substance is in relation to its reference potential at the state of interest and that at its reference state (Prausnitz et al., 1999). If the reference state for all phases is the same, the combination of Equations 3.9 and 3.10 yields the equilibrium criterion that depends on activities:

$$a_i^{(1)} = a_i^{(2)} = \cdots = a_i^{(m)} \tag{3.11}$$

The activity of a species *i* is related to its composition by means of the activity coefficient γ_i:

$$\gamma_i = \frac{a_i}{x_i} \tag{3.12}$$

where x_i is the mole fraction of the species *i*. Hence Equation 3.11 can be transformed into:

$$(\gamma_i \cdot x_i)^{(1)} = (\gamma_i \cdot x_i)^{(2)} = \cdots = (\gamma_i \cdot x_i)^{(m)} \tag{3.13}$$

which is a popular and practical expression for the equilibrium criterion in multiphasic liquid systems. For a system of *N* components, each activity coefficient $\gamma_i^{(k)}$ is a function of the temperature and pressure of the system and of the *N*-1 independent mole fractions in phase *k*.

3.2.2. Liquid-liquid equilibrium in binary systems

In an equilibrium system in which the only significant intensive variables are temperature, pressure, and chemical potential, and under the assumption that no chemical reaction takes place, the famous phase rule (credited to J. W. Gibbs) provides a means of determining the number of intensive variables that can be independently varied without changing the state of the system (Smith et al., 2005; Treybal, 1963):

$$F = 2 - \pi + N \tag{3.14}$$

where *F* represents this number of independent variables (known as the number of degrees of freedom), π is the number of phases, and *N* is the number of components. If a binary system (two components) in which two liquid phases coexist is considered, from application of Equation 3.14 it is clear that *F* = 2. In such binary system, each of the activity coefficients will be a function of temperature, pressure, and one independent mole fraction. Thus, if one of those variables is fixed, the liquid-liquid equilibrium of the binary system can be conveniently represented in the two-

dimensional plane by plotting the other two variables in the corresponding x- and y-axes. For conditions of constant pressure (which is usually the case in the most relevant applications of liquid-liquid equilibrium at industrial level), the most typical representation is a temperature-composition diagram (also known as solubility diagram).

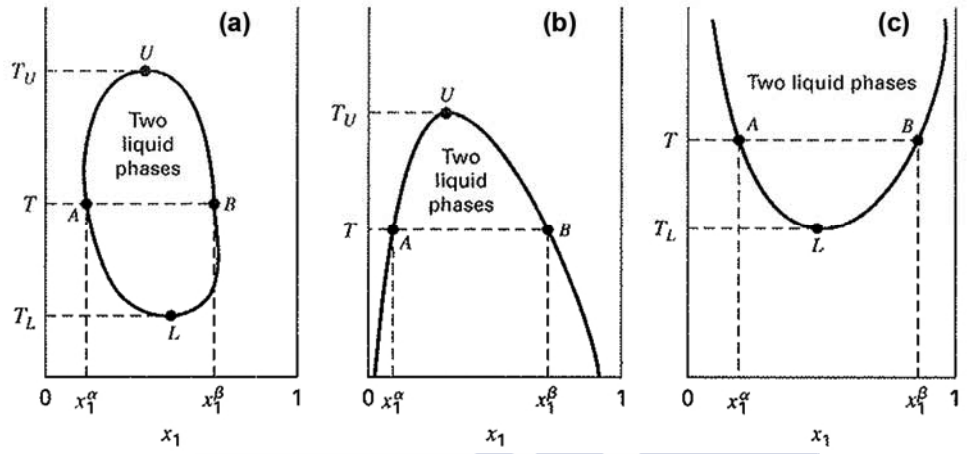

Figure 3.1. Representative types of liquid-liquid equilibria for binary systems, represented in isobaric temperature-composition diagrams: a) "island" type; b) upper critical solution temperature (UCST) type; b) lower critical solution temperature (LCST) type. Reproduced from Smith et al. (2005) by permission of McGraw-Hill.

Figure 3.1 shows three different types of liquid-liquid equilibria for binary systems, plotted in temperature-composition diagrams at constant pressure (Smith et al., 2005), with x_1 in the x-axis being the mole fraction of species 1. In these diagrams, for a given temperature T, points A and B at the intersection of the corresponding horizontal line with the equilibrium curves (or binodal curves) determine the compositions in equilibrium x_1^α and x_1^β for the coexisting liquid phases α (richer in species 2) and β (richer in species 1). Figure 3.1a represents an "island"-type liquid-liquid equilibrium, where the possibility of having two coexisting liquid phases in equilibrium is restricted to the temperature range between T_U and T_L, which are respectively the so-called upper critical solution temperature (UCST) and lower critical solution temperature (LCST). At temperature above T_U or below T_L, only one liquid phase will be obtained over the entire range of composition. "Island"-type liquid-liquid equilibrium behaviours occur rarely, as the binodal curves are usually interrupted by

some other phase transition. If the binodal curves are interrupted by the freezing curve, only a UCST can exist (Figure 3.1b); whereas if they are interrupted by the bubble curve of the vapour-liquid equilibrium, only an LCST can exist (Figure 3.1c) (Smith et al., 2005). A large number of liquid pairs form systems without upper or lower critical solution temperatures, since a solid phase forms before the appearance of an LCST on cooling, and a vapour-liquid condition (vapour phase of the same composition and density as one of the liquid phases) occurs before the appearance of a UCST on heating (Treybal, 1963).

3.3. Experimental

3.3.1. Ionic liquids

The ionic liquids 1-ethyl-3-methylimidazolium chloride ([C_2mim]Cl) and 1-ethyl-3-methylimidazolium acetate ([C_2mim][OAc]) were purchased from Iolitec with nominal purities greater than 98 % and 95 %, respectively. 1-Butyl-3-methylimidazolium chloride ([C_4mim]Cl), 1-methyl-3-octylimidazolium chloride ([C_8mim]Cl), and 1-butyl-3-methylimidazolium acetate ([C_4mim][OAc]) were supplied by Fluka, with nominal purities greater than 95 %, 98 %, and 95 %, respectively. Trihexyl(tetradecyl)phosphonium chloride ([$P_{6\,6\,6\,14}$]Cl) was kindly donated by Cytec with a nominal purity greater than 97 %.

1-Hexyl-3-methylimidazolium chloride ([C_6mim]Cl) was synthesised in-house by alkylation of 1-methylimidazole (Aldrich, >99 %) with 1-chlorohexane (Aldrich, 99,5 %), following an analogous procedure to that reported elsewhere for other 1-alkyl-3-methylimidazolium chlorides (Bradley et al., 2002).

Aliquat 336® (CAS number 63393-96-4) is the trade mark of a product corresponding to a mixture of trialkylmethylammonium chlorides, where the alkyl chains are octyl or decyl, with octyl predominating in a 2:1 mole ratio (Mikkola et al., 2006). Denominated here with the abbreviation [Aliquat]Cl, it was obtained from Sigma with a nominal purity in the range 85 %–95 % (with the impurities being mainly constituted by water and residual alcohols).

The syntheses of trihexyl(tetradecyl)phosphonium acetate ([$P_{6\,6\,6\,14}$][OAc]) and Aliquat acetate ([Aliquat][OAc]) were conducted by a metathesis reaction between

potassium acetate (Sigma Aldrich, >99 %) and the corresponding chlorides of the desired cations, according to the procedure reported by Mikkola et al. (2015) for the synthesis of several tetraalkylphosphonium acetates. Both reactants were dissolved independently in ethanol (Panreac, 99.8 %), and then the alcoholic solutions were mixed and stirred overnight. The precipitate of potassium chloride was filtered off, and the ethanol was removed by rotary evaporation. After cooling to room temperature, acetone (Sigma Aldrich, ≥99.9 %) was added, the mixture was stirred and then placed in the freezer for 48 h. If precipitate was observed, the filtration stage, evaporation of acetone, and re-addition of fresh acetone was repeated; until no further precipitation was observed.

All ionic liquids, regardless of being acquired from a commercial vendor or synthesised in-house, were purified by subjecting them to highly reduced pressure (<1 Pa) while being stirred and heated at ca. 330-340 K, to reduce the level of possible volatile impurities. Water is an impurity of particular concern, given the hygroscopic character of ionic liquids and the strong influence that it can have on their performance (Seddon et al., 2000). After the purification step, the final water content of the ionic liquids was measured by Karl-Fischer titration in a Metrohm 737 KF coulometer (Figure 3.2), and it was found to be 0.0023 in mass fraction for $[P_{6\,6\,6\,14}][OAc]$, 0.0020 for $[C_2mim]Cl$, 0.0012 for $[C_4mim][OAc]$, and in the range 0.0002-0.0008 for the rest of ionic liquids. Their chemical identity and the absence of significant levels of impurities in these purified products were confirmed by ^{1}H and ^{13}C nuclear magnetic resonance (NMR) spectroscopy analyses, run in a Varian Mercury 300 NMR spectrometer (Figure 3.2), or occasionally in a Bruker DRX-500 NMR spectrometer. The corresponding spectra are compiled in Appendix A. For the two ionic liquids prepared in-house by metathesis, the concentration of the spectator ions in the final products was measured, and found to be in the range 1600-1700 ppm for chloride (as determined by ion chromatography) and in the range 100-200 ppm for potassium (as determined by inductively coupled plasma optical emission spectroscopy, ICP-OES); which was considered acceptable for the purposes of this work.

The chemical structures of the constitutive ions of the ionic liquids mentioned in this section are shown in Figure 3.3.

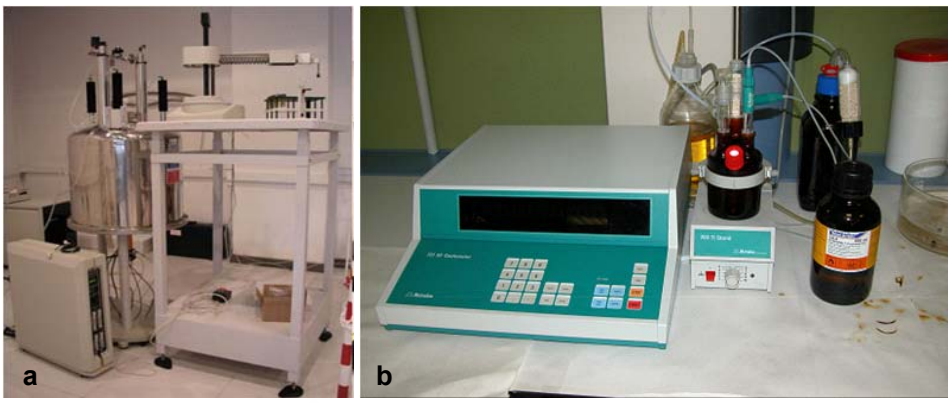

Figure 3.2. Equipment for the characterisation of the purified ionic liquids: Varian Mercury 300 NMR spectrometer (left) and Metrohm 737 KF coulometer (right).

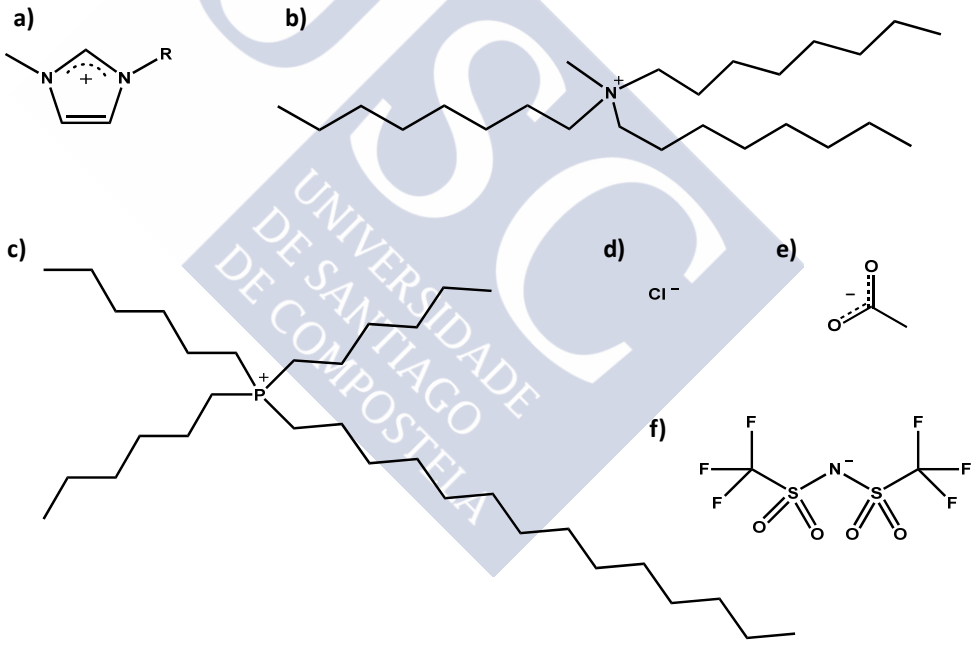

Figure 3.3. Chemical structures of the ions of the ionic liquids involved in this work: a) 1-alkyl-3-methylimidazolium (R = ethyl, butyl, hexyl, or octyl), $[C_n mim]^+$ (where *n* stands for the number of carbon atoms in the alkyl substituent); b) methyltrioctylammonium, as the most representative chemical structure in $[Aliquat]^+$ (see the main text for further details); c) trihexyl(tetradecyl)phosphonium, $[P_{6\,6\,6\,14}]^+$; d) chloride, Cl^-; e) acetate, $[OAc]^-$; f) bis(trifluoromethylsulfonyl)amide, $[NTf_2]^-$.

3.3.2. Thermal analyses

Thermal analyses to identify the range in which the ionic liquids remained thermally stable in the liquid state were carried out in order to determine the temperature ranges to be investigated in the liquid-liquid equilibrium studies.

Thermal stability of the ionic liquids was determined by thermogravimetric analysis (TGA) using a TA Instruments Q500 thermogravimetric analyser with a weight precision of ±0.01 % (Figure 3.4). This apparatus was calibrated in weight with weights of certified mass, and in temperature with nickel of high purity (99.9945 %) by means of the determination of its Curie temperature, in accordance with the instructions by the manufacturer. An open platinum pan loaded with ca. 15-20 mg of sample was used in each case. The TGA runs were carried out at a heating rate of 5 $K \cdot min^{-1}$, from ambient temperature up to 773 K, using N_2 (Praxair, 99.999 %) as balance purge gas and as sample purge gas (with flow rates of 40 $mL \cdot min^{-1}$ and 60 $mL \cdot min^{-1}$, respectively).

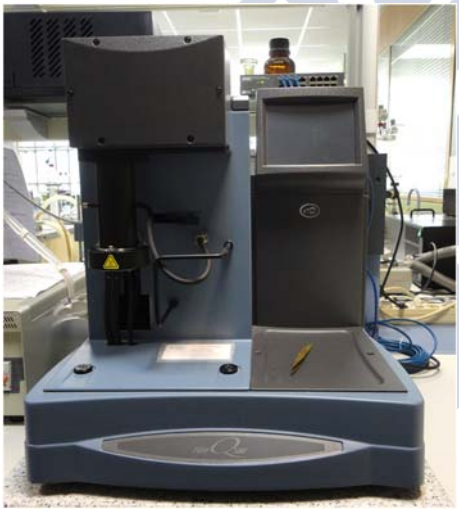

Figure 3.4. TA Instruments Q500 thermogravimetric analyser.

The lower end of the temperature range of the ionic liquids as stable liquids was determined by differential scanning calorimetry (DSC) using a TA Instruments Q2000 differential scanning calorimeter (Figure 3.5) with an RCS 90 refrigerated cooling system attached. The apparatus was calibrated with indium of high purity (99.99 %) by means of the determination of its onset melting temperature, in accordance with the

instructions by the manufacturer. Approximately 10-20 mg of each sample was placed in a 40 μL aluminium pan, sealed hermetically with a lid of the same material and loaded into the measuring chamber with an autosampler. An analogous, empty pan with its corresponding lid was used as reference. An initial heating at 5 $K \cdot min^{-1}$ up to 393 K was the initial step of the thermal program applied, followed by a 5-min isotherm at 393 K, and then two cooling-heating cycles in the temperature range 183-393 K, with cooling/heating ramps of 5 $K \cdot min^{-1}$ and the corresponding 5-min isotherms both at 183 K and at 393 K after finishing each cooling or heating ramp. A 50 $mL \cdot min^{-1}$ flow of N_2 was used as sample purge gas. After ensuring that the DSC curves for the two full cooling-heating cycles were essentially coincident, the signal from the last cooling ramp was used for determination of (midpoint) glass transitions, and the signal from the last heating ramp was used for determination of (onset) melting temperatures.

Figure 3.5. TA Instruments Q2000 differential scanning calorimeter.

The analysis of all the TGA and DSC curves was made by means of the Universal Analysis 2000 software, version 4.5.0.5, by TA Instruments.

3.3.3. Identification of mutually immiscible ionic liquids

Combinations of an imidazolium ionic liquid and a tetraalkylammonium or tetraalkylphosphonium ionic liquid, with either chloride or acetate as common anion,

were explored at different temperatures and compositions, in search of the formation of stable liquid-liquid biphasic mixtures. Jacketed glass cells were used, keeping the temperature of the system constant, with an uncertainty of 0.1 K, by means of the circulation through the jacket of fluid from either a Julabo EH5 oil bath thermostat or an Ultratherm-200 P Selecta water bath thermostat (the latter for temperatures only up to 358.2 K). For a given fixed temperature, one of the ionic liquids was placed in the cell, and the other was gradually added, with an approximate composition step of 0.02 in mole fraction. After each addition, the mixture was magnetically stirred until complete solubilisation, or for a minimum of 1 h to guarantee the persistency of any observed immiscibility. The additions were performed until permanent immiscibility was detected, or until a 0.50 mole fraction was reached. In the latter case, the roles of the ionic liquids were inverted and the same operation was repeated. The same protocol was applied to other temperatures, until obtaining evidence of thermodynamically stable liquid-liquid demixing, or until covering the entire temperature range to be explored in each case. Regarding the latter point, for each system the upper limit of such temperature range was taken as a temperature safely below the decomposition temperature determined by TGA of the less thermally stable of the two ionic liquids, or 423.2 K, whichever were lower; whereas the lower limit was taken as a temperature somewhat above the highest of the melting points determined for the two ionic liquids by DSC, or 298.2 K, whichever were higher. This choice of lower end for the investigated temperature range was done arbitrarily, without intending to neglect the possibility of having the systems totally liquid at lower temperatures, either in a supercooled state (Stark and Seddon, 2007) or as a result of a eutectic behaviour (Stolarska et al., 2015). However, these aspects have not been considered for study herein.

3.3.4. Determination of liquid-liquid equilibrium data

Equilibrium experiments

The determination of liquid-liquid equilibrium (LLE) data was carried out for the binary combinations of ionic liquids found to exhibit immiscibility according to the protocol described in Section 3.3.3. For each system, mixtures of the two ionic liquids lying in the liquid-liquid biphasic domain were loaded into jacketed glass cells especially

designed for liquid-liquid equilibrium experiments, and manufactured at the glassblowing workshop of the University of Santiago de Compostela (Figure 3.6). The content of the cell was thermostated as previously described in Section 3.3.3. At each desired temperature, the mixture within the cell was vigorously stirred by means of magnetic stirring for at least 2 h (a sufficiently large time to guarantee equilibration of the liquid phases). At the time of ceasing the stirring, a plugged metal needle was introduced, through a septum in a lateral neck of the cell, into the heterogeneous mixture, with the tip reaching the bottom of the cell. The mixture was then allowed to settle for no less than 20 h to ensure good separation of the equilibrated phases. A sample from the top phase was taken with a glass Pasteur pipette. By removing the plug of the previously introduced needle and attaching a syringe to it, a sample was taken from the bottom phase without disturbance of the liquid-liquid interphase (thus avoiding the risk of cross-contamination of the phases while collecting samples of them).

Figure 3.6. Liquid-liquid equilibrium jacketed glass cell, mounted on a magnetic stirring plate.

The samples taken from each liquid phase in equilibrium were directly placed in NMR tubes, and dissolved in either $CDCl_3$ (Aldrich, 99.8 atom % D) or CD_3OD (Sigma

Aldrich, 99.8 atom % D) depending on their solubility in these deuteriated solvents, for subsequent compositional analysis by NMR spectroscopy, as described next.

Compositional analysis

A procedure based on ^{1}H NMR spectroscopy was used to determine the compositions of the phases in equilibrium. For each system, a set of spectral peaks for the cations of the ionic liquids was identified so that the mole fraction compositions could be determined by using the relationship existing between the areas per proton under the peaks and the number of moles of each cation. In particular, for the $[C_n\text{mim}]^+$ cations, the quartet/triplet peak (accounting for two hydrogen atoms, 2H) and the singlet peak (3H) in the range 3.5-4.5 ppm (corresponding to the methylene and methyl groups directly bonded to the nitrogen atoms of the imidazolium ring) were considered. For $[N_{8881}]^+$, the peaks at ca. 3 ppm (3H, methyl group bonded to the nitrogen atom) and at ca. 0.9 ppm (9H, terminal methyl groups of the long alkyl chains) were selected; and for $[P_{66614}]^+$, the peaks at ca. 2.0-2.5 ppm (8H, methylene groups bonded to the phosphorous atom) and at ca. 0.5-1.0 ppm (12H, terminal methyl groups of the four alkyl chains) were used. In the particular case of the system $[C_4\text{mim}]\text{Cl} + [N_{8881}]\text{Cl}$, the 9H signal for $[N_{8881}]^+$ overlapped with the 3H signal of the terminal methyl group of the butyl substituent of $[C_4\text{mim}]^+$, and therefore the subtraction of an area equivalent to 3H of the imidazolium cation from the total peak integration was carried out to yield the specific contribution of $[N_{8881}]^+$ to the area under that composed peak. All ^{1}H NMR spectra were recorded in a Varian Mercury 300 spectrometer, with a longitudinal relaxation time (t_1) of 6 s and a total of 64 scans.

The error in the determination of the composition of the phases in equilibrium by the procedure above described was estimated by means of test vials prepared by weight. Homogeneous mixtures of each pair of ionic liquids of the studied liquid-liquid equilibrium systems were prepared in glass vials, with a composition lying in the vicinity of the liquid-liquid demixing boundary. The mass of the added compounds was recorded with a Mettler Toledo AE240 analytical balance with a precision of $\pm 1 \times 10^{-4}$ g (Figure 3.7). A sample of each test vial was taken, placed in an NMR tube, dissolved with the appropriate deuteriated solvent, and subjected to analysis by ^{1}H NMR spectroscopy, following the exact protocol described above for the samples of the liquid-liquid equilibrium experiments. An uncertainty of 0.008 in mole fraction was

estimated, on the basis of the differences found between the real compositions (known by weight) and the calculated compositions (from the recorded NMR spectra) for these test vials. Such degree of accuracy was considered acceptable for the purpose of this work.

Figure 3.7. Mettler Toledo AE 240 analytical balance.

3.4. Results and discussion

3.4.1. Thermal characterisation of ionic liquids

Thermal stability

For each ionic liquid, the regular onset decomposition temperature T_d and the 5 % onset decomposition temperature $T_{d,5\%}$ (corresponding to the onset temperature for a weight loss of 5 % of the original sample mass, instead of for the inflexion point of the entire TGA curve) were calculated, with an estimated uncertainty of 1 K, and are reported in Table 3.1. All processed TGA thermograms, from which the numerical values were obtained, are compiled in Appendix B.

The $T_{d,5\%}$ magnitude constitutes a more conservative and better estimation, as compared to T_d, of the maximum temperature at which the substances can be operated

in a continuous process in the mid- or long-term (Clough et al., 2013; Smiglak et al., 2006). Thus, the $T_{d,5\%}$ values were the ones considered in estimating the temperature ranges for investigation of the liquid-liquid equilibrium in the selected systems of mixtures of two ionic liquids. As observed in Table 3.1, these $T_{d,5\%}$ values are typically several dozens of degrees Kelvin lower than the corresponding T_d values, although higher than 400 K in all cases. The experimental T_d values were valid, nevertheless, to establish a comparison with literature values from other authors for most of the ionic liquids investigated (Table 3.1); the only exception being [Aliquat][OAc], for which no numerical value of T_d was found in the literature. A reasonably good agreement between experimental and literature data sets was observed, particularly if taking into account the rather high dispersion of literature values for some of the ionic liquids (as illustrated by the two or three example references selected for certain ionic liquids). Such dispersion may be attributed to the presence in the samples of different impurities and their levels, as well as to the fact of having carried out the experiments under somewhat different conditions (e.g. at a different heating rate), which affects the T_d value finally obtained.

Table 3.1. Onset decomposition temperature (T_d) and 5 % onset decomposition temperature ($T_{d,5\%}$) for the ionic liquids involved in the liquid-liquid equilibria determined in this work, at atmospheric pressure. "Exp." stands for experimental values determined herein, and "Lit." stands for literature values.

Ionic liquid	T_d (K)		$T_{d,5\%}$ (K)
	Exp.	Lit.‡	Exp.
[C_2mim]Cl	538	534,[a] 551[b]	487
[C_4mim]Cl	535	564,[b] 527,[c] 530[d]	415
[C_6mim]Cl	529	526[c]	485
[C_8mim]Cl	529	516,[c] 549[d]	495
[C_2mim][OAc]	475	494,[d] 489[e]	427
[C_4mim][OAc]	483	489,[d] 492[f]	445
[Aliquat]Cl	453	475,[g] 493[h]	415
[Aliquat][OAc]	426	448[h]	411
[$P_{6\,6\,6\,14}$]Cl	618	604[i]	437
[$P_{6\,6\,6\,14}$][OAc]	574	not found	493

‡ References: [a] Ngo et al. (2000); [b] Meine et al. (2010); [c] Huddleston et al. (2001); [d] Cao and Mu (2014); [e] Clough et al. (2013); [f] Wei et al. (2015); [g] Fraser et al. (2007); [h] Mikkola et al. (2006); [i] Ferreira et al. (2012).

Phase transitions

The melting temperatures and glass transitions obtained by DSC for the ionic liquids, with an estimated uncertainty of 1 K, are reported in Table 3.2. The corresponding thermograms from which the numerical values were obtained are presented in Appendix B. Although the lowest temperature used in the cycles of the thermal program was 183 K, a loss of stability of the baseline was observed in the range 183-200 K approximately, likely due to limitations of the refrigeration system of the apparatus. Consequently, it must be noted that the thermal events identified in the vicinity of 200 K are possibly affected by a greater uncertainty than the rest of the values. This affection may even involve the identification of the nature of the thermal transitions observed, as for example in the case of $[P_{6\,6\,6\,14}]Cl$ and $[P_{6\,6\,6\,14}][OAc]$. For these two ionic liquids, the signals observed in the corresponding thermograms were assigned to melting points; although a glass transition manifested with a pronounced 'hump' could be an alternative interpretation – see Figures B.9 and B.10 in Appendix B. Nevertheless, an acceptable agreement of these experimental values with literature values reported by other authors was found, as it can be also observed in Table 3.2. There is no agreement, however, between the melting temperature of 323 K reported herein for [Aliquat]Cl and that of 253 K reported in the literature by Mikkola et al. (2006). Such difference might be attributed to the utilisation by those authors of a sample of Aliquat 336 with a higher content of its characteristic molecular impurities. In fact, as supplied by the commercial vendor, this ionic liquid is liquid at room temperature; and after intensive application of high vacuum (as described in Section 3.3.1) the purified sample became solid at room temperature.

It must be also pointed out that only a low-temperature glass transition was observed for the $[C_4mim]Cl$ sample, with no signal of crystallisation or melting of any of its two identified polymorphs, as described by Diogo et al. (2013). A similar observation was reported by Fredlake et al. (2004), with the identification of just a glass transition and no melting peaks. The absence of melting peak for this ionic liquid in its DSC thermogram may be attributed to its extremely high tendency to remain as a supercooled liquid (Nishikawa et al., 2007). In any case, the highest among the reported melting temperatures of the identified polymorphs was taken into consideration for

determining the low end of the temperature range for experimental investigation of the liquid-liquid equilibrium in the system involving [C_4mim]Cl.

Table 3.2. Melting temperature (T_m) and/or glass transition temperature (T_g) for the ionic liquids involved in the liquid-liquid equilibria determined in this work, at atmospheric pressure. "Exp." stands for experimental values determined herein, and "Lit." stands for literature values. The values marked with an asterisk correspond to a T_g, while the other values correspond to a T_m.

Ionic liquid	T_m (K) and/or T_g (K)	
	Exp.	Lit.‡
[C_2mim]Cl	357	362;[a] 361[b]
[C_4mim]Cl	221*	343;[b] 314;[c] 222*, 321(m), 345(o)[d,‖]
[C_6mim]Cl	208*	198*;[c] 223*[d]
[C_8mim]Cl	199*	186*;[c] 229*[d]
[C_2mim][OAc]	202*	195*;[e] 198*[f]
[C_4mim][OAc]	210*	203*;[f] 203*[g]
[Aliquat]Cl	323	253[h]
[Aliquat][OAc]	250	251[h]
[$P_{6\,6\,6\,14}$]Cl	207	203*;[i] 216*[j]
[$P_{6\,6\,6\,14}$][OAc]	206	not found

‡ References: [a] Ngo et al. (2000); [b] Kick et al. (2013); [c] Huddleston et al. (2001); [d] Diogo et al. (2013); [e] Troshenkova et al. (2010); [f] Guan et al. (2011); [g] Wei et al. (2015); [h] Mikkola et al. (2006); [i] CYTEC Industries Inc. (2011); [j] Pozo-Gonzalo et al. (2014).
‖ Polymorphs: (m), monoclinic; (o), orthorhombic.

3.4.2. Mutually immiscible pairs of ionic liquids

The ionic liquid [Aliquat]Cl was combined with [$C_n$mim]Cl ionic liquids (n = 2, 4, 6, or 8). Liquid-liquid immiscibility was observed for the systems [C_2mim]Cl + [Aliquat]Cl and [C_4mim]Cl + [Aliquat]Cl, whereas the systems [C_6mim]Cl + [Aliquat]Cl and [C_8mim]Cl + [Aliquat]Cl were found to be totally miscible over the entire composition range and investigated temperature range. This is similar to what was previously reported for mixtures [$C_n$mim]Cl + [$P_{6\,6\,6\,14}$]Cl, which may give rise to liquid-liquid biphasic systems when the alkyl substituent chain of the imidazolium cation is pentyl or shorter, but they total miscibility at any composition for hexyl or longer substituents (Arce et al., 2006).

Regarding the combinations of ionic liquids with acetate as common anion, [C_2mim][OAc] and [C_4mim][OAc] were combined with the acetates of the two tetraalkylpnictogenium cations, i.e. with [Aliquat][OAc] and with [$P_{6\,6\,6\,14}$][OAc]. Following the protocol described in Section 3.3.3, liquid-liquid biphases were found in the binary systems [C_2mim][OAc] + [Aliquat][OAc] and [C_2mim][OAc] + [$P_{6\,6\,6\,14}$][OAc],

but not in the systems with [C_4mim][OAc]. Thus, in analogy with what has been described for the chloride-based systems in the paragraph above, an increase in the length of the alkyl substituent of the imidazolium ionic liquid leads to the disappearance of the liquid-liquid biphasic domain in the systems. A difference, however, is that in the case of the mixtures of acetates, a shorter alkyl substituent (butyl instead of hexyl) is sufficient for the total miscibility to occur.

3.4.3. Experimental liquid-liquid equilibrium data

For the above mentioned systems that showed distinct liquid-liquid biphasic character at some conditions of concentration and temperature, the liquid-liquid equilibrium was rigorously determined, according to the procedure described in Section 3.3.4. The mole fraction compositions of the phases in equilibrium for the binary systems [$C_n$mim]Cl + [Aliquat]Cl (n = 2 or 4), [C_2mim][OAc] + [Aliquat][OAc], and [C_2mim][OAc] + [$P_{6\,6\,6\,14}$][OAc], at the different experimental temperatures tested, are reported in Table 3.3 (systems with chloride as a common ion) and Table 3.4 (systems with acetate as a common ion). Moreover, the liquid-liquid equilibrium data for the system [C_2mim]Cl + [$P_{6\,6\,6\,14}$]Cl, which has already been reported in the literature (Arce et al., 2006) but only in graphical form, were also determined and are numerically reported in Table 3.3. From direct inspection of the tables, it can be observed that the lower phase is (very) rich in the imidazolium ionic liquid in all studied systems, whereas the upper phase is rich in the tetraalkylammonium/tetraalkylphosphonium ionic liquid.

For a better analysis of the influence of different structural features of the ionic liquids on the liquid-liquid equilibria, the corresponding temperature-composition diagrams were built. Figure 3.8 shows a diagram of this type, displaying the liquid-liquid equilibria of the systems [C_2mim]Cl + [$P_{6\,6\,6\,14}$]Cl and [C_2mim][OAc] + [$P_{6\,6\,6\,14}$][OAc]. For these two systems, it can be observed that the presence of phosphonium cations in the imidazolium-rich phase (the lower phase) is very small and even negligible, whereas the imidazolium cations are present in the phosphonium-rich phase (the upper phase) in a relevant concentration. The replacement of the chloride anion with the bigger acetate anion in these systems leads to greater concentrations of the imidazolium cation in the phosphonium-rich phase, increasing the degree of

miscibility (or, equivalently, decreasing the concentration range exhibiting immiscibility) at a given temperature.

Table 3.3. Mole fractions of the imidazolium ionic liquid in the upper and lower phases ($x_{1,up}$ and $x_{1,low}$, respectively) of the liquid-liquid equilibria of systems [C$_n$mim]Cl (1) + [Cation]Cl (2) (where n = 2 or 4, and [Cation]$^+$ stands for [Aliquat]$^+$ or [P$_{6\,6\,6\,14}$]$^+$), at the corresponding temperatures T and atmospheric pressure.

T / K	$x_{1,up}$	$x_{1,low}$
[C$_2$mim]Cl (1) + [Aliquat]Cl (2)		
358.2‡	0.104	0.999
368.2	0.115	0.996
378.2	0.130	0.998
388.2	0.124	0.997
398.2	0.106	0.997
[C$_4$mim]Cl (1) + [Aliquat]Cl (2)		
358.2	0.377	0.969
368.2	0.468	0.949
378.2	0.491	0.952
388.2	0.493	0.954
398.2	0.483	0.951
408.2	0.480	0.951
[C$_2$mim]Cl (1) + [P$_{6\,6\,6\,14}$]Cl (2)		
373.2	0.098	1.000
383.2	0.093	1.000
393.2	0.087	1.000
403.2	0.084	1.000
413.2	0.086	1.000
423.2	0.080	1.000

‡ This temperature is only slightly higher than the reported melting temperature experimentally determined for pure [C$_2$mim]Cl (see Table 3.2), but it was included in the study in order to cover a sufficiently large temperature range, given the upper temperature limitation imposed by the thermal decomposition of [Aliquat]Cl (see Table 3.1).

The influence of temperature in the system [C$_2$mim]Cl + [P$_{6\,6\,6\,14}$]Cl is unclear, but in any case it is small over the studied temperature range, as the mutual solubility of these two ionic liquids can be taken as practically invariant in such range (within the experimental composition uncertainty). Contrarily, for the mixture of [C$_2$mim][OAc] and [P$_{6\,6\,6\,14}$][OAc] a clear decrease in mutual solubility is observed as the temperature is risen. This suggests that the liquid-liquid equilibrium of the system [C$_2$mim][OAc] + [P$_{6\,6\,6\,14}$][OAc] responds to an LCST-type phase behaviour. Interestingly, this is in contrast to the UCST-type behaviour previously observed in the literature (Arce et al.,

2006, 2007) for the system [C_2mim][NTf_2] + [$P_{6\,6\,6\,14}$][NTf_2], with the same cations but with the much bulkier bis(trifluoromethylsulfonyl)amide ([NTf_2]$^-$) as common anion – see its chemical structure in Figure 3.3. The liquid-liquid equilibrium of the latter system is also represented in Figure 3.8 for direct visual comparison. Even though the mutual immiscibility for these pairs of ionic liquids is largely due to the great dissimilarity of their cations, Figure 3.8 evidences the importance that the nature of the common counterion (i.e. the anion) has in the type of liquid-liquid equilibrium generated.

Table 3.4. Mole fractions of the imidazolium ionic liquid in the upper and lower phases ($x_{1,up}$ and $x_{1,low}$, respectively) of the liquid-liquid equilibria of systems [C_2mim][OAc] (1) + [Cation][OAc] (2) (where [Cation]$^+$ stands for [Aliquat]$^+$ or [$P_{6\,6\,6\,14}$]$^+$), at the corresponding temperatures T and atmospheric pressure.

T / K	$x_{1,up}$	$x_{1,low}$
[C_2mim][OAc] (1) + [Aliquat][OAc] (2)		
298.2	0.407	0.985
308.2	0.427	0.979
318.2	0.435	0.982
328.2	0.449	0.981
338.2	0.445	0.978
348.2	0.452	0.979
358.2	0.430	0.981
368.2	0.377	0.983
[C_2mim][OAc] (1) + [$P_{6\,6\,6\,14}$][OAc] (2)		
298.2	0.400	0.992
318.2	0.369	0.995
328.2	0.360	0.997
338.2	0.352	0.996
358.2	0.330	0.993
368.2	0.324	0.994
378.2	0.313	0.995

A different evolution of the liquid-liquid equilibrium with temperature is observed in Figure 3.9 for the systems [C_2mim]Cl + [Aliquat]Cl and [C_2mim][OAc] + [Aliquat][OAc]. In these cases, an initial increase in mutual miscibility occurs with an increase in temperature; but the trend switches at a certain temperature, and the immiscibility gap starts increasing with further increase of the temperature. The result is an hourglass-shaped system. This type of temperature-composition behaviour was previously reported for the liquid-liquid equilibrium of a binary system comprising an ionic liquid and a molecular solvent (Łachwa et al., 2006). However, the systems

reported in Figure 3.9 constitute the first evidence of such type of behaviour for a mixture of two mutually immiscible ionic liquids.

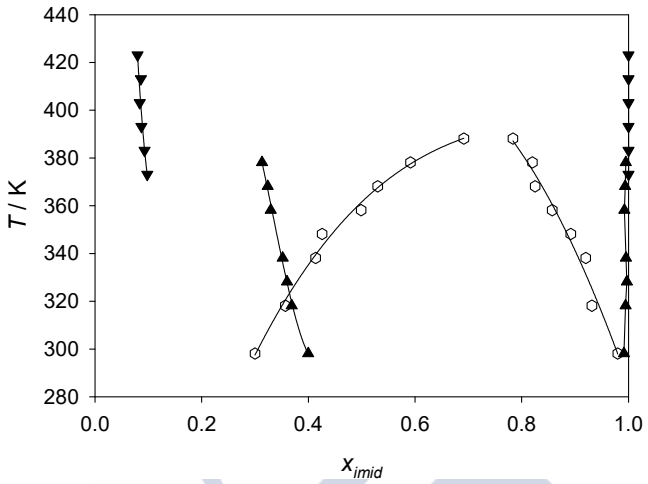

Figure 3.8. Temperature-composition diagram for the liquid-liquid equilibria of the systems $[C_2mim]Cl + [P_{6\,6\,6\,14}]Cl$ (solid inverted triangles) and $[C_2mim][OAc] + [P_{6\,6\,6\,14}][OAc]$ (solid triangles). Literature values for the system $[C_2mim][NTf_2]+[P_{6\,6\,6\,14}][NTf_2]$ (open black hexagons) are also represented (Arce et al., 2007). In the x-axis, the mole fraction of the corresponding imidazolium ionic liquid (x_{imid}) is represented. The liquid-liquid biphasic domain corresponds to the region between the two branches of each system. Solid lines are shown as guides to the eye.

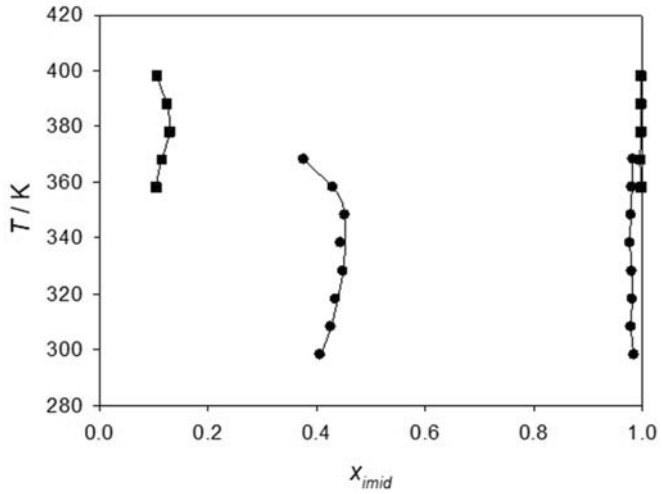

Figure 3.9. Temperature-composition diagram for the liquid-liquid equilibria of the systems $[C_2mim]Cl$ + [Aliquat]Cl (squares) and $[C_2mim][OAc]$ + [Aliquat][OAc] (circles). In the x-axis, the mole fraction of the corresponding imidazolium ionic liquid (x_{imid}) is represented. The liquid-liquid biphasic domain corresponds to the region between the two branches of each system. Solid lines are shown as guides to the eye.

In terms of the degree of mutual immiscibility, a parallelism is observed between the systems in Figure 3.9 and those in Figure 3.8 already discussed. Specifically, the replacement of the chloride anion by the acetate anion (from [C_2mim]Cl + [Aliquat]Cl to [C_2mim][OAc] + [Aliquat][OAc]) leads to an improvement of the mutual solubility of the phases, through the solubilisation of a higher proportion of imidazolium cations in the ammonium-rich phase. On the other hand, the denser, imidazolium-rich phase contains a very small or even negligible concentration of ammonium cations in all cases.

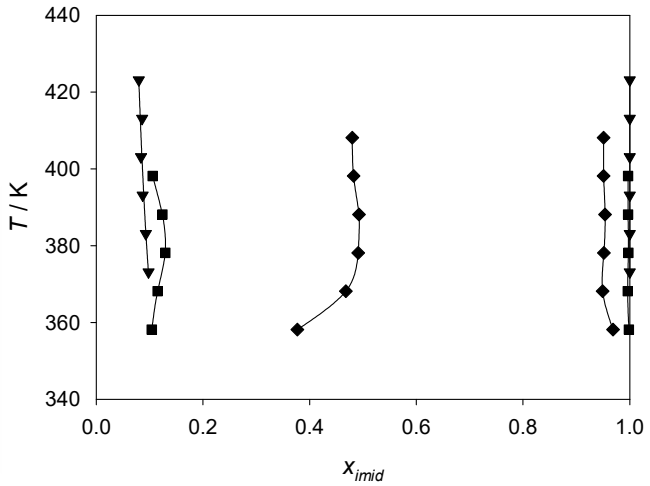

Figure 3.10. Temperature-composition diagram for the liquid-liquid equilibria of the systems [C_2mim]Cl + [Aliquat]Cl (squares), [C_2mim]Cl + [$P_{6\,6\,6\,14}$]Cl (inverted triangles), and [C_4mim]Cl + [Aliquat]Cl (diamonds). In the x-axis, the mole fraction of the corresponding imidazolium ionic liquid (x_{imid}) is represented. The liquid-liquid biphasic domain corresponds to the region between the two branches of each system. Solid lines are shown as guides to the eye.

Figure 3.10 offers a direct visualisation of the comparison of the liquid-liquid equilibria of the systems [C_2mim]Cl + [$P_{6\,6\,6\,14}$]Cl and [C_2mim]Cl + [Aliquat]Cl, enabling an analysis of the effect of the nature of the tetraalkylammonium/tetraalkylphosphonium cation. By replacing the $[P_{6\,6\,6\,14}]^+$ cation with the $[Aliquat]^+$ cation, the immiscibility gap with the imidazolium ionic liquid decreases; although this effect is relatively small. It must be noted that, in $[Aliquat]^+$, the methyl substituent is much shorter than all others substituents, bringing a sort of 'semi-spherical' shape to this cation and locating the centre of charge close to the centre of such semi-sphere. This may result in a little higher polarity for $[Aliquat]^+$ as compared to the more spherical and charge-centred $[P_{6\,6\,6\,14}]^+$. Such difference may

account for the slight decrease observed in the immiscibility gap with [C_2mim]Cl. A more marked effect can be observed in the evolution of the mutual miscibility with temperature, since there is practically no effect in the system with [$P_{6\,6\,6\,14}$]$^+$, while the system with [Aliquat]$^+$ exhibits the hourglass-shaped behaviour mentioned above. An analogous discussion could be applied to the comparison of the systems [C_2mim][OAc] + [$P_{6\,6\,6\,14}$][OAc] and [C_2mim][OAc] + [Aliquat][OAc] (not shown together in the same figure, but easy to compare by simultaneous consideration of Figures 3.8 and 3.9), although noting that in this case a variation from LCST behaviour to hourglass behaviour is actually observed when replacing the [$P_{6\,6\,6\,14}$]$^+$ cation with the [Aliquat]$^+$ cation.

The liquid-liquid equilibrium for the system [C_4mim]Cl + [Aliquat]Cl is also plotted in Figure 3.10, thus enabling a direct analysis of the influence of the length of the alkyl substituent chain of the imidazolium cation, via comparison with the system [C_2mim]Cl + [Aliquat]Cl. In this case, the replacement of the ethyl substituent with a butyl substituent in the imidazolium cation causes a remarkable increase in the mutual miscibility, while maintaining the hourglass type behaviour. A further increase in the length of the substituent, to hexyl or octyl, will result in total miscibility of the two ionic liquids, over the entire temperature range investigated, as already described in Section 3.4.2. Therefore, the evolution of the liquid-liquid equilibrium in the systems [$C_n$mim]Cl + [Aliquat]Cl follows an analogous trend to what was previously reported for the systems [$C_n$mim]Cl + [$P_{6\,6\,6\,14}$]Cl (Arce et al., 2006), for which also gradually smaller immiscibility was observed with an increase in the alkyl substituent length, and from hexyl onwards the ionic liquids became completely miscible in any proportion.

By simultaneous consideration of all the systems in Figure 3.10, it can be noted that the variation of the alkyl substituent length in the imidazolium ionic liquid has a much stronger influence in the liquid-liquid equilibria of the mutually immiscible ionic liquids than the variation of the lengths of the alkyl substituents (or the central atom) in the tetraalkylammonium/tetraalkylphosphonium cations. The reason for this may be the relative modification of the polarity caused by those variations. The butyl substituent in [C_4mim]$^+$ is sufficiently long (in contrast to the ethyl substituent in [C_2mim]$^+$) to create an 'apolar tail' in the cation, leading to a stronger chance of interaction with the 'apolar shells' of [$P_{6\,6\,6\,14}$]Cl or [Aliquat]Cl; hence increasing mutual miscibility. However, the replacement of [$P_{6\,6\,6\,14}$]$^+$ with [Aliquat]$^+$, although involving a change in the length of all four alkyl substituents, does not lead to so relevant

modifications in the charge distribution of the ion, as well as consequently in the interaction with the imidazolium ionic liquid.

3.4.4. Thermodynamic analysis

In the studied liquid-liquid equilibria, the ammonium/phosphonium ionic liquid barely enters the imidazolium-rich phase. Contrarily, the solubility of the imidazolium ionic liquid in the ammonium/phosphonium-rich phase is very significant. Thus, an interesting thermodynamic analysis of the systems can be made from the perspective of solution of the imidazolium ionic liquid in the ammonium/phosphonium ionic liquid.

From the solubility data at several temperatures, the apparent enthalpy change of the solution process (ΔH_{app}) can be obtained from the classical van't Hoff equation:

$$\left(\frac{\partial \ln x_{1,up}}{\partial(1/T)}\right)_p = -\frac{\Delta H_{app}}{R} \tag{3.15}$$

where $x_{1,up}$ stands for the mole fractions of the imidazolium ionic liquid in the ammonium/phosphonium-rich phase, measured at the absolute temperatures T; subscript p indicates constant pressure; and R is the universal gas constant. However, in order to reduce the propagation of errors and to better discriminate between true chemical effects and those effects due exclusively to statistical treatment in the analysis of the corresponding van't Hoff plots, an approach proposed by Krug et al. (1976) has led to the common utilisation of the following modified version of Equation 3.15:

$$\left(\frac{\partial \ln x_{1,up}}{\partial(1/T - 1/T_{hm})}\right)_p = -\frac{\Delta H_{app}}{R} \tag{3.16}$$

where T_{hm} is the harmonic mean of the experimental temperatures, calculated as:

$$T_{hm} = \frac{n}{\sum_{i=1}^{n} \frac{1}{T_i}} \tag{3.17}$$

with n corresponding to the total number of experimental temperatures investigated. If a linear dependence is found when plotting $\ln(x_{1,up})$ against the difference $(1/T - 1/T_{hm})$, ΔH_{app} can be assumed as constant over the explored temperature range, and its value can be easily inferred from the slope of the linear fit. A non-linear behaviour implies that ΔH_{app} changes with temperature in the studied interval, and in

this case a first approach to consider is to carry out a polynomial regression of order two (parabolic model) of the data (Mora et al., 2005):

$$\ln x_{1,up} = a + b \cdot \left(\frac{1}{T} - \frac{1}{T_{hm}} \right) + c \cdot \left(\frac{1}{T} - \frac{1}{T_{hm}} \right)^2 \tag{3.18}$$

where *a*, *b* and *c* are fit parameters. By derivation of this expression and comparison with Equation 3.16, the following equation is obtained for the calculation of ΔH_{app} at each specific temperature:

$$\Delta H_{app} = - R \cdot \left[b + 2 \cdot c \cdot \left(\frac{1}{T} - \frac{1}{T_{hm}} \right) \right] \tag{3.19}$$

Figure 3.11 shows the modified van't Hoff plots for the solution of the imidazolium ionic liquid in the ammonium/phosphonium ionic liquid for the liquid-liquid equilibrium systems investigated in this work; as well as for the system [C_2mim][NTf_2] + [$P_{6\,6\,6\,14}$][NTf_2], built from literature data (Arce et al., 2007), for comparative purposes. An analysis with the F-test (Devore, 2004) determined that the second-order term in Equation 3.18 was not statistically significant, at a significance level of 0.05, in the regression of the systems involving the phosphonium cation ([C_2mim]Cl + [$P_{6\,6\,6\,14}$]Cl and [C_2mim][OAc] + [$P_{6\,6\,6\,14}$][OAc]). Therefore, the data series of these two systems were fit to a straight line, and the numerical values of the slope and intercept are listed in Table 3.5., along with the root mean square deviation values (rmsd). The constant values of ΔH_{app} for these two systems were derived from the corresponding slope values (via their multiplication by *R*), and are reported in Table 3.6.

Table 3.5. Numerical values of the fit parameters of Equation 3.18 for the liquid-liquid equilibrium systems studied in this work (a zero value for parameter *c* is indicative of a linear fit). The corresponding root-mean square deviation (rmsd) values are also shown.

System	*a*	*b* / K	*c* / $10^6 \cdot K^2$	rmsd
[C_2mim]Cl + [Aliquat]Cl	-2.07	-111	-9.75	0.027
[C_4mim]Cl + [Aliquat]Cl	-0.698	-506	-5.24	0.026
[C_2mim]Cl + [$P_{6\,6\,6\,14}$]Cl	-2.43	583	0	0.021
[C_2mim][OAc] + [$N_{8\,8\,8\,1}$][OAc]	-0.794	80.1	-1.31	0.026
[C_2mim][OAc] + [$P_{6\,6\,6\,14}$][OAc]	-1.05	335	0	0.005
[C_2mim][NTf_2] + [$P_{6\,6\,6\,14}$][NTf_2]	-0.820	-1139	0.769	0.027

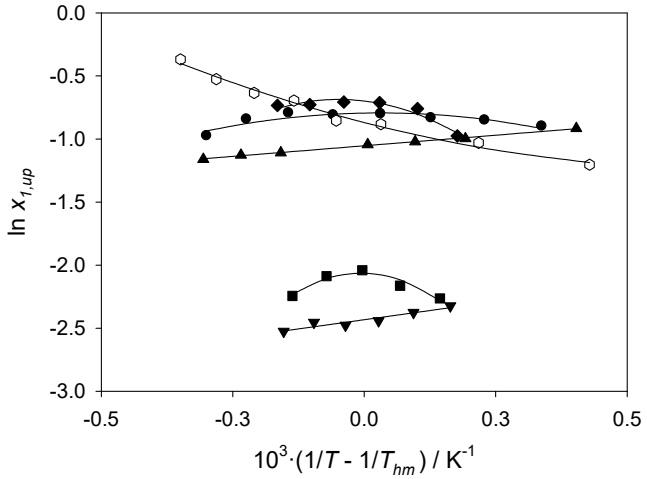

Figure 3.11. Modified van't Hoff plots (natural logarithm of the mole fraction of imidazolium ionic liquid in the phosphonium-rich phase, $x_{1,up}$, versus the difference of inverses of the absolute temperature T and the harmonic mean temperature T_{hm}) for liquid-liquid systems comprising two mutually immiscible ionic liquids: [C$_2$mim]Cl + [Aliquat]Cl (squares); [C$_4$mim]Cl + [Aliquat]Cl (diamonds); [C$_2$mim]Cl + [P$_{6\,6\,6\,14}$]Cl (inverted triangles); [C$_2$mim][OAc] + [Aliquat][OAc] (circles); [C$_2$mim][OAc] + [P$_{6\,6\,6\,14}$][OAc] (triangles); and [C$_2$mim][NTf$_2$] + [P$_{6\,6\,6\,14}$][NTf$_2$] (open hexagons). Solid lines correspond to linear fits or to quadratic fits obtained with Equation 3.18.

Table 3.6. Apparent enthalpy change (ΔH_{app}) and apparent entropy change (ΔS_{app}) for the solution of the imidazolium ionic liquid in the phosphonium ionic liquid in the systems [C$_2$mim]Cl + [P$_{6\,6\,6\,14}$]Cl and [C$_2$mim][OAc] + [P$_{6\,6\,6\,14}$][OAc].

System	ΔH_{app} / kJ·mol^{-1}	ΔS_{app} / J·mol^{-1}·K^{-1}
[C$_2$mim]Cl + [P$_{6\,6\,6\,14}$]Cl	-4.85 ± 0.10	-32.4 ± 0.4
[C$_2$mim][OAc] + [P$_{6\,6\,6\,14}$][OAc]	-2.79 ± 0.01	-17.0 ± 0.1

The apparent entropy change of solution (ΔS_{app}) could then be calculated by means of the rearranged Gibbs equation:

$$\Delta S_{app} = \frac{\Delta H_{app} - \Delta G_{app}}{T} \tag{3.20}$$

where ΔG_{app} is the apparent Gibbs energy change of solution, which was evaluated from the experimental data according to the following expression:

$$\Delta G_{app} = -R \cdot T \cdot \ln x_{1,up} \tag{3.21}$$

For systems with a linear behaviour, an option identified in the specialised literature is to evaluate ΔG_{app} at the specific temperature T_{hm}, getting a single

representative value of ΔG_{app} for the entire temperature range investigated; and then getting the constant value of ΔS_{app} via Equation 3.20 also using T_{hm} as the temperature in the denominator (Krug et al., 1976; Maia et al., 2010; Mora et al., 2005; Panteli and Voutsas, 2009). Nevertheless, herein it was preferred to calculate ΔG_{app} by applying Equation 3.21 to each specific experimental point, to preserve the visibility of the variation of ΔG_{app} with temperature. Subsequently, the constant ΔS_{app} for each system was calculated as the arithmetic mean of all the values obtained by application of Equation 3.20 to each experimental temperature. These averaged values of ΔS_{app}, accompanied by an uncertainty twice the standard deviation associated with the calculation of the above mentioned arithmetic means, are reported in Table 3.6 for the two systems displaying a linear behaviour in the modified van't Hoff plot. The detailed values of ΔG_{app} at all experimental temperatures for these systems are shown in Table 3.7.

Table 3.7. Apparent Gibbs energy change of solution (ΔG_{app}) and the entropic contribution to it (i.e. the product of the temperature T and the apparent entropy change of solution ΔS_{app}) for the solution of imidazolium ionic liquid in phosphonium ionic liquid for the liquid-liquid equilibrium systems showing a linear trend in the modified van't Hoff plot (see Figure 3.11).

T / K	ΔG_{app} / kJ·mol^{-1}	$T\cdot\Delta S_{app}$ / kJ·mol^{-1}
	[C_2mim]Cl + [$P_{6\,6\,6\,14}$]Cl	
373.2	7.21	-12.1
383.2	7.57	-12.4
393.2	7.98	-12.8
403.2	8.30	-13.1
413.2	8.43	-13.4
423.2	8.89	-13.7
	[C_2mim][OAc] + [$P_{6\,6\,6\,14}$][OAc]	
298.2	2.27	-5.07
318.2	2.64	-5.41
328.2	2.79	-5.58
338.2	2.94	-5.75
358.2	3.30	-6.09
368.2	3.45	-6.26
378.2	3.65	-6.43

As observed in Table 3.6, both ΔH_{app} and ΔS_{app} are negative for the process of solution of [C_2mim]Cl in [$P_{6\,6\,6\,14}$]Cl and for that of [C_2mim][OAc] in [$P_{6\,6\,6\,14}$][OAc]. The entropic contributions to ΔG_{app} were calculated multiplying ΔS_{app} by the absolute

temperature T, obtaining values in the range (-12.1 to -13.7) kJ·mol^{-1} for the system [C$_2$mim]Cl + [P$_{6\,6\,6\,14}$]Cl, and in the range (-5.07 to -6.43) kJ·mol^{-1} for the system [C$_2$mim][OAc] + [P$_{6\,6\,6\,14}$][OAc]. The detailed numerical values can also be found in Table 3.7. Compared to the enthalpic contributions to ΔG_{app} (which are directly given by the values of ΔH_{app}), it is observed that the entropic contributions are larger in absolute value (i.e. more negative) in both systems. This set of thermodynamic circumstances ($\Delta H_{app} < 0$, $\Delta S_{app} < 0$, and $|T{\cdot}\Delta S_{app}| > |\Delta H_{app}|$) in solutions of fully liquid components is characteristic of liquid-liquid equilibria driven by unfavourable entropic effects which display an LCST-type behaviour. The exothermic character of the solution processes for the two systems may be explained by the formation of a stronger network of bonds within the phosphonium-rich phase, for instance through hydrogen bonding between the [C$_2$mim]$^+$ cations and the anions, relatively stronger than the weak hydrogen bonding existing between the [P$_{6\,6\,6\,14}$]$^+$ cations and the anions in the pure phosphonium ionic liquid. The described enhancement in the bonding network in the phosphonium-rich phase would also lead to an increase in the degree of ordering of such phase, hence resulting in the negative ΔS_{app} observed.

The solution of [C$_2$mim][NTf$_2$] in [P$_{6\,6\,6\,14}$][NTf$_2$], involving exactly the same cations than the solution of [C$_2$mim]Cl in [P$_{6\,6\,6\,14}$]Cl or the solution of [C$_2$mim][OAc] in [P$_{6\,6\,6\,14}$][OAc], but with the [NTf$_2$]$^-$ anion starkly different than Cl$^-$ or [OAc]$^-$, exhibits a curved trend in the modified van't Hoff plot (Figure 3.11). Equation 3.18 was used for correlation of this data series, and ΔH_{app} and ΔS_{app} could then be calculated by means of Equations 3.19-3.21. Their numerical values, along with those of the entropic contribution to ΔG_{app} (that is, the product $T{\cdot}\Delta S_{app}$), are presented in Table 3.8. Both ΔH_{app} and ΔS_{app} are positive over the investigated temperature range, and in Figure 3.12a it can be observed that they increase with increasing temperature. In addition, Figure 3.12a also shows that ΔH_{app} is greater than $T{\cdot}\Delta S_{app}$, indicating that the solution of [C$_2$mim][NTf$_2$] in [P$_{6\,6\,6\,14}$][NTf$_2$] is enthalpically driven. This is in evident contrast to what was found and previously discussed for the equivalent systems with Cl$^-$ or [OAc]$^-$ as anion, in connection with the large difference between these two anions and [NTf$_2$]$^-$. The latter is much bulkier and with a much more delocalised charge, thus exhibiting a greater similarity from that perspective with the cations in the discussed systems. This may facilitate the exchange of cations between both phases (with the phosphonium cations even accessing the imidazolium-rich phase in relevant

concentrations, as opposed to what was observed for the systems with Cl^- and $[OAc]^-$; see Figure 3.8). As a result, the degree of disorder in each liquid phase of the system is increased (implying $\Delta S_{app} > 0$); but at the same time the interactions existing in the equilibrium phases, and in particular in the phosphonium-rich phase, will be weaker than those in the pure ionic liquids before mixing, thus causing the solution process to be endothermic ($\Delta H_{app} > 0$). By simultaneous consideration of Table 3.6 and Figure 3.12a, the evolution of ΔH_{app} and ΔS_{app} for the studied systems sharing the $[C_2mim]^+$ and $[P_{6\,6\,6\,14}]^+$ cations follows an increasing order (from more negative to more positive) with the following anion sequence: $Cl^- < [OAc]^- << [NTf_2]^-$. The relative order of Cl^- and $[OAc]^-$ in this sequence suggests that a larger increase in the overall strength of the attractive forces network occurs in the solution process when the anion is Cl^- in comparison to when it is $[OAc]^-$.

A curved trend was also observed in Figure 3.11 for the solution of imidazolium ionic liquids in ammonium ionic liquids, namely for the three systems ([C_2mim]Cl + [Aliquat]Cl, [C_4mim]Cl + [Aliquat]Cl, and [C_2mim][OAc] + [Aliquat][OAc]). All the corresponding data series, adequately correlated by Equation 3.18, show a maximum at an intermediate temperature in the studied ranges, as expected from the hourglass shape described by their liquid-liquid equilibria in the temperature-composition diagrams (Figures 3.9 and 3.10). The ΔH_{app} and ΔS_{app} values calculated with Equations 3.19-3.21 were used to build plots of their evolution with temperature in Figure 3.12. The numerical values of ΔH_{app}, ΔS_{app}, ΔG_{app}, and the product $T{\cdot}\Delta S_{app}$ are listed in Table 3.8. Interestingly, in all three systems a transition from positive values of ΔH_{app} and ΔS_{app} to negative ones is observed within the corresponding experimental temperature ranges. In other words, with an increase in temperature the process of solution of the imidazolium ionic liquid in the ammonium ionic liquid changes from endothermic to exothermic, and from increasing to decreasing the degree of disorder. At any given temperature and for any of the mentioned systems, ΔH_{app} is greater (either more positive or less negative) than the product $T{\cdot}\Delta S_{app}$. Combined with the commented switch in the sign of ΔH_{app} and ΔS_{app}, the result is that, in absolute value, the unfavourable (endothermic) apparent enthalpy of solution is higher than the entropic contribution at the low temperatures, whereas the unfavourable (order-increasing) apparent entropy of solution leads to an entropic contribution higher than the enthalpic one at the high temperatures. Consequently, it can be stated that the analysed solution process in these systems is enthalpically driven at the low temperatures of the studied

temperature ranges, whereas it is entropically driven at the high temperatures of such ranges.

Table 3.8. Apparent enthalpy change of solution (ΔH_{app}), apparent entropy change of solution (ΔS_{app}), apparent Gibbs energy change of solution (ΔG_{app}), and the entropic contribution to it (i.e. the product of the temperature T and ΔS_{app}) for the solution of imidazolium ionic liquid in ammonium/phosphonium ionic liquid for the liquid-liquid equilibrium systems showing a non-linear trend in the modified van't Hoff plot (see Figure 3.11).

T / K	ΔH_{app} / kJ·mol^{-1}	ΔS_{app} / J·mol^{-1}·K^{-1}	ΔG_{app} / kJ·mol^{-1}	$T\cdot\Delta S_{app}$ / kJ·mol^{-1}
		[C_2mim]Cl + [Aliquat]Cl		
358.2	24.3	48.9	6.74	17.5
368.2	12.0	14.5	6.62	5.34
378.2	0.33	-16.1	6.42	-6.09
388.2	-10.7	-45.0	6.74	-17.5
398.2	-21.2	-71.9	7.43	-28.6
		[C_4mim]Cl + [Aliquat]Cl		
358.2	19.6	46.7	2.91	16.7
368.2	13.0	29.0	2.32	10.7
378.2	6.76	12.0	2.24	4.52
388.2	0.82	-3.76	2.28	-1.46
398.2	-4.82	-18.1	2.41	-7.23
408.2	-10.2	-31.0	2.49	-12.7
		[C_2mim][OAc] + [Aliquat][OAc]		
298.2	6.68	14.9	2.23	4.45
308.2	4.32	6.93	2.18	2.14
318.2	2.10	-0.32	2.20	-0.10
328.2	0.02	-6.61	2.19	-2.17
338.2	-1.94	-12.5	2.28	-4.22
348.2	-3.79	-17.5	2.30	-6.09
358.2	-5.53	-22.5	2.51	-8.05
368.2	-7.18	-27.6	3.00	-10.2
		[C_2mim][NTf_2] + [$P_{6\,6\,6\,14}$][NTf_2]		
298.2	3.43	1.49	2.99	0.45
318.2	6.13	10.7	2.73	3.40
338.2	8.50	17.8	2.48	6.02
348.2	9.59	20.4	2.47	7.12
358.2	10.6	23.9	2.07	8.54
368.2	11.6	26.2	1.94	9.64
378.2	12.5	28.7	1.65	10.9
388.2	13.4	31.4	1.19	12.2

A parallelism can be established between the variation of the thermodynamically predominant contributions to ΔG_{app} and the evolution with temperature of the mole fraction of the imidazolium ionic liquid in the ammonium ionic liquid (or equivalently the miscibility of the two ionic liquids) in these systems (Figures 3.8 and 3.9): the enthalpically driven part corresponds to the UCST-like lower part of the hourglass

shape of the liquid-liquid domain, while the entropically driven part is associated with its LCST-like upper part. A further feature revealed by comparison of plots b, c and d in Figure 3.12 is the stronger influence of temperature on the apparent enthalpy and entropy of solution of [C_2mim]Cl in [Aliquat]Cl, as compared to that of [C_4mim]Cl in [Aliquat]Cl or, more notably, to that of [C_2mim][OAc] in [Aliquat][OAc].

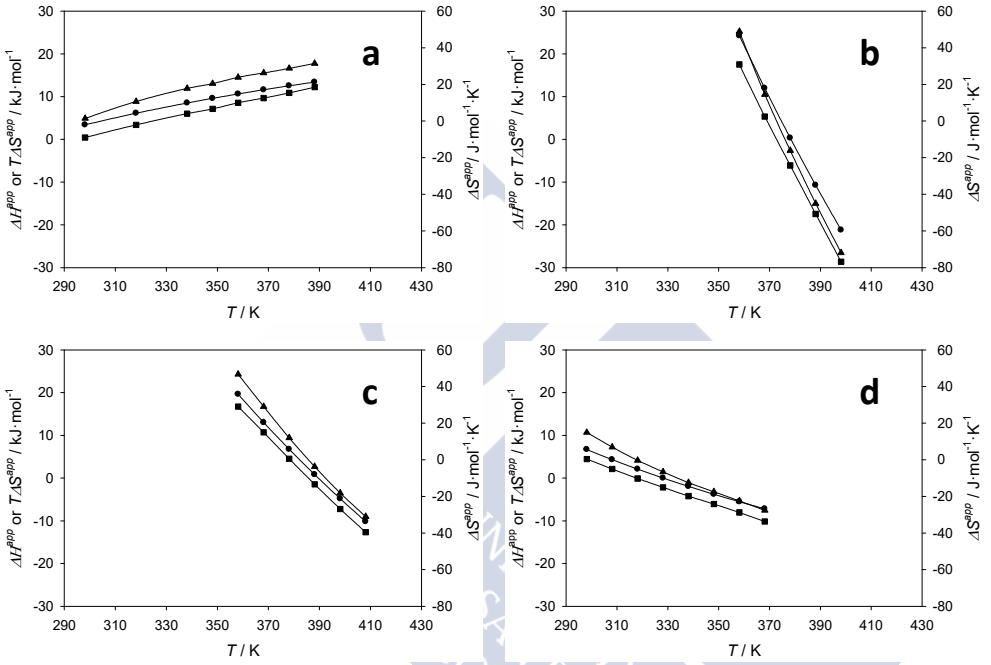

Figure 3.12. Apparent enthalpy change ΔH_{app} (circles), apparent entropy change ΔS_{app} (triangles), and the product $T{\cdot}\Delta S_{app}$ (squares), as a function of temperature T, for the solution of the imidazolium ionic liquid in the phosphonium ionic liquid in the following systems: a) [C_2mim][NTf_2] + [$P_{6\,6\,6\,14}$][NTf_2], b) [C_2mim]Cl + [Aliquat]Cl, c) [C_4mim]Cl + [Aliquat]Cl, and d) [C_2mim][OAc] + [Aliquat][OAc]. Solid lines are shown as guides to the eye.

4. IONIC LIQUID + ALCOHOL SYSTEMS. SOLUBILITY OF BIOPOLYMERS

USC
UNIVERSIDADE
DE SANTIAGO
DE COMPOSTELA

4. IONIC LIQUID + ALCOHOL SYSTEMS. SOLUBILITY OF BIOPOLYMERS

4.1. Motivation

Although ionic liquids often exhibit an appealing set of properties for their use as solvents in potentially sustainable processes (Freemantle, 2010), one of their most recurrent drawbacks is their relatively high viscosity, as compared to conventional molecular solvents. This has been found to impose important limitations in processes such as the dissolution of biopolymers in ionic liquids. For example, in the particular case of dissolution of cellulose in known cellulose-dissolving ionic liquids, higher levels of solubilisation have been experimentally achieved with increasing temperature, in spite of the fact that the process itself has been proven to be thermodynamically exothermic (and therefore it should be favoured at lower temperatures) (Andanson et al., 2015). The explanation for this contradiction has to reside in the kinetic limitation derived from the high viscosity of the ionic liquid medium. The use of molecular solvents as cosolvents of the ionic liquid in this kind of processes, assuming that they do not reduce significantly the dissolution capacity of the ionic liquid, might be of interest since the kinetics of the dissolution process would be facilitated as a result of the diminution of the viscosity (Stark and Seddon, 2007). This lowering in viscosity of the fluid medium would also be a concomitant benefit for the process from an engineering perspective. Moreover, the use of a cosolvent together with the ionic liquid would allow modulation of the solubility capacity by controlling the composition of the resulting solvent fluid, with the advantages that a fractionated solubility of the different biopolymers might have for some specific purposes. Of course, the cosolvent should be miscible with the biomass-dissolving ionic liquid and should also possess reasonably green credentials to fit within the general context of sustainability of the new process.

On the other hand, since ionic liquids and lignocellulose biopolymers are non-volatile, and if the lignocellulosic fractions or any derived solutes still in polymeric form are to be regenerated from the ionic liquid solution prior to any further utilisation, a logical approach for this regeneration is the use of a classical solvent as an antisolvent

to force precipitation. This antisolvent has to be miscible with the biomass-dissolving ionic liquid, while possessing a negligible ability to act as solvent of the solutes to be precipitated. Thus, upon addition of the antisolvent the solute will be precipitated out of the solution and will be recoverable from the medium by simple solid-liquid separation operations (e.g. by filtration); and the antisolvent will be removed from its mixture with the ionic liquid via vaporisation (e.g. by distillation). Due to the latter aspect, a characteristic of interest for the proposed antisolvent would be an intermediate volatility, for balancing two aspects: the energy required for its removal by vaporisation from the mixture with non-volatile ionic liquid for recycling of both substances to the process, and the safety and environmental risks associated with a too volatile compound. Additionally, the proposed antisolvent should again exhibit acceptably good green credentials that would not compromise the general sustainable character of the new process.

In the regeneration of lignocelluloses from ionic liquid solution by addition of antisolvent, no emphasis has been put in the literature on the quantification of the antisolvent added to cause the precipitation of the solutes. This is a critical aspect in the conception and design of a process to be scaled up for real application at an industrial level. Also, water has been typically the antisolvent of choice in most of the literature available to date. Obviously, the green credentials of water *per se* are unbeatable; however, its high specific heat and relatively high boiling temperature pose an excessive energy penalty at the stage of recovering the ionic liquid from its mixture with the antisolvent by vaporisation of the latter. An appealing alternative to water in the above described role may be the use of light alcohols (methanol, ethanol, 1-propanol and 2-propanol), which present lower specific heats and boiling temperatures than water, thus enabling the possibility of a less energy intensive separation of the ionic liquid + antisolvent mixture. In addition, they can be considered to have reasonably good green credentials intrinsic to their nature (Henderson et al., 2011), and therefore they have the potential to lead to an improved environmental friendliness of the overall process, in spite of inconvenient characteristics such as their flammability.

For the pretreatment of lignocellulosic biomass via dissolution, 1-ethyl-3-methylimidazolium acetate ([C_2mim][OAc]) has become an archetypical ionic liquid (Brandt et al., 2013), as it has shown a great capacity for the dissolution of different sources of lignocellulosic biomass and its main biopolymers (Sun et al., 2009, 2011). This ionic liquid has a series of favourable properties for industrial applications (Freire

et al., 2011): a relatively low viscosity (within the context of ionic liquids), low toxicity (with a value of LD_{50}, the dose that would cause the death of 50 % of a group of test animals, greater than 2000 $mg \cdot kg^{-1}$), low corrosiveness, a liquid character far below room temperature, and an acceptably good thermal stability.

Thus, this chapter concentrates on the study of the fluid systems constituted by [C_2mim][OAc] and each of the four lightest alcohols, through their thermal characterisation and the rigorous determination of key thermophysical properties as a function of temperature and composition. These provide both a deeper knowledge for better understanding of the behaviour of the mixtures at a fundamental science level and critical information for an efficient design of an industrial process pretending to utilise these mixtures. The study of all four [C_2mim][OAc] + alcohol systems allows for analysis of the effect of the length of the alkyl chain of the alcohol on the properties, as well as the position of the hydroxyl group in the case of the two propanols. The investigation of the solubility of representative standards of the major biopolymers of lignocellulosic biomass in mixtures of [C_2mim][OAc] and alcohol is considered, in order to preliminary evaluate the potential of the alcohols as cosolvents of [C_2mim][OAc] in processes involving a fractionated solubilisation of lignocellulose biopolymers. Complementary, to analyse the viability of using the alcohols as antisolvents of lignocellulose fractions previously dissolved in the ionic liquid, precipitation tests are also carried out. In fact, the possibility of having versatile substances capable of acting either as cosolvents at certain concentrations or as antisolvents at other concentrations would be highly attractive, as it would permit the fluid system to be operated in a continuous basis without having to totally vaporise the volatile compound from the ionic liquid for the recycling of the latter to the process.

4.2. Theoretical considerations on thermophysical properties

4.2.1. Density, viscosity, refractive index, and surface tension

Density and viscosity are two fundamental properties in the characterisation of any fluid in the context of a chemical process. Surface tension is also a relevant property in the design of process units in which mass transfer between fluid phases plays a relevant

role. Complementarily, refractive index is a practical property which, being a fundamental physical property of substances, can be easily used to ascertain the composition of a mixture (particularly a binary mixture). Knowledge of these properties over the appropriate temperature and composition ranges for fluid mixtures based on ionic liquids is critically valuable for the design of real processes where they will be involved.

The density (ρ) of a substance is defined as its mass per unit volume, and is probably the most useful physical property. It does not only participate directly in many design calculations and simulations, but also in the calculation of many other properties (Riddick et al., 1986). One such property is the molar volume (V), which is defined for a pure compound as:

$$V = \frac{M}{\rho} \tag{4.1}$$

where M represents the molar mass of the compound. In the case of a mixture of different compounds, the use of a weighted average of their individual molar masses M_i (with the mole fractions x_i as weighting coefficients) in the numerator of Equation 4.1 yields the molar volume of the mixture:

$$V = \frac{\sum x_i \cdot M_i}{\rho} \tag{4.2}$$

The dynamic viscosity (η) of a fluid (often referred to as simply –and not unambiguously!– "viscosity") relates to the friction resistance between its molecules, that limits its ability to flow. This resistance opposes the movement of particles on other adjacent particles, and it is considered as an internal friction of the molecules. It is caused by the attractive forces between the liquid molecules. Specifically, dynamic viscosity corresponds to the force per unit area necessary to maintain a unit velocity gradient between two parallel planes a unit distance apart (Riddick et al., 1986). It is defined via Newton's law of viscosity:

$$\tau_{yx} = -\eta \cdot \frac{\partial v_x}{\partial y} \tag{4.3}$$

where τ_{yx} is the force in the x direction on a unit area perpendicular to the y direction, v_x is the component in the x direction of the velocity vector of the fluid, and η acts as the proportionality constant. If Equation 4.3, with a constant value for η, describes well the

resistance to flow of the fluid, independently of the magnitude of the shearing stress or of the velocity gradient, then such fluid is said to be Newtonian.

The kinematic viscosity (ν) is defined as the ratio of the dynamic viscosity and the density of the fluid:

$$\nu = \frac{\eta}{\rho} \tag{4.4}$$

and it happens to be directly proportional to the time required for a liquid to flow down through a capillary tube under its own hydrostatic head (Riddick et al., 1986). Thus, it is the type of viscosity obtained directly in viscometers based on liquid efflux times through capillary tubes. If the density of the liquid is known, the dynamic viscosity can be easily calculated from the kinematic viscosity by means of Equation 4.4.

The refractive index (n) of a substance is defined as the ratio between the velocity of light in vacuum and the velocity of light in the substance (Riddick et al., 1986). This dimensionless physical property is a function of the temperature of the medium and of the wavelength of the incident light. The effect of temperature on the refractive index of a liquid is mainly due to its influence on the degree of packing of the molecules of the liquid. Regarding the incident light, in the most common case the D1 and D2 lines of a sodium lamp are used, with a weighted mean wavelength of 589.26 nm (Riddick et al., 1986). In such chase, the determined refractive index is denoted as n_D, and the dependency on the incident light does no longer apply.

Density and refractive index are both present in the Lorentz-Lorenz expression for the calculation of the molar refraction (R_M):

$$R_M = \frac{n_D^2 - 1}{n_D^2 + 2} \cdot \frac{M}{\rho} \tag{4.5}$$

where all the variables have already been defined.

The surface tension (σ) of a liquid can be defined as the force exerted in the plane of the surface per unit length (Poling et al., 2001). It is a measure of the cohesive forces between liquid molecules present at the surface (Tariq et al., 2012).

4.2.2. Excess properties and property changes of mixing

Excess properties and property changes of mixing derived from thermophysical properties can provide valuable information on the behaviour of real mixtures.

The excess property of an extensive thermodynamic property (e.g. molar volume, internal energy, enthalpy, entropy, etc.) is defined as the difference between the real value of the property and the value of the property calculated for the same conditions of temperature, pressure, and composition by the ideal solution equations (Prausnitz et al., 1999). For a given property M, the mathematical expression is:

$$M^E = M - M^{id} \tag{4.6}$$

where M^E is the excess property, M is the value of the real property, and M^{id} is the property of the ideal mixture. For the particular case of molar volume (V), the value of V^{id} is calculated as the mole-fraction weighted sum of the molar volumes of the pure compounds (V_i):

$$V^{id} = \sum_i x_i \cdot V_i \tag{4.7}$$

The property change of mixing (ΔM), for a given property M, in a multicomponent mixture is defined as:

$$\Delta M = M - \sum_i x_i \cdot M_i \tag{4.8}$$

where M is the property of the solution, and x_i and M_i are respectively the mole fraction and the property of the pure i-th component. Thus, for molar volume, viscosity, molar refraction, and surface tension the corresponding property changes of mixing, or deviation properties, can be written as:

$$\Delta V = V - \sum_i x_i \cdot V_i \tag{4.9}$$

$$\Delta \eta = \eta - \sum_i x_i \cdot \eta_i \tag{4.10}$$

$$\Delta R_M = R_M - \sum_i x_i \cdot R_{M,i} \tag{4.11}$$

$$\Delta \sigma = \sigma - \sum_i x_i \cdot \sigma_i \tag{4.12}$$

For a property that may expand over several orders of magnitude for a given system, the direct calculation of the corresponding property change of mixing may provide little information of value. Such is the case of viscosity in systems involving an ionic liquid and a molecular solvent of low molar mass. For this property, instead, an analysis of the viscosity logarithm change of mixing ($\Delta \ln(\eta/\eta^0)$, with η^0 being a reference viscosity equal to 1 in the units in which η is expressed):

$$\Delta \ln\left(\eta/\eta^0\right) = \ln\left(\eta/\eta^0\right) - \sum_i x_i \cdot \ln\left(\eta_i/\eta^0\right) \quad (4.13)$$

is preferred, especially if considering also that the viscosity of many fluid systems is quite often well described by a simple and classical mixing rule, that can be credited to Arrhenius and Kendall, which for a binary system would take the following form (Kendall and Monroe, 1917):

$$\ln \eta = x_1 \cdot \ln \eta_1 + x_2 \cdot \ln \eta_2 \quad (4.14)$$

By comparing Equation 4.9 with the combination of Equations 4.6 (applied to molar volume) and 4.7, it can be deduced that the expressions of V^E and ΔV are identical, and therefore their numerical values are always coincident. Developing the summations in the expressions of the excess molar volume for the case of a binary system, we get:

$$V^E = V - \left(x_1 \cdot V_1 + x_2 \cdot V_2\right) \quad (4.15)$$

where subscripts 1 and 2 refer to each of the components in the mixture. Similarly, from Equations 4.11-4.13, the following developed expressions for the viscosity logarithm change of mixing, the molar refraction change of mixing, and the surface tension change of mixing of binary systems can be obtained:

$$\Delta \ln\left(\eta/\eta^0\right) = \ln\left(\eta/\eta^0\right) - \left[x_1 \cdot \ln\left(\eta_1/\eta^0\right) + x_2 \cdot \ln\left(\eta_2/\eta^0\right)\right] \quad (4.16)$$

$$\Delta R_M = R_M - \left(x_1 \cdot R_{M1} + x_2 \cdot R_{M2}\right) \quad (4.17)$$

$$\Delta\sigma = \sigma - \left(x_1 \cdot \sigma_1 + x_2 \cdot \sigma_2\right) \quad (4.18)$$

4.2.3. Data correlation: influence of the temperature

Properties of liquids such as density, viscosity, refractive index, or surface tension do generally tend to decrease with an increase with temperature. However, the pattern followed in each case for the evolution with temperature may be substantially different.

For many liquids, the variation of density, refractive index and surface tension with temperature can be acceptably assumed to be linear over a relatively broad range of temperatures.

$$\rho = a_0 + a_1 \cdot T \quad (4.19)$$

$$n_D = b_0 + b_1 \cdot T \quad (4.20)$$

$$\sigma = c_0 + c_1 \cdot T \quad (4.21)$$

where T is the absolute temperature, and a_0, a_1, b_0, b_1, c_0, and c_1 are the fit parameters. In some other situations, however, the correlation by means of a polynomial expression of higher order may be more suitable. For the density of pure ionic liquids, for example, either a linear fit (Gu and Brennecke, 2002; Jacquemin et al., 2008; Deng et al., 2011) or a second order polynomial fit (Gomes de Azevedo et al., 2005; Jacquemin et al., 2007; Hasse et al., 2009) are usually adopted in the literature for the correlation with temperature:

$$\rho = a_0 + a_1 \cdot T + a_2 \cdot T^2 \tag{4.22}$$

where a_2 is the fit parameter corresponding to the second-order term. The statistical Fisher's F-test (Devore, 2004) can be a suitable tool to evaluate whether the addition of the quadratic term will be statistically significant or not in the polynomial correlation of these properties as a function of temperature.

The evolution of the viscosity of liquids with temperature is markedly different. For many liquids, the temperature dependency of the dynamic viscosity over wide temperature ranges can be suitably correlated by means of the Arrhenius-type equation proposed by Andrade (1930), for example in the case of simple solvents such as light alcohols. Its expression is:

$$\eta = \eta_\infty \cdot \exp\left(-\frac{E_a}{R \cdot T}\right) \tag{4.23}$$

where R is the universal gas constant, T is the absolute temperature, and η_∞ ("viscosity at infinitive temperature") and E_a ("activation energy") are the fit parameters. However, the 2-parameter Andrade equation is often unable to provide a good description of the evolution with temperature of the viscosity of other liquids, such as glass-forming liquids, and typically ionic liquids. For the latter, the use of the Vogel-Fulcher-Tammann (VFT) equation (Vogel, 1921; Fulcher, 1925; Tammann, 1926), with three fit parameters, is preferred. In its modified version by Cohen and Turnbull (1959), the VFT equation is expressed as:

$$\eta = A \cdot T^{0.5} \cdot \exp\left(\frac{k}{T - T_0}\right) \tag{4.24}$$

where A, k, and T_0 are the fit parameters. In this expression, thanks to different theoretical rationales (Cohen and Turnbull, 1959; Adam and Gibbs, 1965), a physical meaning can be attributed to T_0: it can be considered as an ideal glass transition temperature, i.e. a temperature below which the fluid exists as an equilibrium glass

where the mass-transporting motions are frozen out (Angell and Moynihan, 1969). Although it cannot be achieved in finite time scale experiments due to kinetic reasons, it should be slightly lower than the experimentally obtained glass transition temperature T_g (Gibbs and DiMarzio, 1958).

Since the dynamic viscosity values for a fluid can span several orders of magnitude in the experimental temperature range explored, a fairer comparison of the evaluation of the quality of the fits provided by Equations 4.23 and 4.24 is better carried out on the basis of the relative standard deviation (SD_{rel}) instead of the regular standard deviation, according to the following expression:

$$SD_{rel} = \left[\frac{1}{n_{dat} - n_p} \sum_{i=1}^{n_{dat}} \left[\frac{\left(\eta_{i,\exp} - \eta_{i,calc}\right)}{\eta_{i,calc}} \right]^2 \right]^{0.5} \tag{4.25}$$

where subscripts "exp" and "calc" refer to the experimental and calculated values respectively, n_{dat} is the total number of experimental data points in the correlated series, and n_p is the number of fit parameters in the correlating equation.

4.2.4. Data correlation: influence of the composition

The description of a physical property of a liquid mixture as a function of composition can be conducted through the adequate correlation of the corresponding excess property or property change of mixing. One of the most common equations used for this purpose is the empirical Redlich-Kister polynomial (Redlich and Kister, 1948), which adopts the following mathematical form for binary mixtures:

$$Q = x_1 \cdot x_2 \cdot \sum_{k=0}^{m} A_k \cdot \left(x_1 - x_2\right)^k \tag{4.26}$$

where Q is the excess property or property change of mixing, x_1 and x_2 are the mole fractions of the components of the mixture, and A_k are the m + 1 polynomial coefficients to be fit (with m representing the degree of the resulting polynomial). The quality of the fit obtained in each case can be evaluated by means of the root mean square deviation (*rmsd*), which is defined as:

$$\text{rmsd} = \left[\frac{1}{n} \cdot \sum_{i=1}^{n} \left(z_{i,\exp} - z_{i,calc}\right)^2 \right]^{0.5} \tag{4.27}$$

where *n* indicates the total number of data points in each series, and subscripts "exp" and "calc" refer respectively to the experimental and calculated values of the property *z* being correlated.

4.3. Experimental

4.3.1. Materials

The ionic liquid 1-ethyl-3-methylimidazolium acetate ([C_2mim][OAc]) (see chemical structure in Figure 4.1) was purchased from Iolitec with a nominal purity greater than 95 %. In order to reduce the presence of volatile impurities, it was subjected to high vacuum (absolute pressure lower than 1 Pa) and moderate temperature (ca. 343 K), while magnetically stirred. Water is an impurity of particular concern in ionic liquids, as a result of their hygroscopic nature and the strong influence that water can have (even if present only in small concentrations) on their properties (Stark and Seddon, 2007). A water content of 0.0012 in mass fraction was found for the purified product, as determined by Karl-Fischer titration using a Metrohm 737 KF coulometer (Figure 3.2), and accepted as sufficiently low to carry out the subsequent experiments. The absence of relevant levels of other impurities and the preservation of the chemical identity in the purified product were verified by ^{1}H and ^{13}C nuclear magnetic resonance (NMR) spectroscopy analyses, run in a Varian Mercury 300 NMR spectrometer (Figure 3.2). The corresponding NMR spectra are presented in Appendix A. The ionic liquid batch was stored in a desiccator under soft vacuum until its use, in order to prevent undesired moisture uptake from the atmospheric air.

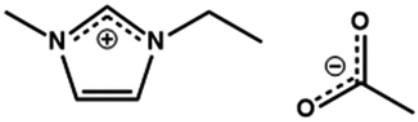

Figure 4.1. Chemical structure of the ionic liquid 1-ethyl-3-methylimidazolium acetate ([C_2mim][OAc]).

Methanol (Aldrich, 99.9 %), ethanol (Panreac, 99.8 %), 1-propanol (Riedel-de Haën, 99.9 %) and 2-propanol (Sigma Aldrich, 99.5 %) were used as received from the suppliers. Gas chromatography analyses did not detect any appreciable level of

impurities. A Metrohm 737 KF coulometer (Figure 3.2) was used to determine the water content of ethanol, 1-propanol, and 2-propanol by the Karl-Fischer titration method, and the values obtained were respectively 0.0006, 0.0005, and 0.0004 in mass fraction. For methanol it was not possible to determine its water content by the mentioned method, as methanol is a major component of the Hydranal™ (Aldrich) solution used in the procedure. It can be noted that the nominal water content of methanol as purchased was lower than 0.001 in mass fraction, and molecules sieves were used to keep it in dry condition.

Values at 298.15 K and atmospheric pressure of selected physical properties of the alcohols and the ionic liquid used in the experiments were experimentally measured (as described below in Section 4.3.2), and are reported and compared to reliable literature values by other authors (Riddick et al., 1986; Lide, 2009; Zarei, 2010; Freire et al., 2011; Quijada-Maldonado et al., 2012; Almeida et al., 2012a; Almeida et al., 2012b) in Table 4.1. A good agreement between the experimental and literature data sets can be observed.

Table 4.1. Experimental and literature values for density (ρ), viscosity (η), refractive index (n_D), and surface tension (σ) of methanol, ethanol, 1-propanol, 2-propanol, and [C_2mim][OAc] at 298.15 K and atmospheric pressure.

Compound	ρ / g·cm^{-3}		η / mPa·s		n_D		σ / mN·m^{-1}	
	Exp.	Lit.‡	Exp.	Lit.‡	Exp.	Lit.‡	Exp.	Lit.‡
Methanol	0.78674	0.78637[a]	0.533	0.5513[a]	1.32701	1.32652[a]	22.7	22.30[a]
		0.78665[b]		0.544[c]				22.07[c]
Ethanol	0.78510	0.78494[a]	1.081	1.082[a]	1.35957	1.35941[a]	22.0	21.97[c]
		0.78515[d]		1.074[c]		1.35950[d]		
1-Propanol	0.79956	0.79960[a]	1.952	1.9430[a]	1.38303	1.38370[a]	23.4	23.10[a,i]
		0.7997[c]		1.945[c]		1.3850[c]		23.32[c]
2-Propanol	0.78084	0.78126[a]	2.018	2.0436[a]	1.37517	1.3752[a]	21.2	21.24[a,i]
		0.7809[c]		2.038[c]		1.3776[c]		20.93[c]
[C_2mim][OAc]	1.09903	1.0993[e]	139.0	143.61[e]	1.50069	1.50091[e]	47.1	42.9[f]
		1.09778[f]		132.91[f]		1.49992[g]		47.1[h]

‡ References: [a] Riddick et al. (1986); [b] Canosa et al. (2000); [c] Lide (2009); [d] Zarei (2010); [e] Freire et al. (2011); [f] Quijada-Maldonado et al. (2012); [g] Almeida et al. (2012a); [h] Almeida et al. (2012b); [i] Value interpolated linearly for 298.15 K from data at other temperatures.

Microcrystalline cellulose, xylan, and Indulin AT were used as representative standards of the major lignocellulosic biopolymers cellulose, hemicellulose, and lignin, respectively. Microcrystalline cellulose (MCC) powder was purchased from Aldrich. Xylan, from beechwood, was supplied by Sigma. Indulin AT, a Kraft pine lignin, was

kindly donated by MeadWestvaco. All three polymers were used without further purification.

4.3.2. Preparation of samples

The ionic liquid [C_2mim][OAc] is fully miscible with light alcohols in all proportions. For the study of these systems, mixtures of [C_2mim][OAc] + alcohol (either methanol, ethanol, 1-propanol, or 2-propanol), with precise composition and covering the entire composition range, were prepared by weight using a Mettler Toledo AE240 analytical balance (Figure 3.7) with a precision of $\pm 1 \times 10^{-4}$ g. The uncertainty in the mole fractions of the prepared mixtures was estimated to be 0.0002. All samples were prepared in septum-sealed open-capped glass vials, immediately prior to the performance of the corresponding measurements in order to avoid relevant variations in composition due to the volatility of the alcohols. Special care was additionally taken in the handling of the prepared samples to minimise their exposure to the atmosphere.

4.3.3. Determination of thermal properties

Thermogravimetric analysis (TGA) and differential scanning calorimetry (DSC) were used to characterise the pure [C_2mim][OAc] and its mixtures with methanol, ethanol, 1-propanol, or 2-propanol, over the entire composition range of each binary system.

The thermal stability of the binary systems [C_2mim][OAc] + alcohol was investigated by TGA using dynamic heating ramps in a TA Instruments Q500 thermogravimetric analyser with a weight precision of ±0.01 % (Figure 3.4), and calibrated as described in Section 3.3.2. The liquid samples (ca. 15-40 mg) were placed in an open platinum pan, which was immediately hung to the balance hook, followed by closing of the furnace chamber and automatic taring just prior to the beginning of the temperature program. A simple heating ramp of 5 K·min^{-1} from room temperature to 673 K was applied, with N_2 (Praxair, 99.999 %) being used both as balance purge gas (with a flow of 40 mL·min^{-1}) and as sample purge gas (with a flow of 60 mL·min^{-1}). An uncertainty of 1 K was estimated for the recorded decomposition temperatures. The version 4.5.0.5 of the Universal Analysis 2000 software, by TA Instruments, was used to process the obtained TGA curves and evaluate the decomposition temperatures.

DSC experiments for the binary systems [C2mim][OAc] + alcohol were run in a TA Instruments Q2000 differential scanning calorimeter (Figure 3.5) equipped with an RCS 90 refrigerated cooling system, and calibrated as described in Section 3.3.2. The liquid samples (ca. 15-20 mg) were encapsulated in aluminium hermetic pans with lids of the same material, and loaded into the measuring chamber with an autosampler. An empty pan with its lid (analogous to those used to encapsulate the samples) was used as reference. N_2 (Praxair, 99.999 %) was used as sample purge gas, at a flow rate of 50 mL·min^{-1}. The thermal program consisted of three cycles, each of them comprising: a cooling ramp at 5 K·min^{-1} down to 183 K, a 5 min isotherm at this temperature, a heating ramp at 5 K·min^{-1} up to 313 K, and a 5 min isotherm at this temperature. It was ensured that the curves for the second and third cycle were essentially coincident, and the results from the third cycle were used in the calculations. An uncertainty of 1 K was estimated for the recorded temperatures. The same software than for the TGA curves (see paragraph above) was used in evaluating the DSC curves obtained. Although the lower temperature used in the cycled runs was 183 K, the portions of the curves below 200 K were systematically disregarded, since loss of stability of the baseline was observed in that region (likely due to limitation of the refrigeration system of the apparatus).

4.3.4. Determination of physical properties

The measurement of density was carried out in an Anton Paar vibrating U-tube DMA 5000 density meter (Figure 4.2) with an uncertainty of 3×10^{-5} g·cm^{-3}, at atmospheric pressure and at constant temperature controlled by means of a built-in system based on the Peltier effect with a precision of $\pm 1 \times 10^{-3}$ K. A correction of the influence of viscosity on the determination of density is automatically performed by the apparatus. For calibration of the apparatus, air and degassed bidistilled water were used. At least two measurements were performed for each sample at each temperature, ensuring that they were repetitive within the estimated uncertainty; and the average values were recorded.

Since [C2mim][OAc] is a Newtonian liquid in the studied temperature ranges (Gericke et al., 2009), and so the alcohols are too, viscosities of the mixtures were determined by means of micro-Ubbelohde glass capillary viscometers (Figure 4.3) manufactured, calibrated, and certified by Schott. An automatic Lauda PVS1 Processor

Viscosity System equipped with a photoelectric cell was used to determine accurately (with a resolution of 0.01 s) the efflux time of the sample through the viscometer (Figure 4.3). The temperature during each measurement was kept constant, with an estimated uncertainty of 0.05 K, by means of a Lauda D 20 KP clear view thermostat filled with water and coupled with a DLK 10 through-flow cooler. For each sample, at least three efflux time measurements were performed, and the average efflux time t was calculated after discarding potential outliers (often resulting from the formation of bubbles or similar in the bulb or capillary section, altering notoriously the efflux time). The kinematic viscosity (ν) was then calculated as:

$$\nu = K \cdot (t - y) \tag{4.28}$$

where K is the certified capillary constant supplied by the manufacturer, and y is the kinetic energy correction factor. The latter was applied in accordance with the tables supplied by the manufacturer, and it was different than zero only in a few cases where the efflux time was relatively short within the valid range for the particular capillary utilised. For all measurements, the resulting value of ν was checked to lie within the prescribed range for the capillary viscometer being used. When this was not the case, the measurements were repeated with another viscometer with a capillary tube of different diameter. Given the relatively large span of viscosity values in the investigated systems, up to five different capillaries (micro-Ubbelohde viscometers of types I, Ic, II, IIc, and III, according to the labelling by the manufacturer), with their corresponding five different diameters, had to be used. The dynamic viscosity was finally calculated from the values of the kinematic viscosity and the density using Equation 4.4. The uncertainty in the determination of the dynamic viscosity was estimated to be 0.5 %.

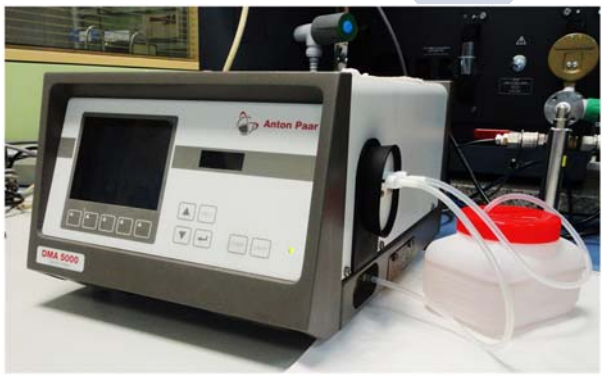

Figure 4.2. Anton Paar vibrating U-tube DMA 5000 density meter.

Figure 4.3. Example of micro-Ubbelohde capillary viscometer (left), and PVS1 systems partially immersed in a Lauda D20 KP clear view thermostat with a Lauda DLK 10 through-flow cooler attached (right).

Refractive indices (n_D) were measured mainly with an Atago RX-5000 refractometer (Figure 4.4) equipped with a sapphire prism at the bottom of a conical measuring chamber built in stainless steel and with a lid of acrylic material to protect it. The temperature was kept constant to within ±0.02 K (although the temperature indicator of the refractometer itself has a resolution of just 0.1 K) by means of a HetoTherm thermostatic bath. The refractometer was accurate to within 4×10^{-5}. For a couple of samples (including pure methanol), their refractive index was out of the range of measurement of the Atago RX-5000 refractometer, and therefore in these specific cases the determination of their refractive indices were carried out in an Anton Paar Abbemat 500 refractometer (Figure 4.4) with a built-in system based on Peltier plates for the temperature control. At least two measurements were performed, ensuring that they were repetitive within the reported uncertainty; and the average values were recorded.

Surface tensions were measured in a Krüss K11 tensiometer using the Wilhelmy plate method (Figure 4.5). A platinium "plate" was used, bended in a cylindrical shape to allow measurements with reduced amounts of sample (Krüss accessory reference PL22), and with dimensions 20 mm (length) × 10 mm (height) × 0.1 mm (thickness) (Figure 4.5). The samples were loaded into cylindrical glass containers, and their temperature was kept constant during the measurements by means of an oil bath with its temperature being controlled by circulating water from a Selecta Frigiterm-10

cryogenic thermostat, with an uncertainty of 0.1 K. Series of twelve consecutive measurements were carried out for each sample, with the first two measurements being systematically disregarded (to allow adequate stabilisation of the liquid surface after contact of the plate and the sample, as well as homogenisation of the wetting of the plate by the sample). The values reported were the average of the remaining ten measurements. An uncertainty of 0.3 $mN \cdot m^{-1}$ was typically observed.

Figure 4.4. Atago RX-5000 refractometer (left) and Anton Paar Abbemat 500 refractometer (right).

Figure 4.5. Krüss K11 tensiometer (left) and detail of the platinum 'plate' folded in a cylindrical shape to perform measurements with smaller amounts of sample (right).

4.3.5. Solubility measurements and precipitation tests

The solubilities of MCC, xylan, and Indulin AT in binary mixtures of [C_2mim][OAc] and alcohol (as well as in the corresponding pure solvents) were determined by gradual addition and dissolution of controlled amounts of the polymer (weighing each added amount in the Mettler Toledo AE240 analytical balance previously mentioned in Section 4.3.2) to the liquid solvent. A mixture of known composition of [C_2mim][OAc] + (methanol or ethanol) was initially placed in a jacketed glass cell (Figure 4.6), connected to an Ultraterm-200 P Selecta thermostatic water bath to maintain the temperature constant to within ±0.1 K throughout the experience. A first addition of biopolymer standard was carried out, with the content of the cell being vigorously stirred for 4-12 h. The stirring in these experiments was performed either by magnetic stirring with a Teflon-coated stirring bar or, in those cases where too high viscosities were achieved, by mechanical stirring with a metal rod coupled to an IKA RW 16 Basic overhead stirrer (Figure 4.6). After ceasing the stirring, the complete dissolution of the added solute was inspected by direct visual observation. Stepwise additions of biopolymer were subsequently repeated in each case, followed by the corresponding stirring period and assessment of dissolution, until the solubility limit was reached. This was typically manifested by undissolved solute at the bottom of the cell, suspended particles, or turbidity in the liquid phase.

In the case of solubility of Indulin AT, occasionally very dark solutions were obtained, which prevented the confirmation of solubilisation by simple visual observation. In such situations, the quantification of the dissolved lignin content was carried out by measurement of the absorbance of the mixtures conveniently diluted with a 0.1 N aqueous solution of NaOH, at a wavelength of 360 nm, in an Agilent Technologies 8453 UV-visible spectrophotometer (Figure 4.7), following a similar procedure to that reported by Lee et al. (2009). The solubility limit would correspond to the lowest concentration for which a plateau of constant absorbance is observed, although in those cases with a particularly high ratio of ionic liquid to alcohol in the solvent, the high solubilisation of the lignin rendered the solution difficult to handle and no absorbance measurement could be carried out suitably.

A microscopic analysis was performed, by means of a Leica DMRE7 optical microscope (Figure 4.8), in order to check the nature of the solubilisation of some of the samples investigated. Moreover, for a specific experiment on selective dissolution of a

mixture of the three aforementioned polymers by mixtures of [C_2mim][OAc] + methanol, FT-IR spectra were carried out in a Varian FT-IR 670 spectrometer (Figure 4.9), using KBr pellets and recording a total of 32 scans in the wavelength range 500-4000 cm^{-1}.

Figure 4.6. Jacketed glass cell used for solubility experiments, with stirring via a metallic rod attached to an IKA RW 16 Basic overhead stirrer.

Figure 4.7. Agilent 8453 Technologies UV-visible spectrophotometer.

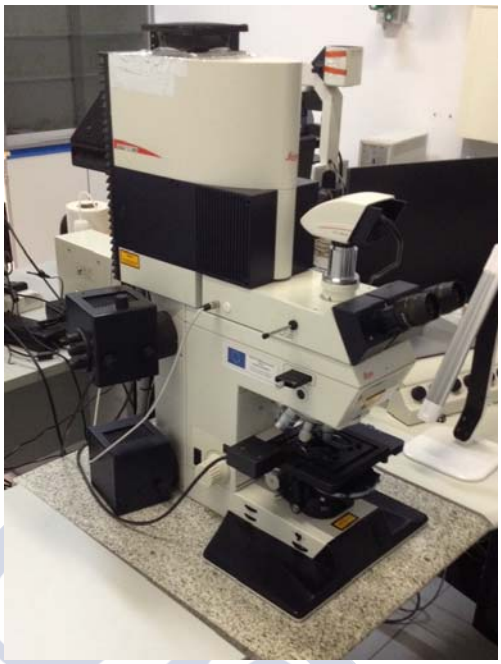

Figure 4.8. Leica DMRE7 optical microscope.

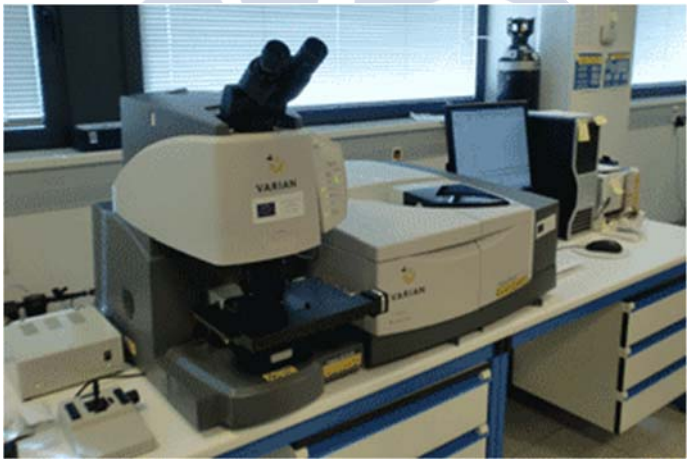

Figure 4.9. Varian FT-IR 670 spectrometer.

On the basis of the solubility results of binary system [C_2mim][OAc] + methanol, precipitation tests to evaluate the ability of methanol as antisolvent were carried out at room temperature. Mixtures of 3 g of [C_2mim][OAc] and 0.15 g of the biopolymer standard (or a combination of polymer standards) were placed in capped glass vials and stirred magnetically until total dissolution. Controlled amounts of methanol were

gradually added. After each addition the resulting system was stirred for 30-45 min and allowed to settle for several minutes.

4.4. Results and discussion

4.4.1. Thermal characterisation of [C_2mim][OAc] + alcohol systems

Either in its role as cosolvent or antisolvent, it is desirable to have a possibility of easily removing the light alcohol from its mixtures with [C_2mim][OAc], to recover the pure ionic liquid as needed. In principle, the vaporisation of the alcohol from the non-volatile ionic liquid at moderate temperatures could be a preferred strategy. To confirm that this is possible for the [C_2mim][OAc] + (methanol, or ethanol, or 1-propanol, or 2-propanol) systems, TGA experiments were carried out for samples covering the composition range of the binary systems studied. Figure 4.10 shows the TGA thermograms for the pure [C_2mim][OAc] and for its mixtures with methanol, ethanol, 1-propanol, or 2-propanol over the entire composition range. No TGA runs were carried out for the pure alcohols due to their totally volatile character.

For pure [C_2mim][OAc] a one-step decomposition curve was obtained, with an onset decomposition temperature (T_d) of 475 K (see Figure B.15 in Appendix B). This value is in reasonably good agreement with the values of 489, 492, and 494 K respectively reported in the literature by Clough et al. (2013), Zhao et al. (2012), and Cao and Mu (2014), taking into account that our TGA runs were carried out at half the heating rate than theirs (5 K·min^{-1} versus 10 K·min^{-1}). Almeida et al. (2012a) also reported 470 K as the temperature at which significant weight loss for this ionic liquid started to occur in their TGA experiments. The more conservative value $T_{d,5\%}$, which provides a better guidance for the maximum temperature at which the ionic liquid can be operated in practice (Clough et al., 2013; Smiglak et al., 2006), was calculated from the TGA curve obtained herein, and it was found to be 427 K (see Figure B.15 in Appendix B).

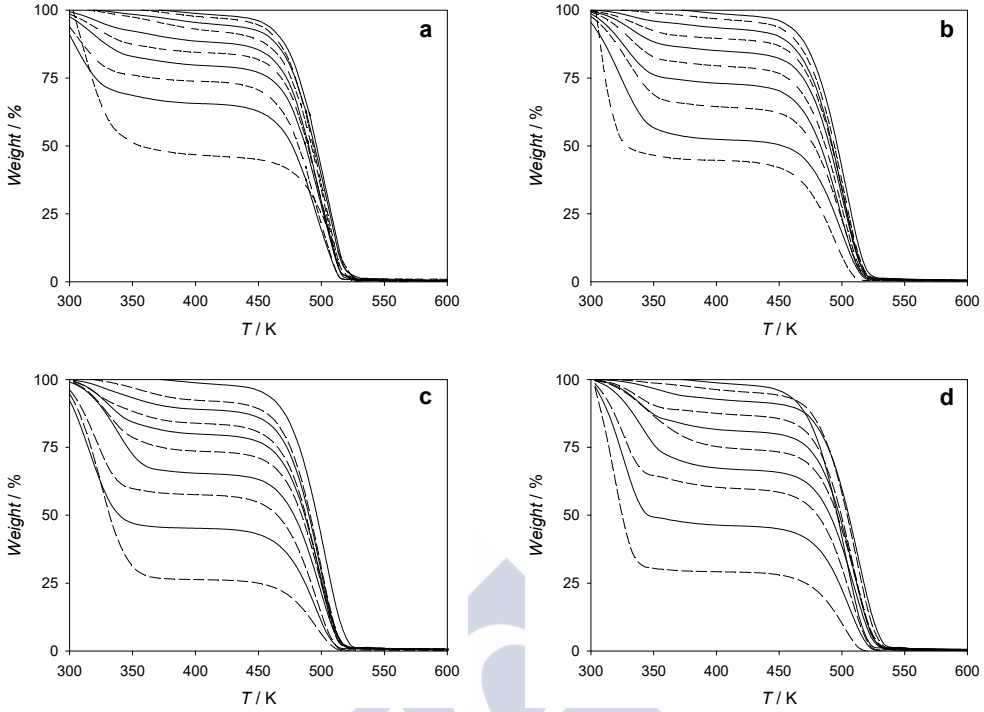

Figure 4.10. TGA thermograms for the binary systems [C2mim][OAc] + alcohol, from pure [C2mim][OAc] (top, right) to a 0.10 mole fraction of [C2mim][OAc], at a step composition of 0.10 in mole fraction. Solid and dashed lines are alternatively used for facilitation of the identification of each thermogram. Alcohol: a) methanol, b) ethanol, c) 1-propanol, d) 2-propanol.

Regarding the mixtures of [C2mim][OAc] with alcohols (methanol, ethanol, 1-propanol, or 2-propanol), all thermograms present a similar pattern (Figure 4.10). Starting at room temperature and with increasing temperature, there is a weight loss from the beginning as a result of the inherent volatility of the alcohol. Next, there is a horizontal inflection point in the curve (transition from convex to concave), occurring at a temperature T_{ip}, and the decomposition proceeds thereafter in a similar way to that observed for the pure ionic liquid. Table 4.2 shows that there is an acceptable correspondence between the sample weight percent remaining at the aforementioned horizontal inflection point ($\%wt_{ip}$) and the mass fraction of the ionic liquid (w_{IL}) in the sample (perhaps with the exception of the samples with the highest concentration of alcohol, for which the correspondence is worse, likely due to higher losses by evaporation during the taring of the TGA balance prior to the start of the heating ramps of the runs). This suggests that the weight loss in the low-temperature part of the

thermogram (below T_{ip}) is due to vaporisation of the alcohol, whereas the weight loss in the high-temperature part (above T_{ip}) is due to the decomposition of the ionic liquid.

Table 4.2. Mole fraction (x_{IL}) and mass fraction (w_{IL}) composition of ionic liquid in the binary mixtures of [C_2mim][OAc] + (methanol, ethanol, 1-propanol, or 2-propanol) for the TGA experiments, along with the temperature (T_{ip}) and remaining sample weight percent ($\%wt_{ip}$) for the low-temperature (from convex to concave) inflexion points of the thermograms, and the corresponding pseudo 5 % onset decomposition temperatures ($T'_{d,5\%}$).

x_{IL}	w_{IL}	T_{ip} / K	$\%wt_{ip}$	$T'_{d,5\%}$/ K
[C_2mim][OAc] + methanol				
0.1000	0.3712	419	46.2	448
0.2000	0.5705	406	65.6	438
0.3000	0.6948	403	73.8	438
0.4000	0.7798	413	79.4	445
0.5000	0.8416	413	84.2	445
0.6000	0.8885	415	88.1	444
0.7000	0.9253	419	92.0	444
0.8003	0.9551	418	94.7	451
0.9003	0.9796	415	97.2	448
[C_2mim][OAc] + ethanol				
0.1000	0.2910	387	44.8	430
0.2000	0.4802	410	52.2	442
0.3000	0.6130	418	64.0	445
0.4000	0.7112	410	72.8	442
0.4999	0.7869	412	79.2	445
0.5998	0.8470	413	84.7	446
0.7001	0.8961	409	89.4	446
0.7990	0.9362	413	93.1	447
0.9000	0.9708	420	96.1	449
[C_2mim][OAc] + 1-propanol				
0.1017	0.2427	401	26.3	436
0.2004	0.4152	398	45.2	436
0.3001	0.5485	400	57.6	436
0.3998	0.6535	411	65.3	445
0.4997	0.7388	409	73.5	443
0.5996	0.8092	412	79.7	444
0.6998	0.8685	408	83.7	441
0.8002	0.9190	407	88.9	443
0.8991	0.9619	410	92.1	444
[C_2mim][OAc] + 2-propanol				
0.1000	0.2394	403	30.0	440
0.2000	0.4145	417	46.1	448
0.3000	0.5483	421	59.7	450
0.4000	0.6537	425	66.7	455
0.5000	0.7390	428	74.2	458
0.5998	0.8093	423	80.9	456
0.7000	0.8686	422	86.8	455
0.7993	0.9186	426	91.9	460
0.9000	0.9622	426	95.3	458

With the exception of the system with 2-propanol, the T_{ip} values are clearly lower than the $T_{d,5\%}$ of [C_2mim][OAc] (427 K). This is indicative of the possibility of achieving a practically total vaporisation of the alcohol (methanol, ethanol, or 1-propanol) in its mixtures with the ionic liquid by a simple heating ramp up to T_{ip}, without causing concomitant thermal degradation of the ionic liquid. Conversely, for the system [C_2mim][OAc] + 2-propanol it is observed that the T_{ip} values of most of the tested samples (in particular above a certain threshold concentration of ionic liquid in the mixture) are rather similar to the $T_{d,5\%}$ calculated for pure [C_2mim][OAc]; so the recovery of pure ionic liquid from the mixture via the heating ramp procedure could be more difficult. Since the specific heats and enthalpies of vaporisation of the alcohols (2.54 $J \cdot g^{-1} \cdot K^{-1}$ and 1.17 $kJ \cdot g^{-1}$ for methanol, 2.44 $J \cdot g^{-1} \cdot K^{-1}$ and 0.92 $kJ \cdot g^{-1}$ for ethanol, and 2.39 $J \cdot g^{-1} \cdot K^{-1}$ and 0.79 $kJ \cdot g^{-1}$ for 1-propanol; all values at 298 K (Riddick et al., 1986)) are largely lower than those of water (4.18 $J \cdot g^{-1} \cdot K^{-1}$ and 2.44 $kJ \cdot g^{-1}$, at 298 K (Riddick et al., 1986)), the use of these alcohols as antisolvents for the precipitation of lignocellulosic biopolymers from ionic liquid solution can be expected to notably reduce, in comparison to the use of water, the energy cost associated with recovering the ionic liquid by vaporisation of the molecular antisolvent. Nevertheless, in order to carry out this recovery by e.g. distillation, the accurate knowledge of vapour-liquid equilibria of the mixtures [C_2mim][OAc] + alcohol should be determined for validation of the alleged savings of energy and viability of the recovery process. In this regard, the vapour-liquid equilibrium data reported by Cai et al. (2011) and Li et al. (2012) on ternary systems [C_2mim][OAc] + alcohol + alkyl acetate look promising, since they point to little effect on the boiling temperature of the alcohols at low concentrations of the ionic liquid in the system. However, at high concentrations of ionic liquid in the system, the distillation of the alcohol could be harder, and appropriate experimental work in addressing this issue should be considered.

Above T_{ip}, the fraction of sample remaining may be assumed to be constituted essentially by the ionic liquid, with some traces of the alcohol. If the horizontal tangent to the TGA curve at T_{ip} is taken as the baseline reference for the calculation of an onset decomposition at the high-temperature part of the curve, a pseudo 5 % onset decomposition temperature ($T'_{d,5\%}$) for the ionic liquid can be determined. The values of $T'_{d,5\%}$ thus calculated are shown in Table 4.2. They lie in the approximate range 430-460 K for all binary samples, being somewhat higher than the $T_{d,5\%}$ found for the pure

ionic liquid. Although the difference is too small as to unambiguously state that there is a stabilising effect of the alcohol on the ionic liquid, it seems clear that the presence of the alcohol does not have a detrimental effect on the thermal stability of [C_2mim][OAc] as compared to that of the ionic liquid in neat.

Since the TGA runs carried out in this work are dynamic experiments, the temperature thresholds of thermal stability must be taken with care. Lower temperature limits might be considered if dealing with process plants operating in the mid- or long-term. However, the values reported in this section can be taken as fair estimations of the actual limiting temperatures at which industrial units in real processes could be operated.

A comparison of the TGA curves of the four binary systems studied, at a given composition, namely for an ionic liquid mole fraction of 0.70, is provided in Figure 4.11. In this figure, a trend can be observed in the thermograms of the systems with primary alcohols (methanol, ethanol, 1-propanol), for which the mass loss upon heating increases with an increase in the alkyl chain length of the alcohol. This seems to correlate well with the simple fact that, as the molar mass of the alcohol is increased, the ionic liquid mole fraction of 0.70 is equivalent to a gradually lower ionic liquid mass fraction: 0.93 in the mixture with methanol; 0.90 in the mixture with ethanol; and 0.87 in the mixture with either of the propanols. However, a somewhat dissimilar behaviour is observed for the system with 2-propanol, which exhibits a relatively enhanced thermal stability. This suggests the presence of alternative/additional ways of interaction of the molecules of 2-propanol with the ions of the ionic liquid.

The determination of the stable liquid range of the investigated systems was completed with a complementary study of thermal events in the mixtures by DSC. Figures 4.12 shows that no thermal events were observed for the different mixtures above ca. 200 K, thus confirming all four systems remain liquid at least down to such low temperature (approximately the lowest reliable temperature of the apparatus used), throughout the entire composition ranges. Therefore, no risk of crystallisation should be expected when using the studied mixtures in a process at temperatures even a far way below conventional ambient temperature.

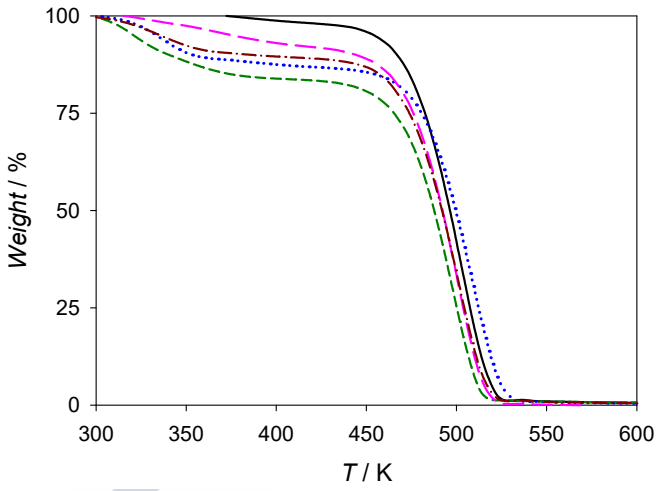

Figure 4.11. TGA thermograms for the binary systems [C2mim][OAc] + alcohol, with a composition of 0.70 in mole fraction. Alcohol: methanol (magenta, long-dashed line), ethanol (brown, dot-dash line), 1-propanol (green, short-dashed line), or 2-propanol (blue, dotted line). The thermogram for pure [C2mim][OAc] (black, solid line) is also depicted for visual reference.

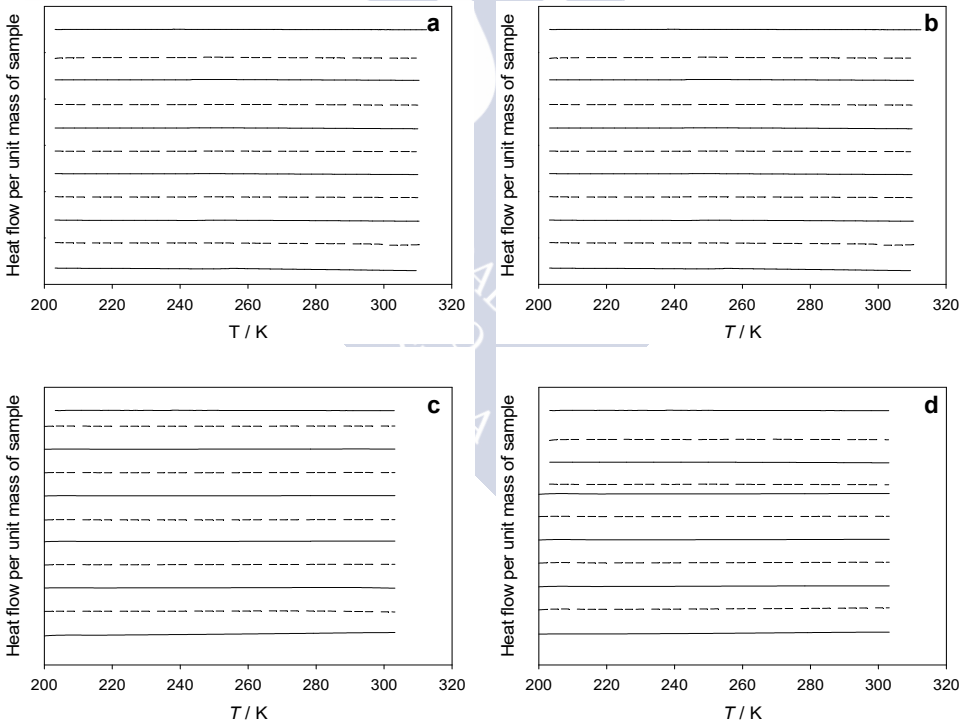

Figure 4.12. Stacked DSC thermograms (heating ramps) for the binary system [C2mim][OAc] + alcohol, from pure [C2mim][OAc] (top) to pure alcohol (bottom) at a step composition of 0.10 in mole fraction. Alcohol: a) methanol, b) ethanol, c) 1-propanol, d) 2-propanol. Solid and dashed lines have been alternatively used to facilitate identification of each thermogram.

4.4.2. Physical properties of [C_2mim][OAc] + alcohol systems

A good knowledge of the physical properties of a fluid system is critical for the design of an efficient process that involves it. Key physical properties such as density, viscosity, and surface tension were determined at atmospheric pressure for the binary systems constituted by [C_2mim][OAc] and methanol, ethanol, 1-propanol, or 2-propanol, over certain temperature ranges of interest (where the mixtures are stable liquids) and over the entire composition range. Additionally, and although its interest in process design may be more limited, the refractive index for the investigated mixtures was also determined at analogous conditions, as it may be useful in the development of models and in the straightforward determination of the composition of samples. The experimental values thus determined for the mentioned properties of the binary systems [C_2mim][OAc] + (methanol, ethanol, 1-propanol, or 2-propanol) are summarised in Tables 4.3 to 4.6. All studied properties are observed to decrease with increasing temperature and with increasing the concentration of alcohol in the mixture. A detailed and insightful analysis of the evolution of each property with temperature and/or composition is provided below, including the calculation of the pertinent excess properties and property changes of mixing.

Effect of temperature

As it can be observed in Tables 4.3 to 4.6, the four investigated properties decrease with an increase of temperature at a given composition, for all binary systems. The pattern described by the different properties as a function of temperature, however, is substantially different in some cases, as discussed next.

Figures 4.13 to 4.16 show the evolution of densities for the binary systems studied, as a function of temperature, for different compositions. This evolution follows an apparently quite linear decrease within the studied temperature ranges for most of the compositions. A more detailed insight on the nature of the trend of density with temperature for these systems was performed by means of the F-test (Devore, 2004). This statistical analysis of the experimental data revealed that the second-order term in a polynomial expression of the density as function of temperature (Equation 4.22) was statistically significant for all series, at a significance level of 0.05. The least-squares quadratic fits for each series at a fixed composition are shown in Figures 4.13 to 4.16 as solid lines, along with the experimental data points. The numerical values of the fit parameters and the corresponding standard deviations are listed in Table 4.7.

Table 4.3. Experimental density (ρ), dynamic viscosity (η), refractive index (n_D), and surface tension (σ) for the binary system [C_2mim][OAc] + methanol, in the temperature range (278.15 to 318.15) K and at atmospheric pressure, as a function of the mole fraction of [C_2mim][OAc] (x_{IL}).

x_{IL}	T / K				
	278.15	288.15	298.15	308.15	318.15
	ρ / g·cm^{-3}				
0.0000	0.80550	0.79614	0.78674	0.77726	0.76768
0.1000	0.91300	0.90499	0.89702	0.88907	0.88112
0.2000	0.97359	0.96612	0.95875	0.95143	0.94413
0.3000	1.01227	1.00520	0.99819	0.99122	0.98431
0.4000	1.03922	1.03237	1.02558	1.01884	1.01216
0.5000	1.05907	1.05239	1.04577	1.03920	1.03269
0.6000	1.07434	1.06780	1.06131	1.05488	1.04849
0.7000	1.08655	1.08016	1.07380	1.06748	1.06120
0.8003	1.09631	1.09002	1.08377	1.07754	1.07136
0.9003	1.10466	1.09826	1.09214	1.08599	1.07989
1.0000	1.11157	1.10520	1.09903	1.09293	1.08686
	η / mPa·s				
0.0000	0.713	0.614	0.533	0.466	0.411
0.1000	2.018	1.693	1.393	1.202	1.050
0.2000	4.358	3.523	2.911	2.444	2.089
0.3000	9.022	6.897	5.410	4.403	3.645
0.4000	18.14	12.97	9.684	7.489	5.972
0.5000	35.84	23.72	16.60	12.22	9.336
0.6000	68.41	41.82	27.37	19.07	13.94
0.6999	144.0	78.55	46.97	30.62	21.14
0.8003	245.4	121.8	69.71	42.85	28.45
0.9003	443.5	198.8	104.4	60.83	38.41
1.0000	690.3	283.8	139.0	77.32	47.37
	n_D				
0.0000	1.33515	1.33085	1.32701	1.32301	1.31902
0.1000	1.39220	1.38864	1.38556	1.38217	1.37893
0.2000	1.42581	1.42298	1.41981	1.41666	1.41376
0.3000	1.44822	1.44501	1.44187	1.43914	1.43598
0.4000	1.46346	1.46058	1.45752	1.45466	1.45167
0.5000	1.47517	1.47231	1.46951	1.46670	1.46382
0.6000	1.48401	1.48131	1.47862	1.47578	1.47303
0.6999	1.49023	1.48844	1.48532	1.48305	1.48029
0.8003	1.49607	1.49457	1.49148	1.48913	1.48643
0.9003	1.50045	1.49828	1.49675	1.49415	1.49140
1.0000	1.50484	1.50285	1.50069	1.49803	1.49527
	σ / mN·m^{-1}				
0.0000	23.8	23.6	22.7	21.9	21.0
0.1000	28.5	28.1	27.5	26.8	26.3
0.2000	32.7	32.1	31.6	31.1	30.6
0.3000	35.9	35.3	35.0	34.5	33.9
0.4000	38.4	38.0	37.5	37.1	36.5
0.5000	40.3	40.0	39.6	39.0	38.7
0.6000	42.1	41.6	41.1	40.8	40.4
0.6999	44.3	43.8	43.3	42.8	42.4
0.8003	45.9	45.1	44.7	44.2	43.9
0.9003	47.6	46.9	46.4	45.9	45.3
1.0000	48.1	47.7	47.1	46.6	46.1

Table 4.4. Experimental density (ρ), dynamic viscosity (η), refractive index (n_D), and surface tension (σ) for the binary system [C_2mim][OAc] + ethanol, in the temperature range (278.15 to 338.15) K and at atmospheric pressure, as a function of the mole fraction of [C_2mim][OAc] (x_{IL}).

x_{IL}	T / K						
	278.15	288.15	298.15	308.15	318.15	328.15	338.15
	ρ / g·cm^{-3}						
0.0000	0.80214	0.79365	0.78510	0.77643	0.76762	0.75861	0.74932
0.1000	0.88099	0.87335	0.86573	0.85809	0.85042	0.84270	0.83490
0.2000	0.93589	0.92865	0.92146	0.91429	0.90713	0.89998	0.89283
0.3000	0.97735	0.97038	0.96345	0.95657	0.94972	0.94291	0.93612
0.4000	1.00892	1.00213	0.99539	0.98871	0.98207	0.97548	0.96892
0.4999	1.03462	1.02799	1.02140	1.01487	1.00839	1.00196	0.99557
0.5998	1.05560	1.04912	1.04266	1.03625	1.02989	1.02358	1.01733
0.7001	1.07294	1.06661	1.06031	1.05410	1.04789	1.04168	1.03552
0.7990	1.08766	1.08137	1.07520	1.06899	1.06281	1.05668	1.05060
0.9000	1.10066	1.09426	1.08814	1.08201	1.07591	1.06985	1.06384
1.0000	1.11157	1.10520	1.09903	1.09293	1.08686	1.08082	1.07483
	η / mPa·s						
0.0000	1.582	1.310	1.081	0.899	0.755	0.638	0.543
0.1000	3.396	2.751	2.264	1.885	1.591	1.355	1.165
0.2000	6.551	5.152	4.145	3.398	2.829	2.391	2.049
0.3000	12.96	9.301	7.198	5.705	4.639	3.833	3.218
0.4000	23.61	16.59	12.20	9.268	7.268	5.840	4.790
0.4999	44.63	28.97	20.04	14.48	10.91	8.487	6.774
0.5998	86.66	49.10	31.80	21.86	15.76	11.82	9.182
0.7001	149.8	81.50	49.24	32.06	22.19	15.99	12.05
0.7990	264.4	130.8	73.27	45.42	29.99	21.00	15.40
0.9000	462.4	206.6	107.7	62.75	39.71	26.89	19.14
1.0000	690.3	283.8	139.0	77.32	47.37	31.29	21.85
	n_D						
0.0000	1.36775	1.36343	1.35957	1.35534	1.35142	1.34704	1.34252
0.1000	1.40274	1.39952	1.39609	1.39260	1.38930	1.38551	1.38222
0.2000	1.42727	1.42397	1.42075	1.41801	1.41451	1.41144	1.40830
0.3000	1.44617	1.44312	1.44003	1.43681	1.43396	1.43089	1.42780
0.4000	1.46096	1.45756	1.45473	1.45202	1.44880	1.44639	1.44299
0.4999	1.47239	1.46945	1.46650	1.46368	1.46086	1.45795	1.45499
0.5998	1.48313	1.47907	1.47631	1.47348	1.47064	1.46777	1.46504
0.7001	1.48967	1.48725	1.48440	1.48164	1.47884	1.47608	1.47341
0.7990	1.49472	1.49298	1.49037	1.48703	1.48484	1.48212	1.47937
0.9000	1.49993	1.49867	1.49606	1.49327	1.49082	1.48812	1.48547
1.0000	1.50484	1.50285	1.50069	1.49803	1.49527	1.49266	1.48995
	σ / mN·m^{-1}						
0.0000	23.3	22.8	22.0	21.4	20.4	19.7	18.9
0.1000	25.6	25.2	24.8	24.2	23.5	22.9	21.8
0.2000	28.8	28.2	27.9	27.3	26.9	26.4	25.8
0.3000	31.2	30.8	30.3	29.8	29.4	28.9	28.4
0.4000	33.6	33.3	32.8	32.3	31.8	31.3	30.9
0.4999	35.9	35.4	35.1	34.7	34.1	33.7	33.4
0.5998	38.0	37.6	37.2	36.6	36.4	36.0	35.6
0.7001	40.4	39.9	39.4	39.0	38.5	38.2	38.0
0.7990	42.7	42.3	41.8	41.2	41.0	40.7	40.6
0.9000	45.5	45.2	44.5	44.1	43.6	43.3	43.0
1.0000	48.1	47.7	47.1	46.6	46.1	45.9	45.4

Table 4.5. Experimental density (ρ), dynamic viscosity (η), refractive index (n_D), and surface tension (σ) for the binary system [C_2mim][OAc] + 1-propanol, in the temperature range (288.15 to 348.15) K and at atmospheric pressure, as a function of the mole fraction of [C_2mim][OAc] (x_{IL}).

x_{IL}	T / K						
	288.15	298.15	308.15	318.15	328.15	338.15	348.15
	ρ / g·cm^{-3}						
0.0000	0.80755	0.79956	0.79146	0.78320	0.77472	0.76598	0.75691
0.1017	0.86940	0.86203	0.85463	0.84719	0.83968	0.83208	0.82434
0.2004	0.91548	0.90840	0.90133	0.89427	0.88721	0.88013	0.87302
0.3001	0.95382	0.94694	0.94010	0.93329	0.92651	0.91975	0.91299
0.3998	0.98605	0.97934	0.97266	0.96603	0.95944	0.95289	0.94636
0.4997	1.01352	1.00695	1.00041	0.99392	0.98748	0.98108	0.97471
0.5996	1.03716	1.03070	1.02428	1.01790	1.01158	1.00530	0.99906
0.6998	1.05765	1.05129	1.04496	1.03868	1.03245	1.02626	1.02012
0.8002	1.07560	1.06933	1.06309	1.05689	1.05074	1.04463	1.03857
0.8991	1.09097	1.08489	1.07875	1.07262	1.06653	1.06048	1.05449
1.0000	1.10520	1.09903	1.09293	1.08686	1.08082	1.07483	1.06888
	η / mPa·s						
0.0000	2.506	1.952	1.545	1.238	1.006	0.824	0.684
0.1017	4.866	3.822	3.038	2.461	2.018	1.680	1.413
0.2004	7.990	6.163	4.878	3.952	3.268	2.686	2.260
0.3001	13.36	9.963	7.657	6.043	4.878	3.946	3.292
0.3998	22.26	15.81	11.70	8.961	7.050	5.672	4.651
0.4997	36.38	24.44	17.30	12.78	9.766	7.675	6.175
0.5996	57.47	36.48	24.75	17.58	13.01	9.978	7.866
0.6998	90.15	53.65	34.59	23.68	17.05	12.68	9.810
0.8002	135.0	75.63	46.49	30.86	21.36	15.57	11.81
0.8991	196.8	103.9	60.98	37.98	25.84	18.49	13.78
1.0000	283.8	139.0	77.32	47.37	31.29	21.85	16.01
	n_D						
0.0000	1.38694	1.38303	1.37914	1.37500	1.37075	1.36667	1.36201
0.1017	1.41146	1.40825	1.40453	1.40109	1.39753	1.39391	1.39115
0.2004	1.42938	1.42622	1.42291	1.41973	1.41631	1.41301	1.41033
0.3001	1.44451	1.44134	1.43827	1.43523	1.43208	1.42910	1.42601
0.3998	1.45711	1.45401	1.45119	1.44803	1.44542	1.44211	1.43912
0.4997	1.46775	1.46473	1.46189	1.45888	1.45593	1.45308	1.45026
0.5996	1.47687	1.47411	1.47127	1.46830	1.46570	1.46267	1.45993
0.6998	1.48500	1.48219	1.47942	1.47661	1.47372	1.47110	1.46823
0.8002	1.49189	1.48919	1.48632	1.48365	1.48089	1.47818	1.47546
0.8991	1.49712	1.49506	1.49221	1.48899	1.48673	1.48324	1.48030
1.0000	1.50285	1.50069	1.49803	1.49527	1.49266	1.48995	1.48721
	σ / mN·m^{-1}						
0.0000	23.9	23.4	22.4	22.0	20.9	19.7	19.0
0.1017	25.8	25.2	24.7	23.9	23.0	22.3	21.5
0.2004	27.4	26.5	25.8	25.3	25.0	24.0	23.6
0.3001	29.7	29.2	28.7	28.5	27.9	27.3	27.1
0.3998	31.7	31.0	30.7	30.2	30.0	29.5	29.3
0.4997	33.7	33.1	32.7	32.2	31.7	31.3	30.8
0.5996	35.6	34.7	34.2	33.3	33.1	32.6	31.8
0.6998	37.7	37.2	36.6	36.1	35.8	35.5	34.5
0.8002	40.2	39.7	39.2	38.8	38.1	37.9	37.6
0.8991	43.2	42.7	42.2	41.8	41.4	41.2	41.0
1.0000	47.7	47.1	46.6	46.1	45.9	45.4	45.1

Table 4.6. Experimental density (ρ), dynamic viscosity (η), refractive index (n_D), and surface tension (σ) for the binary system [C_2mim][OAc] + 2-propanol, in the temperature range (288.15 to 338.15) K and at atmospheric pressure, as a function of the mole fraction of [C_2mim][OAc] (x_{IL}).

x_{IL}	T / K					
	288.15	298.15	308.15	318.15	328.15	338.15
			ρ / g·cm^{-3}			
0.0000	0.78918	0.78084	0.77223	0.76327	0.75389	0.74402
0.1000	0.85268	0.84522	0.83768	0.82999	0.82214	0.81408
0.2000	0.90160	0.89412	0.88704	0.87994	0.87280	0.86560
0.3000	0.94178	0.93495	0.92814	0.92135	0.91457	0.90778
0.4000	0.97637	0.96970	0.96307	0.95647	0.94991	0.94337
0.5000	1.00601	0.99947	0.99298	0.98652	0.98011	0.97374
0.5998	1.03155	1.02512	1.01874	1.01239	1.00610	0.99984
0.7000	1.05383	1.04751	1.04121	1.03496	1.02876	1.02260
0.7993	1.07297	1.06677	1.06056	1.05438	1.04825	1.04217
0.9000	1.09017	1.08405	1.07792	1.07181	1.06574	1.05972
1.0000	1.10520	1.09903	1.09293	1.08686	1.08082	1.07483
			η / mPa·s			
0.0000	2.752	2.018	1.507	1.150	0.895	0.704
0.1000	5.550	4.171	3.204	2.511	1.998	1.617
0.2000	8.842	6.640	5.142	4.067	3.272	2.683
0.3000	14.85	10.84	8.186	6.344	5.049	4.086
0.4000	24.85	17.31	12.60	9.506	7.378	5.876
0.5000	40.69	26.86	18.61	13.61	10.28	8.019
0.5998	64.17	40.40	26.86	18.87	13.77	10.46
0.7000	100.7	58.42	36.90	25.08	17.83	13.23
0.7993	147.9	81.31	49.32	32.33	22.39	16.22
0.9000	212.4	109.9	63.37	40.36	27.23	19.37
1.0000	283.8	139.0	77.32	47.37	31.29	21.85
			n_D			
0.0000	1.37933	1.37517	1.37093	1.36643	1.36173	1.35682
0.1000	1.40475	1.40107	1.39762	1.39423	1.39112	1.38677
0.2000	1.42939	1.42604	1.42276	1.41947	1.41637	1.41309
0.3000	1.43991	1.43669	1.43360	1.43066	1.42763	1.42464
0.4000	1.45344	1.45075	1.44750	1.44471	1.44229	1.43908
0.5001	1.46510	1.46242	1.46177	1.45641	1.45352	1.45107
0.5998	1.47535	1.47243	1.46954	1.46689	1.46489	1.45943
0.7000	1.48406	1.48131	1.47840	1.47561	1.47293	1.47054
0.7994	1.49120	1.48861	1.48593	1.48324	1.48046	1.47775
0.9000	1.49776	1.49526	1.49257	1.48986	1.48714	1.48466
1.0000	1.50285	1.50069	1.49803	1.49527	1.49266	1.48995
			σ / mN·m^{-1}			
0.0000	21.6	21.2	20.5	19.6	18.7	17.4
0.1000	23.6	23.2	22.5	21.8	20.8	20.1
0.2000	25.5	25.1	24.6	24.1	23.5	22.6
0.3000	27.5	26.9	26.6	26.1	25.5	25.0
0.4000	29.4	29.0	28.3	27.9	27.4	26.9
0.5000	31.5	31.2	30.5	29.9	29.6	29.1
0.5997	33.0	32.6	32.1	31.6	31.5	30.7
0.7000	35.1	34.5	34.1	33.7	33.4	32.9
0.7994	37.7	37.4	37.0	36.8	36.4	36.0
0.9000	41.2	40.9	40.5	40.2	40.0	39.3
1.0000	47.7	47.1	46.6	46.1	45.9	45.4

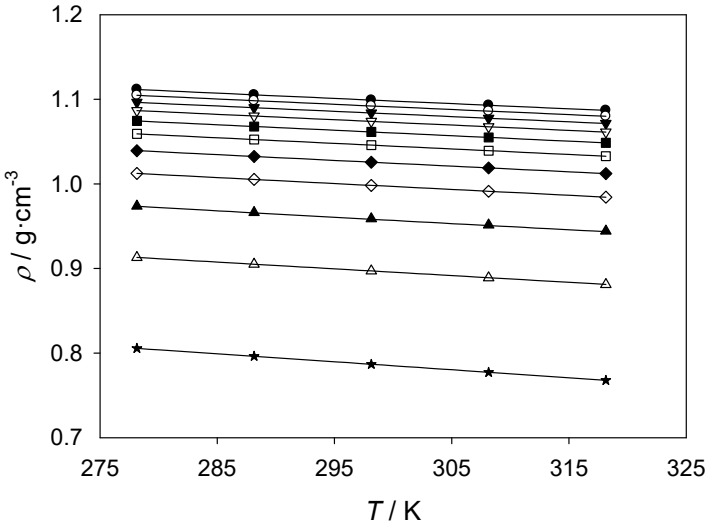

Figure 4.13. Density ρ for the binary system [C_2mim][OAc] + methanol, at atmospheric pressure and as a function of temperature (T), at different mole fractions of [C_2mim][OAc] (x_{IL}): ★, 0.00; △, 0.10; ▲, 0.20; ◇, 0.30; ◆, 0.40; □, 0.50; ■, 0.60; ▽, 0.70; ▼, 0.80; ○, 0.90; ●, 1.00. (For a greater degree of precision of the mole fractions, please refer to Table 4.3.) Solid lines correspond to the correlation by means of a second-degree polynomial.

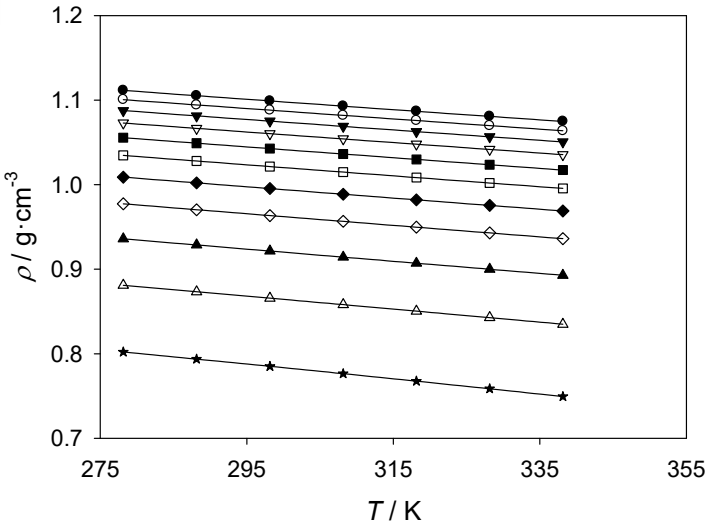

Figure 4.14. Density ρ for the binary system [C_2mim][OAc] + ethanol, at atmospheric pressure and as a function of temperature (T), at different mole fractions of [C_2mim][OAc] (x_{IL}): ★, 0.00; △, 0.10; ▲, 0.20; ◇, 0.30; ◆, 0.40; □, 0.50; ■, 0.60; ▽, 0.70; ▼, 0.80; ○, 0.90; ●, 1.00. (For a greater degree of precision of the mole fractions, please refer to Table 4.4.) Solid lines correspond to the correlation by means of a second-degree polynomial.

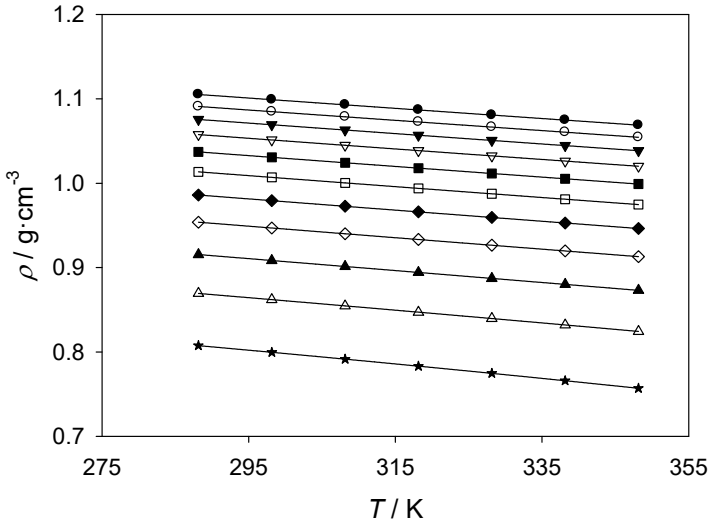

Figure 4.15. Density ρ for the binary system [C_2mim][OAc] + 1-propanol, at atmospheric pressure and as a function of temperature (T), at different mole fractions of [C_2mim][OAc] (x_{IL}): ★, 0.00; △, 0.10; ▲, 0.20; ◇, 0.30; ◆, 0.40; □, 0.50; ■, 0.60; ▽, 0.70; ▼, 0.80; ○, 0.90; ●, 1.00. (For a greater degree of precision of the mole fractions, please refer to Table 4.5.) Solid lines correspond to the correlation by means of a second-degree polynomial.

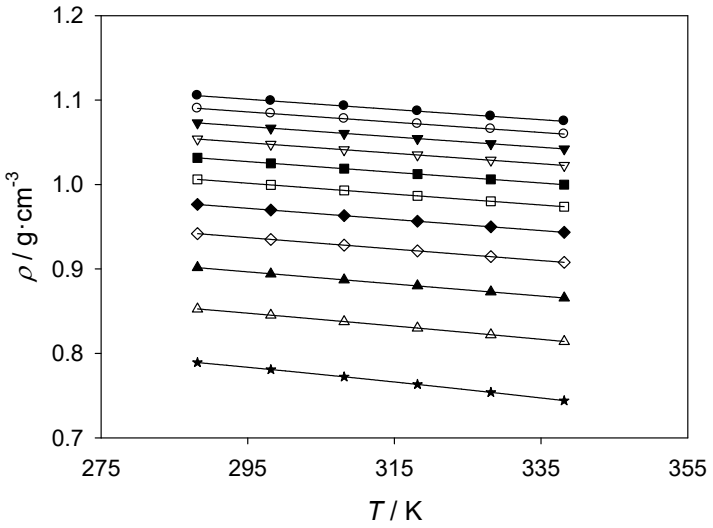

Figure 4.16. Density ρ for the binary system [C_2mim][OAc] + 2-propanol, at atmospheric pressure and as a function of temperature (T), at different mole fractions of [C_2mim][OAc] (x_{IL}): ★, 0.00; △, 0.10; ▲, 0.20; ◇, 0.30; ◆, 0.40; □, 0.50; ■, 0.60; ▽, 0.70; ▼, 0.80; ○, 0.90; ●, 1.00. (For a greater degree of precision of the mole fractions, please refer to Table 4.6.) Solid lines correspond to the correlation by means of a second-degree polynomial.

Table 4.7. Fit parameters (a_0, a_1, a_2) of the quadratic fit of the density of the binary systems [C_2mim][OAc] + (methanol, ethanol, 1-propanol, or 2-propanol) for its correlation as a function of temperature, at different mole fractions of ionic liquid (x_{IL}), by means of Equation 4.22. The corresponding standard deviations (*SD*) are also shown.

x_{IL}	Fit parameters and standard deviation ‡			
	a_0	$a_1 \times 10^4$	$a_2 \times 10^7$	*SD*
[C_2mim][OAc] + methanol				
0.0000	1.03615	-7.27936	-3.64286	0.00002
0.1000	1.14356	-8.57142	1.01429	0.00001
0.2000	1.27591	-13.8225	10.6071	0.00088
0.3000	1.22945	-8.52334	2.57143	0.00000
0.4000	1.25211	-8.43048	2.79286	0.00000
0.5000	1.26682	-8.23413	2.75000	0.00000
0.6000	1.27680	-7.99414	2.57143	0.00000
0.7000	1.27873	-7.40994	1.80000	0.00001
0.8003	1.28527	-7.27827	1.74286	0.00000
0.9003	1.31203	-8.57096	4.00714	0.00006
1.0000	1.32415	-8.93278	4.63571	0.00004
[C_2mim][OAc] + ethanol				
0.0000	0.97231	-3.92673	-7.88452	0.00006
0.1000	1.07893	-6.66002	-1.64405	0.00003
0.2000	1.14305	-7.67354	0.81071	0.00001
0.3000	1.18602	-8.02204	1.86905	0.00001
0.4000	1.21652	-8.12168	2.36429	0.00000
0.4999	1.23922	-8.05301	2.50714	0.00000
0.5998	1.25518	-7.82805	2.34762	0.00001
0.7001	1.26104	-7.19943	1.56905	0.00002
0.7990	1.27456	-7.16539	1.60357	0.00002
0.9000	1.29686	-7.82047	2.75000	0.00005
1.0000	1.31034	-7.99955	3.06190	0.00004
[C_2mim][OAc] + 1-propanol				
0.0000	0.94212	-1.56821	-10.7714	0.00009
0.1017	1.04992	-5.24234	-3.55119	0.00004
0.2004	1.11726	-6.94495	-0.20119	0.00002
0.3001	1.16250	-7.60661	1.26429	0.00001
0.3998	1.19596	-7.84051	1.92857	0.00001
0.4997	1.22111	-7.81397	2.11548	<0.00001
0.5996	1.24306	-7.80302	2.28214	<0.00001
0.6998	1.26085	-7.71062	2.28690	<0.00001
0.8002	1.27492	-7.53289	2.13690	0.00001
0.8991	1.27815	-6.83106	1.16667	0.00003
1.0000	1.30025	-7.36225	2.05833	0.00001
[C_2mim][OAc] + 2-propanol				
0.0000	0.86245	2.97206	-19.1429	0.00007
0.1000	1.00119	-2.97437	-7.56607	0.00004
0.2000	1.12865	-8.48619	2.09643	0.00013
0.3000	1.14395	-7.20131	0.64286	0.00001
0.4000	1.18261	-7.63239	1.64821	<0.00001
0.5000	1.21264	-7.78044	2.11607	<0.00001
0.5998	1.23567	-7.71625	2.19464	<0.00001
0.7000	1.25469	-7.58652	2.13750	<0.00001
0.7993	1.26630	-7.17374	1.61250	0.00001
0.9000	1.27905	-6.94639	1.36071	0.00002
1.0000	1.29981	-7.33391	2.01250	0.00001

‡ Units: a_0 and the standard deviation, in g·cm^{-3}; a_1, in g·cm^{-3}·K^{-1}; a_2, in g·cm^{-3}·K^{-2}.

The quadratic fit adopted here is in contrast to the linear fit adopted by Quijada-Maldonado et al. (2012) for the density of pure [C_2mim][OAc] in their study of the binary system [C_2mim][OAc] + ethanol. A direct comparison of their density data and those reported herein for this specific system are possible at the temperatures of 298.15 K and 328.15 K. Figure 4.17 depicts such comparison, in which a very good agreement is observed between the two datasets at each indicated temperature.

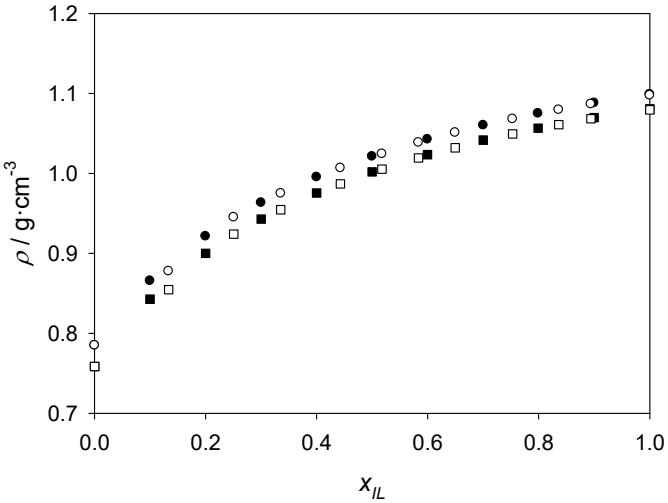

Figure 4.17. Comparison of the experimental density data (ρ) reported for the binary system [C_2mim][OAc] + ethanol in this work (solid symbols) and those reported by Quijada-Maldonado et al. (2012) (open symbols), as a function of the mole fraction of ionic liquid (x_{IL}), at atmospheric pressure and at the temperatures 298.15 K (circles) and 328.15 K (squares).

A visual evolution of the viscosity with the temperature, at different constant compositions over the entire composition range for the binary systems studied, is provided in Figures 4.18 to 4.21. As it can be easily observed, the evolution of this property with the temperature, obeying a typical exponential decay, is starkly different than that described above for the density. From an application perspective in a chemical process context, it is obvious that low temperatures should be avoided especially with streams rich in the ionic liquid, due to their high viscosity. For the correlation of the experimental data of dynamic viscosity with temperature, two equations were tested: the classical Arrhenius-like equation proposed by Andrade (1930), which is known to provide a good description of the viscosity of simple solvents such as alcohols (Equation 4.23); and the Vogel-Fulcher-Tammann (VFT) equation (Equation 4.24), more

appropriate for the viscosity of substances that tend to form glasses, such as ionic liquids. The values obtained for the fit parameters of Equations 4.23 and 4.24 after correlation of all data series at a fixed composition for all the binary systems studied, along with the relative standard deviations (calculated by means of Equation 4.25), are reported in Table 4.8. For all compositions and systems, by comparison of the SD_{rel} values, the VFT equation led to a clearly better description of the experimental data for the pure ionic liquid and most of its mixtures with any of the alcohols. However, attempts to correlate the series corresponding to the pure alcohols and the mixtures with x_{IL}=0.10 with the VFT equation led to abnormally low values of the T_0 parameter (with the exception of the system involving methanol). For this reason, only the Andrade equation was used in these cases. Thus, the fits shown as solid lines in Figures 4.18 to 4.21 correspond to the VFT equation for all series with x_{IL}=0.20 or higher, while they correspond to the Andrade equation for the series with x_{IL}=0.10 or x_{IL}=0.00 (pure alcohol). An exception to this was the series with x_{IL}=0.10 for the system [C_2mim][OAc] + methanol, which was also carried out with the VFT equation. A good agreement between the experimental viscosity data and these correlations can be qualitatively observed throughout.

Quijada-Maldonado et al. (2012) also investigated the viscosity of mixtures of [C_2mim][OAc] and ethanol. The comparison of their data and experimental data presented herein at 298.15 K and at 328.15 K is provided in Figure 4.22. In spite of a general good agreement, the literature data are somewhat lower than those reported herein, especially at 298.15 K and at high concentrations of the ionic liquid. This may be due to a lower water content of the ionic liquid used in the present work.

Figures 4.23 to 4.26 show the experimental refractive index for the binary systems studied, as a function of temperature, for different compositions. The linearity of the variation of the refractive index with temperature was evaluated by means of an *F*-test analysis, which yielded a statistically negligible quadratic term for practically all series at a significance level of 0.05 (as opposed to what was found for density). Therefore, a lineal polynomial expression (Equation 4.20) was used to fit the data of each composition series of all binary systems studied. The corresponding fit parameters and standard deviations are listed in Table 4.9, and the resulting straight lines are plotted along with the experimental data in Figures 4.23 to 4.26.

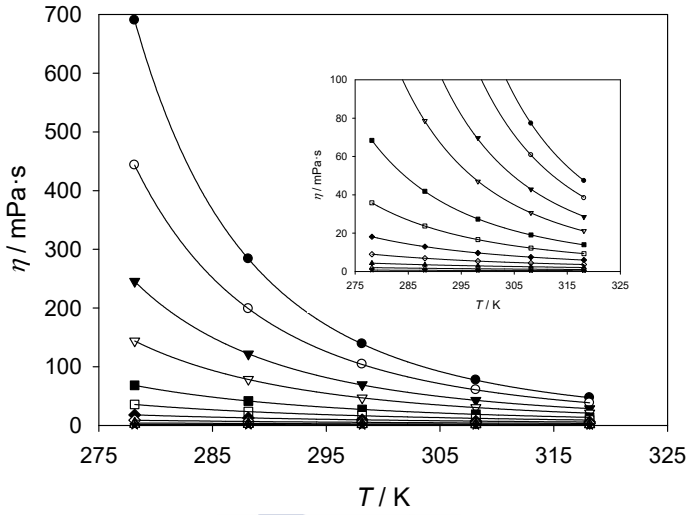

Figure 4.18. Viscosity η for the binary system [C_2mim][OAc] + methanol, at atmospheric pressure and as a function of temperature (T), at different mole fractions of [C_2mim][OAc] (x_{IL}): ★, 0.00; △, 0.10; ▲, 0.20; ◇, 0.30; ◆, 0.40; □, 0.50; ■, 0.60; ▽, 0.70; ▼, 0.80; ○, 0.90; ●, 1.00. (For a greater degree of precision of the mole fractions, please refer to Table 4.3.) The inset plot provides a detailed view of the low viscosity range (below 100 mPa·s). Solid lines correspond to the correlation by means of the VFT equation ($x_{IL} \geq 0.10$) or the Andrade equation ($x_{IL} = 0.00$).

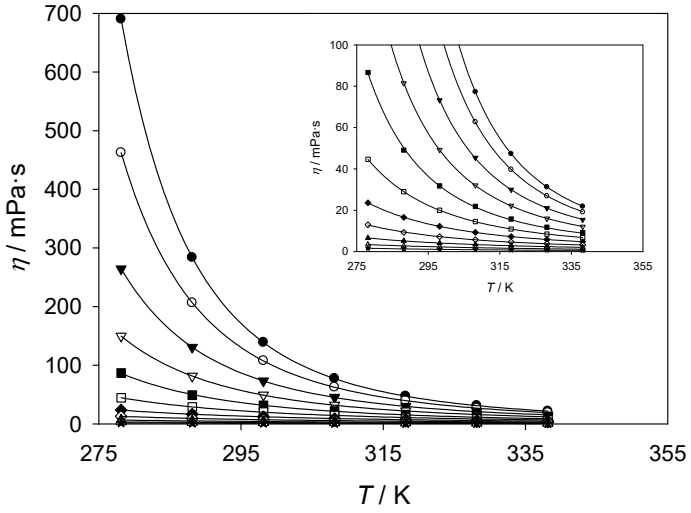

Figure 4.19. Viscosity η for the binary system [C_2mim][OAc] + ethanol, at atmospheric pressure and as a function of temperature (T), at different mole fractions of [C_2mim][OAc] (x_{IL}): ★, 0.00; △, 0.10; ▲, 0.20; ◇, 0.30; ◆, 0.40; □, 0.50; ■, 0.60; ▽, 0.70; ▼, 0.80; ○, 0.90; ●, 1.00. (For a greater degree of precision of the mole fractions, please refer to Table 4.4.) The inset plot provides a detailed view of the low viscosity range (below 100 mPa·s). Solid lines correspond to the correlation by means of the VFT equation ($x_{IL} \geq 0.20$) or the Andrade equation ($x_{IL} \leq 0.10$).

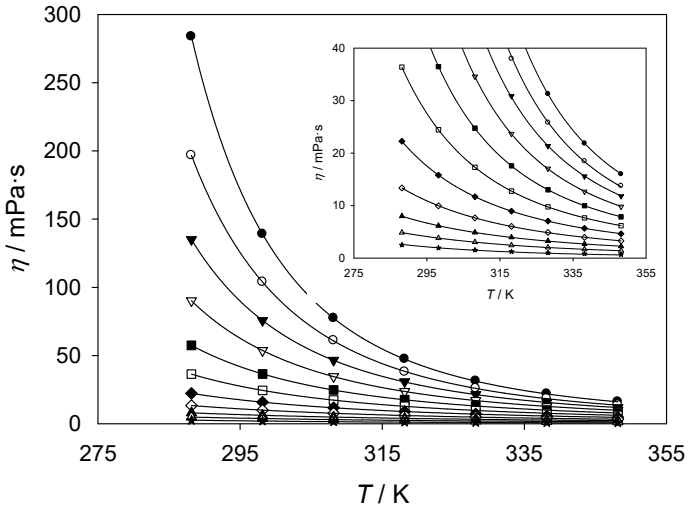

Figure 4.20. Viscosity η for the binary system [C_2mim][OAc] + 1-propanol, at atmospheric pressure and as a function of temperature (T), at different mole fractions of [C_2mim][OAc] (x_{IL}): ★, 0.00; Δ, 0.10; ▲, 0.20; ◇, 0.30; ◆, 0.40; □, 0.50; ■, 0.60; ▽, 0.70; ▼, 0.80; ○, 0.90; ●, 1.00. (For a greater degree of precision of the mole fractions, please refer to Table 4.5.) The inset plot provides a detailed view of the low viscosity range (below 40 mPa·s). Solid lines correspond to the correlation by means of the VFT equation ($x_{IL} \geq 0.20$) or the Andrade equation ($x_{IL} \leq 0.10$).

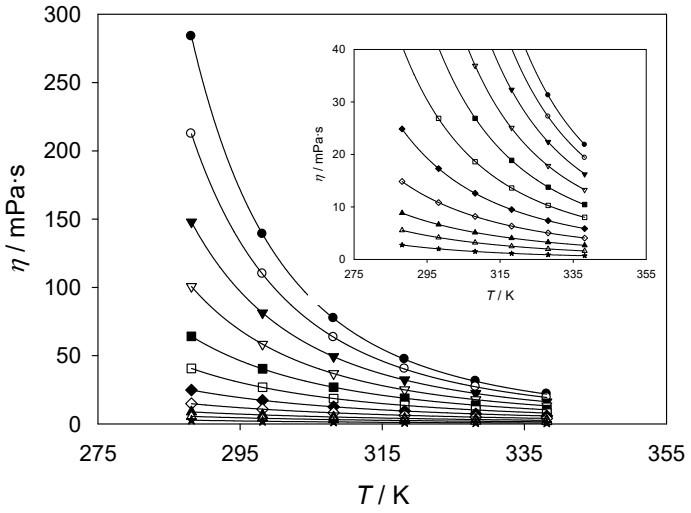

Figure 4.21. Viscosity η for the binary system [C_2mim][OAc] + 2-propanol, at atmospheric pressure and as a function of temperature (T), at different mole fractions of [C_2mim][OAc] (x_{IL}): ★, 0.00; Δ, 0.10; ▲, 0.20; ◇, 0.30; ◆, 0.40; □, 0.50; ■, 0.60; ▽, 0.70; ▼, 0.80; ○, 0.90; ●, 1.00. (For a greater degree of precision of the mole fractions, please refer to Table 4.6.) The inset plot provides a detailed view of the low viscosity range (below 40 mPa·s). Solid lines correspond to the correlation by means of the VFT equation ($x_{IL} \geq 0.20$) or the Andrade equation ($x_{IL} \leq 0.10$).

Table 4.8. Fit parameters (η_∞, E_a, A, k, T_0) of the Andrade equation (Equation 4.23) and of the VFT equation (Equation 4.24) for the correlation of viscosity as a function of temperature in the binary systems [C$_2$mim][OAc] + (methanol, ethanol, 1-propanol, or 2-propanol), at different mole fractions of [C$_2$mim][OAc] (x_{IL}). The corresponding relative standard deviations (SD_{rel}), calculated according to Equation 4.25, are also shown.

x_{IL}	Andrade equation ‡			VFT equation ‡,‖			
	η_∞ x 10^3	E_a	SD_{rel}	A x 10^3	k	T_0	SD_{rel}
			[C$_2$mim][OAc] + methanol				
0.0000	9.074	-10.09	0.00	-	-	-	-
0.1000	10.09	-12.25	0.01	1.223	975.0	66.07	0.008
0.2000	11.93	-13.64	0.01	2.383	911.6	84.06	0.001
0.3000	5.835	-16.97	0.02	4.936	718.2	125.2	0.002
0.4000	21.06	-20.94	1.16	5.141	758.9	136.4	0.000
0.5000	0.546	-25.63	0.04	6.068	740.8	151.9	0.001
0.6000	0.119	-30.64	0.05	5.365	796.4	158.2	0.001
0.6999	0.012	-37.69	0.09	5.942	775.2	171.1	0.002
0.8003	0.002	-43.02	0.13	9.829	674.3	185.9	0.006
0.9003	0.000	-49.76	0.15	8.905	702.2	190.4	0.004
1.0000	0.000	-55.54	0.26	8.590	708.6	194.6	0.001
			[C$_2$mim][OAc] + ethanol				
0.0000	4.142	-13.77	0.01	-	-	-	-
0.1000	8.161	-13.95	0.00	-	-	-	-
0.2000	8.585	-15.34	0.01	1.316	1205	66.76	0.000
0.3000	3.802	-18.77	0.04	3.055	894.2	116.5	0.016
0.4000	2.036	-21.62	0.04	3.736	894.2	127.6	0.001
0.4999	0.531	-26.10	0.07	5.161	808.8	148.8	0.002
0.5998	0.066	-32.52	0.17	6.077	747.0	167.4	0.029
0.7001	0.019	-36.68	0.19	7.039	747.0	173.7	0.006
0.7990	0.002	-42.72	0.31	8.136	719.6	183.2	0.005
0.9000	0.000	-49.33	0.46	8.460	715.6	189.8	0.005
1.0000	0.000	-54.93	0.63	8.459	711.4	194.4	0.002
			[C$_2$mim][OAc] + 1-propanol				
0.0000	1.380	-17.98	0.00	-	-	-	-
0.1017	3.611	-17.26	0.00	-	-	-	-
0.2004	5.008	-17.65	0.01	0.812	1418	65.29	0.007
0.3001	3.387	-19.82	0.02	1.295	1267	90.48	0.005
0.3998	1.812	-22.53	0.04	3.118	959.0	129.4	0.002
0.4997	0.717	-25.93	0.06	4.182	877.8	147.5	0.002
0.5996	0.256	-29.49	0.08	4.503	867.0	157.2	0.001
0.6998	0.074	-33.53	0.12	5.609	809.7	170.0	0.003
0.8002	0.021	-37.49	0.17	6.017	795.7	177.4	0.005
0.8991	0.005	-41.76	0.23	5.002	837.5	180.1	0.009
1.0000	0.001	-46.42	0.33	7.945	725.0	193.4	0.002
			[C$_2$mim][OAc] + 2-propanol				
0.0000	0.268	-22.13	0.00	-	-	-	-
0.1000	1.268	-20.08	0.00	-	-	-	-
0.2000	2.512	-19.55	0.01	0.798	1329	83.12	0.002
0.3000	2.017	-21.32	0.02	1.566	1145	107.2	0.001
0.4000	1.059	-24.09	0.03	2.899	962.7	133.5	0.001
0.5000	0.411	-27.53	0.05	4.168	866.4	151.8	0.002
0.5998	0.159	-30.91	0.06	2.895	997.4	149.1	0.003
0.7000	0.037	-35.44	0.10	6.952	744.4	177.8	0.003
0.7993	0.012	-39.04	0.13	6.983	755.6	182.2	0.003
0.9000	0.003	-43.12	0.18	8.251	719.0	190.0	0.004
1.0000	0.001	-46.79	0.23	8.029	722.8	193.6	0.001

‡ Units: η_∞, in mPa·s; E_a, in kJ·mol^{-1}; A, in mPa·s·K$^{-0.5}$; k and T_0, in K.

‖ Abnormally low values of T_0 were obtained when attempting to correlate with the VFT equation the data series with x_{IL} = 0.00 (pure alcohol) and x_{IL} = 0.10. These correlations were discarded.

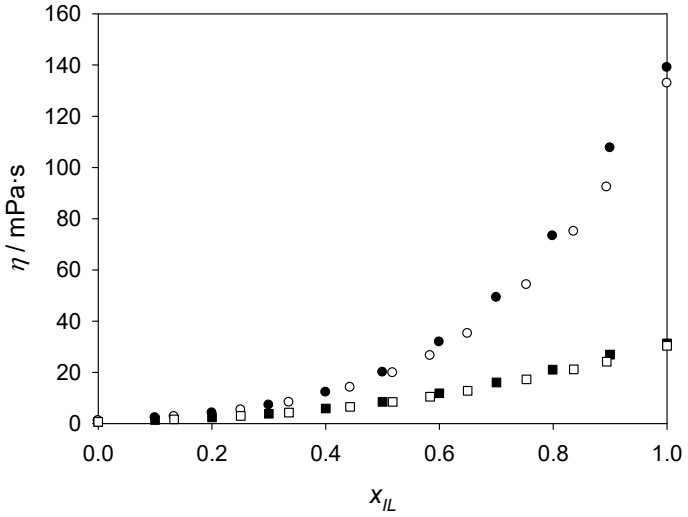

Figure 4.22. Comparison of the experimental dynamic viscosity data (η) reported for the binary system [C_2mim][OAc] + ethanol in this work (solid symbols) and those reported by Quijada-Maldonado et al. (2012) (open symbols), as a function of the mole fraction of ionic liquid (x_{IL}), at atmospheric pressure and at the temperatures 298.15 K (circles) and 328.15 K (squares).

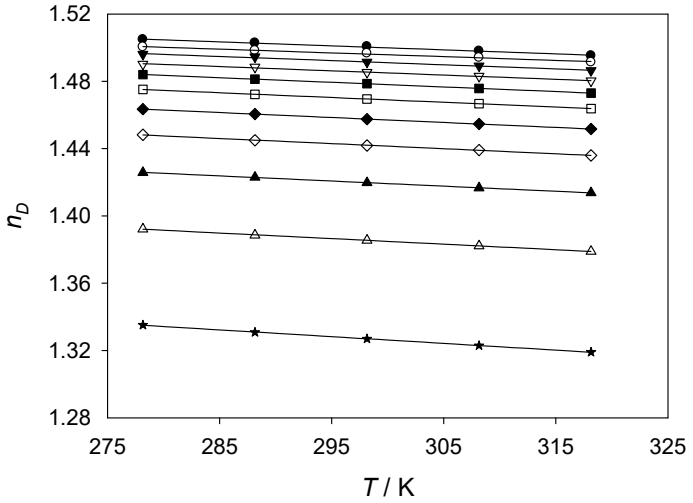

Figure 4.23. Refractive index (n_D) for the binary system [C_2mim][OAc] + methanol, at atmospheric pressure and as a function of temperature (T), at different mole fractions of [C_2mim][OAc] (x_{IL}): ★, 0.00; △, 0.10; ▲, 0.20; ◇, 0.30; ◆, 0.40; □, 0.50; ■, 0.60; ▽, 0.70; ▼, 0.80; ○, 0.90; ●, 1.00. (For a greater degree of precision of the mole fractions, please refer to Table 4.3.) Solid lines correspond to linear fits.

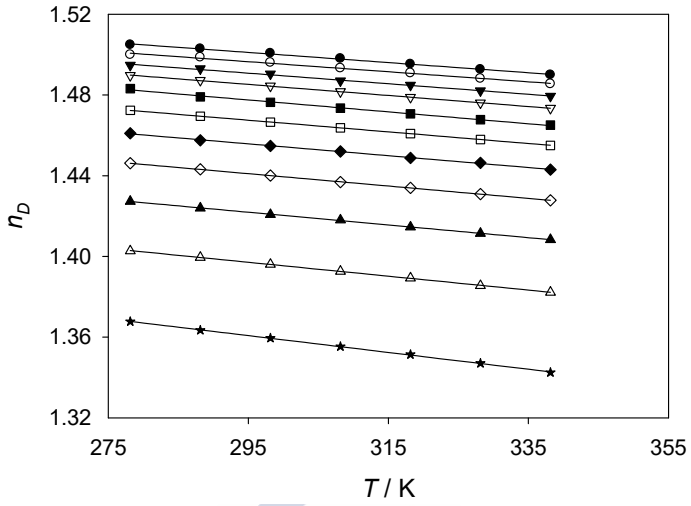

Figure 4.24. Refractive index (n_D) for the binary system [C_2mim][OAc] + ethanol, at atmospheric pressure and as a function of temperature (T), at different mole fractions of [C_2mim][OAc] (x_{IL}): ★, 0.00; △, 0.10; ▲, 0.20; ◇, 0.30; ◆, 0.40; □, 0.50; ■, 0.60; ▽, 0.70; ▼, 0.80; ○, 0.90; ●, 1.00. (For a greater degree of precision of the mole fractions, please refer to Table 4.4.) Solid lines correspond to linear fits.

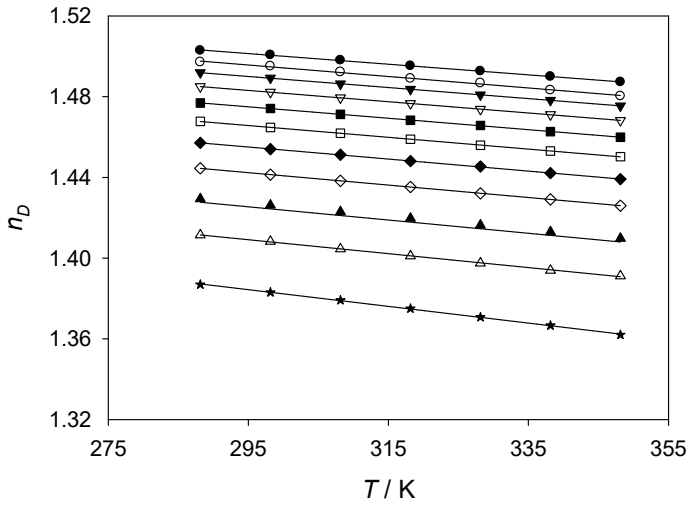

Figure 4.25. Refractive index (n_D) for the binary system [C_2mim][OAc] + 1-propanol, at atmospheric pressure and as a function of temperature (T), at different mole fractions of [C_2mim][OAc] (x_{IL}): ★, 0.00; △, 0.10; ▲, 0.20; ◇, 0.30; ◆, 0.40; □, 0.50; ■, 0.60; ▽, 0.70; ▼, 0.80; ○, 0.90; ●, 1.00. (For a greater degree of precision of the mole fractions, please refer to Table 4.5.) Solid lines correspond to linear fits.

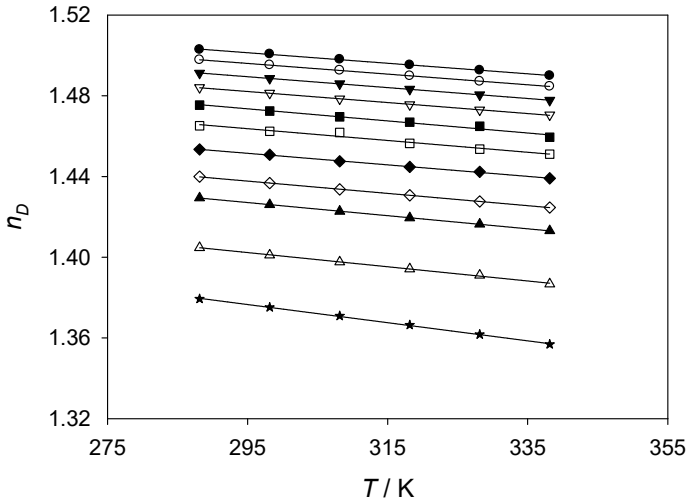

Figure 4.26. Refractive index (n_D) for the binary system [C_2mim][OAc] + 2-propanol, at atmospheric pressure and as a function of temperature (T), at different mole fractions of [C_2mim][OAc] (x_{IL}): ★, 0.00; △, 0.10; ▲, 0.20; ◇, 0.30; ◆, 0.40; □, 0.50; ■, 0.60; ▽, 0.70; ▼, 0.80; ○, 0.90; ●, 1.00. (For a greater degree of precision of the mole fractions, please refer to Table 4.6.) Solid lines correspond to linear fits.

The evolution of the surface tension of mixtures of [C_2mim][OAc]+(methanol, ethanol, 1-propanol, or 2-propanol) with temperature at different compositions covering the entire composition range is shown in Figures 4.27 to 4.30. Analogously to what was described for the refractive index, the apparent linear trend observed for the surface tension with temperature for all binary systems studied was confirmed by means of the F-test, and a straight line was used to correlate the experimental data of surface tension with temperature (Equation 4.21). Least-squares regressions led to the fit parameters listed in Table 4.9. The quality of the proposed fits for correlation of the experimental data can be graphically corroborated in Figures 4.27 to 4.30.

Table 4.9. Fit parameters (b_0, b_1, c_0, c_1) of the linear fits of refractive index (n_D) and surface tension (σ), for the correlation of these properties as a function of temperature at different mole fractions of ionic liquid (x_{IL}) in the binary systems [C_2mim][OAc] + (methanol, ethanol, 1-propanol, or 2-propanol), according to Equations 4.20 and 4.21. The corresponding standard deviations (SD_{nD} for the correlation of refractive index and SD_σ for the correlation of surface tension) are also shown.

x_{IL}	Fit parameters and standard deviations ‡					
	b_0	$b_1 \times 10^4$	SD_{nD}	c_0	$c_1 \times 10^2$	SD_σ
			[C_2mim][OAc] + methanol			
0.0000	1.44657	-4.01000	0.00012	44.32	-7.28	0.2
0.1000	1.48392	-3.30100	0.00012	44.40	-5.68	<0.1
0.2000	1.51050	-3.04200	0.00011	47.22	-5.23	<0.1
0.3000	1.53253	-3.03500	0.00015	49.33	-4.84	<0.1
0.4000	1.54553	-2.95000	0.00005	51.17	-4.59	<0.1
0.5000	1.55391	-2.83100	0.00002	51.88	-4.15	<0.1
0.6000	1.56051	-2.74900	0.00005	53.41	-4.10	<0.1
0.7000	1.56081	-2.52700	0.00033	57.45	-4.74	<0.1
0.8003	1.56524	-2.47200	0.00042	58.71	-4.68	0.2
0.9003	1.56248	-2.22300	0.00041	63.71	-5.61	<0.1
1.0000	1.57177	-2.39600	0.00032	62.04	-5.00	<0.1
			[C_2mim][OAc] + ethanol			
0.0000	1.48364	-4.16500	0.00021	44.63	-7.60	0.1
0.1000	1.49863	-3.44179	0.00014	43.16	-6.22	0.2
0.2000	1.51483	-3.15036	0.00015	42.59	-4.96	<0.1
0.3000	1.53122	-3.05857	0.00008	44.39	-4.73	<0.1
0.4000	1.54236	-2.93500	0.00024	46.53	-4.63	<0.1
0.4999	1.55266	-2.88714	0.00005	47.88	-4.30	<0.1
0.5998	1.56447	-2.94786	0.00040	49.31	-4.07	<0.1
0.7001	1.56600	-2.73857	0.00011	51.40	-4.01	0.1
0.7990	1.56802	-2.61786	0.00037	52.56	-3.60	0.2
0.9000	1.56992	-2.49000	0.00045	57.41	-4.30	0.1
1.0000	1.57531	-2.51679	0.00033	60.68	-4.54	<0.1
			[C_2mim][OAc] + 1-propanol			
0.0000	1.50648	-4.13929	0.00019	48.6	-8.48	<0.1
0.1017	1.51090	-3.45036	0.00018	47.2	-7.36	<0.1
0.2004	1.52215	-3.27886	0.00156	45.3	-6.26	<0.1
0.3001	1.53313	-3.07750	0.00003	42.5	-4.46	<0.1
0.3998	1.54306	-2.98357	0.00010	42.9	-3.96	<0.1
0.4997	1.55180	-2.91893	0.00005	47.2	-4.71	<0.1
0.5996	1.55848	-2.83107	0.00006	52.2	-5.84	<0.1
0.6998	1.56545	-2.79250	0.00004	52.2	-5.03	<0.1
0.8002	1.57085	-2.74071	0.00003	53.1	-4.51	<0.1
0.8991	1.57952	-2.84214	0.00026	54.1	-3.81	<0.1
1.0000	1.57906	-2.63464	0.00012	59.6	-4.20	<0.1
			[C_2mim][OAc] + 2-propanol			
0.0000	1.50920	-4.49629	0.00022	46.1	-8.37	<0.1
0.1000	1.50610	-3.51829	0.00022	44.9	-7.30	<0.1
0.2000	1.52301	-3.25143	0.00005	42.0	-5.68	<0.1
0.3000	1.52745	-3.04200	0.00006	41.5	-4.85	<0.1
0.4000	1.53574	-2.85629	0.00015	43.9	-5.03	<0.1
0.5000	1.54983	-2.92029	0.00074	45.9	-4.99	<0.1
0.5998	1.56192	-2.99629	0.00061	45.7	-4.40	<0.1
0.7000	1.56261	-2.72943	0.00012	47.3	-4.27	<0.1
0.7993	1.56898	-2.69686	0.00004	47.1	-3.24	<0.1
0.9000	1.57403	-2.64486	0.00006	51.7	-3.63	<0.1
1.0000	1.57831	-2.61000	0.00012	60.3	-4.42	<0.1

‡ Units: b_0 and SD_{nD}, dimensionless; b_1, in K^{-1}; c_0 and SD_σ, in $mN \cdot m^{-1}$; c_1, in $mN \cdot m^{-1} \cdot K^{-1}$.

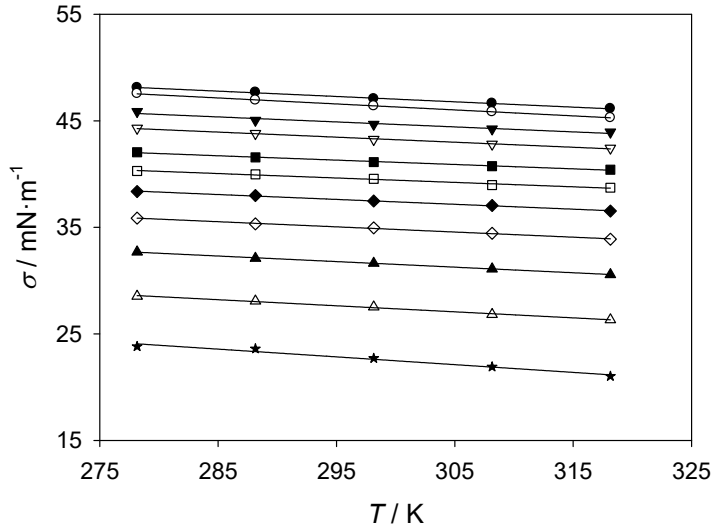

Figure 4.27. Surface tension (σ) for the binary system [C_2mim][OAc] + methanol, at atmospheric pressure and as a function of temperature (T), at different mole fractions of [C_2mim][OAc] (x_{IL}): ★, 0.00; △, 0.10; ▲, 0.20; ◇, 0.30; ◆, 0.40; □, 0.50; ■, 0.60; ▽, 0.70; ▼, 0.80; ○, 0.90; ●, 1.00. (For a greater degree of precision of the mole fractions, please refer to Table 4.2.) Solid lines correspond to linear fits.

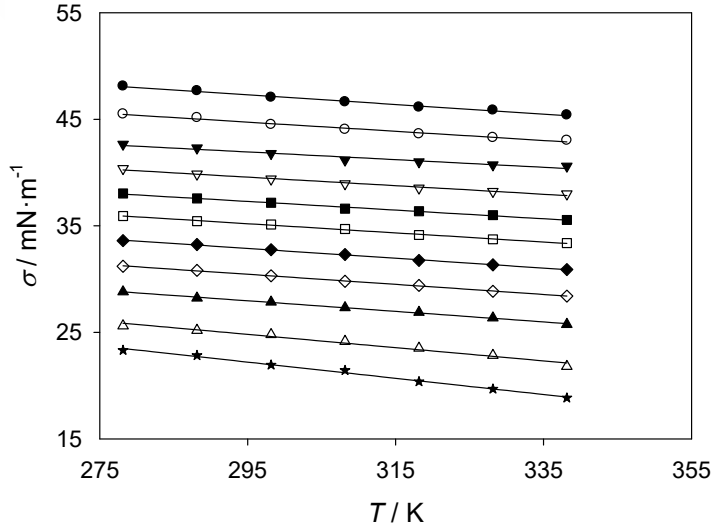

Figure 4.28. Surface tension (σ) for the binary system [C_2mim][OAc] + ethanol, at atmospheric pressure and as a function of temperature (T), at different mole fractions of [C_2mim][OAc] (x_{IL}): ★, 0.00; △, 0.10; ▲, 0.20; ◇, 0.30; ◆, 0.40; □, 0.50; ■, 0.60; ▽, 0.70; ▼, 0.80; ○, 0.90; ●, 1.00. (For a greater degree of precision of the mole fractions, please refer to Table 4.3.) Solid lines correspond to linear fits.

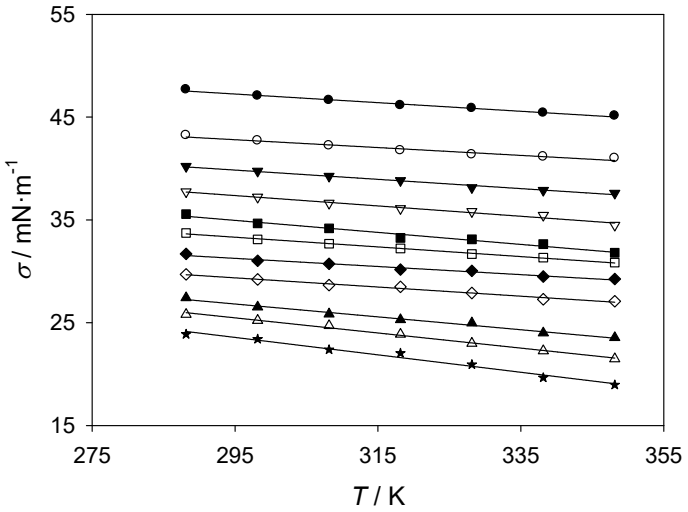

Figure 4.29. Surface tension (σ) for the binary system [C_2mim][OAc] + 1-propanol, at atmospheric pressure and as a function of temperature (T), at different mole fractions of [C_2mim][OAc] (x_{IL}): ★, 0.00; △, 0.10; ▲, 0.20; ◇, 0.30; ◆, 0.40; □, 0.50; ■, 0.60; ▽, 0.70; ▼, 0.80; ○, 0.90; ●, 1.00. (For a greater degree of precision of the mole fractions, please refer to Table 4.4.) Solid lines correspond to linear fits.

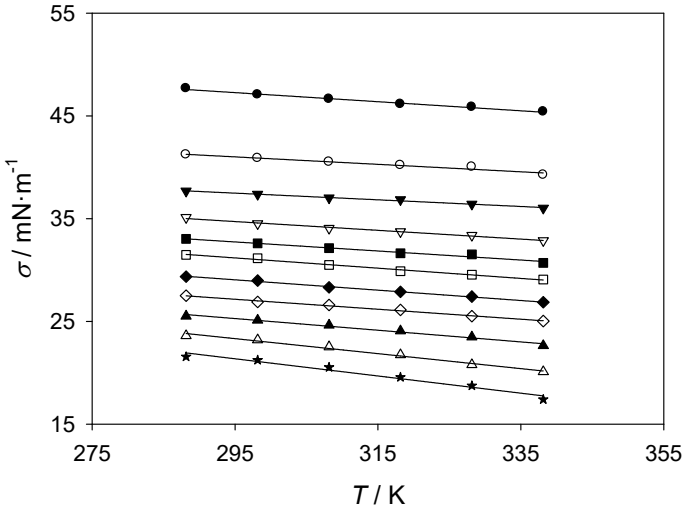

Figure 4.30. Surface tension (σ) for the binary system [C_2mim][OAc] + 2-propanol, at atmospheric pressure and as a function of temperature (T), at different mole fractions of [C_2mim][OAc] (x_{IL}): ★, 0.00; △, 0.10; ▲, 0.20; ◇, 0.30; ◆, 0.40; □, 0.50; ■, 0.60; ▽, 0.70; ▼, 0.80; ○, 0.90; ●, 1.00. (For a greater degree of precision of the mole fractions, please refer to Table 4.5.) Solid lines correspond to linear fits.

Effect of composition

Excess properties and property changes of mixing are suitable for a detailed analysis of the effect of composition on the thermophysical properties of a fluid system. For the case of the thermophysical properties studied herein, the excess molar volume (V^E), viscosity logarithm change of mixing ($\Delta\ln(\eta/\eta_0)$), molar refraction change of mixing (ΔR_M), and surface tension change of mixing ($\Delta\sigma$) were calculated from the data in Tables 4.3 to 4.6 for all binary systems studied, by means of Equations 4.15 to 4.18, with auxiliary use of Equations 4.2 and 4.5 for intermediate calculation of molar volumes and molar refractions. Tables 4.10 to 4.13 report the numerical values of V^E, $\Delta\ln(\eta/\eta_0)$, ΔR_M, and $\Delta\sigma$.

Figures 4.31 to 4.34 show the excess molar volumes of the binary systems, as a function of the ionic liquid mole fraction in the mixtures, for the different isotherms experimentally investigated. All excess molar volumes are negative, over the entire composition range, at all the investigated temperatures, and for all binary systems studied. This is an indication of the existence of attractive forces at a molecular level between the ionic liquid and the alcohol, among which hydrogen bonding and ion-dipole interactions (Zafarani-Moattar and Shekaari, 2005) are probably predominating. This type of interaction would be expected to weaken with increasing temperature and consequently diminish the absolute value of V^E; however, the opposite is observed (Figures 4.31 to 4.34). This is likely due to the contribution of a second factor: the increment of molar volumes of the pure compounds (both ionic liquid and alcohol) when temperature is increased, in the temperature ranges investigated. This increment in the V_i values is speculated to facilitate a more compact spatial arrangement of the species in the liquid mixture. With this effect occurring at a faster pace than the weakening of the attractive interactions mentioned above, the overall effect would be an increase in the absolute value of the excess molar volume (i.e., V^E becoming more negative) with an increase in temperature, as it is in fact observed. The minima of V^E in the isotherms is located approximately in the range of 0.25-0.30 in mole fraction of ionic liquid, thus suggesting that the combination of attractive forces and spatial enhanced arrangement is maximised at this particular composition range.

Table 4.10. Excess molar volume (V^E), viscosity logarithm change of mixing ($\Delta\ln(\eta/\eta^0)$), molar refraction change of mixing (ΔR_M), and surface tension change of mixing ($\Delta\sigma$) for the binary system [C_2mim][OAc] + methanol, at atmospheric pressure and different temperatures (T), as a function of the mole fraction of [C_2mim][OAc] (x_{IL}).

x_{IL}	T / K				
	278.15	288.15	298.15	308.15	318.15
	V^E / cm³·mol⁻¹				
0.0000	0.000	0.000	0.000	0.000	0.000
0.1000	-0.884	-0.948	-1.018	-1.093	-1.179
0.2000	-1.154	-1.230	-1.313	-1.404	-1.505
0.3000	-1.181	-1.262	-1.345	-1.434	-1.535
0.4000	-1.103	-1.179	-1.253	-1.333	-1.425
0.5000	-0.967	-1.036	-1.101	-1.170	-1.249
0.6000	-0.797	-0.859	-0.912	-0.968	-1.033
0.7000	-0.618	-0.676	-0.720	-0.762	-0.813
0.8003	-0.402	-0.451	-0.483	-0.513	-0.549
0.9003	-0.213	-0.228	-0.256	-0.273	-0.294
1.0000	0.000	0.000	0.000	0.000	0.000
	$\Delta\ln(\eta/\eta^0)$				
0.0000	0.000	0.000	0.000	0.000	0.000
0.1000	0.353	0.401	0.404	0.435	0.462
0.2000	0.435	0.520	0.585	0.634	0.676
0.3000	0.476	0.578	0.648	0.712	0.758
0.4000	0.486	0.596	0.674	0.731	0.777
0.5000	0.480	0.586	0.657	0.711	0.749
0.6000	0.439	0.540	0.600	0.644	0.675
0.6999	0.496	0.557	0.584	0.607	0.618
0.8003	0.339	0.379	0.421	0.430	0.438
0.9003	0.243	0.256	0.269	0.270	0.264
1.0000	0.000	0.000	0.000	0.000	0.000
	ΔR_M				
0.0000	0.000	0.000	0.000	0.000	0.000
0.1000	0.018	0.016	0.019	0.020	0.025
0.2000	0.034	0.041	0.032	0.033	0.043
0.3000	0.061	0.044	0.026	0.038	0.034
0.4000	0.059	0.044	0.022	0.026	0.025
0.5000	0.074	0.050	0.033	0.036	0.038
0.6000	0.074	0.050	0.032	0.031	0.038
0.6999	0.026	0.045	-0.005	0.025	0.029
0.8003	0.024	0.058	0.001	0.026	0.032
0.9003	-0.017	-0.026	0.017	0.023	0.025
1.0000	0.000	0.000	0.000	0.000	0.000
	$\Delta\sigma$ / mN·m⁻¹				
0.0000	0.0	0.0	0.0	0.0	0.0
0.1000	2.3	2.1	2.4	2.4	2.8
0.2000	4.0	3.7	4.0	4.3	4.6
0.3000	4.8	4.5	5.0	5.2	5.4
0.4000	4.9	4.8	5.0	5.3	5.5
0.5000	4.3	4.3	4.7	4.8	5.2
0.6000	3.7	3.5	3.8	4.1	4.3
0.6999	3.5	3.3	3.5	3.6	3.8
0.8003	2.7	2.2	2.5	2.5	2.8
0.9003	1.9	1.6	1.7	1.8	1.7
1.0000	0.0	0.0	0.0	0.0	0.0

Table 4.11. Excess molar volume (V^E), viscosity logarithm change of mixing ($\Delta\ln(\eta/\eta^0)$), molar refraction change of mixing (ΔR_M), and surface tension change of mixing ($\Delta\sigma$) for the binary system [C_2mim][OAc] + ethanol, at atmospheric pressure and different temperatures (T), as a function of the mole fraction of [C_2mim][OAc] (x_{IL}).

x_1	T / K						
	278.15	288.15	298.15	308.15	318.15	328.15	338.15
	V^E / cm^3·mol^{-1}						
0.0000	0.000	0.000	0.000	0.000	0.000	0.000	0.000
0.1000	-0.620	-0.681	-0.747	-0.821	-0.907	-1.006	-1.123
0.2000	-0.817	-0.895	-0.977	-1.070	-1.177	-1.302	-1.449
0.3000	-0.898	-0.980	-1.065	-1.160	-1.270	-1.398	-1.547
0.4000	-0.832	-0.911	-0.989	-1.078	-1.180	-1.299	-1.439
0.4999	-0.761	-0.835	-0.905	-0.983	-1.074	-1.180	-1.303
0.5998	-0.651	-0.720	-0.781	-0.845	-0.922	-1.011	-1.115
0.7001	-0.488	-0.554	-0.609	-0.671	-0.737	-0.808	-0.889
0.7990	-0.343	-0.394	-0.441	-0.477	-0.520	-0.570	-0.627
0.9000	-0.192	-0.208	-0.239	-0.260	-0.285	-0.313	-0.345
1.0000	0.000	0.000	0.000	0.000	0.000	0.000	0.000
	$\Delta\ln(\eta/\eta^0)$						
0.0000	0.000	0.000	0.000	0.000	0.000	0.000	0.000
0.1000	0.156	0.204	0.254	0.295	0.332	0.364	0.394
0.2000	0.205	0.293	0.373	0.439	0.493	0.543	0.589
0.3000	0.279	0.346	0.439	0.511	0.574	0.625	0.671
0.4000	0.272	0.388	0.481	0.551	0.609	0.657	0.699
0.4999	0.301	0.408	0.492	0.552	0.602	0.642	0.677
0.5998	0.358	0.398	0.469	0.520	0.556	0.585	0.612
0.7001	0.295	0.365	0.419	0.456	0.483	0.496	0.513
0.7990	0.262	0.306	0.336	0.363	0.375	0.384	0.393
0.9000	0.207	0.220	0.230	0.237	0.237	0.238	0.237
1.0000	0.000	0.000	0.000	0.000	0.000	0.000	0.000
	ΔR_M						
0.0000	0.000	0.000	0.000	0.000	0.000	0.000	0.000
0.1000	0.022	0.037	0.032	0.038	0.042	0.038	0.056
0.2000	0.044	0.040	0.031	0.058	0.044	0.056	0.067
0.3000	0.073	0.068	0.054	0.054	0.063	0.066	0.072
0.4000	0.119	0.084	0.075	0.094	0.081	0.112	0.095
0.4999	0.126	0.102	0.079	0.088	0.093	0.092	0.093
0.5998	0.212	0.112	0.092	0.096	0.097	0.094	0.104
0.7001	0.149	0.134	0.100	0.100	0.100	0.100	0.110
0.7990	0.051	0.073	0.046	0.006	0.047	0.045	0.047
0.9000	0.004	0.062	0.029	0.022	0.045	0.040	0.046
1.0000	0.000	0.000	0.000	0.000	0.000	0.000	0.000
	$\Delta\sigma$ / mN·m^{-1}						
0.0000	0.0	0.0	0.0	0.0	0.0	0.0	0.0
0.1000	-0.2	-0.1	0.3	0.2	0.6	0.5	0.3
0.2000	0.5	0.4	0.9	0.8	1.4	1.4	1.6
0.3000	0.4	0.5	0.8	0.8	1.3	1.3	1.6
0.4000	0.4	0.5	0.8	0.8	1.1	1.2	1.4
0.4999	0.2	0.2	0.6	0.7	0.9	1.0	1.2
0.5998	-0.2	-0.2	0.2	0.1	0.6	0.6	0.8
0.7001	-0.3	-0.4	-0.1	-0.1	0.1	0.2	0.5
0.7990	-0.5	-0.4	-0.2	-0.4	0.0	0.1	0.5
0.9000	-0.1	0.0	0.0	-0.1	0.1	0.0	0.3
1.0000	0.0	0.0	0.0	0.0	0.0	0.0	0.0

Table 4.12. Excess molar volume (V^E), viscosity logarithm change of mixing ($\Delta\ln(\eta/\eta^0)$), molar refraction change of mixing (ΔR_M), and surface tension change of mixing ($\Delta\sigma$) for the binary system [C_2mim][OAc] + 1-propanol, at atmospheric pressure and different temperatures (T), as a function of the mole fraction of [C_2mim][OAc] (x_{IL}).

x_{IL}	T / K						
	288.15	298.15	308.15	318.15	328.15	338.15	348.15
	V^E / cm³·mol⁻¹						
0.0000	0.000	0.000	0.000	0.000	0.000	0.000	0.000
0.1017	-0.511	-0.565	-0.628	-0.704	-0.794	-0.903	-1.033
0.2004	-0.618	-0.686	-0.765	-0.860	-0.975	-1.114	-1.283
0.3001	-0.651	-0.722	-0.804	-0.903	-1.022	-1.166	-1.340
0.3998	-0.647	-0.714	-0.792	-0.887	-1.000	-1.136	-1.299
0.4997	-0.606	-0.669	-0.739	-0.824	-0.925	-1.046	-1.190
0.5996	-0.539	-0.593	-0.652	-0.723	-0.809	-0.911	-1.032
0.6998	-0.437	-0.481	-0.526	-0.582	-0.649	-0.729	-0.823
0.8002	-0.313	-0.347	-0.377	-0.417	-0.463	-0.518	-0.582
0.8991	-0.144	-0.180	-0.199	-0.219	-0.244	-0.272	-0.306
1.0000	0.000	0.000	0.000	0.000	0.000	0.000	0.000
	$\Delta\ln(\eta/\eta^0)$						
0.0000	0.000	0.000	0.000	0.000	0.000	0.000	0.000
0.1017	0.183	0.238	0.279	0.316	0.347	0.378	0.405
0.2004	0.211	0.295	0.365	0.430	0.489	0.524	0.563
0.3001	0.254	0.350	0.426	0.491	0.547	0.582	0.625
0.3998	0.293	0.386	0.461	0.522	0.573	0.618	0.656
0.4997	0.312	0.396	0.461	0.513	0.555	0.593	0.625
0.5996	0.297	0.370	0.428	0.468	0.499	0.528	0.552
0.6998	0.273	0.328	0.370	0.401	0.425	0.440	0.457
0.8002	0.202	0.243	0.273	0.299	0.305	0.316	0.325
0.8991	0.111	0.139	0.157	0.147	0.155	0.164	0.168
1.0000	0.000	0.000	0.000	0.000	0.000	0.000	0.000
	ΔR_M						
0.0000	0.000	0.000	0.000	0.000	0.000	0.000	0.000
0.1017	0.016	0.026	0.015	0.024	0.029	0.023	0.076
0.2004	0.027	0.027	0.025	0.036	0.034	0.030	0.072
0.3001	0.045	0.034	0.037	0.048	0.050	0.054	0.065
0.3998	0.053	0.035	0.046	0.045	0.069	0.049	0.059
0.4997	0.052	0.029	0.035	0.036	0.035	0.037	0.051
0.5996	0.047	0.031	0.032	0.032	0.047	0.035	0.049
0.6998	0.056	0.029	0.031	0.037	0.029	0.040	0.041
0.8002	0.048	0.019	0.011	0.023	0.020	0.023	0.031
0.8991	-0.007	-0.001	-0.013	-0.044	-0.015	-0.073	-0.086
1.0000	0.000	0.000	0.000	0.000	0.000	0.000	0.000
	$\Delta\sigma$ / mN·m⁻¹						
0.0000	0.0	0.0	0.0	0.0	0.0	0.0	0.0
0.1017	-0.5	-0.6	-0.1	-0.6	-0.5	0.0	-0.1
0.2004	-1.2	-1.6	-1.4	-1.6	-1.0	-0.8	-0.7
0.3001	-1.3	-1.3	-1.0	-0.8	-0.5	-0.1	0.3
0.3998	-1.7	-1.8	-1.3	-1.5	-0.9	-0.5	-0.2
0.4997	-2.1	-2.1	-1.8	-1.9	-1.7	-1.2	-1.2
0.5996	-2.6	-2.9	-2.7	-3.2	-2.8	-2.5	-2.8
0.6998	-2.8	-2.8	-2.7	-2.8	-2.6	-2.2	-2.8
0.8002	-2.7	-2.6	-2.6	-2.5	-2.7	-2.4	-2.3
0.8991	-2.0	-2.0	-2.0	-2.0	-2.0	-1.7	-1.5
1.0000	0.0	0.0	0.0	0.0	0.0	0.0	0.0

Table 4.13. Excess molar volume (V^E), viscosity logarithm change of mixing ($\Delta\ln(\eta/\eta^0)$), molar refraction change of mixing (ΔR_M), and surface tension change of mixing ($\Delta\sigma$) for the binary system [C_2mim][OAc] + 2-propanol, at atmospheric pressure and different temperatures (T), as a function of the mole fraction of [C_2mim][OAc] (x_{IL}).

x_{IL}	T / K					
	288.15	298.15	308.15	318.15	328.15	338.15
	V^E / cm^{-3}·mol^{-1}					
0.0000	0.000	0.000	0.000	0.000	0.000	0.000
0.1000	-0.544	-0.626	-0.727	-0.851	-1.001	-1.184
0.2000	-0.641	-0.703	-0.829	-0.987	-1.182	-1.421
0.3000	-0.622	-0.727	-0.856	-1.018	-1.216	-1.459
0.4000	-0.632	-0.732	-0.853	-1.004	-1.189	-1.415
0.5000	-0.616	-0.705	-0.813	-0.946	-1.110	-1.308
0.5998	-0.566	-0.643	-0.734	-0.846	-0.983	-1.148
0.7000	-0.482	-0.545	-0.616	-0.704	-0.810	-0.939
0.7993	-0.344	-0.396	-0.445	-0.507	-0.581	-0.670
0.9000	-0.192	-0.228	-0.255	-0.289	-0.328	-0.375
1.0000	0.000	0.000	0.000	0.000	0.000	0.000
	$\Delta\ln(\eta/\eta^0)$					
0.0000	0.000	0.000	0.000	0.000	0.000	0.000
0.1000	0.238	0.303	0.360	0.409	0.448	0.488
0.2000	0.240	0.345	0.439	0.520	0.586	0.650
0.3000	0.295	0.411	0.511	0.592	0.664	0.728
0.4000	0.346	0.456	0.548	0.625	0.688	0.747
0.5000	0.376	0.472	0.545	0.612	0.664	0.715
0.5998	0.369	0.458	0.519	0.568	0.602	0.638
0.7000	0.354	0.403	0.441	0.479	0.504	0.529
0.7993	0.278	0.313	0.340	0.364	0.378	0.391
0.9000	0.174	0.188	0.195	0.212	0.216	0.223
1.0000	0.000	0.000	0.000	0.000	0.000	0.000
	ΔR_M					
0.0000	0.000	0.000	0.000	0.000	0.000	0.000
0.1000	0.026	0.020	0.027	0.045	0.079	0.059
0.2000	0.307	0.313	0.319	0.328	0.346	0.357
0.3000	0.075	0.061	0.065	0.081	0.088	0.099
0.4000	0.081	0.086	0.074	0.093	0.127	0.118
0.5001	0.082	0.079	0.216	0.077	0.078	0.109
0.5998	0.102	0.077	0.075	0.094	0.147	-0.019
0.7000	0.102	0.078	0.071	0.078	0.083	0.112
0.7994	0.076	0.054	0.059	0.069	0.063	0.068
0.9000	0.062	0.039	0.039	0.045	0.039	0.058
1.0000	0.000	0.000	0.000	0.000	0.000	0.000
	$\Delta\sigma$ / mN·m^{-1}					
0.0000	0.0	0.0	0.0	0.0	0.0	0.0
0.1000	-0.6	-0.6	-0.6	-0.5	-0.7	-0.1
0.2000	-1.3	-1.3	-1.1	-0.8	-0.7	-0.4
0.3000	-1.9	-2.1	-1.8	-1.4	-1.4	-0.8
0.4000	-2.7	-2.6	-2.7	-2.3	-2.2	-1.7
0.5000	-3.1	-3.0	-3.1	-3.0	-2.8	-2.3
0.5997	-4.2	-4.1	-4.1	-3.9	-3.5	-3.5
0.7000	-4.7	-4.8	-4.8	-4.4	-4.4	-4.1
0.7994	-4.8	-4.5	-4.4	-4.0	-4.0	-3.8
0.9000	-3.8	-3.6	-3.5	-3.3	-3.1	-3.3
1.0000	0.0	0.0	0.0	0.0	0.0	0.0

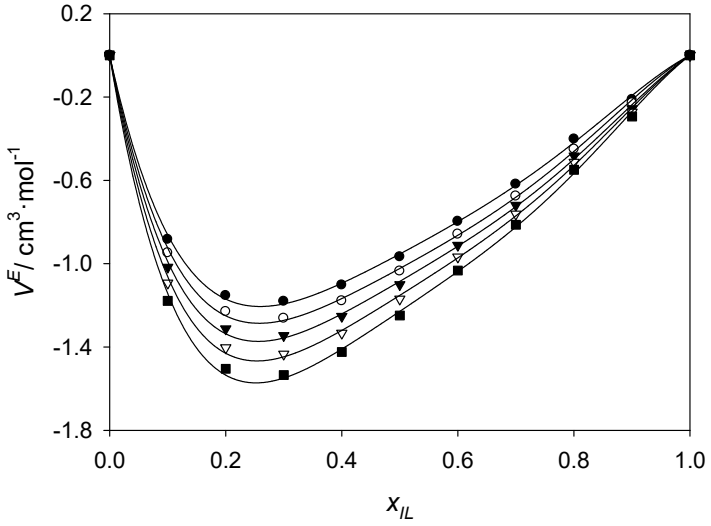

Figure 4.31. Excess molar volume (V^E) for the binary system [C_2mim][OAc] + methanol as a function of the mole fraction of [C_2mim][OAc] (x_{IL}) at different temperatures: : ●, 278.15 K; ○, 288.15 K; ▼, 298.15 K; ▽, 308.15 K; ■, 318.15 K. Solid lines represent the corresponding correlations by Redlich-Kister polynomials.

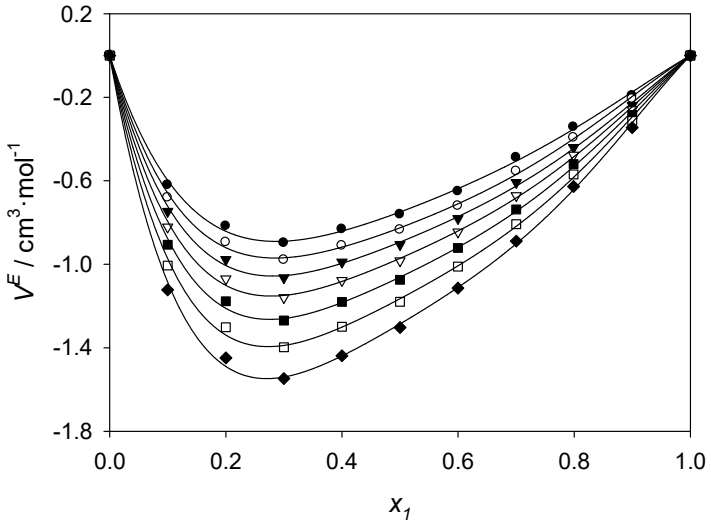

Figure 4.32. Excess molar volume (V^E) for the binary system [C_2mim][OAc] + ethanol as a function of the mole fraction of [C_2mim][OAc] (x_{IL}) at different temperatures: ●, 278.15 K; ○, 288.15 K; ▼, 298.15 K; ▽, 308.15 K; ■, 318.15 K; □, 328.15 K; ◆, 338.15 K. Solid lines represent the corresponding correlations by Redlich-Kister polynomials.

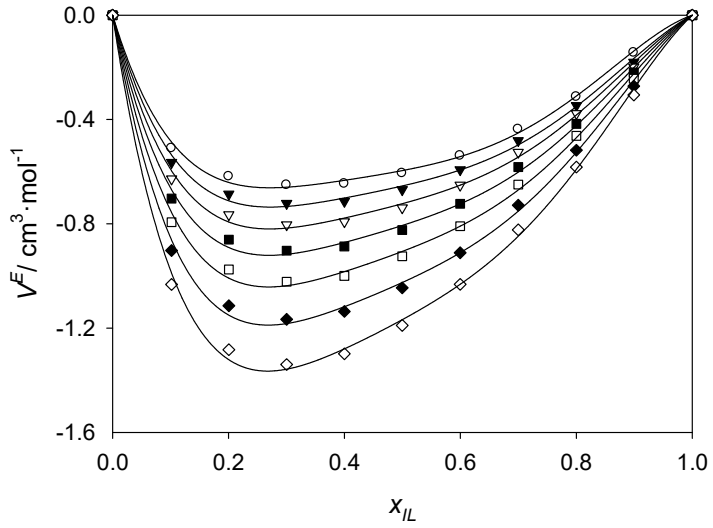

Figure 4.33. Excess molar volume (V^E) for the binary system [C_2mim][OAc] + 1-propanol as a function of the mole fraction of [C_2mim][OAc] (x_{IL}) at different temperatures: ○, 288.15 K; ▼, 298.15 K; ∇, 308.15 K; ■, 318.15 K; □, 328.15 K; ◆, 338.15 K; ◇, 348.15 K. Solid lines represent the corresponding correlations by Redlich-Kister polynomials.

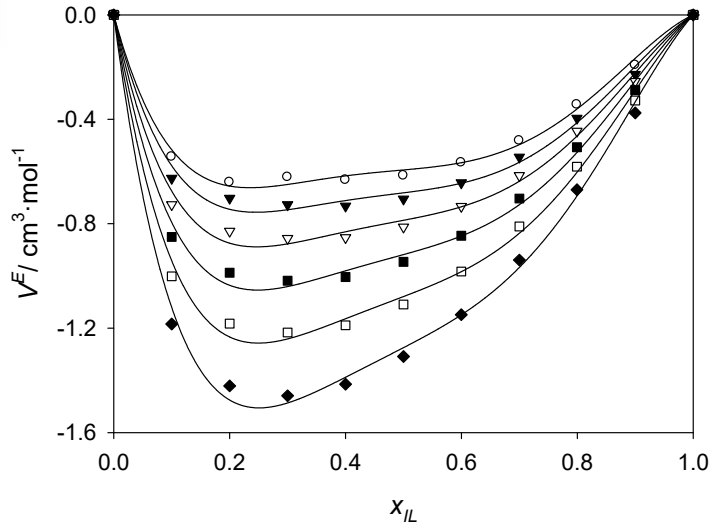

Figure 4.34. Excess molar volume (V^E) for the binary system [C_2mim][OAc] + 2-propanol as a function of the mole fraction of [C_2mim][OAc] (x_{IL}) at different temperatures: ○, 288.15 K; ▼, 298.15 K; ∇, 308.15 K; ■, 318.15 K; □, 328.15 K; ◆, 338.15 K. Solid lines represent the corresponding correlations by Redlich-Kister polynomials.

The series of viscosity logarithm change of mixing at constant temperature are depicted as a function of composition in Figures 4.35 to 4.38 for each binary system. It can be observed that, for any of the systems, the viscosity logarithm change of mixing is positive over the entire range for any of the isotherms experimentally investigated, and it increases with increasing temperature for any given composition. This means that the viscosity of the mixtures is higher than that predicted by the mixing rule by Arrhenius and Kendall (Equation 4.14). All systems exhibit maxima of $\Delta\ln(\eta/\eta_0)$ shifting from $x_{IL} \approx 0.5$-0.6 at low temperatures to $x_{IL} \approx 0.3$-0.4 at high temperatures.

For the molar refraction change of mixing, unfortunately, the relatively small values obtained and reported in Tables 4.10 to 4.13 precluded the possibility of getting sufficiently smooth trends as to solidly discuss any composition effect in this magnitude for the studied systems.

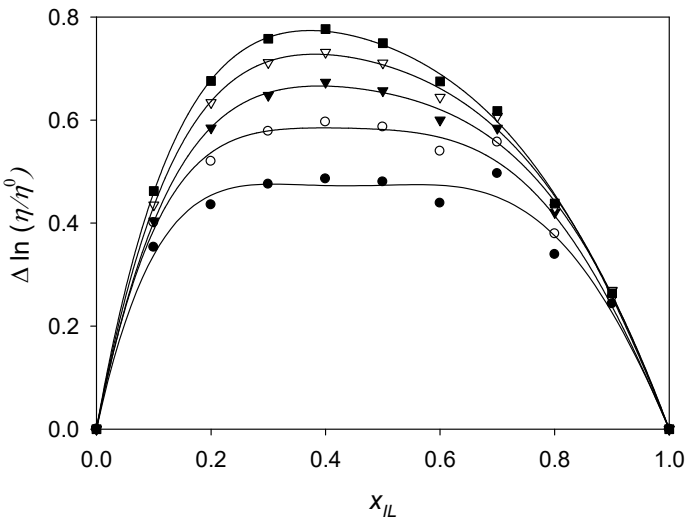

Figure 4.35. Viscosity logarithm change of mixing ($\Delta\ln(\eta/\eta^0)$) for the binary system [C_2mim][OAc] + methanol as a function of the mole fraction of [C_2mim][OAc] (x_{IL}) at different temperatures: ●, 278.15 K; ○, 288.15 K; ▼, 298.15 K; ▽, 308.15 K; ■, 318.15 K. Solid lines represent the corresponding correlations by Redlich-Kister polynomials.

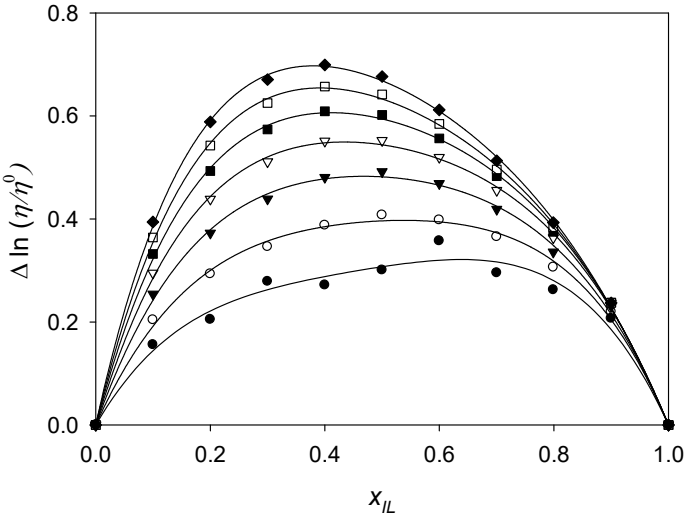

Figure 4.36. Viscosity logarithm change of mixing ($\Delta\ln(\eta/\eta^0)$) for the binary system [C_2mim][OAc] + ethanol as a function of the mole fraction of [C_2mim][OAc] (x_{IL}) at different temperatures: ●, 278.15 K; ○, 288.15 K; ▼, 298.15 K; ▽, 308.15 K; ■, 318.15 K; □, 328.15 K; ◆, 338.15 K. Solid lines represent the corresponding correlations by Redlich-Kister polynomials.

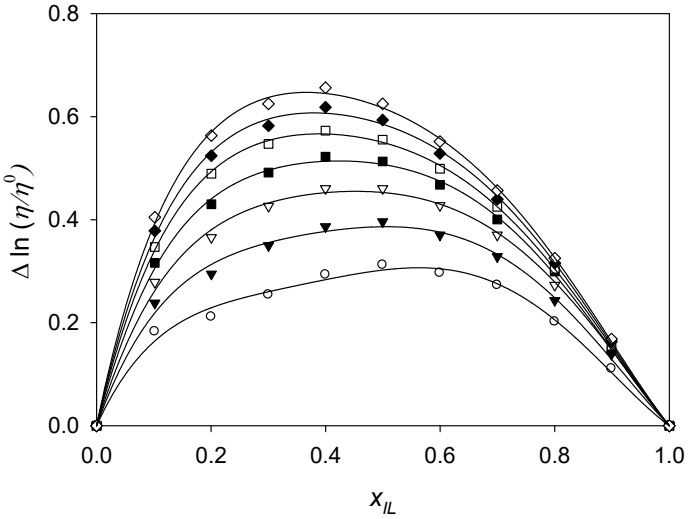

Figure 4.37. Viscosity logarithm change of mixing ($\Delta\ln(\eta/\eta^0)$) for the binary system [C_2mim][OAc] + 1-propanol as a function of the mole fraction of [C_2mim][OAc] (x_{IL}) at different temperatures: ○, 288.15 K; ▼, 298.15 K; ▽, 308.15 K; ■, 318.15 K; □, 328.15 K; ◆, 338.15 K; ◇, 348.15 K. Solid lines represent the corresponding correlations by Redlich-Kister polynomials.

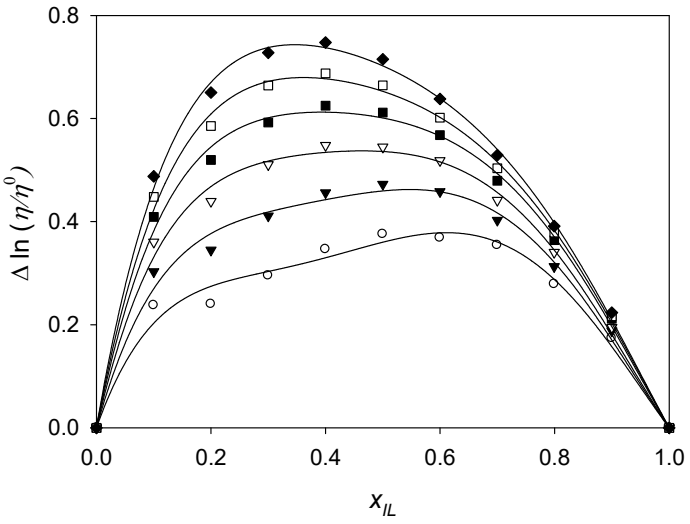

Figure 4.38. Viscosity logarithm change of mixing ($\Delta\ln(\eta/\eta^0)$) for the binary system [C_2mim][OAc] + 2-propanol as a function of the mole fraction of [C_2mim][OAc] (x_{IL}) at different temperatures: ○, 288.15 K; ▼, 298.15 K; ▽, 308.15 K; ■, 318.15 K; □, 328.15 K; ◆, 338.15 K. Solid lines represent the corresponding correlations by Redlich-Kister polynomials.

The surface tension change of mixing is plotted, as a function of composition, for the different isotherms investigated, in Figures 4.39 to 4.42 for all four studied binary systems. As it can be observed in Figure 4.39, the binary system [C_2mim][OAc] + methanol presents values of $\Delta\sigma$ clearly positive throughout the entire composition range, with maxima in the band of composition x_{IL} = 0.3-0.5 for all the isotherms. In the case of the system [C_2mim][OAc] + ethanol (Figure 4.40), the smoothness of the series is not as good as it would be desired, likely due to the fact that the uncertainty of the calculated values of $\Delta\sigma$ in this case is relatively higher in comparison to their magnitude. No particular smooth trend with composition was found, nor an evident evolution with temperature for a given composition, although general trends can still be intuited. Thus, in general there seems to be a positive maximum for the mixtures rich in ethanol, which would imply that in these mixtures the surface of the liquid tends to get enriched in the ionic liquid (which is the pure compound with the highest surface tension) with respect to the bulk composition. And for the evolution with temperature, a shift towards less negative/more positive values with increasing temperature is loosely apparent, which could be connected with a higher concentration of ionic liquid at the surface of the liquid mixture promoted by a rise in temperature. Regarding the system

[C2mim][OAc] + 1-propanol (Figure 4.41), again problems to identify smooth trends and evolutions were noticeable, obtaining a plot of series with quite scattered data. Nevertheless, it can still be stated that its values of $\Delta\sigma$ are typically negative and the different isotherms reach a minimum (a maximum in absolute value) in the band of mole fraction of ionic liquid x_{IL} = 0.60-0.90 for all the temperatures investigated. In the propanol-rich region, the $\Delta\sigma$ values are generally less negative, being even slightly positive for some of the data points at the higher temperatures, resembling somehow the behaviour described above for the system [C2mim][OAc] + ethanol. In contrast, the system [C2mim][OAc] + 2-propanol (Figure 4.42) shows values of $\Delta\sigma$ exclusively negative, with its absolute values being greater (i.e., $\Delta\sigma$ more negative), concomitantly leading to a less scattered plot since the uncertainty in this case is smaller in relation to the magnitude of the property change of mixing. Nevertheless, even in the case of this system it is hard to elucidate a clear evolution of $\Delta\sigma$ with temperature, as all the isotherms are too close to each other.

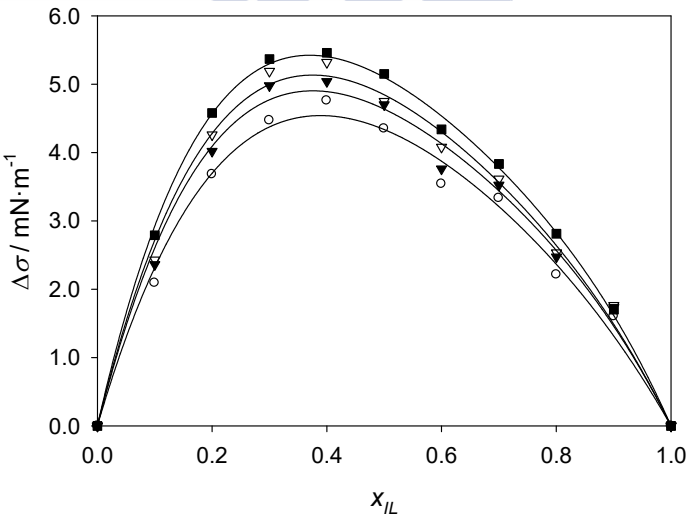

Figure 4.39. Surface tension change of mixing ($\Delta\sigma$) for the binary system [C2mim][OAc] + methanol as a function of the mole fraction of [C2mim][OAc] (x_{IL}) at different temperatures: ●, 278.2 K; ○, 288.2 K; ▼, 298.2 K; ▽, 308.2 K; ■, 318.2 K. Solid lines represent the corresponding correlations by Redlich-Kister polynomials.

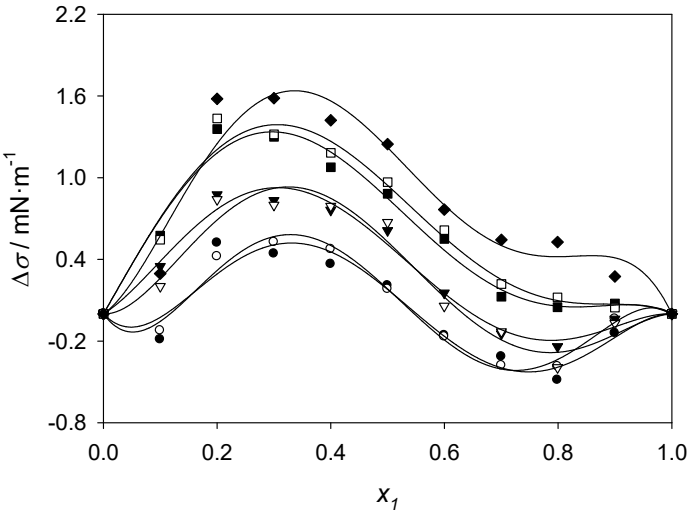

Figure 4.40. Surface tension change of mixing ($\Delta\sigma$) for the binary system [C_2mim][OAc] + ethanol as a function of the mole fraction of [C_2mim][OAc] (x_{IL}) at different temperatures: ●, 278.2 K; ○, 288.2 K; ▼, 298.2 K; ▽, 308.2 K; ■, 318.2 K; □, 328.2 K; ◆, 338.2 K. Solid lines represent the corresponding correlations by Redlich-Kister polynomials.

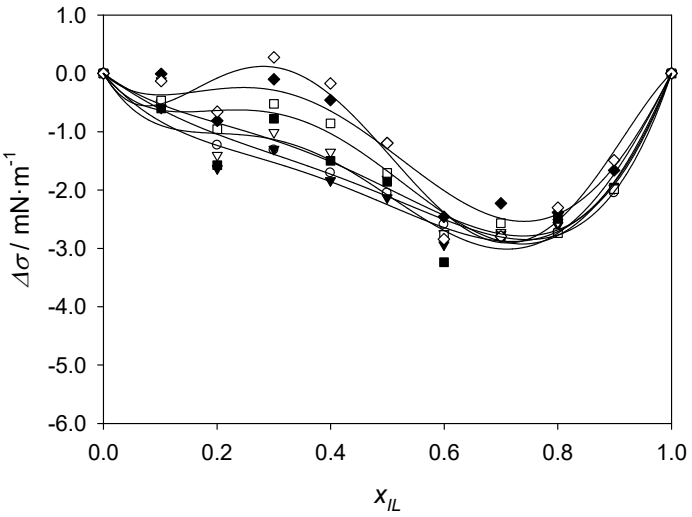

Figure 4.41. Surface tension change of mixing ($\Delta\sigma$) for the binary system [C_2mim][OAc] + 1-propanol as a function of the mole fraction of [C_2mim][OAc] (x_{IL}) at different temperatures: ○, 288.2 K; ▼, 298.2 K; ▽, 308.2 K; ■, 318.2 K; □, 328.2 K; ◆, 338.2 K; ◇, 348.2 K. Solid lines represent the corresponding correlations by Redlich-Kister polynomials.

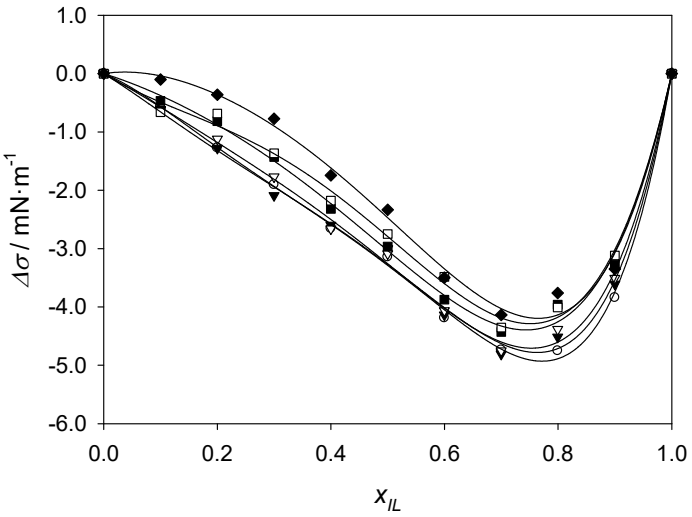

Figure 4.42. Surface tension change of mixing ($\Delta\sigma$) for the binary system [C_2mim][OAc] + 2-propanol, as a function of the mole fraction of [C_2mim][OAc] (x_{IL}) at different temperatures: ○, 288.2 K; ▼, 298.2 K; ▽, 308.2 K; ■, 318.2 K; □, 328.2 K; ◆, 338.2 K. Solid lines represent the corresponding correlations by Redlich-Kister polynomials.

The evolution of the excess molar volumes, viscosity logarithm change of mixing, and surface tension change of mixing with the composition of the mixtures was correlated, at all the investigated temperatures, by means of Redlich-Kister polynomials (Equation 4.26). Polynomials with m = 3 were found to adequately correlate the series of V^E and $\Delta\ln(\eta/\eta^0)$ in the studied systems, whereas polynomials with m = 2 were selected for $\Delta\sigma$., as they already produced sufficiently low values of the root mean square deviations (*rmsd*). The Redlich-Kister coefficients obtained by least-squares fits are listed in Tables 4.14 to 4.17, where the corresponding *rmsd* values obtained with Equation 4.27 are also included. The corresponding correlation functions are depicted, along with the experimental data points, in Figures 4.31 to 4.42 as solid lines for each of the isotherms experimentally investigated. The quality of these correlations can thus be visually assessed.

Table 4.14. Coefficients A_k of the Redlich-Kister polynomials (Equation 4.26) for the correlation of the excess molar volume (V^E), viscosity logarithm change of mixing ($\Delta\ln(\eta/\eta^0)$), and surface tension change of mixing ($\Delta\sigma$) as a function of composition, for the binary system [C_2mim][OAc] + methanol. Root mean square deviations (*rmsd*) (calculated by means of Equation 4.27), expressed in the units of the corresponding property, are also shown.

Coefficient	T / K			
	288.15	298.15	308.15	318.15
	V^E / cm³·mol⁻¹			
A_0	-3.8150	-4.0927	-4.3402	-4.6086
A_1	2.9734	3.0466	3.2612	3.4940
A_2	-3.1964	-3.4890	-3.8719	-4.2049
A_3	2.6093	2.9549	3.0716	3.3361
rmsd	0.013	0.013	0.015	0.017
	$\Delta\ln(\eta/\eta^0)$			
A_0	1.894	2.327	2.614	2.829
A_1	0.057	-0.136	-0.442	-0.653
A_2	1.941	1.793	1.662	1.593
A_3	-1.294	-1.391	-0.845	-0.846
rmsd	0.02	0.02	0.01	0.01
	$\Delta\sigma$ / mN·m⁻¹			
A_0	17.7	17.3	18.5	19.4
A_1	-6.82	-6.94	-7.94	-8.53
A_2	9.44	4.44	6.30	6.24
rmsd	0.2	0.2	0.2	0.2

Table 4.15. Coefficients A_k of the Redlich-Kister polynomials (Equation 4.26) for the correlation of the excess molar volume (V^E), viscosity logarithm change of mixing ($\Delta\ln(\eta/\eta^0)$), and surface tension change of mixing ($\Delta\sigma$) as a function of composition, for the binary system [C_2mim][OAc] + ethanol. Root mean square deviations (*rmsd*) (calculated by means of Equation 4.27), expressed in the units of the corresponding property, are also shown.

Coefficient	T / K						
	288.15	298.15	308.15	318.15	328.15	338.15	348.15
	V^E / cm³·mol⁻¹						
A_0	-2.9991	-3.3014	-3.5757	-3.8871	-4.2471	-4.6611	-5.1444
A_1	2.0651	2.0936	2.2568	2.4319	2.6601	2.9506	3.2947
A_2	-2.0237	-2.2661	-2.6510	-2.9618	-3.3155	-3.7197	-4.1912
A_3	1.3712	1.7622	1.8654	2.1769	2.4712	2.7764	3.1501
rmsd	0.014	0.013	0.014	0.014	0.016	0.018	0.020
	$\Delta\ln(\eta/\eta^0)$						
A_0	1.229	1.586	1.927	2.176	2.377	2.533	2.674
A_1	0.333	0.098	-0.127	-0.322	-0.525	-0.741	-0.898
A_2	0.937	0.958	0.954	1.024	1.050	1.094	1.153
A_3	-0.074	-0.017	-0.101	-0.154	-0.222	-0.227	-0.318
rmsd	0.02	0.01	0.01	0.01	0.01	0.01	0.01
	$\Delta\sigma$ / mN·m⁻¹						
A_0	0.72	0.73	2.03	2.12	3.39	3.77	4.88
A_1	-6.82	-7.71	-7.16	-7.87	-7.73	-7.56	-8.42
A_2	-2.85	-2.16	-0.65	-2.34	1.32	0.84	0.93
rmsd	0.1	0.1	0.1	0.1	0.1	0.1	0.2

Table 4.16. Coefficients A_k of the Redlich-Kister polynomials (Equation 4.26) for the correlation of the excess molar volume (V^E), viscosity logarithm change of mixing ($\Delta\ln(\eta/\eta^0)$), and surface tension change of mixing ($\Delta\sigma$) as a function of composition, for the binary system [C_2mim][OAc] + 1-propanol. Root mean square deviations (*rmsd*) (calculated by means of Equation 4.27), expressed in the units of the corresponding property, are also shown.

Coefficient	T / K						
	288.15	298.15	308.15	318.15	328.15	338.15	348.15
	V^E / cm³·mol⁻¹						
A_0	-2.3829	-2.6184	-2.8905	-3.2246	-3.6225	-4.0992	-4.6690
A_1	0.8532	1.0280	1.2151	1.4320	1.6963	2.0242	2.4314
A_2	-1.6381	-1.9420	-2.1748	-2.4424	-2.7646	-3.1548	-3.6268
A_3	2.4204	2.3719	2.5543	2.7900	3.0707	3.4089	3.7971
rmsd	0.013	0.015	0.017	0.018	0.020	0.021	0.023
	$\Delta\ln(\eta/\eta^0)$						
A_0	1.209	1.546	1.811	2.029	2.200	2.341	2.467
A_1	0.262	0.023	-0.197	-0.361	-0.595	-0.718	-0.873
A_2	0.414	0.578	0.691	0.728	0.812	0.852	0.924
A_3	-1.064	-0.996	-0.916	-1.124	-1.076	-1.108	-1.101
rmsd	0.01	0.01	0.01	0.01	0.00	0.01	0.01
	$\Delta\sigma$ / mN·m⁻¹						
A_0	-8.43	-9.00	-7.87	-8.33	-6.70	-5.18	-5.45
A_1	-8.92	-7.74	-9.56	-9.23	-11.4	-11.4	-13.5
A_2	-9.67	-9.23	-8.77	-9.53	-11.0	-8.90	-7.50
rmsd	0.1	0.2	0.2	0.3	0.2	0.3	0.4

Table 4.17. Coefficients A_k of the Redlich-Kister polynomials (Equation 4.26) for the correlation of the excess molar volume (V^E), viscosity logarithm change of mixing ($\Delta\ln(\eta/\eta^0)$), and surface tension change of mixing ($\Delta\sigma$) as a function of composition, for the binary system [C_2mim][OAc] + 2-propanol. Root mean square deviations (rmsd) (calculated by means of Equation 4.27), expressed in the units of the corresponding property, are also shown.

Coefficient	T / K					
	288.15	298.15	308.15	318.15	328.15	338.15
	V^E / cm³·mol⁻¹					
A_0	-2.3758	-2.7264	-3.1472	-3.6725	-4.3157	-5.0984
A_1	0.3998	0.5633	0.8550	1.2327	1.7025	2.2965
A_2	-2.2149	-2.4669	-2.8661	-3.3510	-3.9413	-4.6482
A_3	3.1738	3.2509	3.5795	3.9572	4.4187	4.9549
rmsd	0.018	0.025	0.027	0.030	0.032	0.034
	$\Delta\ln(\eta/\eta^0)$					
A_0	1.440	1.838	2.144	2.404	2.611	2.809
A_1	0.559	0.216	-0.136	-0.430	-0.732	-0.978
A_2	0.875	0.95	1.093	1.260	1.353	1.460
A_3	-1.367	-1.42	-1.418	-1.342	-1.241	-1.242
rmsd	0.02	0.02	0.01	0.01	0.01	0.01
	$\Delta\sigma$ / mN·m⁻¹					
A_0	-13.2	-13.1	-13.0	-12.1	-11.2	-9.88
A_1	-18.5	-17.4	-17.6	-17.5	-17.0	-19.5
A_2	-16.8	-16.0	-14.0	-10.8	-13.0	-11.6
rmsd	0.2	0.2	0.1	0.1	0.1	0.2

Effect of alcohol

In order to analyse the effect of the nature of the alcohol in the four binary systems investigated in this chapter, a direct comparison of the excess properties and property changes of mixing of the combinations of [C_2mim][OAc] with each of the four lightest alcohols (methanol, ethanol, 1-propanol, and 2-propanol) as a function of the mole fraction of ionic liquid was carried out at two intermediate temperatures within the experimental temperature ranges: 298.15 K and 318.15 K.

The comparison of the selected isotherms for V^E is displayed in Figure 4.43. While negative in all cases, at the 318.15 K isotherms the absolute value of the magnitude becomes smaller in the following order of alcohols: methanol > ethanol > 2-propanol > 1-propanol. In principle this order correlates with the strength of the attractive forces existing between the ionic liquid and the alcohol. At the 298.15 K isotherms, the trend is similar, but the difference between the values for the two systems with propanols becomes practically negligible. Thus, the attractive interaction between the ionic liquid and the propanols is stronger for the case of 2-propanol at high temperatures, but at low temperatures the interactions with 2-propanol or 1-propanol are practically the same.

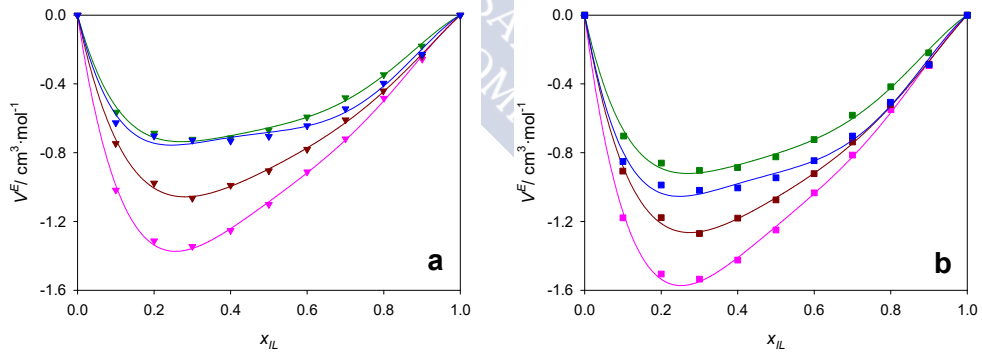

Figure 4.43. Excess molar volume (V^E) for binary systems [C_2mim][OAc] + alcohol, as a function of the mole fraction of ionic liquid, at (a) 298.15 K, and (b) 318.15 K. Alcohol (from bottom to top): methanol (magenta), ethanol (brown), 2-propanol (blue), and 1-propanol (green).

Trends for $\Delta\ln(\eta/\eta_0)$, always positive for the four systems, can be also observed with the nature of the alcohol in Figure 4.44. At any of the selected temperatures, the values of this property change of mixing decrease in the following order: methanol >

ethanol ≈ 2-propanol > 1-propanol (Figure 4.44). This trend is similar to that discussed above for V^E in absolute values, with the difference that for $\Delta\ln(\eta/\eta_0)$ the isotherms that are the closest are the ones corresponding to the systems with ethanol and with 2-propanol, while a clear difference is maintained between the two systems involving the propanols. In any case, the mixtures of [C2mim][OAc] with methanol would be the ones showing a strongest deviation from the classical mixing rule given by Equation 4.14.

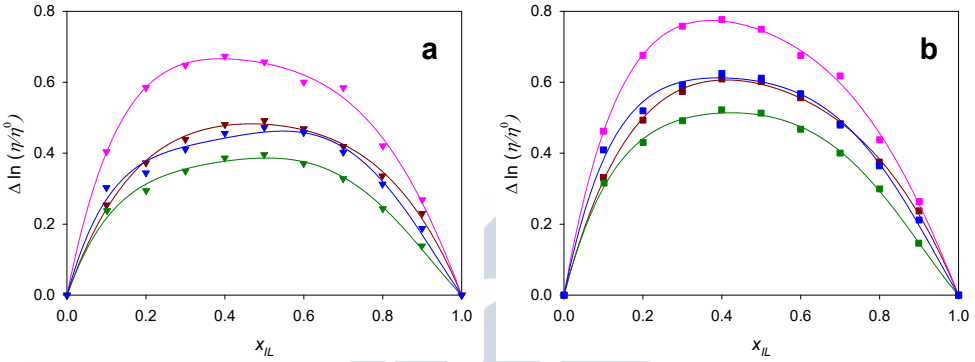

Figure 4.44. Viscosity logarithm change of mixing ($\Delta\ln(\eta/\eta^0)$) for binary systems [C2mim][OAc] + alcohol, as a function of the mole fraction of ionic liquid, at (a) 298.15 K, and (b) 318.15 K. Alcohol (from top): methanol (magenta), ethanol (brown), 2-propanol (blue), and 1-propanol (green).

Regarding $\Delta\sigma$, from Figure 4.45 a gradual evolution with the varying polarity of the alcohol in the systems [C2mim][OAc] + alcohol can be inferred: from totally positive for the mixtures with methanol, to positive-negative for the mixtures with ethanol, then a transition to negative for the mixtures with 1-propanol, and then becoming more negative for the mixtures with 2-propanol. Moreover, the maxima in absolute value of each isotherm shift roughly towards compositions richer in ionic liquid in the same order. No remarkable differences are observed between one temperature and the other.

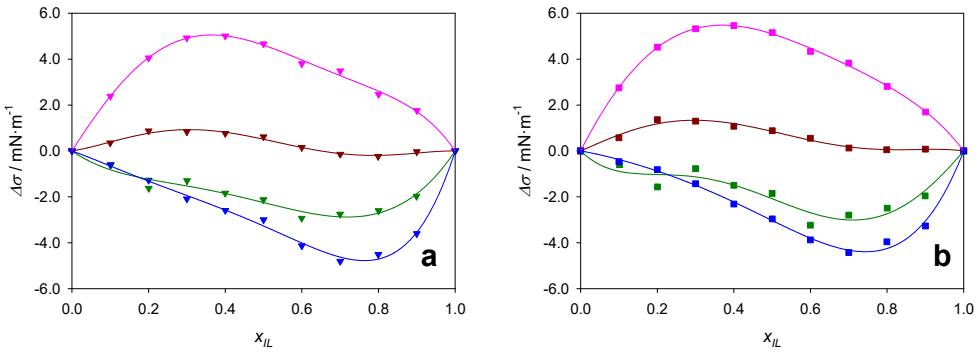

Figure 4.45. Surface tension change of mixing ($\Delta\sigma$) for binary systems [C_2mim][OAc] + alcohol, as a function of the mole fraction of ionic liquid, at (a) 298.15 K, and (b) 318.15 K. Alcohol (from top): methanol (magenta), ethanol (brown), 1-propanol (green), and 2-propanol (blue).

4.4.3. Solubility of biopolymer standards: the alcohol as cosolvent

In view of the results shown and discussed in Section 4.4.2, together with the intrinsic characteristics of all four alcohols explored, it was decided to select methanol and ethanol as the most interesting candidates for their use as cosolvents or antisolvents of the ionic liquid [C_2mim][OAc] in the pretreatment (with possible dissolution and partial fractionation) of lignocellulosic biomass. As a first approach for such purpose, the solubility of MCC, xylan, and Indulin AT (taken as standards of the three major biopolymers of lignocellulosic biomass) in mixtures of [C_2mim][OAc] + (methanol or ethanol) were investigated as function of the relative composition of the solvent. The values obtained and at 298.2 K are reported in Table 4.18. It must be noted, however, that for one of the systems (namely [C_2mim][OAc] + ethanol) these solubilities were tested additionally at 318.2 K and 338.2 K, not detecting significant solubility differences with the variation in temperature in that range. Nevertheless, in the case of appreciable solubility of xylan, a characteristic behaviour was identified: the amount reported was not soluble when added directly at 298.2 K, but it fully dissolved upon heating to 338.2 K. After cooling down to 298.2 K, no precipitation was observed. A possible explanation of this phenomenon could be that, at the low temperature, the intra- and intermolecular forces in the xylan are too strong as to be overcome by the solute-solvent interactions; whereas a sufficient energy for this to happen may be supplied at higher temperature. Once the solute is dissolved, the solute-solvent

interactions can keep the solution stable even if the temperature is lowered to its original value.

Table 4.18. Solubilities of the biopolymer standards (MCC, xylan, and Indulin AT) in mixtures of [C_2mim][OAc] + (methanol or ethanol), at different mole fractions of ionic liquid (x_{IL}), at 298.2 K and atmospheric pressure.

x_{IL}	Solubility (g biopolymer / 100 g solvent)		
	MCC	Xylan	Indulin AT [a]
	[C_2mim][OAc] + methanol		
0.00	<0.1	<0.1	<0.1
0.20	<0.1	<1.0	>20
0.40	<0.5	<0.1	>20
0.60	7	<0.1	>20
0.80	11	<0.1	n.a.
1.00	15	5	n.a.
	[C_2mim][OAc] + ethanol		
0.00	<0.1	<0.1	<0.1
0.20	<0.1	<0.1	>20
0.40	<0.1	<0.1	>20
0.60	1	2	>20
0.80	4	5	n.a.
1.00	15	5	n.a.

[a] n.a.: Quantitative solubility data not available. The mixtures become extremely viscous, and its handling is impracticable upon solubilisation of large quantities of the biopolymer.

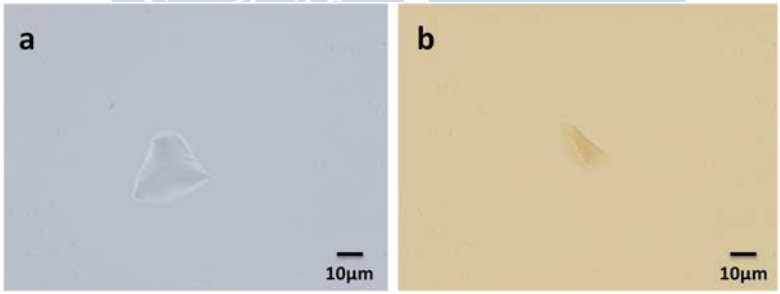

Figure 4.46. Examples of microscopic heterogeneities constituted by solvated portions of biopolymer in visually transparent solutions of biopolymer in liquid mixtures of [C_2mim][OAc] and ethanol. Solute: a) MCC; b) Indulin AT.

It should be also taken into account that most of the values reported in Table 4.18 were determined by direct visual inspection as the limiting concentrations at which transparent solutions to the naked eye were obtained (see Section 4.3.5). However, samples of transparent solutions were identified as not completely homogeneous via

confocal microscopy. Thus, in some microscopic images corresponding to transparent solutions, small heterogeneities constituted by solvated portions of biopolymer were observed (Figure 4.46). In any case, for the results and effect of the work reported herein, the criterion of transparent solution was the one on which the "soluble" condition was decided.

In Table 4.18, it can be clearly observed that none of the biopolymer standards was appreciably soluble in pure alcohol (a value of solubility lower than 0.1 g of solute per 100 g of alcohol). Conversely, the solubility of MCC was quite high in pure [C_2mim][OAc], as compared to the solubility of cellulose in other solvents, or even in other ionic liquids (Wang et al., 2012). This solubility shows a similar trend for both systems [C_2mim][OAc] + methanol and [C_2mim][OAc] + ethanol: its value decreases moderately with a moderate increase in the percentage of alcohol in the solvent composition (x_{IL} = 0.60, 0.80). The solubility in the system with ethanol is significantly lower than in the system with methanol for a given molar concentration (for example: for a composition x_{IL} = 0.60, the solubility in the system with methanol is 11 g of MCC per 100 g of solvent, whereas in the system with ethanol it is 4 g of MCC per 100 g of solvent). With a further increase in the concentration of alcohol (x_{IL} = 0.40 or lower), MCC became practically insoluble (less than 0.5 g per 100 g of solvent in any case). For xylan, a lower solubility than that of MCC in the pure ionic liquid was found. Interestingly, this solubility decreases much more rapidly if methanol is added than if ethanol is added. In fact, for a solvent composition with x_{IL} = 0.80, in the case of ethanol the solubility of xylan was still equivalent to that of the pure ionic liquid, whereas for the case of methanol the solubility of xylan was already negligible at that composition (<0.1 g per 100 g of solvent). A slightly higher solubility of xylan (although still very low: in the range 0.5-1.0 g per 100 g solvent) was experimentally found in the [C_2mim][OAc] + methanol mixture with x_{IL} = 0.20 (corresponding to w_{IL} = 0.57). This non-monotonic evolution of the solubility with composition was previously reported for the case of biopolymers in mixed solvents; for example in the case of lignin in a mixture with acetone and water (Sun et al., 2011). It is not improbable that there be a local maximum of solubility of xylan in the mixtures of methanol and [C_2mim][OAc] in the region relatively rich in methanol; but, due to the low solubilities in absolute terms, this aspect was not further investigated. Regarding the solubility of Indulin AT, it was practically negligible in pure alcohol (<0.1 g per 100 g of solvent), but very large (>20 g per 100 g of solvent) in the solvent combination tested: x_{IL} = 0.20, 0.40, and 0.60;

whereas for x_{IL} = 0.80 or 1.00, the system became like a gel and its handling turned impracticable in the process of solubilising the large amounts of solute added. Such large solubility looks consistent with the dissolution of up to 300 g of Indulin AT per 1 kg of [C2mim][OAc] reported in the literature at a temperature of 363 K (Lee et al., 2009). In trying to refine the abrupt transition from negligible solubility in pure alcohol to a solubility higher than 20 g of Indulin AT per 100 g of solvent in the mixture of [C2mim][OAc] with alcohol (methanol or ethanol) with x_{IL} = 0.20, solubility tests were carried out in mixtures of ionic liquid and alcohol in that range with a step of 0.01 in mole fraction. It was found that a sharp solubility boost occurred at concentrations of ca. x_{IL} = 0.08 for the system [C2mim][OAc] + methanol (equivalent to an ionic liquid mass fraction w_{IL} = 0.32), and ca. x_{IL} = 0.15 for the system [C2mim][OAc] + ethanol (equivalent to w_{IL} = 0.39). The explanation of this behaviour is not clear at present, but it is remarkable to see that it is observed for both systems.

A solubility test was also carried out for MCC in the pure ionic liquid at higher temperature of 358 K, more in connection with other cellulose solubility experiments in the literature. A rise in the experimental solubility up to 30 g of MCC per 100 g of [C2mim][OAc] was observed. This value is higher than others reported in the literature for other sources of cellulose (e.g., eucalyptus prehydrolysis sulphate pulp (Eu-569), cellulose from *Trichoderma reesei*, or different types of Avicel) at the same or similar temperatures (Kosan et al., 2008; Zhao et al., 2008; Balensiefer et al., 2008; Vitz et al., 2009; Zavrel et al., 2009; Fu et al., 2010), perhaps due to a lower degree of polymerisation of the cellulose standard used herein.

In a hypothetical case of dissolution of biomass, with all three biopolymers involved, the individual solubility values reported in Table 4.18 are expected to be affected by the presence of the other biopolymers in the solution. Nevertheless, those individual solubilities provide a reasonable estimate of the compositions of the solvent system [C2mim][OAc] + alcohol for which each specific biopolymer will precipitate out of the solution or not. Thus, the composition of the solvent system could be conveniently adjusted, for example at different stages in a process, to dissolve one or several of the biopolymers, according to the interest in each particular case. In view of the values in Table 4.18, the pure ionic liquid will dissolve all three biopolymers (up to a certain limit) and the pure alcohol will not dissolve any of them; and, in between, there exist solvent composition ranges in which the carbohydrates and lignin will be codissolved simultaneously, or in which only lignin will dissolve. In a context of

fractionation of biomass, these results suggest the possibility of using the [C_2mim][OAc]+ alcohol system to separate, via selective dissolution, a mixture of the major lignocellulose biopolymers. Figure 4.47 shows a possible scheme for the fractionated recovery of the biopolymer fractions from "disengaged biomass" (an idealisation of a lignocellulosic biomass previously treated so that all the lignocellulosic bonds linking the biopolymers to each other were fully broken), exemplified for the solvent system [C_2mim][OAc] + methanol.

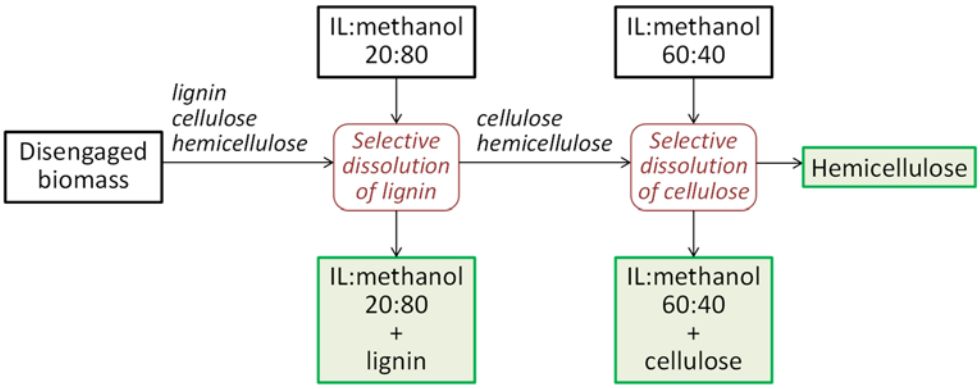

Figure 4.47. Proposed process scheme for the fractionation of a mixture of the major lignocellulose biopolymers ("disengaged biomass") via selective dissolution with different combinations of [C_2mim][OAc] (IL) and methanol. The ratios indicated for the IL + methanol mixtures are in a molar basis.

An experiment was attempted to verify the validity of the scheme in Figure 4.47, using a mixture of 0.25 g of each of the biopolymer standards (for a total of 0.75 g of mixture). This mixture was first combined with 5.0 g of a 20:80 mol/mol mixture of [C_2mim][OAc] + methanol (which is only capable of dissolving lignin appreciable at that concentration). Upon vigorous stirring for several hours and subsequent filtration (under soft vacuum using a fritted glass Allihn filter tube), the remaining solid was combined with 5.0 g of a 60:40 mol/mol mixture of [C_2mim][OAc] + methanol (which exhibits a negligible solubility capacity for xylan, but can dissolve cellulose in appreciable levels). The filtration in the second stage turned out to be difficult due to very high viscosity, and therefore only the first separation stage in Figure 4.47 was effectively carried out in the experiment. By elimination of solvents from the separated fractions, 0.14 g of a black precipitate was obtained from the filtrate of the first stage

('Precipitate-1'), and 0.61 g of a brown precipitate was obtained from the mixture in the second stage ('Precipitate-2'). Photographs of 'Precipitate-1' and 'Precipitate-2' are shown in Figure 4.48a. The FT-IR spectra of both samples, as well as of those of the equivalently regenerated biopolymer standards, are shown in Figure 4.48b (zoomed in the wavenumber range 500-2000 cm^{-1}). The similarity between the spectra of 'Precipitate-1' and Indulin AT is evident, as it is between the spectra of 'Precipitate-2' and of MCC and xylan. Among the set of characteristic vibration bands (Casas et al., 2013; Labbé et al., 2005), specific analysis of signals at 897 cm^{-1} (characteristic of carbohydrates) and at 1459 cm^{-1} and 1510 cm^{-1} (characteristic of lignin) in the obtained spectra reveals in this particular case the preferential presence of Indulin AT in 'Precipitate-1' and the preferential presence of carbohydrates (MCC and xylan) in 'Precipitate-2'. This is in good agreement with what would be expected from the colourations observed for the precipitates (Figure 4.48a).

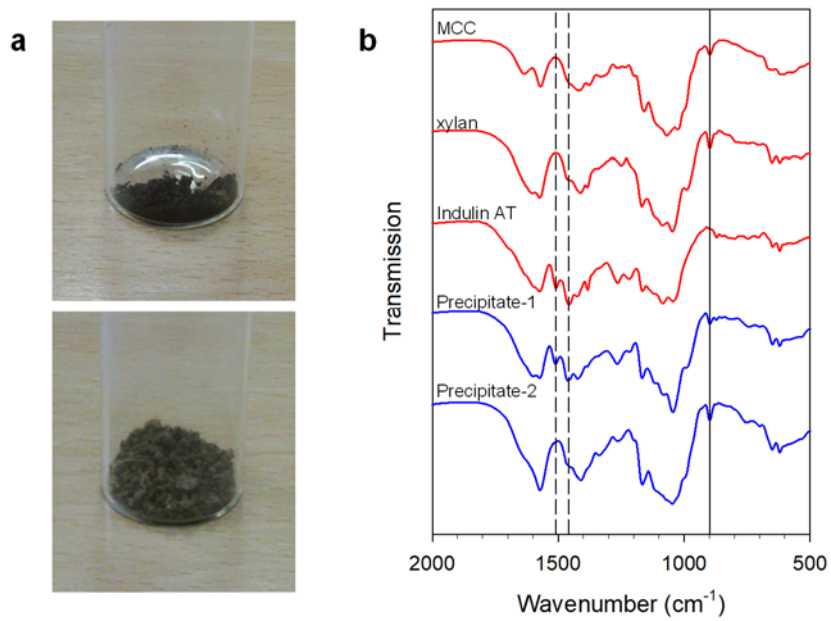

Figure 4.48. a) Photographs of 'Precipitate-1' (top) and 'Precipitate-2' (bottom). b) FT-IR spectra, in the wavenumber range 500-2000 cm^{-1}, of regenerated biopolymer standards and of regenerated precipitates of the selective dissolution experiment (see details in the text); from top to bottom: MCC, xylan, Indulin AT, 'Precipitate-1', and 'Precipitate-2'. The solid vertical line indicates a characteristic signal of cellulose/hemicellulose, and the dashed vertical lines indicate characteristic signals of lignin (Casas et al., 2013; Labbé et al., 2005).

4.4.4. Precipitation tests: the alcohol as antisolvent

On the basis of the differences in the solubilities reported in Table 4.18 for the biopolymer standards in mixtures of [C_2mim][OAc] + alcohol of varied compositions, a precipitation scheme could be considered for the fractionated recovery of biopolymer fractions from lignocellulosic biomass dissolved in [C_2mim][OAc] by gradual additions of controlled amounts of alcohol acting as antisolvent. In order to evaluate the ability of the alcohol to act as antisolvent for this fractionated recovery, some precipitation tests were carried out. In particular, the precipitation of the biopolymer standards, previously dissolved in [C_2mim][OAc], by addition of methanol was investigated. Solutions of 0.15 g of biopolymer standard (MCC, xylan, or Indulin AT) in 3.00 g of [C_2mim][OAc] (a solute-to-solvent mass ratio of 5:100) were made and subsequently subjected to the addition of different amounts of methanol at ambient temperature. Although the values reported in Table 4.18 would suggest the precipitation of at least the MCC and the xylan with the addition of moderate amounts of methanol (less than 1:1 wt/wt ratio to the ionic liquid), a clean precipitation of solids was not observed in the tests. Instead, a kind of emulsion or gel-like phase was formed (exemplified in the photographs of Figure 4.49 for the case of cellulose and xylan). Similar gel phase formations have been previously reported in the literature for similar systems (Dibble et al., 2011). This fact would hinder the utilisation of the alcohol in moderate amounts as a direct antisolvent for the regeneration of lignocellulose fractions previously dissolved in [C_2mim][OAc] or for the fractionated precipitation of the different biopolymers from a [C_2mim][OAc] solution by gradual addition of methanol (see scheme in Figure 4.50). This emulsion/gel formation was observed even after the addition of as much as five times the mass of methanol with regard to the ionic liquid (methanol-to-[C_2mim][OAc] ratio of 5:1 wt/wt). No large amounts of methanol were attempted to force a clean precipitation, since this would lead to an excessively high amount of volatile organic used in the process, as well as to the consumption of too much energy in the elimination of the antisolvent for recycling of the ionic liquid in the cooking step (see Figure 4.50) in a continuous process.

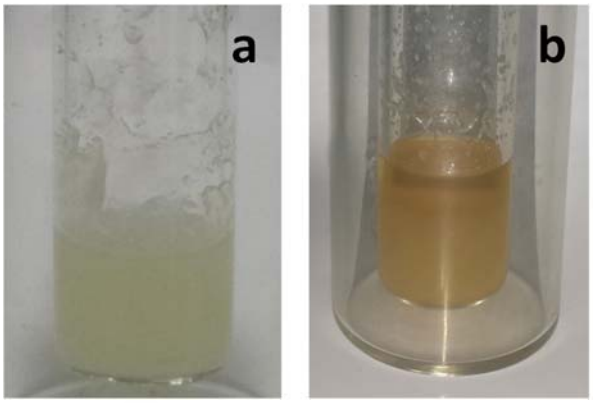

Figure 4.49. Illustrative pictures from the precipitation tests: a) gel formation upon addition of methanol, in a ratio of 1:1 wt/wt relative to ionic liquid, to a solution of cellulose in [C_2mim][OAc]; b) emulsion formed upon addition of methanol, in a ratio of 1:1 wt/wt relative to ionic liquid, to a solution of xylan in [C_2mim][OAc]. See the text for further details.

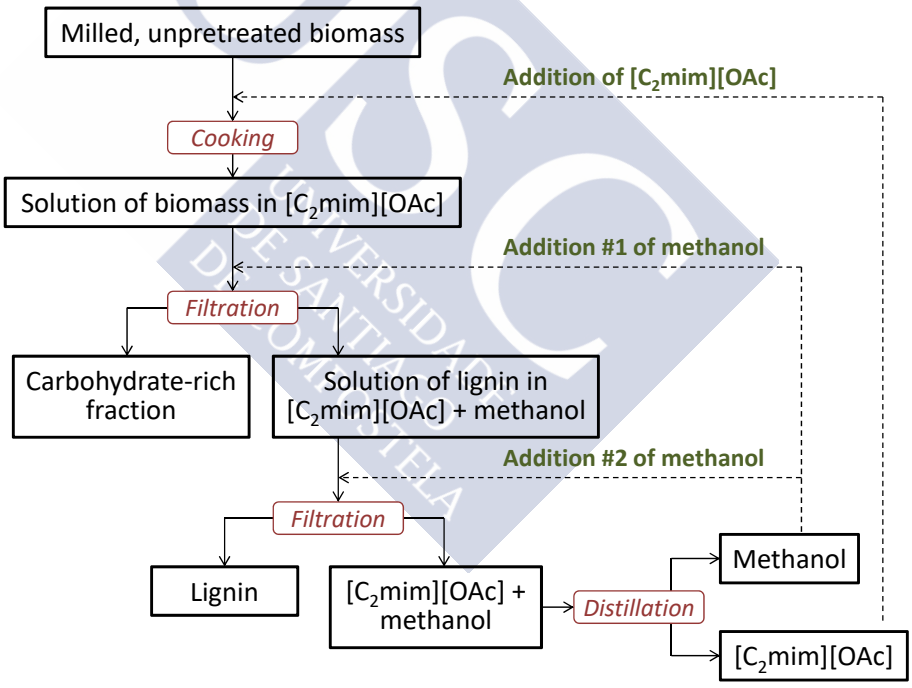

Figure 4.50. Potential scheme for the dissolution and fractional precipitation of lignocellulosic biomass using [C_2mim][OAc] as solvent and methanol as antisolvent. This scheme would not be viable with the use of moderate amounts of methanol, due to the formation of gel-like phases.

USC
UNIVERSIDADE
DE SANTIAGO
DE COMPOSTELA

5. PRETREATMENT OF EUCALYPTUS WOOD WITH AN IONIC LIQUID + ETHANOL MIXTURE

USC
UNIVERSIDADE
DE SANTIAGO
DE COMPOSTELA

5. PRETREATMENT OF EUCALYPTUS WOOD WITH AN IONIC LIQUID + ETHANOL MIXTURE

5.1. Motivation

Much of the research efforts made to date on the pretreatment of lignocellulosic biomass with ionic liquids has put its emphasis on the partial or total dissolution of the biomass in the ionic liquid. Due to the non-volatile nature of both the ionic liquid and the biopolymeric constituents of the biomass, the recovery of the dissolved fractions has typically been addressed by the addition of large amounts of a molecular liquid miscible with the ionic liquid and acting as antisolvent of the lignocelluloses. To avoid the large input of energy associated with the recovery of the ionic liquid from its mixture with the antisolvent by vaporisation of the latter, an alternative pretreatment scheme based on non-dissolving conditions may be envisioned.

In a non-dissolving pretreatment, no fractions of lignocellulosic material would be actually dissolved in the pretreatment fluid at relevant levels. Instead, the pretreatment fluid would interact with the biopolymers in the solid phase (without carrying out their dissolution), in a way that would facilitate the reaction and transformation of these biopolymers in subsequent stages. An example of this might be a non-dissolving pretreatment in which the crystallinity of the cellulose fraction in the lignocellulosic biomass is reduced, thus facilitating its reactivity in later steps within the biorefinery scheme. Given the non-dissolving character of this approach, the use of antisolvents to precipitate dissolved fractions would not be necessary, and the reclaim of the pretreated biomass would be doable by simple filtration.

In proposing a fluid solvent for the non-dissolving pretreatment, an ionic liquid able to interact with the lignocellulosic biomass or its constituent biopolymers under certain conditions could be an interesting choice. Moreover, the consideration of the mixture of such ionic liquid with a molecular cosolvent capable of conveniently tuning this dissolution capacity, as well as other properties of the solvent, could be also of

interest. In Chapter 4 it has been found that the ionic liquid [C_2mim][OAc], or its mixtures with a light alcohol within a certain concentration range, can dissolve representative standards of the different major biopolymers of lignocellulosic biomass up to different concentrations, even at room temperature. This solubility capacity is indicative of the favourable interactions that can be established between such fluids and the diverse components of the biomass, a key aspect for a successful pretreatment. At the same time, the utilisation of low temperatures may imply two advantageous aspects: on the one hand, the capacity of the solvent to dissolve the biomass as such in an appreciable extent may be hampered, thus leading to a pretreatment in non-dissolving conditions; and on the other hand, the consumption of energy during the pretreatment step may be substantially reduced, while also helping to prevent undesired thermal degradation of substances in the system.

In choosing a woody biomass to be tested, white eucalyptus (*Eucalyptus globulus*) has been selected due to the current relevance that it has in the forestry industries in Galicia, and more broadly in other regions of the Iberian Peninsula, as well.

Therefore, in this chapter the use as solvents of neat [C_2mim][OAc] and of a mixture of this ionic liquid with ethanol is proposed for the pretreatment of *E. globulus* particles, at conditions at which the capacity of the ionic liquid to truly dissolve wood is very low, thus benefiting from the advantages of a non-dissolving pretreatment

5.2. Experimental

5.2.1. Materials

Chips of *E. globulus* were kindly supplied by the factory that the company Financiera Madedera S.A. has in Padrón (Spain). In a preliminary grinding, their size was reduced to lower than ca. 0.5 cm by means of a Waring HGBTWT laboratory blender (Figure 5.1). The particle size was further reduced by milling in a Retsch ZM200 ultra-centrifugal mill (Figure 5.2), using a 500-μm internal sieve. The particles obtained therein were sieved and classified according to their size by means of a Filtra FTL-200 mechanical screener consisting of several fitted sieves with meshes of different light path (Figure 5.3). Particle size ranges of 250-500 μm and 125-250 μm were selected, and these *E. globulus* samples were stored at 277 K in polyethylene plastic bags under

vacuum (using a Sammic V201 vacuum-packer) until their utilisation in the experiments reported in this chapter.

Figure 5.1. Waring HGBTWT laboratory blender.

Figure 5.2. Retsch ZM200 ultra-centrifugal mill.

Figure 5.3. Filtra FTL-200 mechanical screener.

The ionic liquid 1-ethyl-3-methylimidazolium acetate ([C_2mim][OAc]), with nominal purity >95 %, was purchased from Iolitec. It was purified in-house, as already described in Section 4.3.1. A water content of 0.0012 in mass fraction was determined by Karl-Fischer titration using a Metrohm 737 KF coulometer (Figure 3.2). The chemical structure of the ionic liquid can be seen in Figure 4.1.

Ethanol was supplied by Panreac with a nominal purity of 99.8 %, and used as received.

5.2.2. Equipment and procedure

Pretreatment

Neat [C_2mim][OAc] and its 95:5 wt/wt mixture with ethanol were used as solvents for the pretreatment of *E. globulus* particles (125-250 μm and 250-500 μm size ranges) at relatively low temperatures, thus disabling the capacity of the ionic liquid to dissolve wood and therefore resulting in conditions of non-dissolving pretreatment.

Approximately 5.7 g of either pure ionic liquid [C_2mim][OAc] or a 95:5 wt/wt mixture of [C_2mim][OAc] + ethanol was loaded into a jacketed glass cell (Figure 5.4), along with ca. 0.3 g of *E. globulus*; thus yielding a 5 wt% concentration of biomass in the mixture. After addition of the components, the lid of the cell was tightly screwed, and the mixture was magnetically stirred at constant temperature for 16 h. Two different pretreatment temperatures were tested: 318 K and 338 K. The desired temperature for each experiment was kept constant by means of the circulation of water from a Julabo F12-EH water bath thermostat through the jacket of the cell.

Figure 5.4. Jacketed glass cell for carrying out the wood pretreatment experiments, placed on a stirring plate and connected to a Julabo F12-EH water bath thermostat.

After completion of the pretreatment time, the mixture of solvent + wood was filtered under soft vacuum using a fritted glass Allihn filter tube. The recovered solid was washed with ethanol (specifically four times, using each time a mass of ethanol equivalent to the mass of solvent used) to remove any residual ionic liquid. On the other hand, an amount of ethanol of five times the mass of solvent used in the pretreatment was added to the filtrate, verifying that no precipitation of any dissolved biomass occurred.

Complementary, the reusability of the ethanol + [C_2mim][OAc] mixture was checked by taking the diluted filtrate and mixing it with the ethanol washings, and then vaporising most of the ethanol in a Büchi R-200 rotary evaporator (Figure 5.5). The liquid residue in the flask was analysed by ^{1}H NMR in a Varian Mercury 300 spectrometer (Figure 3.2), obtaining a spectrum essentially in agreement with that of the original [C_2mim][OAc] (Figure A.5 in Appendix A). Therefore, this confirmed the preservation of the chemical identity of the ionic liquid (no degradation) as well as the absence of residual non-volatile lignocellulosic fractions building up in relevant levels in the solvent.

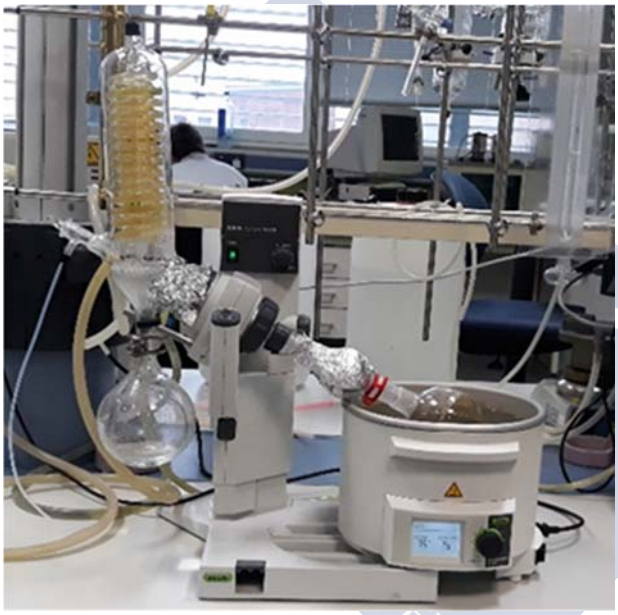

Figure 5.5. Büchi R-200 rotary evaporator.

The pretreated biomass was oven-dried at 378 K for no less than 4 h until constant weight, and different aliquots were used in the different analyses, as described below.

All weighing was carried out in a Mettler-Toledo AT261 DeltaRange analytical balance (Figure 5.6) with a precision of $\pm 1 \times 10^{-4}$ g.

Figure 5.6. Mettler-Toledo AT261 DeltaRange analytical balance.

Morphology and crystallinity analyses

The morphology of both untreated and pretreated samples was examined by means of photographs taken in bright field with a Leica M205FA stereoscopic microscope (Figure 5.7).

For investigation of the degree of crystallinity, both untreated and pretreated samples were analysed by powder X-ray diffractometry (PXRD), using a Philips diffractometer handled by a PW1710 control unit with a PW1820/00 vertical goniometer and an Enraf Nonius FR590 generator operating at 40 kV and 30 mA (Figure 5.8). X-rays were obtained from a Cu sealed tube, and the radiation was monochromatised with a graphite monochromator (λ(Kα1) = 1.5406 Å). The diffraction patterns were obtained in the 2θ angular range 10-40° with a step of 0.02° and an accumulation time of 4 s. The samples were mounted on a silicon zero-background holder plate, where they were rotated during the measurements to obtain the optimal peak profiles for analysis, as well as to minimise the effect of preferential orientation.

The crystallinity index (CI) was calculated by means of the technique known as "amorphous subtraction method", which is currently considered to lead to the numerically more reliable results (Park et al., 2010). In order to apply this technique, a totally amorphous sample for reference is needed. Given that the crystallinity in

lignocellulosic biomass is essentially due to the crystallinity of cellulose in it, the amorphous reference sample selected was a sample of totally amorphous cellulose. This sample was prepared by charging ca. 1 g of microcrystalline cellulose (MCC) powder, supplied by Aldrich, into the grinding cell of a Retsch MM2 laboratory mixer mill (Figure 5.9), which was operated at a grinding frequency of 15 Hz with a 2-mm ball. A sequence of several grinding times, namely 4×30 min followed by 4×1 h, were applied in order to obtain a sample of cellulose that could be considered fully amorphous.

After eliminating the contribution of the instrument and adjusted the intensity of the diffractograms at low angles (*background normalisation*), the crystallinity index was calculated as the difference between the area under the diffractogram of the measured sample and that of the diffractogram corresponding to the amorphous reference. All mathematical fits of the diffractograms were performed with the software HighScore Plus (version 3.0d).

Figure 5.7. Leica M205FA stereoscopic microscope.

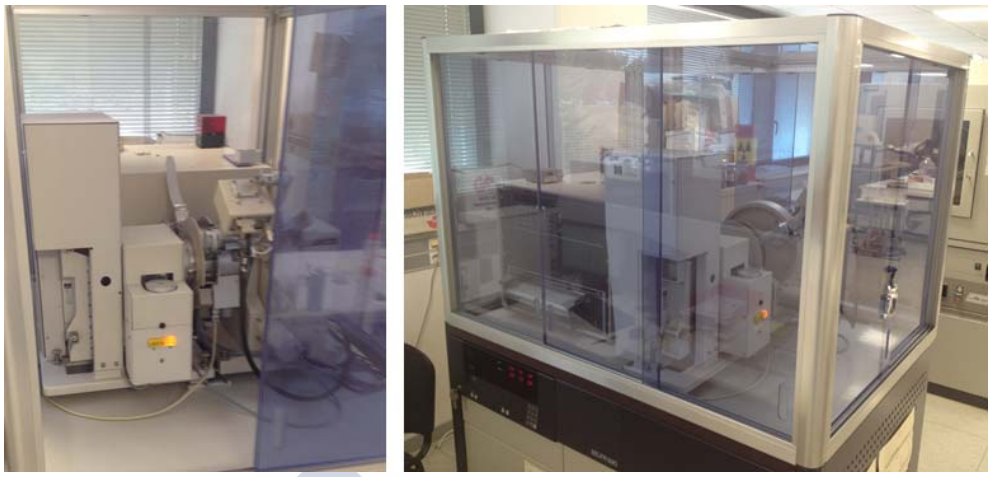

Figure 5.8. Front and lateral views of the Philips diffractometer used in this work.

Figure 5.9. Retsch MM2 laboratory mixer mill.

Compositional analysis

A procedure based on the Laboratory Analytical Procedure developed by Sluiter et al. (2012) at the National Renewable Energy Laboratory (NREL) of the United States of America was used to determine the percentage compositions of cellulose, hemicellulose, and lignin in the pretreated biomass samples. This procedure uses a two-step acid hydrolysis to transform the biomass into forms that are more easily quantified. The lignin fractionates into acid insoluble material and acid soluble material. The acid insoluble material may also include ash and protein, which must be accounted

for by means of gravimetric analysis. The acid soluble lignin is measured by UV-Vis spectroscopy.

Portions of 50.0±0.5 mg of the pretreated biomass samples were weighted and loaded into autoclave tubes with a capacity of 15 mL. Half a millilitre of a 72 % H_2SO_4 aqueous solution was added to each tube, for digestion of the solids for 1 h. During this period, the content of the tubes was occasionally vortexed in order to guarantee a good and uniform contact between the solid particles and the acid solution. Next, 14 mL of distilled water were added to each tube (thus reducing the concentration of the acid solution to 4 %), and the tubes were autoclaved for 1 h at 394 K in a P-Selecta MED 20 autoclave (Figure 5.10). After completion of the autoclave cycle, the samples were allowed to slowly cool to near room temperature before removing the caps and proceeding with their filtration through a fritted glass Allihn filter tube under soft vacuum conditions. The resulting liquid filtrate and solid residue followed different pathways, as explained next.

Figure 5.10. P-Selecta MED-20 autoclave.

Aliquots of ca. 1.5 mL of the liquid filtrates were re-filtered through 0.22-μm pore-size filtering discs, and analysed by high-performance liquid chromatography (HPLC) in an Agilent 1100 Series HPLC chromatograph equipped with a 300 mm ×

7.8 mm Aminex HPX-87H column (by BioRad Laboratories) and an Agilent 1260 Infinity Series refractive index detector (Figure 5.11). An aqueous 0.005 M (0.01 N) H_2SO_4 solution was used as HPLC mobile phase, with a flow rate of 0.3 mL·min^{-1}, at 313 K. A volume of 20 µL was injected. For building the calibration curves, the following standard compounds were used: cellobiose (Fluka, ≥99.0%, cat. #22150), D-(+)-glucose (Sigma-Aldrich, ≥99.5%, cat. #G7528), D-(+)-xylose (Sigma-Aldrich, ≥99.0%, cat. #X3877), L-(+)-arabinose (Sigma-Aldrich, ≥99.0%, cat. #A3256), sodium acetate (Sigma-Aldrich, ≥99.0%, cat. #71183), 5-(hydroxymethyl)furfural (Sigma-Aldrich, ≥99.0%, cat. #W3877) and furfural (Sigma-Aldrich, 99.0%, cat. #185914). The percentage of cellulose in the biomass sample (*%Cell*) was calculated from the concentrations of glucose ([*Glu*]) and 5-(hydroxymethyl)furfural ([*HMF*]), whereas the percentage of hemicellulose (*%HC*) was calculated from the concentrations of xylose ([*Xyl*]), arabinose ([*Ara*]), acetate ([*Ace*]), and furfural ([*Fur*]), as follows:

$$\%Cell = \frac{0.9 \times \left([Glu] + \frac{180}{126.11} \times [HMF] \right) \times V}{W} \times 100 \quad (5.2)$$

$$\%HC = \frac{0.88 \times \left([Xyl] + [Ara] + \frac{150.13}{96.08} \times [Fur] \right) \times V + \frac{42}{59} \times [Ace] \times V}{W} \times 100 \quad (5.3)$$

where *V* corresponds to the total volume of liquid in the tube (14.5 mL) and *W* to the total mass of sample originally placed in it (50 mg).

The liquid filtrates were also used to determine the acid-soluble lignin in the samples by measuring their absorbance at a wavelength of 278 nm in an Agilent 8453 UV-vis spectrophotometer (Figure 4.7). As recommended by Sluiter et al. (2012), the absorbance of the samples was carried out within six hours of hydrolysis, or in the following day after being stored in a refrigerator overnight. A dilution factor of 20 was used to ensure that the actually measured absorbance values were in a suitable range (0.3-0.7 absorbance units). The percentage of acid-soluble lignin (%*ASL*) was calculated as:

$$\%ASL = \frac{\frac{A}{b \times a} \times DF \times V}{W} \times 100 \quad (5.4)$$

where *A* is the absorbance at 278 nm, *b* is the path length of the UV quartz cuvette used (1 cm), *a* is the absorptivity (or extinction coefficient) at 278 nm, *DF* is the dilution

factor, V is the volume of filtrate (14.5 mL, assuming negligible change in volume due to dissolution of part of the solid biomass samples in the heterogeneous mixtures inside the autoclave tubes), and W is the mass of solid placed in the tubes for digestion and autoclaving (50 mg). A value of absorptivity of 20 $L \cdot g^{-1} \cdot cm^{-1}$ at 278 nm, generally acceptable for natural softwood and hardwood lignin, was used (Parasuraman et al., 2007).

Figure 5.11. Agilent 1100 Series HPLC chromatograph.

The solids obtained in the filtration stage were oven-dried in the filters themselves, at 378 K, for no less than 4 h. After removing them from the oven and allowing them to cool down to room temperature, the solids were transferred to previously tared crucibles. They were weighed and then they were introduced in a Hobersal HD-230 furnace (Figure 5.12), where they were ashed at 848 K for 18-24 h. (It should be noted that the empty crucibles were subjected to the same thermal treatment before use, to eliminate any possible organic residual contamination on their surface.) The percentage of acid-insoluble lignin (%AIL) was calculated by the following equation:

$$\%AIL = \frac{m_{non-ashed} - m_{ashed}}{W} \times 100 \qquad (5.5)$$

where $m_{non\text{-}ashed}$ and m_{ashed} are respectively the masses of the crucible plus sample before and after the ashing step in the furnace, and W is as in Equation 5.3.

The total percentage of lignin in the samples was obtained as the sum of *%ASL* and *%AIL*.

All acid hydrolyses and subsequent determinations of composition of structural carbohydrates and lignin were carried out in triplicate. The results of the replicates typically agreed to within less than 3 %. The average values are reported herein.

Figure 5.12. Hobersal HD-230 furnace.

5.3. Results and discussion

5.3.1. Morphology modification and crystallinity reduction

Microscope photographs of the untreated wood and of the wood obtained after pretreatment at different conditions are shown in Figures 5.13 and 5.14, for the case of particles of size in the ranges 125-250 μm and 250-500 μm respectively. In both figures it is observed that the pretreatments at 318 K have little effect on the morphology of the wood particles. Conversely, at 338 K a remarkable level of fibrillation of the

biomass is observed. The effect of fibrillation seems to be stronger when using the [C_2mim][OAc] + ethanol mixture instead of the neat ionic liquid, likely due to the facilitation of the particle-fluid contact caused by the viscosity reduction resulting from the addition of the alcohol (see Section 4.4.2).

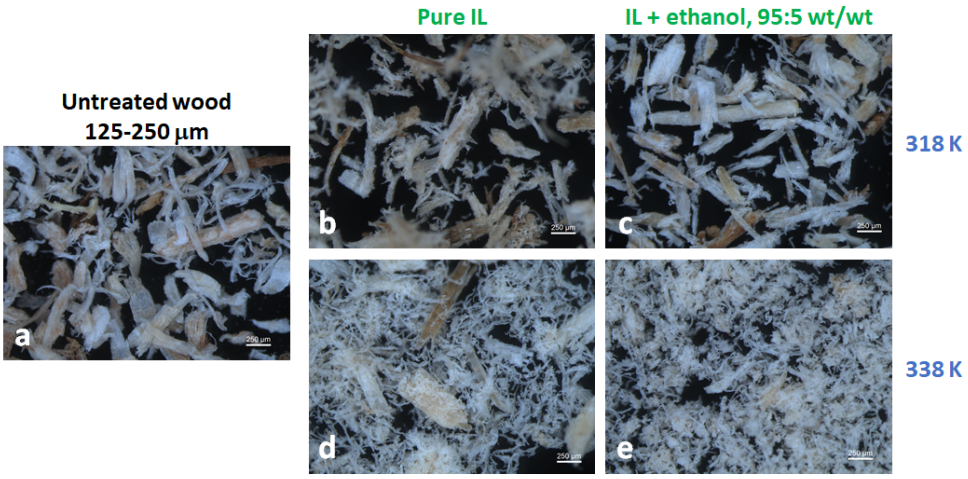

Figure 5.13. Microscope images, at a magnification of 50x, of a) untreated *E. globulus* particles of size 125-250 μm; and b) the corresponding particles pretreated with the solvent and at the temperatures indicated. ("IL" stands for [C_2mim][OAc].)

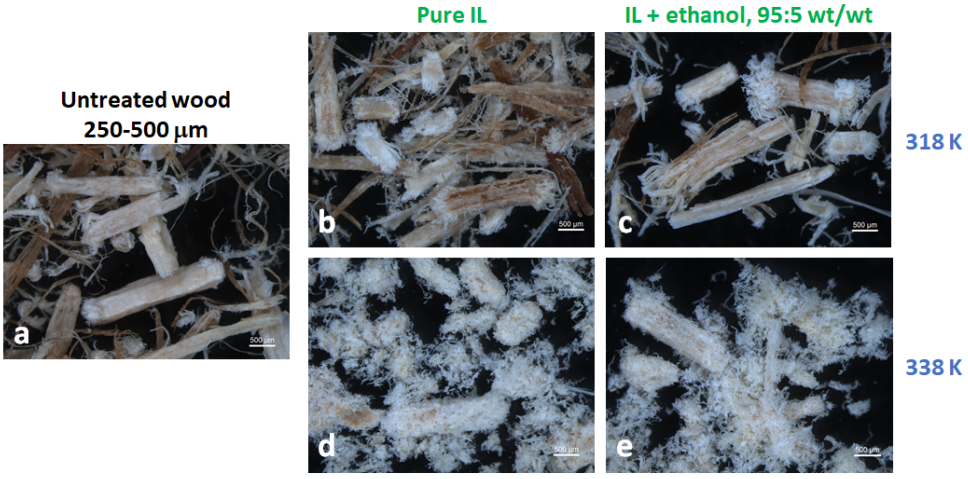

Figure 5.14. Microscope images, at a magnification of 25x, of a) untreated *E. globulus* particles of size 250-500 μm; and b) the corresponding particles pretreated with the solvent and at the temperatures indicated. ("IL" stands for [C_2mim][OAc].)

Trying to link the observed fibrillation with the potential changes induced in the biopolymeric matrix of the wood particles by the pretreatment, powder X-ray diffraction analyses were carried out. Comparing the diffractograms of the untreated wood particles and of the particles after the non-dissolving pretreatment, an important reduction of the crystallinity of cellulose in the wood is noticed. This is numerically shown in Figure 5.15, where a good correspondence of the reduction in the crystallinity index with the increased level of fibrillation previously discussed can be observed. In essence, a low reduction of the degree of crystallinity occurs for the pretreatments performed at 318 K; whereas a remarkable reduction is noticeable for the pretreatments carried out at 338 K, with the reduction being even stronger if the 95:5 wt/wt [C_2mim][OAc] + ethanol mixture is utilised as solvent instead of the neat [C_2mim][OAc]. Regarding the influence of the particle size, and as possibly expected, a smaller particle size improves the decrease of the degree of crystallinity, especially in those pretreatment conditions under which decrystallisation is notably undergone. A maximum decrystallisation of ca. 50 %, relative to the untreated wood, was obtained for the wood particles of size 125-250 μm pretreated at 338 K with the 95:5 wt/wt [C_2mim][OAc] + ethanol mixture.

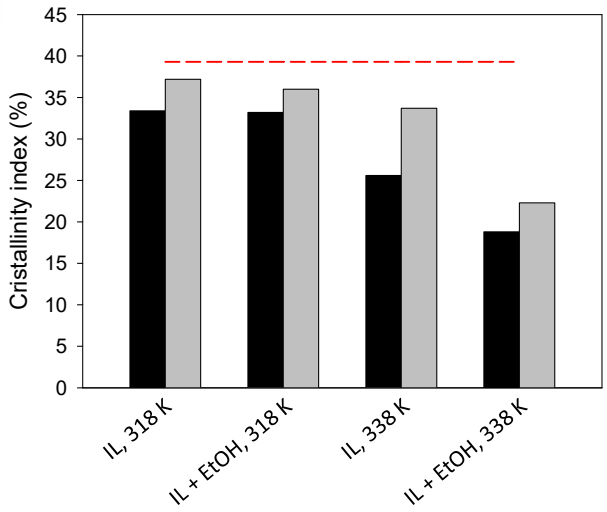

Figure 5.15. Crystallinity index for eucalyptus particles pretreated with neat [C_2mim][OAc] (IL) or a 95:5 wt/wt mixture of [C_2mim][OAc] + ethanol (IL + EtOH), at the indicated temperatures. Black columns correspond to particles in the size range 125-250 μm, and gray columns correspond to particles in the size range 250-500 μm. The red horizontal dashed line at 39.3 % indicates the crystallinity index of the untreated particles (calculated as the average of independent determinations on particles of the two size ranges investigated).

The morphological fibrillation, together with a notable decrease of the degree of crystallinity of cellulose in the wood, are promising elements for a more facilitated reactivity of the cellulose and its transformation, by means of miscellaneous downstream processes, into other chemicals of relevance within a biorefinery scheme.

5.3.2. Composition and yield of the pretreated wood

The percentage compositions of cellulose, hemicellulose, and lignin of the original *E. globulus* wood and of the wood obtained after pretreatment under different conditions are presented in Figure 5.16. At a first glance, it can be observed that the conditions at which the pretreatment is carried out do not affect strongly the relative concentration of the major biopolymers in the wood. The most relevant variation corresponds to lignin, with all pretreatments leading to a certain decrease of the lignin percentage in the wood with respect to the original material. Nevertheless, this reduction in the lignin content is much smaller than the one typically obtained in conventional pretreatments, which heavily focus on delignification for improving the access to the carbohydrate polymers for their facilitated transformation in downstream processes. The non-dissolving pretreatment proposed herein, while being successful in improving the accessibility to cellulose (and likely to hemicellulose as well), as discussed in Section 5.3.1, is also able to keep most of the lignin in its polymeric form in the pretreated wood (instead of degrading it, as the conventional pretreatment methods usually do, in a way that does not permit its high added-value valorisation). This observation is consistent with the high values of yield (amount of washed and dried pretreated wood over amount of original wood prior to the pretreatment) that have been consistently obtained in the different experiments, and which are reported in Table 5.1. Thus, this non-dissolving method would permit, within the framework of a biorefinery process, a more versatile and high added-value exploitation of the lignin fraction present in the lignocellulosic raw material being treated.

Regarding the effect of the different variables analysed in the pretreatment, a first noticeable aspect is that the particle size, within the range studied, seems to have generally little influence in the composition of the pretreated wood obtained. However, this must be considered in combination with the fact that, as described in Section 5.3.1, a smaller particle size will favour the decrease in crystallinity of cellulose (and allegedly its subsequent reactivity).

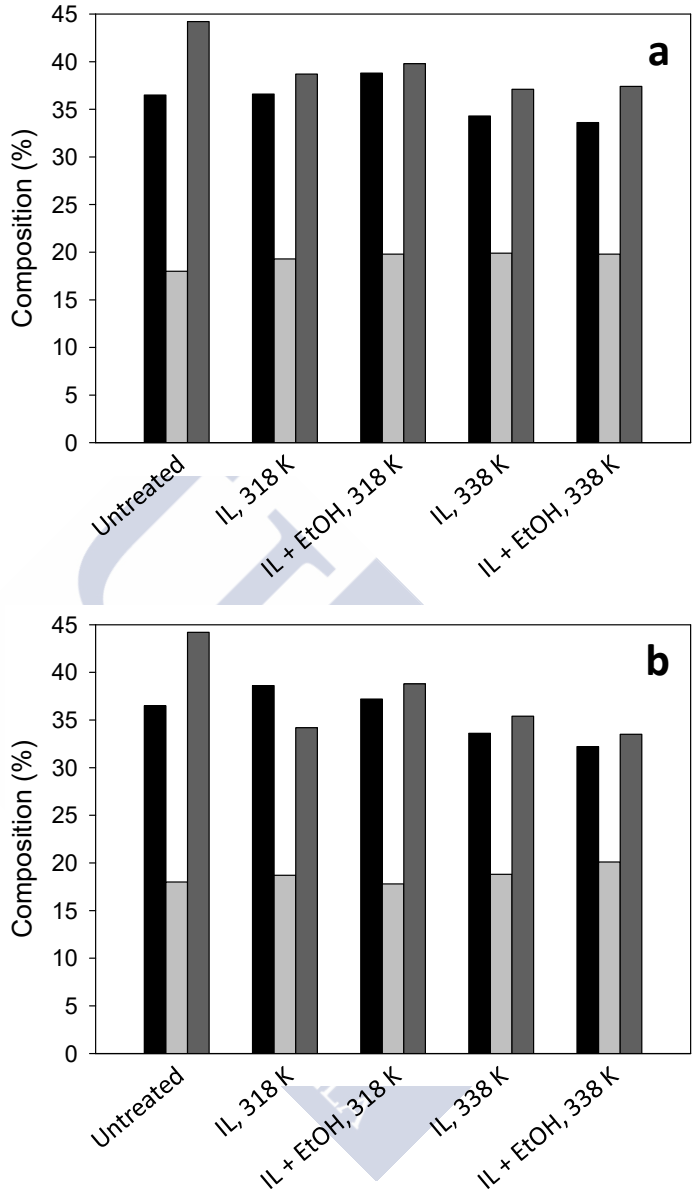

Figure 5.16. Content of cellulose (black bars), hemicellulose (light gray bars), and lignin (dark gray bars) of the untreated eucalyptus wood and of the wood pretreated with neat [C_2mim][OAc] (IL) or a 95:5 wt/wt mixture of [C_2mim][OAc] + ethanol (IL + EtOH), at the indicated temperatures. Particles size range: a) 125-250 μm; b) 250-500 μm.

Table 5.1. Mass percentage of solids recovered after pretreatment, with respect to the mass of the original wood, for the different pretreatment experiments, using neat [C_2mim][OAc] ("IL") or with a 95:5 wt/wt mixture of [C_2mim][OAc] + ethanol ("IL + EtOH") as solvents, of particles of E. globulus of the indicated particle size for 16 h at the indicated temperature.

Solvent	Particle size / μm	Temperature / K	Recovered solid (%)
IL	125-250	318	90.7
		338	87.9
	250-500	318	83.5
		338	96.7
IL + EtOH	125-250	318	90.9
		338	87.9
	250-500	318	95.4
		338	93.3

With respect to the effect of temperature, a lower contribution of the three biopolymers to the total composition is observed in the case of the samples pretreated at the high temperature (338 K). This may be due to the occurrence of polymer degradation to a somewhat larger extent at this temperature. Therefore, the temperature 318 K might be preferable from this point of view, although this preference is in conflict with the larger degree of decrystallinisation that was observed in the pretreatments at 338 K (see Figure 5.15).

Finally, the introduction of ethanol as pretreatment cosolvent does not affect in a relevant manner the resulting composition of the pretreated eucalyptus, while it is beneficial from the point of view of crystallinity reduction, as well as in terms of the engineering of the process as a result of its capacity to lower the viscosity of the neat ionic liquid (see Section 4.4.2).

6. PRETREATMENT OF SPRUCE WOOD WITH PHOSPHONIUM IONIC LIQUIDS

USC
UNIVERSIDADE
DE SANTIAGO
DE COMPOSTELA

6. PRETREATMENT OF SPRUCE WOOD WITH PHOSPHONIUM IONIC LIQUIDS

6.1. Motivation

Phosphonium ionic liquids are, in general, more thermally stable compared to their imidazolium analogues (Bradaric et al., 2003), thus extending the range of operating temperatures and allowing for increased kinetic and thermodynamic control. In addition, tetraalkylphosphonium ionic liquids may be typically derived from trialkylphosphines which are produced in large-scale industrial processes, thus contributing to the possibility of a low-cost manufacturing of the ionic liquid if implemented in scaled-up in industrial processes (Bradaric et al., 2003). Given these good characteristics of phosphonium ionic liquids, their use in a non-dissolving pretreatment of woody biomass (analogous to that presented in Chapter 5) will be explored.

There are no reports of tetraalkylphosphonium ionic liquids dissolving wood. It has been recently found, nevertheless, that ionic liquids with a tetraalkylphosphonium cation and the acetate anion can dissolve cellulose when combined with a molecular solvent such as dimethylsulfoxide (DMSO) (Holding et al., 2014). This can be taken as a promising fact for the desired interaction that a fluid system based on these ionic liquids may have on the non-dissolving pretreatment of wood.

Compared to the neat phosphonium ionic liquid, the presence of DMSO leads to a notable reduction of the viscosity of the solution. This is an aspect of critical importance in a large-scale industrial process for wood pretreatment. Nevertheless, in trying to improve the sustainability credentials of the pretreatment system suggested, it would be of interest to replace the polar aprotic DMSO with another solvent of renewable origin and similarly low volatility. An attractive candidate can be γ-valerolactone, (GVL), a recognised green solvent with great potential in this type of applications, which is obtained from renewable sources (Horváth et al., 2008).

The purpose of this chapter is therefore the development of a procedure for the non-dissolving pretreatment of wood based on the ability of some representative

tetraalkylphosphonium acetates, alternatively in combination with polar aprotic solvents such as DMSO or GVL.

The work presented in this chapter was carried out in the Department of Chemistry of the University of Helsinki, in Finland. In this country, as well as in the Scandinavian Peninsula, forestry is a tremendously abundant renewable resource, with coniferous species being of particular relevance. Among them, the so-called Norway spruce (*Picea abies*) has been selected for investigation of the pretreatment of its wood with the above mentioned fluid systems.

6.2. Experimental

6.2.1. Materials

Two tetraalkylphosphonium acetate ionic liquids were aim of study, with alkyl substituent chains of different lengths: tetrabutylphosphonium acetate [P_{4444}][OAc] and methyltrioctylphosphonium acetate [P_{8881}][OAc] (see chemical structures in Figure 6.1).

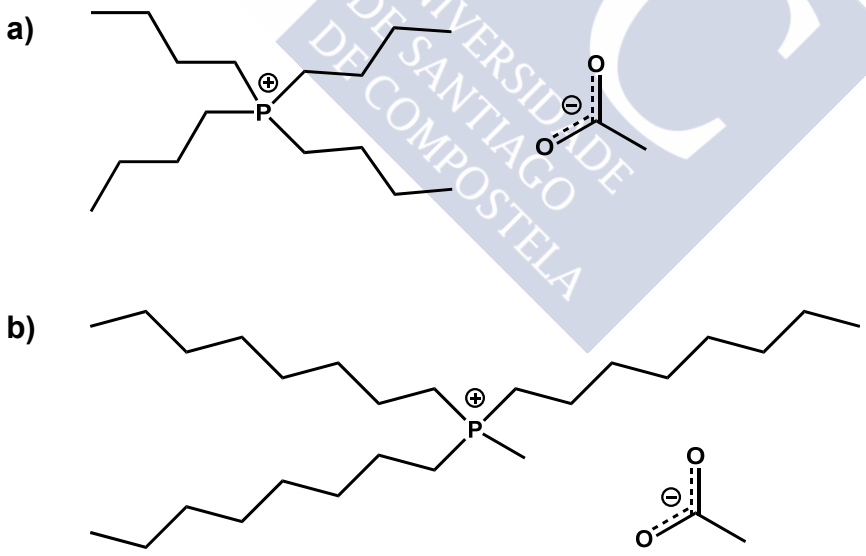

Figure 6.1. Chemical structures of: a) tetrabutylphosphonium acetate ([P_{4444}][OAc]); and b) methyltrioctylphosphonium acetate ([P_{8881}][OAc]).

The ionic liquid [P_{4444}][OAc] was synthesised by metathesis between tetrabutylphosphonium chloride (obtained in a dry form by evaporation of water under vacuum from its 80 % aqueous solution, donated by CYTEC) and potassium acetate (Sigma Aldrich, 99 %), using 2-propanol (Sigma Aldrich, 99.5 %) as solvent, following the procedure reported by Mikkola et al. (2015). A 20 % excess of potassium acetate over the stoichiometric amount was used, and the mixture was stirred overnight at 358 K with reflux. The heterogeneous mixture obtained (as a result of the precipitation of potassium chloride) was filtered through a celite bed, and the filtrate was evaporated to dryness in a rotary evaporator. Acetone (Sigma Aldrich, ≥99.9 %) was added and mixed with the dry filtrate, and then it was stored in the fridge for several hours, to promote the precipitation of any excess potassium salts. Then the solution was filtered through a celite bed again, and the acetone being removed by rotary evaporation. The steps from the addition of acetone were repeated until no further precipitate was observed in the medium.

The ionic liquid [P_{8881}][OAc] was synthesised by personnel of the Department of Chemistry of the University of Helsinki, following a previously published method by Fabris et al. (2009) which uses the carbonated-based ionic liquid synthesis process (Kalb, 2011).

Both ionic liquids were purified under reduced pressure with heating and stirring. Absence of relevant levels of impurities in the purified products, including water, was verified by NMR spectroscopy. In Appendix A, ^{1}H and ^{13}C NMR spectra of both [P_{4444}][OAc] and [P_{8881}][OAc] are presented.

Dimethylsulfoxide (DMSO) and γ-valerolactone (GVL) were supplied by Sigma Aldrich with nominal purities of ≥99.9 and 99 %, respectively, and used as received. Their chemical structures are shown in Figure 6.2.

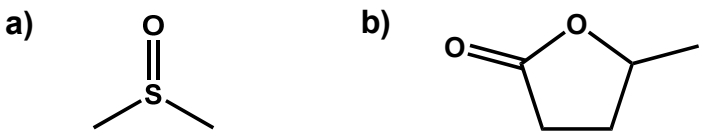

Figure 6.2. Chemical structures of: a) dimethylsulfoxide (DMSO); and b) γ-valerolactone (GVL).

Dry Norway spruce (*Picea abies*) chips were cut from the dry heartwood to an approximate size of $1 \times 1 \times 0.5$ cm^3. Wet industrial chips with a water content of

ca. 5 %, supplied by the company Metsä Fiber, were chopped down to a similar size. Industrial sawdust of the same species, also with an approximate water content of 5 %, was also provided by Metsä Fiber. As representative standards of the biopolymers cellulose, hemicellulose, and lignin in the spruce chips, the following were respectively used: Avicel® PH-101 cellulose powder supplied by Sigma Aldrich; galactoglucomannan recovered by spray-drying waters from Norway spruce thermomechanical pulping, donated by Stefan Willför from Åbo Academy University; and dioxane acidolysis lignin from Norway spruce, extracted with a 0.2 N solution of HCl in a 9:1 v/v mixture of dioxane and water, according to the procedure reported by Holding et al. (2014).

6.2.2. Equipment and procedure

Pretreatment experiments

In an initial set of experiments, pure ionic liquid [P_{4444}][OAc], pure DMSO, pure GVL, and the 50:50 wt/wt combinations of the ionic liquid with each of the molecular solvents were explored as fluid media for the pretreatment of dry spruce chips. A schematic of the experimental procedure followed is shown in Figure 6.3. Approximate masses of 0.1 g of wood and 2.0 g of solvent, yielding a solid-to-liquid ratio of 5:100 wt/wt, were systematically used. Four different temperatures were investigated for the cooking step: 353 K, 373 K, 393 K, and 413 K. Each solid-liquid mixture was loaded into a glass vial, capped and partially immersed in a silicon oil bath at the desired temperature (monitored by a thermometer) on a hot plate with magnetic stirring function. After vigorous stirring of the heterogeneous mixture overnight (ca. 16 h), the chips were removed from the vial (either by filtration or, in the case of high viscosity of the liquid, with the help of tweezers), leaving behind the solution phase. The chips obtained at this point were thoroughly washed in refluxing ethanol at 333 K for 4 h and, after filtration with a fritted glass Allihn filter tube under soft vacuum, they were dried in a vacuum oven overnight at 353 K. The solution phase previously obtained was also washed with ethanol, ensuring that no precipitation of dissolved materials occurred.

In a subsequent set of analogous experiments, the pure ionic liquid [P_{8881}][OAc] was used as fluid medium for the pretreatment of dry spruce chips as well as of wet industrial spruce chips. The solids loading, temperatures investigated, pretreatment time, and work-up procedure were the same as in the paragraph above.

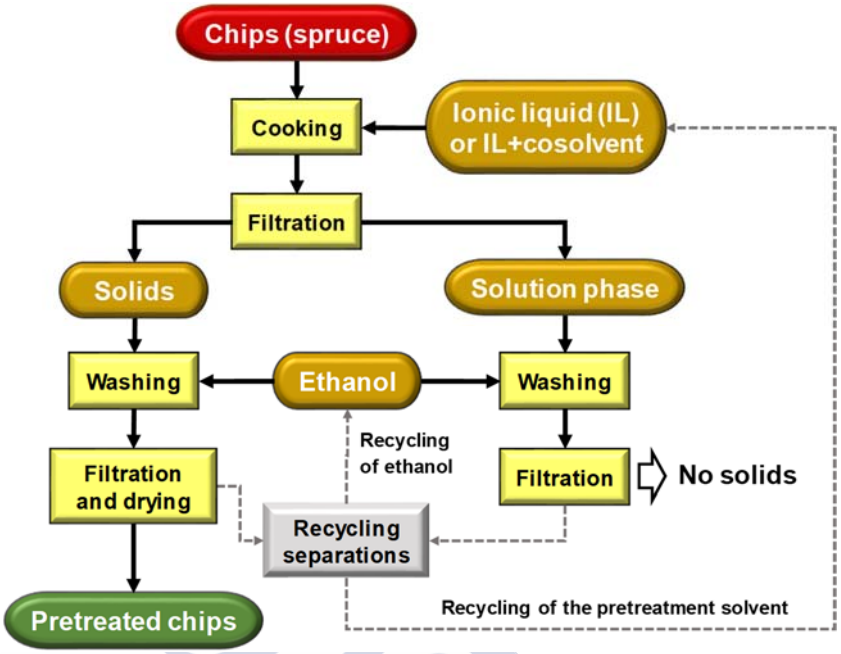

Figure 6.3. Scheme of the procedure for the experiments of pretreatment of spruce chips. The gray dashed lines and the gray box correspond to steps not considered in the experimental work developed, but which visualise the potential for recycling of the solvents in a continuous process.

In selected cases, some of the experiments described were reproduced at a higher temperature (433 K) during a shorter period of time (6 h).

Pretreatment experiments at a larger scale, using either wet industrial chips or industrial sawmill sawdust as lignocellulosic material, were also carried out in a 50-mL jacketed glass reactor made in-house (Figure 6.4). Pure $[P_{4444}][OAc]$ or pure $[P_{8881}][OAc]$ were used as solvents, with a 10:100 solid-to-solvent ratio. The temperature was kept at 413 K by circulating oil from a Julabo CF41 thermostatic bath through the reactor jacket. After pretreatment overnight (ca. 16 h), the solids were removed and washed with refluxing ethanol at 373 K for 1 h, followed by washing with refluxing water at 393 K for 1 h and subsequent drying in a vacuum oven.

An Olympus BX51 microscope (Figure 6.5) was used for microscopic photographing of pretreated biomass in selected experiments.

All weighing was carried out in a Precisa Series 321 LX analytical balance (Figure 6.6) with a readability of 10^{-4} g.

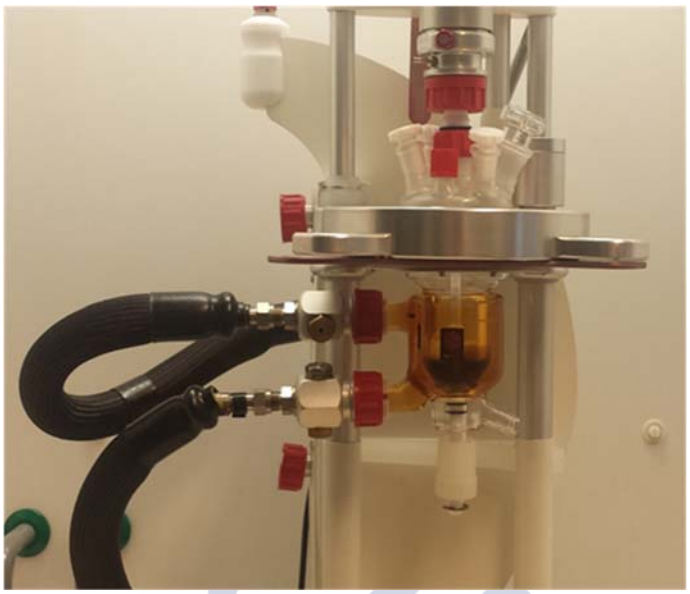

Figure 6.4. Jacketed glass reactor for larger-scale experiments of pretreatment of industrial chips.

Figure 6.5. Olympus BX51 microscope.

Figure 6.6. Precisa Series 321 LX analytical balance.

Compositional characterisation of extracts and pretreated wood

The solution phase after pretreatment in selected experiments was analysed by ^{1}H NMR spectroscopy. A certain amount of the liquid was placed in an NMR tube and diluted with deuteriated DMSO (abbreviated as DMSO-d_6, purchased from Eurisotop with a deuterisation of 99.80 % D) up to a ratio of 20:80 wt/wt of solution phase to deuteriated solvent. The homogeneous sample thus obtained was run in a Varian Mercury Plus 300 spectrometer with a frequency of 300 MHz for ^{1}H. This spectrum was compared to those of the representative standards of the three major biopolymers (see Section 6.2.1) dissolved in a 20:80 wt/wt mixture of [P_{4444}][OAc] + DMSO-d_6.

The compositional analysis of the biomass pretreated in the large-scale experiments was performed at the Department of Forest Products Technology in Aalto University, according a protocol based on that by Sluiter et al. (2012), although using high-performance anion exchange chromatography with pulsed amperometric detection for the quantification of sugars resulting from the hydrolysis of the carbohydrates (Hauru et al., 2013).

6.3. Results and discussion

6.3.1. Pretreatment experiments

The appearance of the untreated chips and those pretreated under different conditions with [P_{4444}][OAc], DMSO, GVL, and their 50:50 wt/wt combinations of ionic liquid and molecular solvent, are shown in Figure 6.7. Either little change or an evident thermal degradation of the biomass is observed in those cases involving the molecular solvents, at the different temperatures tested. Conversely, fibrillation could be clearly observed in the wood treated with the pure [P_{4444}][OAc] at 413 K and, to a lesser extent, at 393 K (see zoomed-up photographs in Figure 6.7b). The microscope image shown in Figure 6.8 corroborates the occurrence of such fibrillation, allowing for observation of the breakdown of fibres in greater detail.

Given the negative effect caused by the presence in the pretreatment fluid of the molecular solvents on [P_{4444}][OAc] to induce significant fibrillation of the spruce chips, with [P_{8881}][OAc] only experiments with the ionic liquid in neat were tried. In this case not only the dried spruce chips were pretreated, but also wet industrial spruce chips, which have a water content of ca. 5 wt%. The appearance of the pretreated biomass obtained after these experiments is shown in the photographs in Figure 6.9. This time an incipient fibrillation is observed exclusively in the case of the pretreatment experiments conducted at 413 K, although it happens not only with the dry chips but also with the wet industrial chips.

From comparison of the results observed in Figures 6.7 and 6.9 it can be stated that [P_{4444}][OAc] performs better than [P_{8881}][OAc] as solvent for the pretreatment, at least in terms of fibrillation, of dry spruce chips.

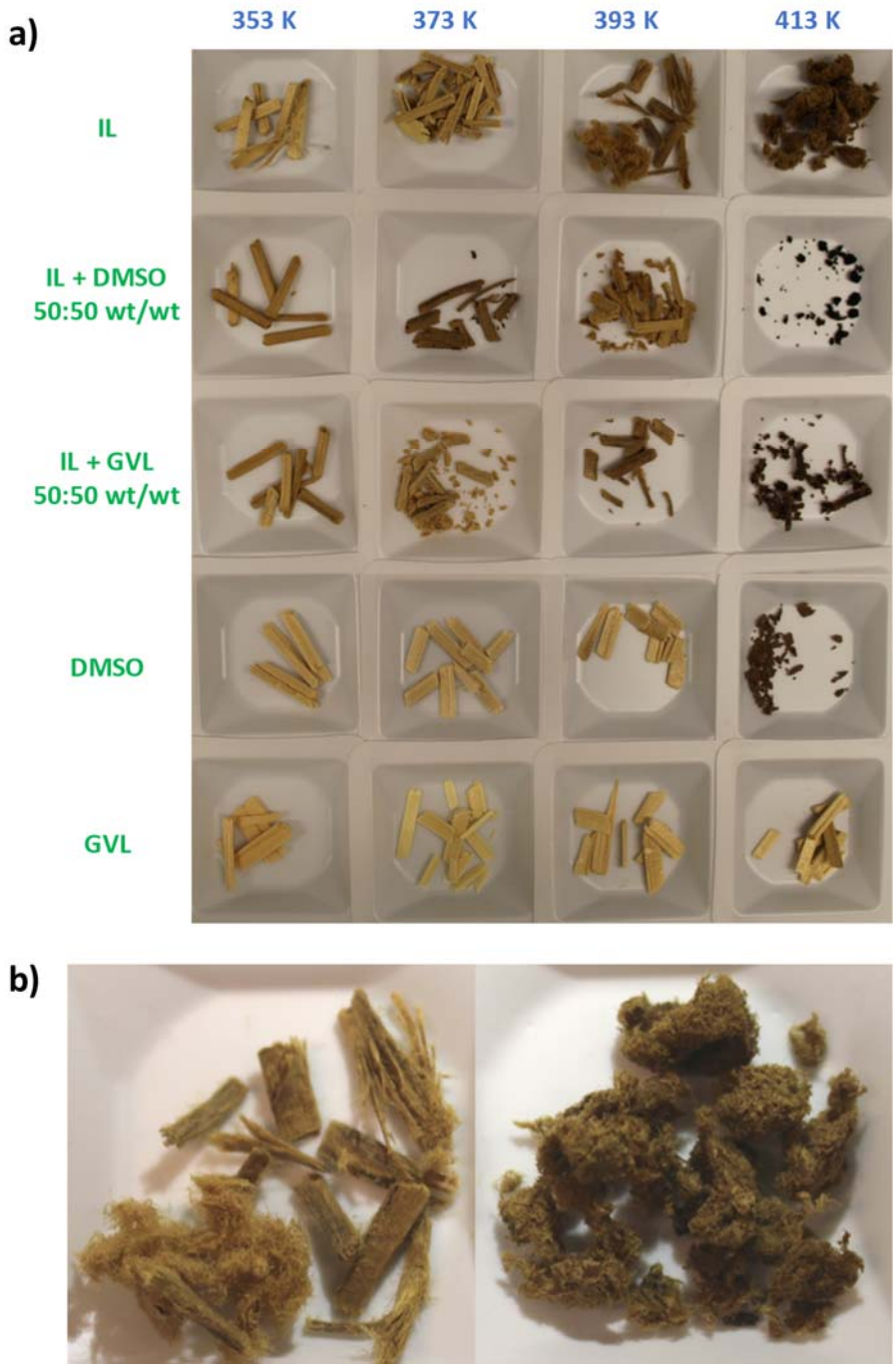

Figure 6.7. a) Photographs of dry spruce chips after overnight pretreatment at the indicated temperatures, at a solids load of 5 g of chips per 100 g of solvent, in different fluid systems (rows from top to bottom): pure $[P_{4\,4\,4\,4}][OAc]$ (IL), 50:50 wt/wt mixture of IL + DMSO, 50:50 wt/wt mixture of IL + GVL, pure DMSO, and pure GVL. b) Zoomed-up photographs of the chips pretreated with pure $[P_{4\,4\,4\,4}][OAc]$ at 393 K (left) and at 413 K (right).

Figure 6.8. Microscope image of the dry spruce chips pretreated with [P_{4444}][OAc] at 413 K.

Figure 6.9. Photographs of dry and wet industrial spruce chips after overnight pretreatment at the indicated temperatures in [P_{8881}][OAc], with a solids load of 5 g of chips per 100 g of solvent.

6.3.2. Compositional characterisation of extracts and pretreated wood

In order to shed some light on the main constituents of wood biomass possibly extracted during the pretreatment experiments into the solution phase, the latter was analysed by ^{1}H NMR spectroscopy. In principle the spectra obtained resembled that of the solvent (ionic liquid), indicating that negligible or very little amount of biomass is actually extracted into the solution phase. Nevertheless, by zooming-up sufficiently the spectra, peaks of those extracted traces could be identified. As an example, Figure 6.10 shows the spectrum corresponding to the case of pretreatment of dry spruce chips with

[P_{4444}][OAc] (solid-to-liquid ratio of 5:100 wt/wt) at 433 K for 6 h, along with the spectra of the representative standards of the main biopolymers; all of them largely zoomed-up in the approximate x-axis range 2.8-8.2 ppm. By direct visual comparison, in the spectrum of the liquid phase after pretreatment it is possible to observe signals that can be connected to each one of the standards, although perhaps characteristic peaks of the standards of the carbohydrates (and in particular of hemicellulose) are more noticeably identifiable. Therefore, it can be assumed that small amounts of cellulose, hemicellulose, and lignin have been extracted from the chips during the pretreatment, possibly with preference of hemicellulose; although it is difficult to quantify by ^{1}H NMR spectroscopy the relative amounts of each, due to the low intensity of the peaks in the spectrum.

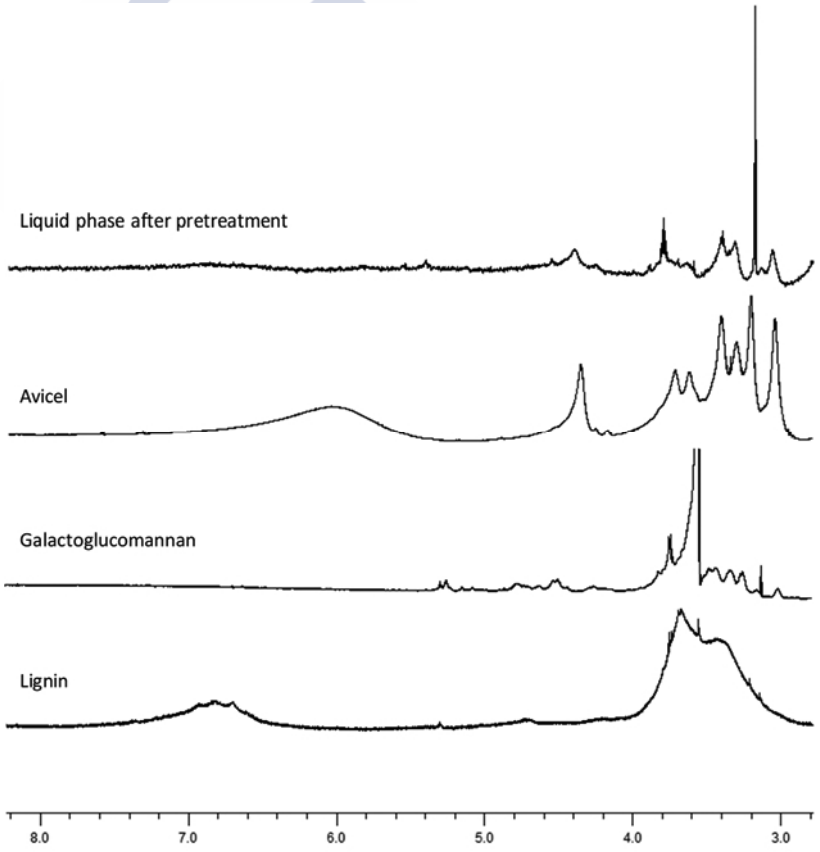

Figure 6.10. ^{1}H NMR spectrum of the liquid phase after pretreatment of dry spruce chips with [P_{4444}][OAc] (solid-to-liquid ratio of 5:100 wt/wt) at 433 K for 6 h, together with the ^{1}H NMR spectra of standards of the different biopolymers (Avicel, galactoglucomannan, and dioxane acidolysis spruce lignin – see Section 6.2.1). The bottom scale is expressed in ppm.

In an alternative approach, a focus on the pretreated solid was put for the experiments carried out in a larger scale. Thus, the contents in the three major biopolymers of the fibrillated materials obtained after pretreatment of 10 wt% industrial chips or sawmill sawdust with [P_{4444}][OAc] or with [P_{8881}][OAc] were determined, and are shown in Figure 6.11, together with those corresponding to the untreated materials. In general, an important reduction of the hemicellulose content is observed in the materials after the pretreatment (inherently causing a slight increment in the percentages of cellulose and lignin in most cases). This reduction in the hemicellulose content is stronger in the case of the pretreatment with [P_{4444}][OAc], regardless of the type of spruce raw material (chips or sawdust). Hemicellulose is crucial in the establishment of chemical linkages of the different biopolymers in biomass, so probably the fibrillation observed macroscopically is a result of the loss of hemicellulose identified in Figure 6.11. The pretreatments with [P_{8881}][OAc] lead to a lower reduction of hemicellulose, thus being consistent with the previous observation of this ionic liquid leading to a less effective fibrillation of the target biomass than the one achieved with [P_{4444}][OAc].

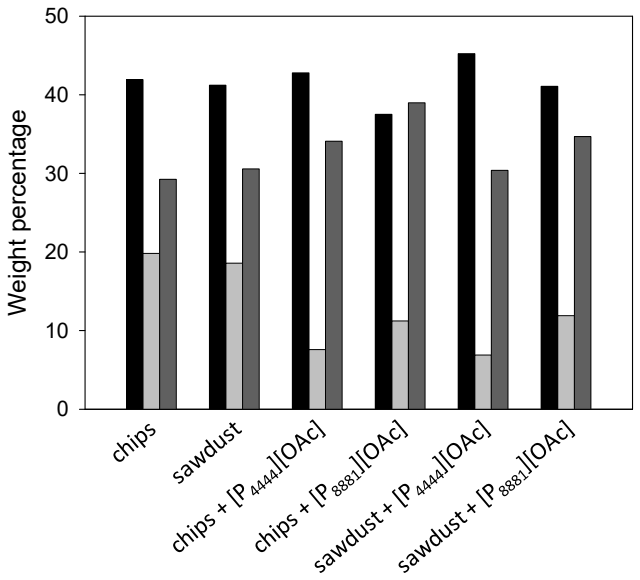

Figure 6.11. Weight percentages of cellulose (black, columns on the left), hemicellulose (light gray, central columns), and lignin (dark gray, columns on the right) of wet industrial spruce chips and spruce sawdust, before and after pretreatment with [P_{4444}][OAc] or [P_{8881}][OAc] in the large-scale experiments at 413 K overnight with a loading of 10 g of solid per 100 g of solvent.

7. CONCLUSIONS

USC
UNIVERSIDADE
DE SANTIAGO
DE COMPOSTELA

7. CONCLUSIONS

The conclusions drawn from the original results reported and discussed in this thesis are presented below, grouped according to the distribution of the contents in Chapters 3-6.

Mutually immiscible ionic liquids

1-Alkyl-3-methylimidazolium chlorides or acetates with a sufficiently short alkyl substituent chain give rise to liquid-liquid biphasic systems when combined with ionic liquids with the same anion and the $[P_{6\,6\,6\,14}]^+$ or $[Aliquat]^+$ cations. The presence of the ammonium/phosphonium ionic liquid in the imidazolium-rich phase is very low or even negligible; whereas a substantially higher concentration of the imidazolium ionic liquid is present in the ammonium/phosphonium-rich phase. The systems confronting the $[C_2mim]^+$ and $[P_{6\,6\,6\,14}]^+$ cations are entropically driven, whereas the systems confronting the $[C_nmim]^+$ and $[Aliquat]^+$ cations display an hourglass-shaped liquid-liquid domain in the temperature-composition diagrams, progressing from enthalpically driven to entropically driven with increasing temperature. The UCST or LCST points of these systems are not achieved within the temperature range of liquid stability of the ionic liquids involved in the different mixtures. This is unfortunate for the application of these mixtures as integrated solvent-antisolvent fluid systems for the pretreatment of lignocellulosic materials. Nevertheless, given the remarkable thermal stability and non-volatile character of ionic liquids, the biphasic systems described herein can be of particular interest for liquid-liquid extractions at elevated temperature.

Mixtures of $[C_2mim][OAc]$ + alcohol. Solubility of biopolymers

The density, viscosity, refractive index, and surface tension of the binary systems $[C_2mim][OAc]$ + (methanol, or ethanol, or 1-propanol, or 2-propanol) decrease with an increase in temperature and/or alcohol concentration. Refractive index and surface tension can be adequately correlated as a function of temperature by means of a linear

fit; whereas a second-order polynomial fit is preferable for density. The VFT is suitable to describe the exponential decay observed in viscosity with increasing temperature (with the exception of the pure alcohols and mixtures with very low concentrations of ionic liquid, where the Arrhenius-type equation proposed by Andrade is preferable). Redlich-Kister polynomials correlated satisfactorily the excess molar volume, viscosity logarithm change of mixing, molar refraction change of mixing, and surface tension change of mixing for all four studied systems. Attractive forces such as hydrogen bonding and ion-dipole interactions can be assumed to predominate in the fluid mixtures, in view of the negative values of excess molar volume. Despite such attractive forces, [C_2mim][OAc] is recoverable from its mixtures with the alcohol via vaporisation of the latter by simple increase of the temperature up to temperatures safely below the decomposition temperature of the ionic liquid. Moreover, the presence of the alcohols in the liquid mixture does not have a negative effect on the thermal stability of [C_2mim][OAc].

Besides a beneficial reduction of viscosity, the addition of specific amounts of alcohol to the ionic liquid [C_2mim][OAc] allows tuning of the capacity of the ionic liquid to dissolve lignocellulosic biopolymers in relevant levels. Thus, these alcohols have an interesting potential as cosolvents of [C_2mim][OAc] in the dissolution of lignocellulose-derived fractions for their chemical conversion into other products and materials. On the other hand, the use of the alcohol as antisolvent for precipitation of the biopolymers dissolved in [C_2mim][OAc] may potentially pose serious difficulties with the use of moderate amounts of alcohol relative to the amount of ionic liquid, since undesired emulsions and gel-like phases may be formed upon the addition of the alcohol.

Pretreatment of *Eucalyptus globulus* wood particles with [C_2mim][OAc] or a mixture [C_2mim][OAc] + alcohol at low temperatures

The pretreatment of *E. globulus* (white eucalyptus) wood particles with [C_2mim][OAc] or with a 95:5 wt/wt mixture of [C_2mim][OAc] and ethanol at 338 K leads to a high degree of fibrillation and an important reduction of the crystallinity of the wood at non-dissolving conditions. These effects are expected to facilitate the further processing and transformation of the biopolymers contained in the wood. Moreover, a high percentage of the original biomass is recovered after the pretreatment, thus minimising the loss of raw material. In this way, the proposed pretreatment would guarantee that most of the

original biomass enters the processing stages after the pretreatment in a biorefinery context, optimally exploiting it.

Pretreatment of *Picea abies* wood particles with [P_{4444}][OAc] or [P_{8881}][OAc]

The pretreatment of *P. abies* (Norway spruce) chips with the ionic liquid [P_{4444}][OAc] at 413 K leads to substantial fibrillation of the wood. The use of DMSO or GVL as cosolvents has an inhibiting effect in this pretreatment efficacy, though. The pretreatment with [P_{8881}][OAc] also leads to some fibrillation of the particles, but more incipient than when using [P_{4444}][OAc]. In the pretreated solids, a significant reduction in the content of hemicellulose occurs, which is likely degraded during the pretreatment, as practically negligible concentrations of biopolymers are detected in the solvent after the pretreating.

USC
UNIVERSIDADE
DE SANTIAGO
DE COMPOSTELA

List of symbols

USC
UNIVERSIDADE
DE SANTIAGO
DE COMPOSTELA

List of symbols

A	absorbance
A	fit parameter in the VFT equation for viscosity
A_k	fit parameter in the Redlich-Kister equation
a	absorptivity
a	activity
a	fit parameter in Equation 3.18
a_0	fit parameter in Equations 4.19 and 4.22
a_1	fit parameter in Equations 4.19 and 4.22
a_2	fit parameter in Equation 4.22
b	fit parameter in Equation 3.18
b	path length of the UV quartz cuvette
b_0	fit parameter in Equation 4.20
b_1	fit parameter in Equation 4.20
c	fit parameter in Equation 3.18
c_0	fit parameter in Equation 4.21
c_1	fit parameter in Equation 4.21
DF	dilution factor
E_a	'activation' energy; fit parameter in the Andrade equation for viscosity
F	number of degrees of freedom
f	fugacity
G	Gibbs free energy
H	enthalpy
k	fit parameter in the VFT equation for viscosity
$LCST$	lower critical solution temperature
M	molar mass
m	degree of the polynomial expansion
m	mass
m	number of experimental data points
N	number of components
n	number of moles
n	total number of experimental data

n_D	refractive index
P	pressure
R	universal constant of gases
R_M	molar refraction
rmsd	root mean square deviation
S	entropy
SD	standard deviation
T	temperature
T_0	fit parameter in the VFT equation for viscosity
$UCST$	upper critical solution temperature
V	volume
V	molar volume
v	velocity
W	total mass of sample
x	mole fraction in the liquid phase
x	spatial direction
y	spatial direction

Subscripts

app	apparent
ashed	after ashing in the furnace
calc	calculated value
d	decomposition
dat	data
exp	experimental value
g	glass transition
hm	harmonic mean
i	component void counter
id	ideal mixture
IL	ionic liquid
j	component void counter
k	void counter
low	lower phase

m	melting
m	mixture
non-ashed	before ashing in the furnace
P	constant pressure
p	parameter
rel	relative value
T	constant temperature
up	upper phase
x	vector component in the *x* direction
0	value at the initial time

Superscripts

E	excess property
id	ideal solution property
ip	inflection point
k	phase void counter
L	liquid phase
L	lower phase
m	number of phases
U	upper phase
V	vapour phase
0	standard state

Greek letters

α	liquid phase richer in component 2
β	liquid phase richer in component 1
γ	activity coefficient
Δ	variation of property
η	dynamic viscosity
$\eta\infty$	dynamic viscosity at infinite temperature; fit parameter in the Andrade equation for viscosity
μ	chemical potential

ν	kinematic viscosity
π	number of phases
ρ	density
σ	surface tension
τ_{yx}	shear stress in the x direction on a unit area perpendicular to the y direction

References

USC
UNIVERSIDADE
DE SANTIAGO
DE COMPOSTELA

References

A

Adam, G.; Gibbs, J. H. (1965). "On the Temperature Dependence of Cooperative Relaxation Properties in Glass-Forming Liquids", *J. Chem. Phys.*, 43, 139-146.

Almeida, H. F. D.; Passos, H.; Lopes-da-Silva, J. A.; Fernandes, A. M.; Freire, M. G.; Coutinho, J. A. P. (2012a). "Thermophysical Properties of Five Acetate-Based Ionic Liquids", *J. Chem. Eng. Data*, 57, 3005-3013.

Almeida, H. F. D.; Teles, A. R. R.; Lopes-da-Silva, J. A.; Freire, M. G.; Coutinho, J. A. P., (2012b). "Influence of the anion on the surface tension of 1-ethyl-3-methylimidazolium-based ionic liquids", *J. Chem. Thermodyn.*, 54, 49-54.

Andanson, J.-M.; Pádua, A. A. H.; Costa Gomes, M. F. (2015). "Thermodynamics of cellulose dissolution in an imidazolium acetate ionic liquid", *Chem. Commun.*, 51, 4485-4487.

Andrade, E. N. da C. (1930). **"**The viscosity of liquids", *Nature*, 125, 309-310.

Angell, C. A.; Moynihan, C. T. (1969). "Transport Processes in Low-Melting Molten Salt Systems", in: *Molten Salts. Characterization and Analysis* (Ed.: G. Mamantov), Marcel Dekker, New York (USA).

Arce, A.; Earle, M. J.; Katdare, S. P.; Rodríguez, H.; Seddon, K. R. (2006). "Mutually immiscible ionic liquids", *Chem. Commun.*, 2548-2550.

Arce, A.; Earle, M. J.; Katdare, S. P.; Rodríguez, H.; Seddon, K. R. (2007). "Phase equilibria of mixtures of mutually immiscible ionic liquids", *Fluid Phase Equilibr.*, 261, 427-433.

B

Badgujar, K. C.; Bhanage, B. M. (2015). "Factors governing dissolution process of lignocellulosic biomass in ionic liquid: Current status, overview and challenges", *Bioresour. Technol.*, 178, 2-18.

Balensiefer, T.; Brodersen, J.; D'Andola, G.; Massonne, K.; Freyer, S.; Stegmann, V. (2008). "Method for producing glucose by enzymatic hydrolysis of cellulose that can be pretreated with an ionic liquid containing a polyatomic anion", *PCT Int. Appl.*, WO 2008/090155.

Binder, J. B.; Raines, R. T. (2010). "Fermentable sugars by chemical hydrolysis of biomass", *Proc. Natl. Acad. Sci. U. S. A*., 107, 4516-4521.

Bradaric, C. J.; Downard, A.; Kennedy, C.; Robertson, A. J.; Zhou, Y. (2003). "Industrial preparation of phosphonium ionic liquids", *Green Chem.*, 5, 143-152.

Bradley, A. E.; Hardacre, C.; Holbrey, J. D.; Johnston, S.; McMath, S. E. J.; Nieuwenhuyzen, M. (2002). "Small-angle X-ray Scattering Studies of Liquid Crystalline 1-Alkyl-3-methylimidazolium Salts", *Chem. Mater*., 14, 629-635.

Brandt, A.; Gräsvik, J.; Hallett, J. P.; Welton, T. (2013). "Deconstruction of lignocellulosic biomass with ionic liquids", *Green Chem*., 15, 550-583.

C

Cai, J.; Cui, X.; Zhang, Y.; Li, R.; Feng, T. (2011). "Vapor-Liquid Equilibrium and Liquid-Liquid Equilibrium of Methyl Acetate + Methanol + 1-Ethyl-3-methylimidazolium Acetate", *J. Chem. Eng. Data*, 56, 282-287.

Canosa, J.; Rodríguez, A.; Tojo, J. (2000). "Dynamic viscosities of the binary mixtures (methyl acetate or methanol + 2-methyl-2-butanol) and the ternary mixtures (methyl acetate + methanol + 2-propanol, or 2-butanol, or 2-methyl-2-butanol) at *T* = 298.15 K", *J. Chem. Thermodyn*., 32, 551-565.

Cao, Y.; Mu, T. (2014). "Comprehensive Investigation on the Thermal Stability of 66 Ionic Liquids by thermogravimetric Analysis", *Ind. Eng. Chem. Res*., 53, 8651-8664.

Casas, A.; Oliet, M.; Alonso, M. V.; Santos, T. M.; Rodríguez, F. (2013). "Dissolution of Pinus radiata and Eucalyptus Globulus Woods in 1-Allyl-3-methylimidazolium Chloride for Cellulose or Lignin Regeneration", *Ind. Eng. Chem. Res.*, 52, 3628-3636.

Cherubini, F.; Jungmeier, G.; Wellisch, M.; Willke, T.; Skiadas, I.; Ree, R. V.; Jong, E. (2009). "Toward a common classification approach for biorefinery systems", *Biofuels Bioprod. Biorefin*., 3, 534-546.

Chirat, C.; Lachenal, D.; Sanglard, M. (2012). "Extraction of xylans from hardwood chips prior to kraft cooking", *Process Biochem.*, 47, 381-385.

Chum, H. L.; Johnson, D. K.; Black, S. (1998). "Organosolv pretreatment for enzymatic hydrolysis of poplars: 1. Enzyme hydrolysis of cellulosic residues", *Biotechnol. Bioeng.*, 31, 643-649.

Clark, J. H.; Deswarte, F. E. I.; Farmer, T. J. (2009). "The integration of green chemistry into future biorefineries", *Biofuels Bioprod. Biorefin.*, 3, 72-90.

Clough, M. T.; Geyer, K.; Hunt, P. A.; Mertes, J.; Welton, T. (2013). "Thermal decomposition of carboxylate ionic liquids: trends and mechanisms", *Phys. Chem. Chem. Phys*., 15, 20480-20495.

Cohen, M. H.; Turnbull, D. (1959). "Molecular Transport in Liquids and Glasses", *J. Chem. Phys*., 31, 1164-1169.

CYTEC Industries Inc. (2011). CYPHOS® IL 101 product data sheet, available online at: http://www.rsc.org/suppdata/cp/b9/b920530f/b920530f-12.pdf (last accessed: October 2018).

D

da Costa Lopes, A. M.; João, K. G.; Morais, A. R. C.; Bogel-Łukasik, E.; Bogel-Łukasik, R. (2013). "Ionic liquids as a tool for lignocellulosic biomass fractionation", *Sus. Chem. Proc.*, 1: 3.

Dadi, A. P., Schall, C. A.; Varanasi, S. (2007). "Mitigation of cellulose recalcitrance to enzymatic hydrolysis by ionic liquid pretreatment", *Appl. Biochem. Biotechnol.*, 137, 407-421.

Deng, Y.; Husson, P.; Delort, A.-M.; Besse-Hoggan, P.; Sancelme, M.; Costa Gomes, M. F. (2011). "Influence of an Oxygen Functionalization on the Physicochemical Properties of Ionic Liquids: Density, Viscosity, and Carbon Dioxide Solubility as a Function of Temperature", *J. Chem. Eng. Data*, 56, 4194-4202.

Devore, J. L. (2004). *Probability and Statistics for Engineering and the Sciences*, 6th ed., Brooks/Cole, Belmont, CA (USA).

Dibble, D. C.; Li, C.; Sun, L.; George, A.; Cheng, A.; Çetinkol, Ö. P.; Benke, P.; Holmes, B. M.; Singh, S.; Simmons, B. A. (2011). "A facile method for the recovery of ionic liquid and lignin from biomass pretreatment", *Green Chem.*, 13, 3255-3264.

Diogo, H. P.; Pinto, S. S.; Moura Ramos, J. J. (2013). "Slow molecular mobility in the amorphous solid and the metastable liquid states of three 1-alkyl-3-methylimidazolium chlorides", *J. Mol. Liq*., 178, 142-148.

E

Earle, M. J.; Seddon, K. R. (2000). "Ionic liquids. Green solvents for the future", *Pure Appl. Chem*., 72, 1391-1398.

F

Fabris, M.; Lucchini, V.; Noè, M.; Perosa, A.; Selva, M. (2009). "Ionic Liquids Made with Dimethyl Carbonate: Solvents as well as Boosted Basic Catalysts for the Michael Reaction", *Chem. Eur. J.*, 15, 12273-12282.

Fengel, D.; Wegener, G. (1989). *Wood: chemistry, ultrastructure, reactions*, De Gruyter, Berlin (Germany).

Ferreira, A. F.; Simões, P. N.; Ferreira, A. G. M. (2012). "Quaternary phosphonium-based ionic liquids: Thermal stability and heat capacity of the liquid phase", *J. Chem. Thermodyn.*, 45, 16-27.

FitzPatrick, M.; Champagne, P.; Cunningham, M. F.; Whitney, R. A. (2010). "A biorefinery processing perspective: Treatment of lignocellulosic materials for the production of value-added products", *Bioresour. Technol.*, 101, 8915-8922.

Fort, D. A.; Remsing, R. C.; Swatloski, R. P.; Moyna, P.; Moyna, G.; Rogers, R. D. (2007). "Can ionic liquids dissolve wood? Processing and analysis of lignocellulosic materials with 1-n-butyl-3-methylimidazolium chloride", *Green Chem.*, 9, 63-69.

Fraser, K. J.; Izgorodina, E. I.; Forsyth, M.; Scott, J. L.; MacFarlane, D. R. (2007). "Liquids intermediate between "molecular" and "ionic" liquids: Liquid Ion Pairs?", *Chem. Commun.*, 3817-3819.

Fredlake, C. P.; Crosthwaite, J. M.; Hert, D. G.; Aki, S. N. V. K.; Brennecke, J. F. (2004). "Thermophysical Properties of Imidazolium-Based Ionic Liquids", *J. Chem. Eng. Data,* 49, 954-964.

Freemantle, M. (2010). *An Introduction to Ionic Liquids*, RSC Publishing, Cambridge (UK).

Freemantle, M. (2016). "From trickle to torrent", *Chemistry World*, 7 October 2016. Avaliable online at: https://www.chemistryworld.com/features/ionic-liquids-revisted/1017383.article (last accessed: October 2018).

Freire, M. G.; Teles, A. R. R.; Rocha, M. A. A.; Schröder, B.; Neves, C. M. S. S.; Carvalho, P. J.; Evtuguin, D. V.; Santos, L. M. N. B. F.; Coutinho, J. A. P. (2011). "Thermophysical Characterization of Ionic Liquids Able To Dissolve Biomass", *J. Chem. Eng. Data*, 56, 4813-4822.

Fu, D.; Mazza, G.; Tamaki, Y. (2010). "Lignin Extraction from Straw by Ionic Liquids and Enzymatic Hydrolysis of the Cellulosic Residues", *J. Agric. Food Chem.*, 58, 2915-2922.

Fujita, M.; Harada, H. (2000). "Ultrastructure and formation of wood cell wall", in: *Wood and Cellulosic Chemistry* (Ed.: Hon, D. N.), Marcel Dekker, New York (USA).

Fulcher, G. S. (1925). "Analysis of Recent Measurements of the Viscosity of Glasses", *J. Am. Ceram. Soc.*, 8, 339-355.

G

Gericke, M.; Schlufter, K.; Liebert, T.; Heinze, T.; Buktova, T. (2009). "Rheological Properties of Cellulose/Ionic Liquid Solutions: From Dilute to Concentrated States", *Biomacromol.*, 10, 1188-1194.

Gibbs, J. H.; DiMarzio, E. A. (1958). "Nature of the Glass Transition and the Glassy State", *J. Chem. Phys.*, 28, 373-383.

Gomes de Azevedo, R.; Esperança, J. M. S. S.; Szydlowski, J.; Visak, Z. P.; Pires, P. F.; Guedes, H. J. R.; Rebelo, L. P. N. (2005). "Thermophysical and thermodynamic properties of ionic liquids over an extended pressure range: [bmim][NTf_2] and [hmim][NTf_2]", *J. Chem. Thermodyn.*, 37, 888-899.

Gu, Z.; Brennecke, J. F. (2002). "Volume Expansivities and Isothermal Compressibilities of Imidazolium and Pyridinium-Based Ionic Liquids", *J. Chem. Eng. Data*, 47, 339-345.

Guan, W.; Ma, X.-X.; Li, L.; Tong, J.; Fang, D.-W.; Yang, J.-Z. (2011). "Ionic parachor and its application in acetic acid ionic liquid homologue 1-alkyl-3-methylimidazolium acetate {[$C_n$mim][OAc] (n = 2, 3, 4, 5, 6)}", *J. Phys. Chem. B.*, 115, 12915-12920.

H

Hansen, C. M.; Björkman, A. (1998). "The Ultrastructure of Wood from a Solubility Parameter Point of View", *Holzforschung*, 52, 335-344.

Hasse, B.; Lehmann, J.; Assenbaum, D.; Wassercheid, P.; Leipertz, A.; Fröba, A. P. (2009). "Viscosity, Interfacial Tension, Density, and Refractive Index of Ionic Liquids [EMIM][$MeSO_3$], [EMIM][$MeOHPO_2$], [EMIM][$OcSO_4$], and [BBIM][NTf_2] in Dependence on Temperature at Atmospheric Pressure", *J. Chem. Eng. Data*, 54, 2576-2583.

Hauru, L. K. J.; Ma, Y.; Hummel, M.; Alekhina, M.; King, A. W. T.; Kilpeläinen, I.; Penttilä; Serimaa, R.; Sixta, H. (2013). "Enhancement of ionic liquid-aided fractionation of birchwood. Part 1: autohydrolysis pretreatment", *RSC Adv.*, 3, 16365-16373.

Henderson, R. K.; Jiménez-González, C.; Constable, D. J. C.; Alston, S. R.; Inglis, G. G. A.; Fisher, G.; Sherwood, J.; Binks, S. P.; Curzons, A. D. (2011). "Expanding GSK's solvent selection guide – embedding sustainability into solvent selection starting at medicinal chemistry", *Green Chem.*, 13, 854-862.

Hendriks, A. T. W. M; Zeeman, G. (2009). "Pretreatment to enhance the digestibility of lignocellulosic biomass", *Bioresour. Technol*., 100, 10-18.

Holding, A. J.; Heikkilä, M.; Kilpeläinen, I.; King, A. W. T. (2014). "Amphiphilic and Phase-Separable Ionic Liquids for Biomass Processing", *ChemSusChem*, 7, 1422-1434.

Horváth, I. T.; Mehdi, J.; Fábos, V.; Boda, L.; Mika, L. T. (2008). "γ-Valerolactone – a sustainable liquid for energy and carbon-based chemicals", *Green Chem.*, 10, 238-242.

Hou, Q.; Ju, M.; Li, W.; Liu, L.; Chen, Y.; Yang, Q. (2017). "Pretreatment of Lignocellulosic Biomass with Ionic Liquids and Ionic Liquid-Based Solvent Systems", *Molecules*, 22: 490.

Huddleston, J. G.; Visser, A. E.; Reichert, W. M.; Willauer, H. D.; Broker, G. A; Rogers, R. D. (2001). "Characterization and comparison of hydrophilic and hydrophobic room temperature ionic liquids incorporating the imidazolium cation", *Green Chem*., 3, 156-164.

I

Iolitec GmbH (2017). Online resource, available at: https://iolitec.de/products/ionic_liquids/applications (last accessed: October 2018).

Ishii, T.; Shimizu, K. (2000). "Chemistry of Cell Wall Polysaccharides", in: *Wood and Cellulosic Chemistry* (Ed.: Hon, D. N.), Marcel Dekker, New York (USA).

Isikgor, F. H.; Becer, C. R. (2015). "Lignocellulosic biomass: a sustainable platform for the production of bio-based chemicals and polymers", *Polym. Chem*., 6, 4497-4559.

J

Jacquemin, J.; Husson, P.; Majer, V.; Padua, A. A. H.; Costa Gomes, M. F. (2008). "Thermophysical properties, low pressure solubilities and thermodynamics of solvation of carbon dioxide and hydrogen in two ionic liquids based on the alkylsulfate anion", *Green Chem.*, 10, 944-950.

Jacquemin, J.; Husson, P.; Mayer, V.; Cibulka, I. (2007). "High-Pressure Volumetric Properties of Imidazolium-Based Ionic Liquids: Effect of the anion", *J. Chem. Eng. Data*, 52, 2204-2211.

Jiang, J.; Wang, J.; Zhang, X.; Wolcott, M. (2016). "Evaluation of physical structural features on influencing enzymatic hydrolysis efficiency of micronized wood", *RSC Adv.*, 6, 103026-103034.

K

Kalb, R. (2011). "Method for producing ionic liquids, ionic solids or mixtures thereof", *U.S. Patent*, patent number US 8,075,803.

Kamm, B.; Kamm, M. (2004). "Principles of biorefineries", *Appl. Microbiol Biot.*, 64, 137-145.

Keating, M. Y.; Gao, F.; Ramsey, J. B. (2011). "TGA-MS study of the decomposition of phosphorus-containing ionic liquids trihexyl(tetradecyl)phosphonium decanoate and trihexyltetradecylphosphonium bis[(trifluoromethyl)sulfonyl]amide", *J. Thermal Analysis and Calorimetry*, 106, 207-211.

Kendall, J.; Monroe, K. P. (1917). "The viscosity of liquids. II. The viscosity-composition curve for ideal liquid mixtures", *J. Am. Chem. Soc.*, 39, 1787-1802.

Kick, M.; Keil, P.; König, A. (2013). "Solid–liquid phase diagram of the two Ionic Liquids EMIMCl and BMIMCl", *Fluid Phase Equilibr.*, 338, 172-178.

Kilpeläinen, I.; Xie, H.; King, A.; Granstrom, M.; Heikkinen, S.; Argyropoulos, D. S. (2007). "Dissolution of Wood in Ionic Liquids", *J. Agric. Food. Chem.*, 5, 9142-9148.

Klein-Marcuschamer, D.; Simmons, B. A.; Blanch, H. W. (2011). "Techno-economic analysis of a lignocellulosic ethanol biorefinery with ionic liquid pre-treatment", *Biofuels Bioprod. Biorefin.*, 5, 562-569.

Klemm, D.; Heublein, B.; Fink, H.-P.; Bohn, A. (2005). "Cellulose: Fascinating Biopolymer and Sustainable Raw Material", *Angew. Chem. Int. Ed.*, 44, 3358-3393.

Klemm, D.; Philipp, B.; Heinze, T.; Heinze, U.; Wagenknecht, W. (1998). "General considerations on structure and reactivity of cellulose", in *Comprehensive Cellulose Chemistry*, Wiley-VCH, Weinheim (Germany).

Koch, G. W.; Sillett, S. C.; Jennings, G. M.; Davis, S. D. (2004). "The limits to tree height", *Nature,* 428, 851-854.

Kosan, B.; Michels, C.; Meister, F. (2008). "Dissolution and forming of cellulose with ionic liquids", *Cellulose*, 15, 59-66.

Krishnan, C.; Sousa, L. C.; Jin, M.; Chang, L.; Dale, B. E.; Balan, V. (2010). "Alkali-based AFEX pretreatment for the conversion of sugarcane bagasse and cane leaf residues to ethanol", *Biotechnol. Bioeng.*, 107, 441-450.

Krug, R. R.; Hunter, W. G.; Grieger, R. A. (1976). "Enthalpy-Entropy Compensation. 2. Separation of the Chemical from the Statistical Effect", *J. Phys. Chem*., 80, 2341-2351.

Kuga, S.; Takagi, S.; Brown, R. M. (1993). "Native folded-chain cellulose II", *Polymer*, 34, 3293-3297.

Kumar, P.; Barrett, D. M.; Delwiche, M. J.; Stroeve, P. (2009), "Methods for Pretreatment of Lignocellulosic Biomass for Efficient Hydrolysis and Biofuel Production", *Ind. Eng. Chem. Res.*, 48, 3713-3729.

L

Labbé, N.; Rials, T. G.; Kelley, S. S.; Cheng, Z. M.; Kim, J.-Y.; Li, Y. (2005). "FT-IR imaging and pyrolysis-molecular beam mass spectrometry: new tools to investigate wood tissues", *Wood Sci. Technol*., 39, 61-76.

Łachwa, J.; Szydłowski, J.; Makowska, A.; Seddon, K. R.; Esperança, J. M. S. S.; Guedes, H. J. R.; Rebelo, L. P. N. (2006). "Changing from an unusual high-temperature demixing to a UCST-type in mixtures of 1-alkyl-3-methylimidazolium bis{(trifluoromethyl)sulfonyl}amide and arenes", *Green Chem*., 8, 262-267.

Lee, S. H.; Doherty, T. V.; Linhardt, R. J.; Dordick, J. S. (2009). "Liquid-Mediated Selective Extraction of Lignin From Wood Leading to Enhanced Enzymatic Cellulose Hydrolysis", *Biotechnol. Bioeng*., 102, 1368-1376.

Li, R.; Cui, X.; Zhang, Y.; Feng, T.; Cai, J. (2012). "Vapor-Liquid Equilibrium and Liquid-Liquid Equilibrium of Ethyl Acetate + Ethanol + 1-Ethyl-3-methylimidazolium Acetate", *J. Chem. Eng. Data*, 57, 911-917.

Lide, D. R. (Ed.) (2009). *CRC Handbook of Chemistry and Physics*, 90th ed., Taylor and Francis, Boca Raton, FL (USA).

Lin, S. Y.; Dence, C. W. (Eds.) (1992). *Methods in Lignin Chemistry*, Springer, Berlin (Germany).

M

Maase, M. (2008). "Industrial applications of ionic liquids", in: *Ionic liquids in synthesis* (Eds.: Wasserscheid, P.; Welton, T.), 2nd ed., Wiley-VCH, Weinheim (Germany).

Maia, F. M.; Rodríguez, O.; Macedo, E. A. (2010). "LLE for (water + ionic liquid) binary systems using [$C_x$mim][BF_4] (x = 6, 8) ionic liquids", *Fluid Phase Equilibr.*, 296, 184-191.

Mäki-Arvela, P.; Anugwom, I.; Virtanen, P.; Sjöholm, R.; Mikkola, J. P. (2010). "Dissolution of lignocellulosic materials and its constituents using ionic liquids – A review", *Ind. Crop. Prod.*, 32, 175-201.

Manley, J. B.; Anastas, P. T.; Cue, B. W. (2008). "Frontiers in Green Chemistry: meeting the grand challenges for sustainability in R&D and manufacturing", *J. Clean. Prod.*, 16, 743-750.

Martín, C.; Galbe, M.; Nilvebrant, N.-O.; Jönsson, L. J. (2002). "Comparison of the Fermentability of Enzymatic Hydrolyzates of Sugarcane Bagasse Pretreated by Steam Explosion Using Different Impregnating Agents", *Appl. Biochem. Biotechnol.*, 98-100, 699-716.

McMillian, J. D. (1994). "Pre-treatment of lignocellulosic biomass", in: *Enzymatic conversion of biomass for fuels production* (Eds.: Himmel, M. E.; Baker, J. O.; Overend, R. P.), ACS Symposium Series, vol. 566, American Chemical Society, Washington, DC (USA).

Meine, N.; Benedito, F.; Rinaldi, R. (2010). "Thermal stability of ionic liquids assessed by potentiometric titration", *Green Chem.*, 12, 1711-1714.

Mikkola, J.-P.; Virtanen, P.; Sjöholm, R. (2006). "Aliquat 336® – a versatile and affordable cation source for an entirely new family of hydrophobic ionic liquids", *Green Chem.*, 8, 250-255.

Mikkola, S.-K.; Robciuc, A.; Lokajová, J.; Holding, A. J.; Lämmerhofer, M.; Kilpeläinen, I.; Holopainen, J. M.; King, A. W. T.; Wiedmer, S. K. (2015). "Impact of Amphiphilic Biomass-Dissolving Ionic Liquids on Biological Cells and Liposomes", *Environ Sci. Technol.*, 49, 1870-1878.

Mora, C. P.; Lozano, H. R.; Martínez, F. (2005). "Aspectos termodinámicos de la miscibilidad parcial entre el *n*-octanol y el agua", *Braz. J. Pharm. Sci.*, 41, 13-26.

Mosier, N.; Wyman, C.; Dale, B.; Elander, R.; Lee, Y. Y.; Holtzapple, M.; Ladisch, M. (2005), "Features of promising technologies for pretreatment of lignocellulosic biomass", *Bioresour. Technol.*, 96, 673-686.

Muhammad, N.; Man, Z.; Mutalib, M. I. A.; Azmi Bustam, M.; Wilfred, C. D.; Sada Khan, A.; Ullah, Z.; Gonfa, G.; Nasrullah, A. (2015). "Dissolution and Separation of Wood Biopolymers Using Ionic Liquids", *ChemBioEng Rev.*, 2, 257-278.

N

Nagarajan, S.; Skillen, N. C.; Irvine, J. T. S.; Lawton, L. A.; Robertson, P. K. J. (2017). "Cellulose II as bioethanol feedstock and its advantages over native cellulose", *Renew. Sust. Energ. Rev*., 77, 182-192.

Ngo, H. L.; LeCompte, K.; Hargens, L.; McEwen, A. B. (2000). "Thermal properties of imidazolium ionic liquids", *Thermochim. Acta*., 357, 97-102.

Nishikawa, K.; Wang, S.; Katayanagi, H.; Hayashi, S.; Hamaguchi, H.; Koga, Y.; Tozaki, K. (2007). "Melting and Freezing Behaviors of Prototype Ionic Liquids, 1-Butyl-3-methylimidazolium Bromide and Its Chloride, Studied by Using a Nano-Watt Differential Scanning Calorimeter", *J. Phys. Chem. B.,* 111, 4894-4900.

O

O'Sullivan, A. C. 1997. "Cellulose: the structure slowly unravels", *Cellulose*, 4, 173-207.

P

Pal, S.; Padmanabhan, S.; Joy, S.; Kimbhar, P.; Trimukhe, K. D.; Varma, A. J. (2015). "An Overview of Studies on Pilot Scale: Lignocellulosic Biomass Pretreatment Processes Used in the Production of Second Generation Bioethanol", *Trends Carbohydr. Res.*, 7, 41-59.

Panteli, E. K.; Voutsas, E. K. (2009). "Solubilities of Cinnamic Acid Esters in Ionic Liquids", *J. Chem. Eng. Data*, 54, 812-818.

Parasuraman, P.; Singh, R.; Bolton, T. S.; Omori, S.; Francis R. C. (2007). "Estimation of hardwood lignin concentrations by UV spectroscopy and chlorine demethylation", *BioResources*, 2, 459-471.

Park S.; Baker, J. O.; Himmel, M. E; Parilla, P. A.; Johnson, D. K. (2010). "Cellulose crystallinity index: measurement techniques and their impact on interpreting cellulase performance", *Biotechnol. Biofuels*, 3: 10.

Pauly, M.; Keegstra, K. (2008). "Cell–wall carbohydrates and their modification as a resource for biofuels", *Plant J.*, 54, 559-568.

Pinkert, A.; Marsh, K. N.; Pang, S.; Staiger, M. P. (2009). "Ionic Liquids and Their Interaction with Cellulose", *Chem. Rev.*, 109, 6712-6728.

Plechkova, N. V.; Seddon, K. R. (2008). "Applications of ionic liquids in the chemical industry", *Chem. Soc. Rev*., 37, 123-150.

Poling, B. E.; Prausnitz, J. M.; O'Connell, J. P. (2001). *The Properties of Gases and Liquids*, 5th ed., McGraw-Hill, New York (USA).

Pozo-Gonzalo, C.; Howlett, P. C.; Hodgson, J. L.; Madsen, L. A.; MacFarlane, D. R.; Forsyth, M. (2014). "Insights into the reversible oxygen reduction reaction in a series of phosphonium-based ionic liquids", *Phys. Chem. Chem. Phys*., 16, 25062-25070.

Prausnitz, J. M.; Lichtenthaler, R. N.; Gomes de Azevedo, E. (1999). *Molecular Thermodynamics of Fluid-Phase Equilibria*, 3th ed., Prentice Hall, Upper Saddle River, NJ (USA).

Q

Quijada-Maldonado, E.; van der Boogaart, S.; Lijbers, J. H.; Meindersma, G. W.; de Haan, A. B. (2012). "Experimental densities, dynamic viscosities and surface tension of ionic liquids series 1-ethyl-3-methylimidazolium acetate and dicyanamide and their binary and ternary mixtures with water and ethanol at *T* = (298.15 to 343.15 K)", *J. Chem. Thermodyn.*, 51, 51-58.

R

Ragauskas, A. J.; Nagy, M.; Kim, D. H.; Eckert, C. A.; Hallett, J. P.; Liotta, C. L. (2006). "From wood to fuels: Integrating biofuels and pulp production", *Ind. Biotechnol.*, 2, 55-65.

Redlich, O.; Kister, A. T. (1948). "Thermodynamics of Nonelectrolyte Solutions – Algebraic representation of thermodynamic properties and the classification of solutions", *Ind. Eng. Chem.*, 40, 345-348.

Riddick, J. A.; Bunger, W. B.; Sakano, T. K. (1986). *Organic Solvent – Physical Properties and Methods of Purification*, 4th ed., Wiley, New York (USA).

Rodríguez, H. (2016). "Ionic Liquids in the Context of Separation Processes", in: *Ionic Liquids for Better Separation Processes* (Ed.: Rodríguez, H.), Springer-Verlag, Berlin (Germany).

Rowell, R. M.; Pettersen, R.; Tshabalada, M. A. (2013). "Cell wall chemistry", in: *Handbook of Wood Chemistry and Wood Composites* (Ed.: Rowell, R. M.), 2nd ed., CRC Press, Boca Raton, FL (USA).

Rubin, E. M. (2008). "Genomics of cellulosic biofuels", *Nature*, 454, 841-845.

S

Salan, T. (2017). "A Brief Review of the Thermochemical Platform as a Promising Way to Produce Sustainable Liquid Biofuels in Biorefinery Concept", *Pet. Petrochem. Eng. J*., 1: 000123.

Seddon, K. R. (1997). "Ionic liquids for clean technology", *J. Chem. Technol. Biotechnol*., 68, 351-356.

Seddon, K. R.; Stark, A.; Torres, M. J. (2000). "Influence of chloride, water, and organic solvents on the physical properties of ionic liquids", *Pure Appl. Chem.*, 72, 2275-2287.

Sheldon, R. A. (2014). "Green and sustainable manufacture of chemicals from biomass: state of art", *Green Chem.*, 16, 950-963.

Shibazaki, H.; Saito, M.; Kuga, S.; Okano, T. (1998). "Native cellulose II production by acetobacter xylinum under physical constraints", *Cellulose*, 5, 165-173.

Simmons, B. A.; Singh, S; Holmes, B. M.; Blanch, H. W. (2010). "Ionic Liquid Pretreatment", *Chem. Eng. Proc.*, vol. 106, no. 3 (March 2010), pp. 50-55.

Sjöström, E. (1993). *Wood chemistry, Fundamentals and Applications*, 2nd ed., Academic Press, San Diego, CA (USA).

Sluiter, A.; Hames, B.; Ruiz, R.; Scarlata, C.; Sluiter, J.; Templeton, D.; Crocker, D. (2012), "Determination of Structural Carbohydrates and Lignin in Biomass – Laboratory Analytical Procedure" (issue date: April 2008; revision date: August 2012), Technical Report NREL/TP-510-42618, revised August 2012, National Renewable Energy Laboratory, U.S. Department of Energy, Office of Energy Efficiency & Renewable Energy (USA). Available online at: https://www.nrel.gov/docs/gen/fy13/42618.pdf (last accessed: October 2018).

Smiglak, M.; Reichert, W. M.; Holbrey, J. D.; Wilkes, J. S.; Sun, L.; Thrasher, J. S.; Kirichenko, K.; Singh, S.; Katritzky, A. R.; Rogers, R. D. (2006). "Combustible ionic liquids by design: is laboratory safety another ionic liquid myth?", *Chem. Commun*., 2554-2556.

Smith, J. M.; Van Ness, H. C.; Abbott, M. M. (2005). *Introduction to Chemical Engineering Thermodynamics*, 7th ed., McGraw-Hill, New York (USA).

Speck, T.; Burgert, I. (2011). "Plant stems: functional design and mechanics", *Annu. Rev. Mater. Res*., 41, 169-193.

Stark, A.; Seddon, K. R. (2007). "Ionic liquids", in: *Kirk-Othmer Encyclopedia of Chemical Technology* (Ed.: Seidel, A.), 5th ed., vol. 26, pp. 836-920, Wiley, Hoboken, NJ, (USA).

Stöcker, M. (2008). "Biofuels and Biomass-To-Liquid Fuels in the Biorefinery: Catalytic Conversion of Lignocellulosic Biomass using Porous Materials", A*ngew. Chem. Int. Ed.*, 47, 9200-9211.

Stolarska, O.; Soto, A.; Rodríguez, H.; Smiglak, M. (2015). "Properties modification by eutectic formation in mixtures of ionic liquids", *RSC Adv.*, 5, 22178-22187.

Sun, N.; Rahman, M.; Qin, Y.; Maxim, M. L.; Rodríguez, H.; Rogers, R. D. (2009). "Complete dissolution and partial delignification of wood in the ionic liquid 1-ethyl-3-methylimidazolium acetate", *Green Chem.*, 11, 646-655.

Sun, N.; Rodríguez, H.; Rahman, M.; Rogers, R. D. (2011). "Where are ionic liquids strategies most suited in the pursuit of chemicals and energy from lignocellulosic biomass?", *Chem. Commun.*, 47, 1405-1421.

Swatloski, R. P.; Spear, S. K.; Holbrey, J. D.; Rogers, R. D. (2002). "Dissolution of Cellulose with Ionic Liquids", *J. Am. Chem. Soc*., 124, 4974-4975.

T

Taherzadeh, M. J.; Karimi, K. (2008). "Pretreatment of lignocellulosic wastes to improve ethanol and biogas production: a review", *Int. J. Mol. Sci*., 9, 1621-1651.

Tammann, G.; Hesse, W. (1926). "Die Abhängigkeit der Viscosität von der Temperatur bei unterkühlten Flüssigkeiten", *Z. anorg. allg. Chem.*, 156, 245-257.

Tan, S. S. Y.; MacFarlane, D. R. (2009). "Ionic liquids in biomass processing", in: *Ionic Liquids* (Ed.: Kirchner, B.), Topics in Current Chemistry book series, Springer-Verlag, Berlin (Germany).

Tariq, M.; Freire M. G.; Saramago, B.; Coutinho, J. A. P.; Canongia Lopes, J. N.; Rebelo, L. P. N. (2012). "Surface tension of ionic liquids and ionic liquid solutions", *Chem. Soc. Rev.*, 41, 829-868.

Treybal, R. E. (1963), Liquid extraction, 2nd ed., McGraw-Hill, New York (USA).

Troshenkova, S. V.; Sashina, E. S.; Novoselov, N. P.; Arndt, K.-F.; Jankowsky, S. (2010). "Structure of ionic liquids on the basis of imidazole and their mixtures with water", *Russ. J. Gen. Chem*., 80, 106-111.

U

U.S. DOE. 2005. *Genomics: GTL Roadmap*, DOE/SC-0090, U.S. Department of Energy Office of Science, p. 27.

U.S. DOE. 2007. *Biofuels Primer Placemat: From Biomass to Cellulosic Ethanol and Understanding Biomass: Plant Cell Walls*, U.S. Department of Energy Office of Science.

V

Vitz, J.; Erdmenger, T.; Haensch, C.; Schubert, U. S. (2009). "Extended dissolution studies of cellulose in imidazolium based ionic liquids", *Green Chem*., 11, 417-424.

Vogel, H. (1921). "Das Temperatur-abhängigkeitsgesetz der Viskosität von Flüssigkeiten", *Phys. Z.*, 22, 645-646.

W

Wang, H.; Gurau, G.; Rogers, R. D. (2012). "Ionic liquids processing of cellulose", *Chem. Soc. Rev*., 41, 1519-1537.

Wei, J.; Bu, X.; Guan, W.; Xing, N.; Fang, D.; Wu, Y. (2015). "Measurement of vaporization enthalpy by isothermogravimetrical method and prediction of the polarity for 1-alkyl-3- methylimidazolium acetate {[Cnmim][OAc] (n = 4, 6)} ionic liquids", *RSC Adv.,* 5, 70333-70338.

Windeisen, E.; Wegener, G. (2009). "Wood", in: *Sustainable solutions for modern economies* (Ed.: Hofer, R.), RSC Publishing, Cambridge (UK).

Wyman, C. E.; Dale, B. E.; Elander, R. T.; Holtzapple, M.; Ladisch, M. R.; Lee, Y. Y. (2005a). "Coordinated development of leading biomass pretreatment technologies", *Bioresour. Technol.*, 96, 1959-1966.

Wyman, C. E.; Dale, B. E.; Elander, R. T.; Holtzapple, M.; Ladisch, M. R.; Lee, Y. Y.; Mitchinson, C.; Saddler, J. N. (2009). "Comparative Sugar Recovery and Fermentation Data Following Pretreatment of Poplar Wood by Leading Technologies", *Biotechnol. Prog.*, 25, 333-339.

Wyman, C. E.; Decker, S. R.; Himmel, M. E.; Brady, J. W.; Skopec, C. E.; Viikari, L. (2005b). "Hydrolysis of Cellulose and Hemicellulose", in: *Polysaccharides: Structural Diversity and Functional Versatility*, (Ed.: Dumitriu, S.), 2nd ed., Marcel Dekker, New York (USA).

X

Xie, H.; Gathergood, N. (Eds.) (2013). *The role of green chemistry in biomass processing and conversion*, Wiley, Hoboken, NJ (USA).

Z

Zafarani-Moattar, M. T.; Shekaari, H. (2005). "Volumetric and Speed of Sound of Ionic Liquid, 1-Butyl-3-methylimidazolium Hexafluorophosphate with Acetonitrile and Methanol at *T* = (298.15 to 318.15) K", *J. Chem. Eng. Data*, 50, 1694-1699.

Zakzeski, J.; Bruijnincx, P. C.; Jongerius, A. L.; Weckhuysen, B. M. (2010). "The Catalytic Valorization of Lignin for the Production of Renewable Chemicals", *Chem. Rev*., 110, 3552-3599.

Zarei, H. A. (2010). "Excess Molar Enthalpies of Benzyl Alcohol + Alkanols (C1-C6) and Their Correlations at 298.15 K and Ambient Pressure", *J. Chem. Eng. Data*, 55, 4021-4024.

Zavrel, M.; Bross, D.; Funke, M.; Büchs, J.; Spiess, A. C. (2009). "Highthroughput screening for ionic liquids dissolving (ligno)-cellulose", *Bioresour. Technol*., 100, 2580-2587.

Zhang, Q.; Hu, J.; Lee, D.-J. (2017). "Pretreatment of biomass using ionic liquids: Research updates", *Renew. Ener.*, 111, 77-84.

Zhang, Y. P.; Ding, S.; Mielenz, J. R.; Cui, J.; Elander, R. T.; Laser, M.; Himmerl, M. E.; McMillan, J. R.; Lynd, L. R. (2007). "Fractionating Recalcitrant Lignocellulose at Modest Reaction Conditions", *Biotechnol. Bioeng.*, 97, 214-223.

Zhao, B.; Greiner, L.; Leitner, W. (2012). "Cellulose solubilities in carboxylate-based ionic liquids", *RSC Adv*., 2, 2476-2479.

Zhao, H.; Baker, G. A.; Song, Z.; Olubajo, O.; Crittle, T.; Peters, D. (2008). "Designing enzyme-compatible ionic liquids that can dissolve carbohydrates", *Green Chem*., 10, 696-705. [Correction: *Green Chem*. (2008), 10, 1342.]

USC
UNIVERSIDADE
DE SANTIAGO
DE COMPOSTELA

Appendix A:

^{1}H and ^{13}C NMR spectra of ionic liquids

USC
UNIVERSIDADE
DE SANTIAGO
DE COMPOSTELA

Appendix A:

^{1}H and ^{13}C NMR spectra of ionic liquids

In this Appendix, the ^{1}H and ^{13}C NMR spectra of the ionic liquids used in this Thesis are presented. Please refer to Chapters 3 and 6 for further details (supplier/synthesis, purification, NMR spectrometer and recording of the spectra, etc.).

The alphabetically-ordered list of ionic liquids, with full names and the corresponding abbreviations, is shown in Table A.1. In Figures A.1 to A.24 in the following pages, for each of them the ^{1}H NMR spectrum is presented first, and then the ^{13}C NMR spectrum.

Table A.1. Full names and abbreviations of the ionic liquids involved in the experimental work of this Thesis, and for which the ^{1}H and ^{13}C NMR spectra are collected in this Appendix.

Name	Abbreviation
1-Butyl-3-methylimidazolium acetate	$[C_4mim][OAc]$
1-Butyl-3-methylimidazolium chloride	$[C_4mim]Cl$
1-Ethyl-3-methylimidazolium acetate	$[C_2mim][OAc]$
1-Ethyl-3-methylimidazolium chloride	$[C_2mim]Cl$
1-Hexyl-3-methylimidazolium chloride	$[C_6mim]Cl$
1-Methyl-3-octylimidazolium chloride	$[C_8mim]Cl$
Aliquat 336®	[Aliquat]Cl
Aliquat acetate	[Aliquat][OAc]
Methyltrioctylphosphonium acetate	$[P_{8\,8\,8\,1}][OAc]$
Tetrabutylphosphonium acetate	$[P_{4\,4\,4\,4}][OAc]$
Trihexyl(tetradecyl)phosphonium chloride	$[P_{6\,6\,6\,14}]Cl$
Trihexyl(tetradecyl)phosphonium acetate	$[P_{6\,6\,6\,14}][OAc]$

1-Butyl-3-methylimidazolium acetate ([C4mim][OAc])

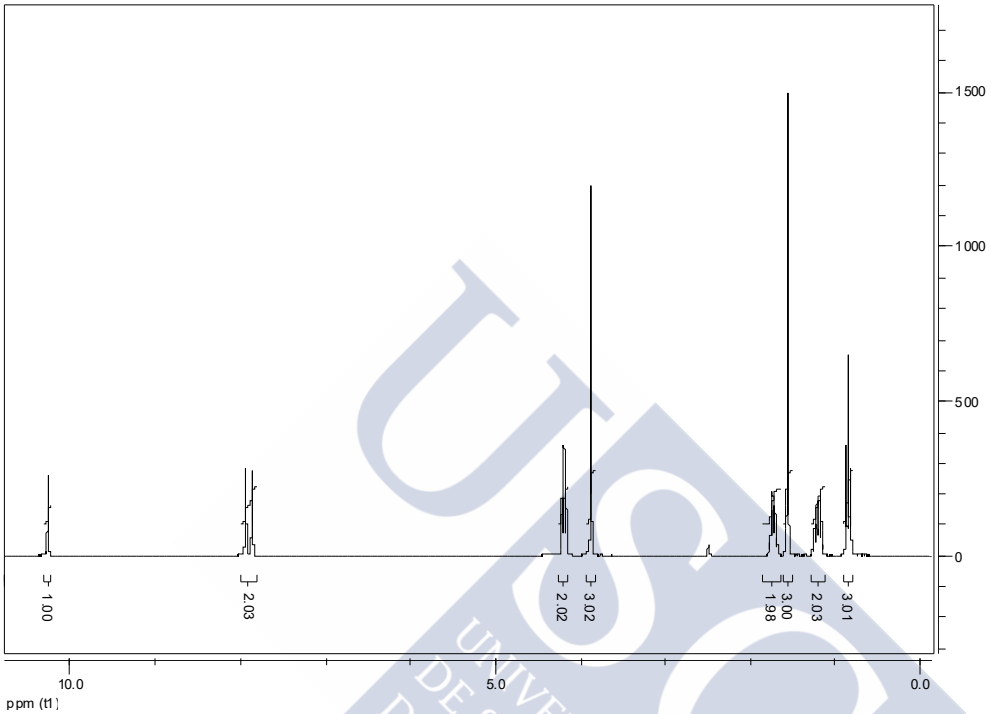

Figure A.1. ^{1}H NMR spectrum of [C$_4$mim][OAc]. δ_H (DMSO-d_6, 300 MHz): 0.86 (t, J = 7.4 Hz, 3H, N(CH$_2$)$_3$C$\underline{H}_3$), 1.21 (sex, J = 7.4 Hz, 2H, N(CH$_2$)$_2$C$\underline{H}_2$), 1.57 (s, 3H, CH$_3$COO), 1.74 (quin, J = 7.4 Hz, 2H, NCH$_2$C$\underline{H}_2$), 3.88 (s, 3H, NCH$_3$), 4.20 (q, J = 7.1 Hz, 2H, NCH$_2$), 7.82-8.00 (unresolved, 2H, C(5)H and C(4)H), 10.27 (s, 1H, C(2)H).

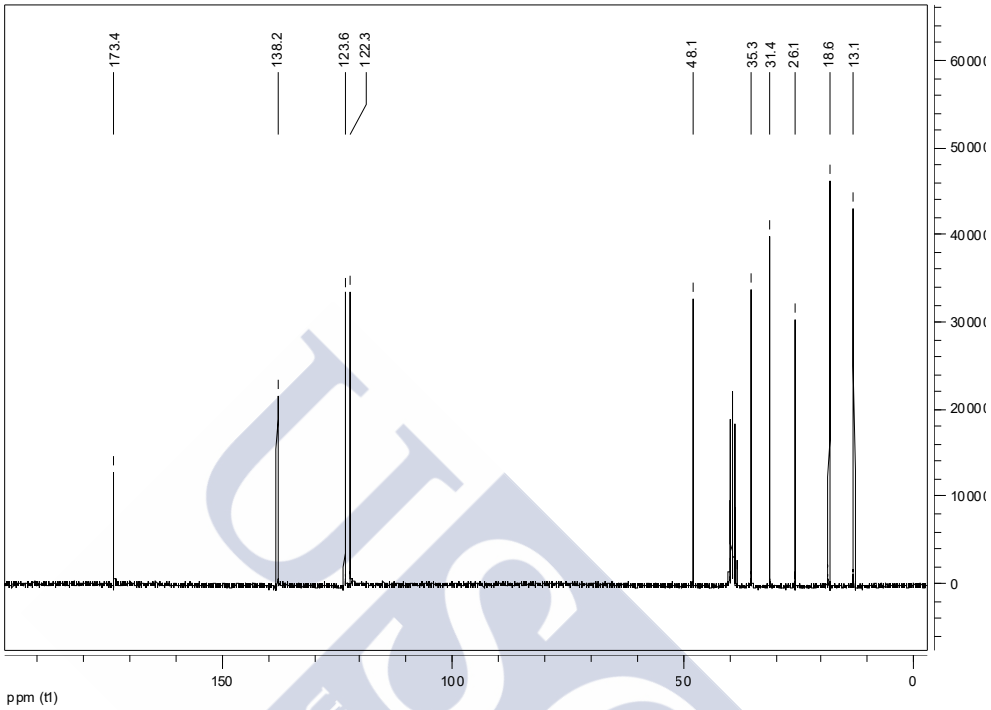

Figure A.2. ^{13}C NMR spectrum of [C_4mim][OAc]. δ_C (DMSO-d_6, 75.4 MHz): 13.1 ($N(CH_2)_3\underline{C}H_3$), 18.6 ($N(CH_2)_2\underline{C}H_2$), 26.1 ($\underline{C}H_3COO$), 31.4 $NCH_2\underline{C}H_2$), 35.3 (NCH_3), 48.1 (NCH_2), 122.3 (C(4)H), 123.6 (C(5)H), 138.2 (C(2)H), 173.4 ($CH_3\underline{C}OO$).

1-Butyl-3-methylimidazolium chloride ([C4mim]Cl)

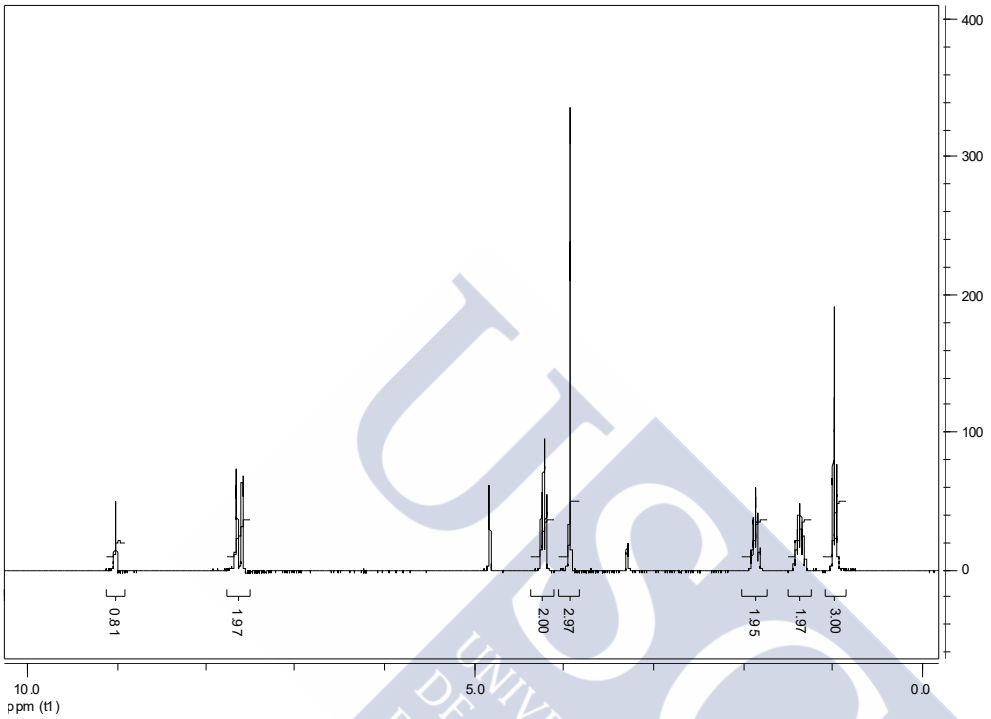

Figure A.3. ^{1}H NMR spectrum of [C4mim]Cl. δ_H (CD_3OD, 300 MHz): 1.00 (t, J= 7.4 Hz, 3H, $N(CH_2)_3C\underline{H}_3$), 1.40 (sex, J= 7.5 Hz, 2H, $N(CH_2)_2C\underline{H}_2$), 1.90 (quin, J= 7.5 Hz, 2H, $NCH_2C\underline{H}_2$), 3.97 (s, 3H, NCH_3), 4.26 (t, J= 7.3 Hz, 2H, NCH_2), 7.66 (dd, J= 20.7 Hz, 2H, C(5)H and C(4)H), 9.05 (s, 1H, C(2)H).

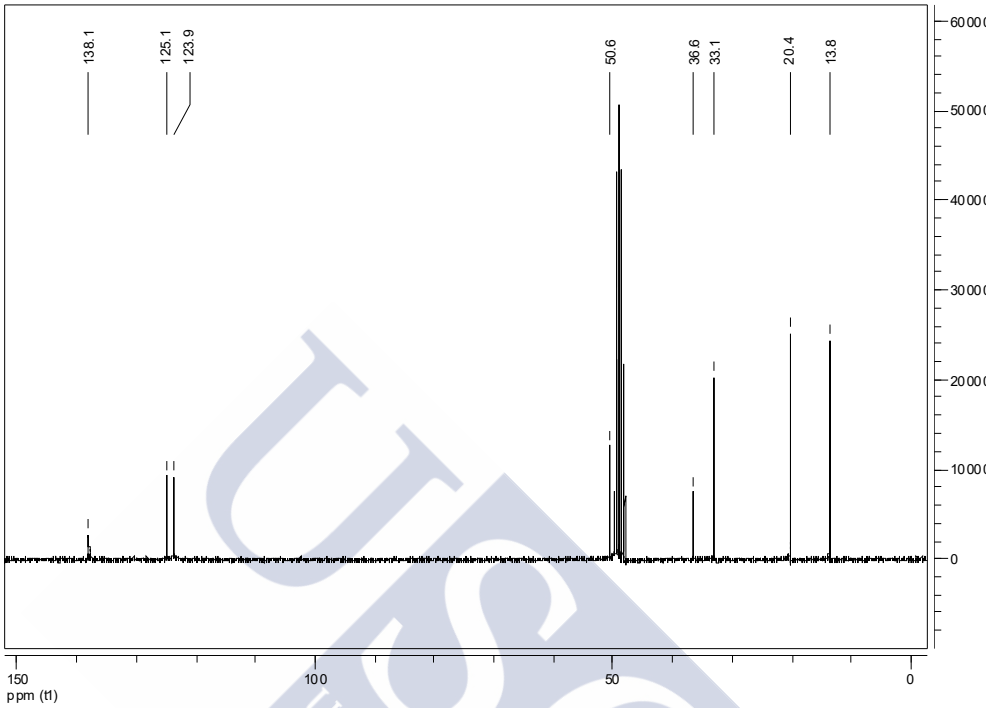

Figure A.4. ^{13}C NMR spectrum of [C_4mim]Cl. δ_C (CD_3OD, 75.4 MHz): 13.8 ($N(CH_2)_3\underline{C}H_3$), 20.4 $N(CH_2)_2\underline{C}H_2$), 33.1 $NCH_2\underline{C}H_2$), 36.6 (NCH_3), 50.6 (NCH_2), 123.9 (C(4)H), 125.1 (C(5)H), 138.1 (C(2)H).

1-Ethyl-3-methylimidazolium acetate ([C2mim][OAc])

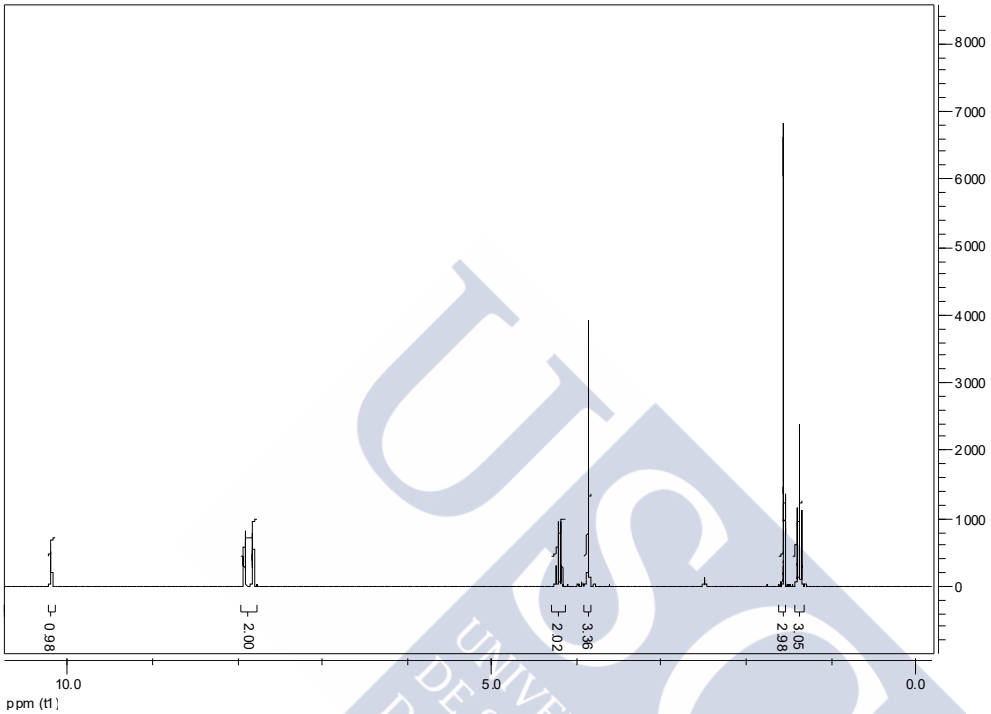

Figure A.5. ^{1}H NMR spectrum of [C_2mim][OAc]. δ_H (DMSO-d_6, 300 MHz): 1.39 (t, J = 7.3 Hz, 3H, $NCH_2C\underline{H}_3$), 1.56 (s, 3H, CH_3COO), 3.87 (s, 3H, NCH_3), 4.22 (q, J = 7.3 Hz, 2H, NCH_2), 7.78-7.96 (unresolved, 2H, C(5)H and C(4)H), 10.20 (s, 1H, C(2)H).

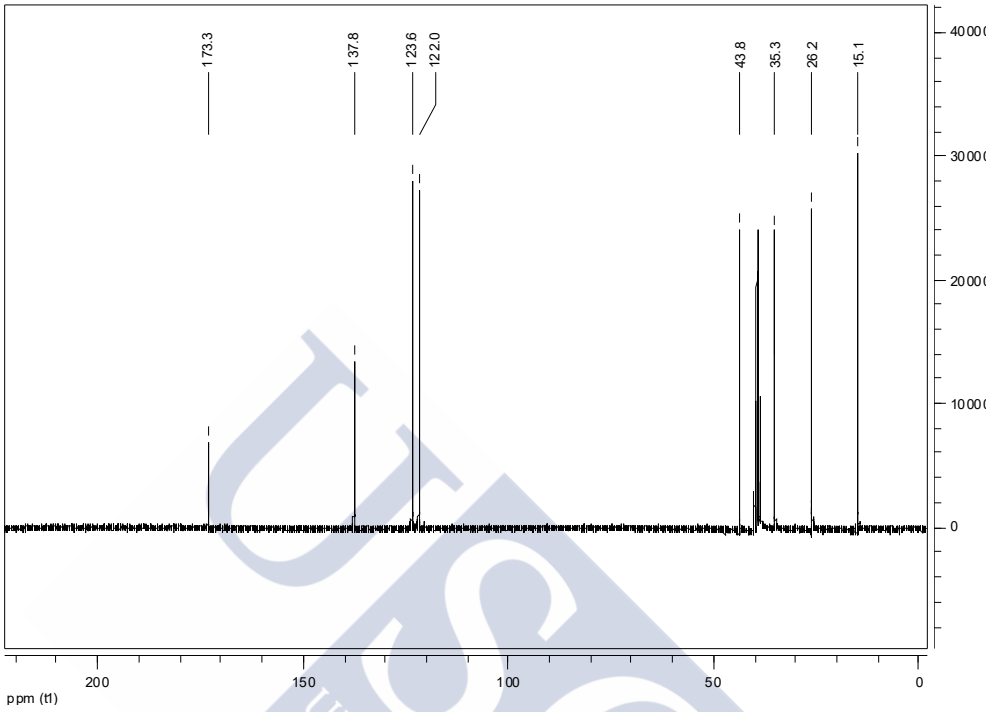

Figure A.6. ^{13}C NMR spectrum of [C_2mim][OAc]. δ_C (DMSO-d_6, 75.4 MHz): 15.1 ($NCH_2\underline{C}H_3$), 26.2 ($\underline{C}H_3COO$), 35.3 (NCH_3), 43.8 (NCH_2), 122.0 (C(4)H), 123.6 (C(5)H), 137.8 (C(2)H), 173.3 ($CH_3\underline{C}OO$).

1-Ethyl-3-methylimidazolium chloride ([C_2mim]Cl)

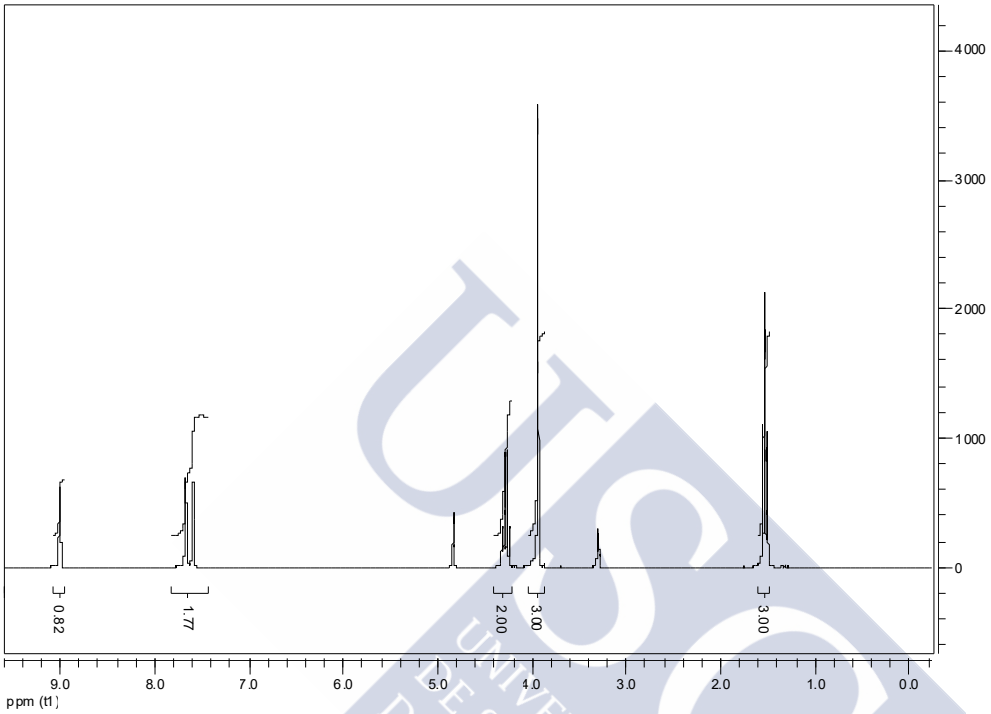

Figure A.7. ^{1}H NMR spectrum of [C_2mim]Cl. δ_H (CD_3OD, 300 MHz): 1.54 (t, J= 7.4 Hz, 3H, $NCH_2C\underline{H}_3$), 3.95 (s, 3H, NCH_3), 4.29 (q, J= 7.3 Hz, 2H, NCH_2), 7.64 (dd, J= 24.2 Hz, 2H, C(5)H and C(4)H), 9.01 (s, 1H, C(2)H).

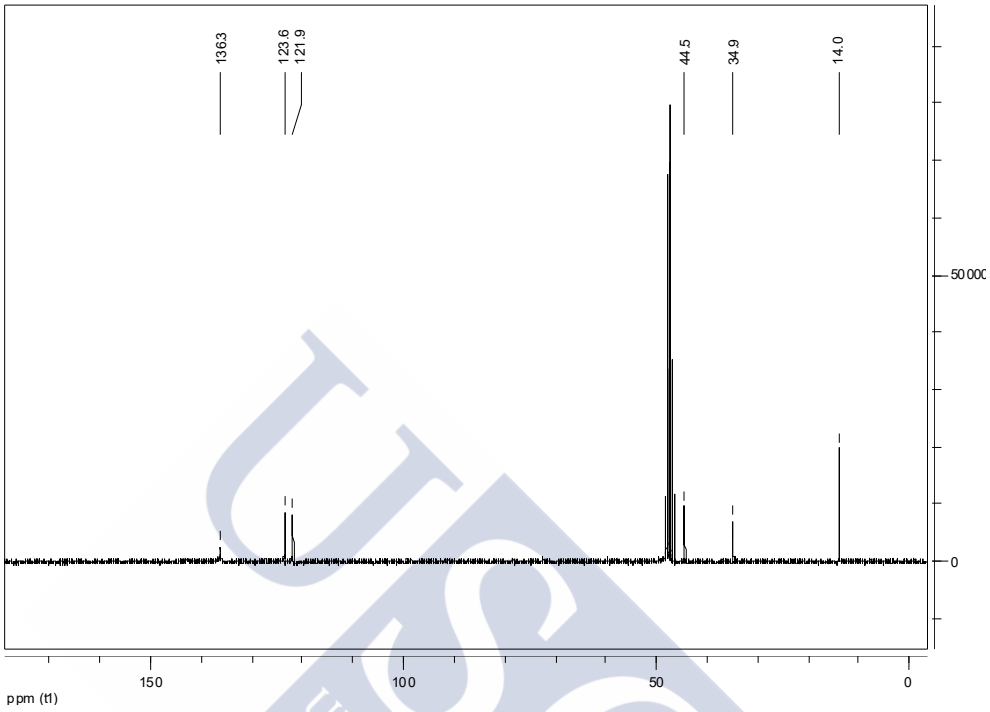

Figure A.8. ^{13}C NMR spectrum of [C_2mim]Cl. δ_C(CD_3OD, 75.4 MHz): 14.0 ($NCH_2\underline{C}H_3$), 34.9 (NCH_3), 44.5 (NCH_2), 121.9 (C(4)H), 123.6 (C(5)H), 136.3 (C(2)H).

1-Hexyl-3-methylimidazolium chloride ([C_6mim]Cl)

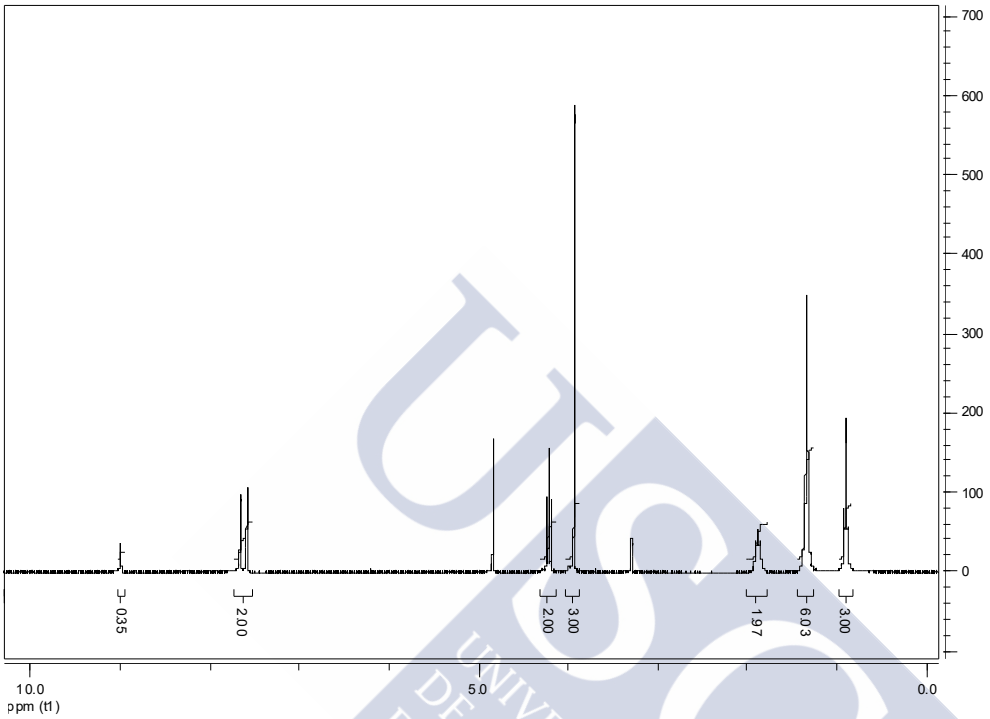

Figure A.9. ^{1}H NMR spectrum of [C_6mim]Cl. δ_H (CD_3OD, 300 MHz): 0.91 (t, J= 6.6 Hz, 3H, $N(CH_2)_5C\underline{H}_3$), 1.25-1.44 (unresolved, 6H, $N(CH_2)_2(C\underline{H}_2)_3$), 1.89 (quin, J= 7.2 Hz, 2H, $NCH_2C\underline{H}_2$), 3.94 (s, 3H, NCH_3), 4.22 (t, J= 7.3 Hz, 2H, NCH_2), 7.53-7.73 (unresolved, 2H, C(5)H and C(4)H), 9.00 (s, 1H, C(2)H). For the hydrogen bonded to the C2 position of the imidazolium ring (peak at 9.00 ppm) the integration is notably shorter than the theorerical value, likely due to deuterium exchange with the deuteriated solvent.

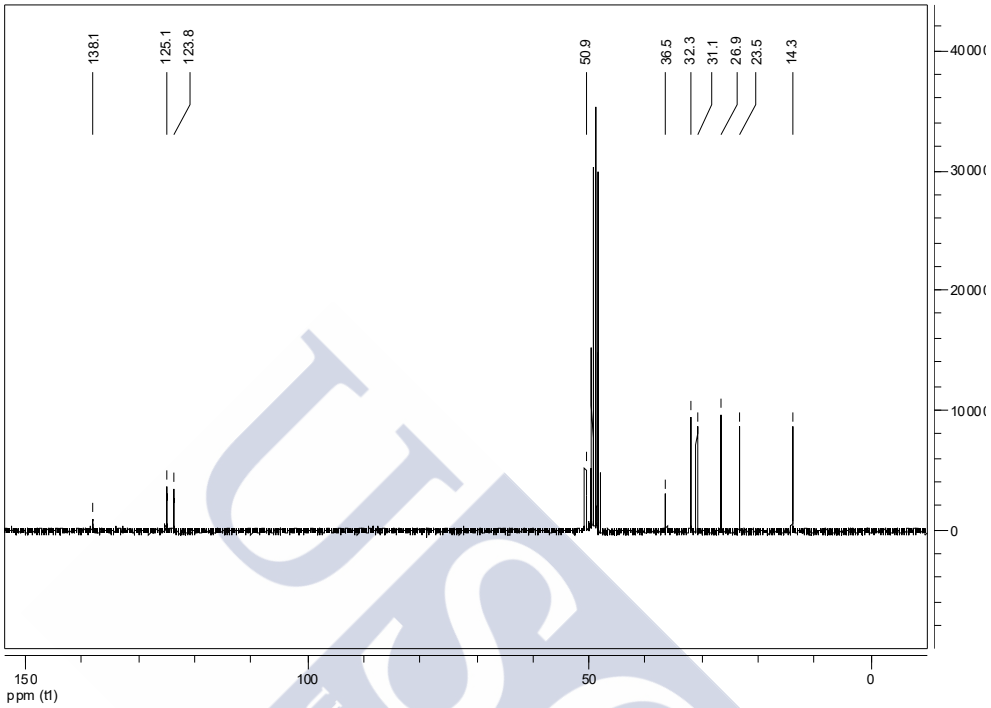

Figure A.10. ^{13}C NMR spectrum of $[C_6mim]Cl$. δ_C (CD_3OD, 75.4 MHz): 14.3 ($N(CH_2)_5\underline{C}H_3$), 23.5 ($N(CH_2)_4\underline{C}H_2$), 26.9 ($N(CH_2)_3\underline{C}H_2$), 31.1 ($N(CH_2)_2\underline{C}H_2$), 32.3 ($NCH_2\underline{C}H_2$), 36.5 ($NCH_3$), 50.9 ($NCH_2$), 123.8 (C(4)H), 125.1 (C(5)H), 138.1 (C(2)H).

1-Methyl-3-octylimidazolium chloride ([C$_8$mim]Cl)

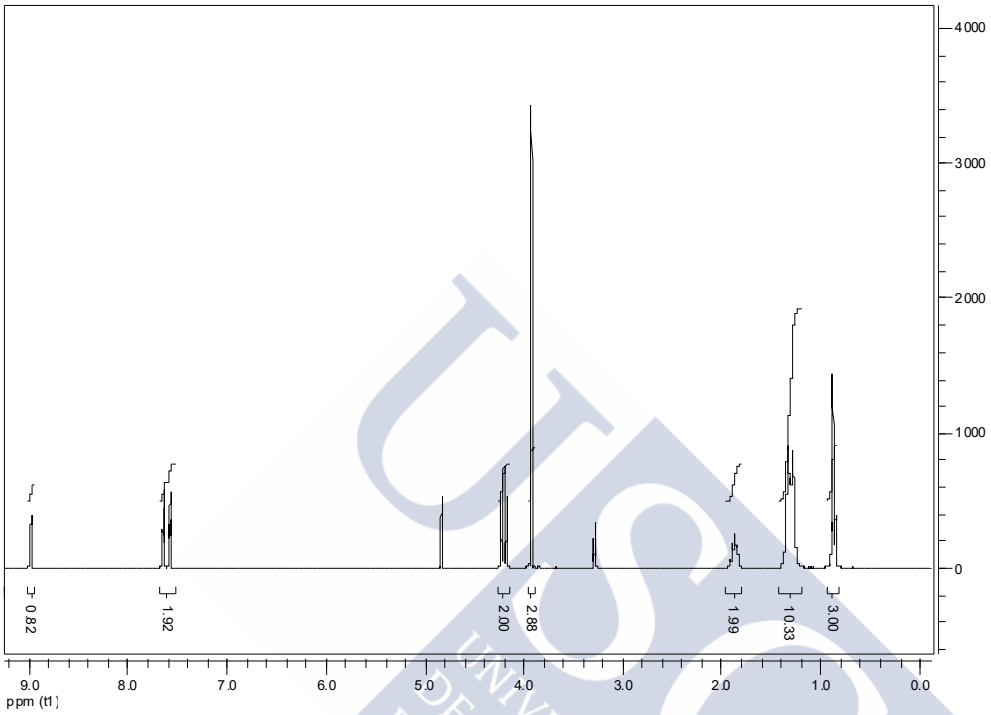

Figure A.11. ^{1}H NMR spectrum of [C$_8$mim]Cl. δ_H (CD_3OD, 300 MHz): 0.88 (t, J= 6.8 Hz, 3H, $N(CH_2)_7C\underline{H}_3$), 1.20-1.43 (unresolved, 10H, $N(CH_2)_2(C\underline{H}_2)_5$), 1.88 (quin, J= 7.3 Hz, 2H, $NCH_2C\underline{H}_2$), 3.93 (s, 3H, NCH_3), 4.21 (t, J= 7.4 Hz, 2H, NCH_2), 7.53-7.69 (unresolved, 2H, C(5)H and C(4)H), 8.98 (s, 1H, C(2)H).

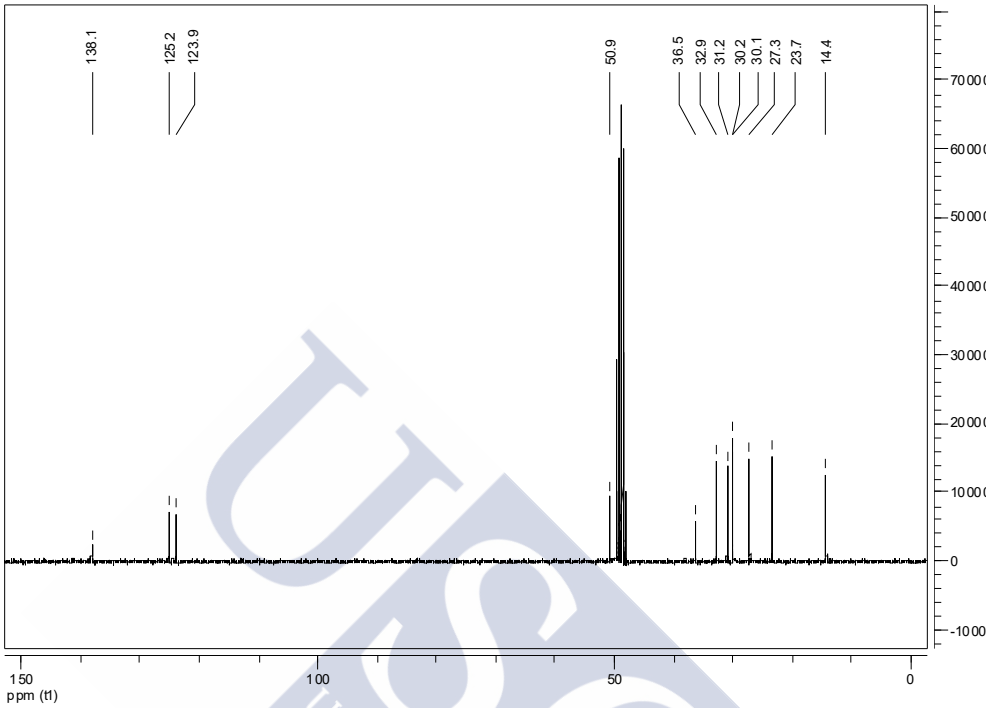

Figure A.12. ^{13}C NMR spectrum of $[C_8mim]Cl$. δ_C (CD_3OD, 75.4 MHz): 14.4 ($N(CH_2)_7\underline{C}H_3$), 23.7 ($N(CH_2)_6\underline{C}H_2$), 27.3 ($N(CH_2)_5\underline{C}H_2$), 30.1 ($N(CH_2)_4\underline{C}H_2$), 30.2 ($N(CH_2)_3\underline{C}H_2$), 31.2 ($N(CH_2)_2\underline{C}H_2$), 32.9 ($NCH_2\underline{C}H_2$), 36.5 ($NCH_3$), 50.9 ($NCH_2$), 123.9 C(4)H, 125.2 C(5)H, 138.1 C(2)H.

Aliquat 336® ([Aliquat]Cl)

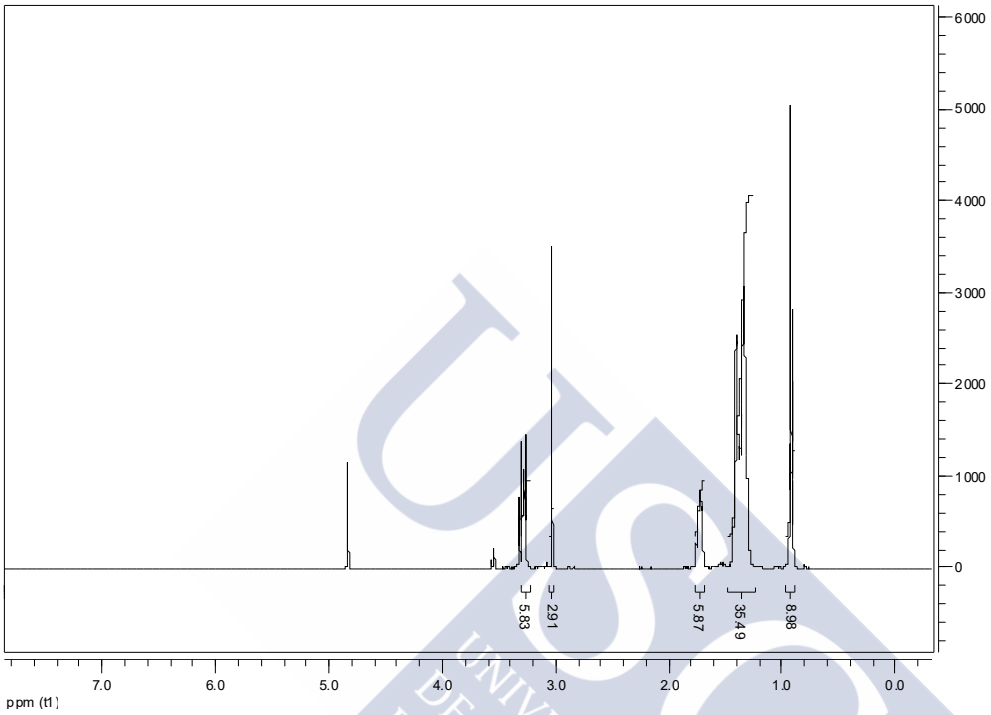

Figure A.13. ^{1}H NMR spectrum of [Aliquat]Cl. δ_H (CD_3OD, 500 MHz): 0.88-0.96 (unresolved, 9H, $3 \times N(CH_2)_2(CH_2)_nC\underline{H}_3$, 1.25-1.48 (unresolved, ca. 34H, $3 \times N(CH_2)_2(C\underline{H}_2)_nCH_3$), 1.69-1.77 (unresolved, 6H, $3 \times NCH_2C\underline{H}_2$), 3.07 (s, 3H, NCH_3), 3.22-3.30 (unresolved, 6H, $3 \times NCH_2$). Subscript *n* takes values 5 or 7 (see Section 3.3.1 in Chapter 3 for details).

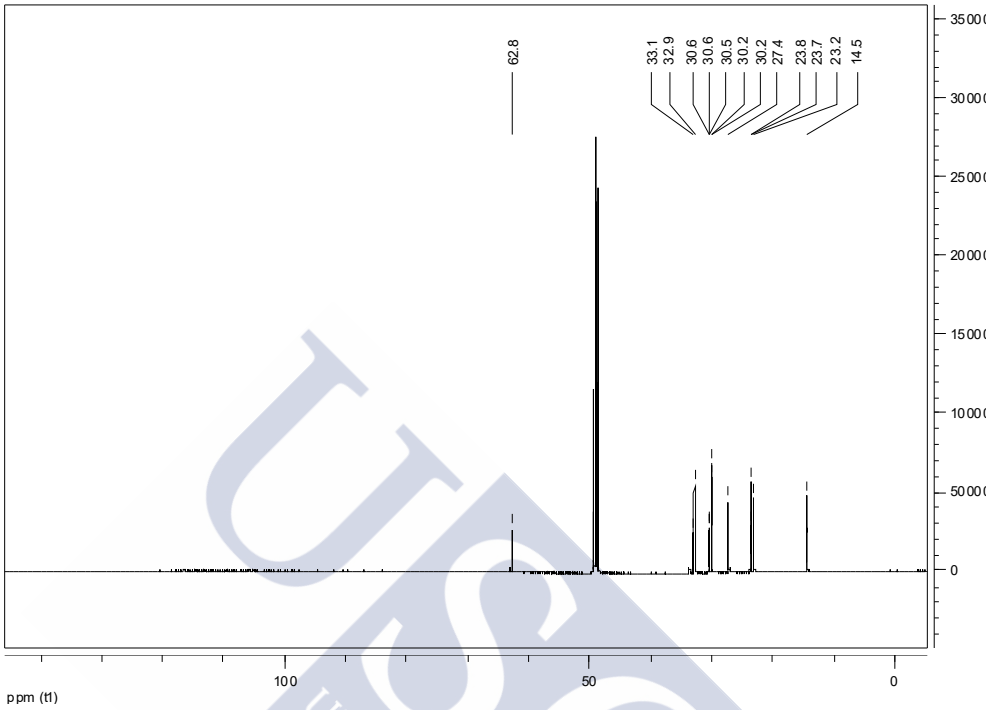

Figure A.14. ^{13}C NMR spectrum of [Aliquat]Cl. δ_C (CD_3OD, 125.7 MHz): 14.5 ($3 \times NCH_2(CH_2)_n\underline{C}H_3$), 23-33 (unresolved, $3 \times NCH_2(\underline{C}H_2)_nCH_3$), 62.8 ($3 \times \underline{C}H_2$). The peak corresponding to the methyl group bonded to the nitrogen atom, expected at ca. 49 ppm, is hidden by the residual signal of the deuteriated solvent. Subscript *n* takes values 6 or 8 (see Section 3.3.1 in Chapter 3 for details).

Aliquat acetate ([Aliquat][OAc])

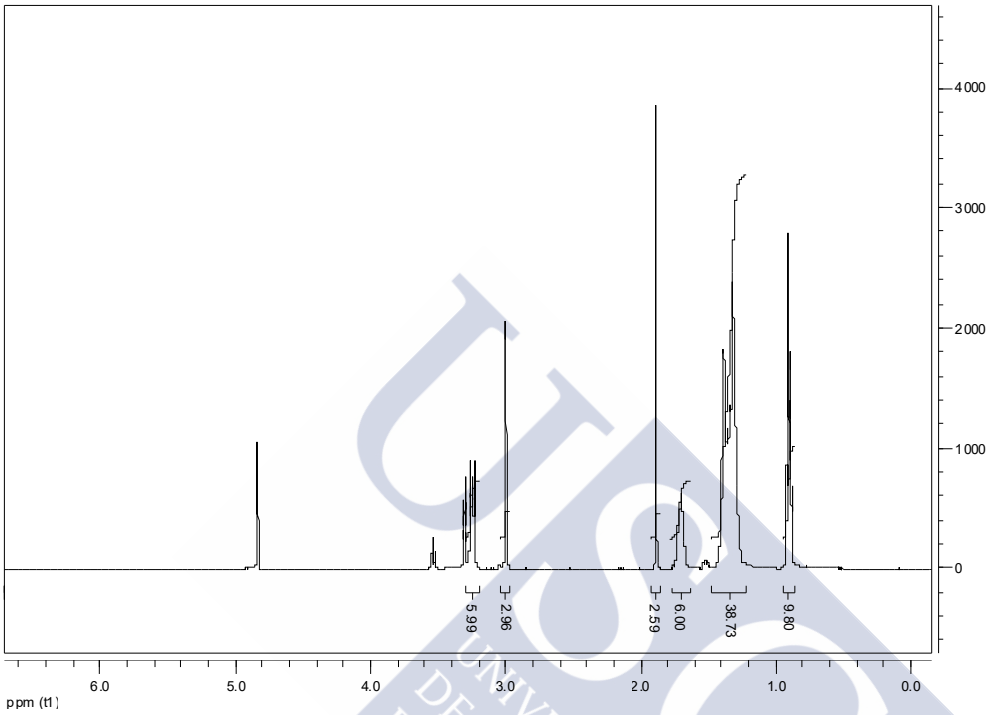

Figure A.15. ^{1}H NMR spectrum of [Aliquat][OAc]. δ_H (CD_3OD, 500 MHz): 0.86-0.94 (unresolved, 9H, 3 × $N(CH_2)_2(CH_2)_nC\underline{H}_3$, 1.21-1.47 (unresolved, ca. 34H, 3 × $N(CH_2)_2(C\underline{H}_2)_nCH_3$), 1.63-1.78 (unresolved, 6H, 3 × $NCH_2C\underline{H}_2$), 1.89 (s, 3H, CH_3COO), 3.07 (s, 3H, NCH_3), 3.20-3.29 (unresolved, 6H, 3 × NCH_2). Subscript *n* takes values 5 or 7 (see Section 3.3.1 in Chapter 3 for details).

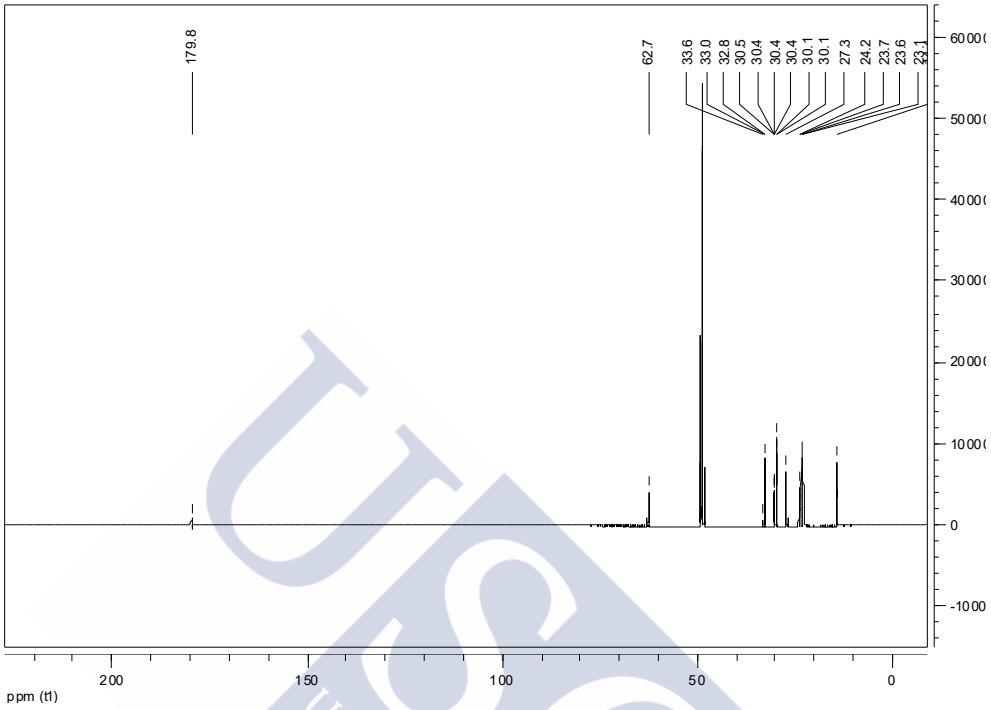

Figure A.16. ^{13}C NMR spectrum of [Aliquat][OAc]. δ_C (CD_3OD, 125.7 MHz): 14.4 ($3 \times NCH_2(CH_2)_n\underline{C}H_3$), 23-34 (unresolved, $3 \times NCH_2(\underline{C}H_2)_nCH_3$ and $\underline{C}H_3COO$), 62.7 ($3 \times NCH_2$), 179.8 ($CH_3\underline{C}OO$). The peak corresponding to the methyl group bonded to the nitrogen atom, expected at ca. 49 ppm, is hidden by the residual signal of the deuteriated solvent. Subscript n takes values 6 or 8 (see Section 3.3.1 in Chapter 3 for details).

Methyltrioctylphosphonium acetate ([P8881][OAc])

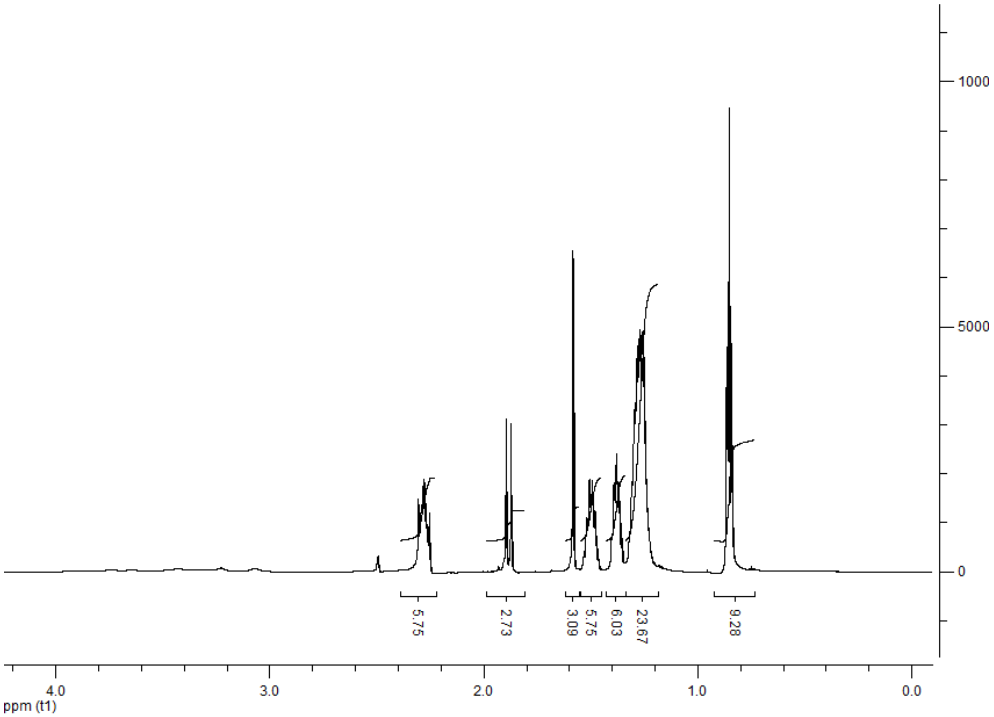

Figure A.17. ^{1}H NMR spectrum of [P8881][OAc]. δ_H (DMSO-d_6, 300 MHz): 0.85 (t, J= 7.0 Hz, 9H, 3 × P(CH$_2$)$_7$C$\underline{H}_3$), 1.19-1.34 (unresolved, 24H, 3 × P(CH$_2$)$_3$(C$\underline{H}_2$)$_4$) 1.38 (quin, J= 7.1 Hz, 6H, 3 × P(CH$_2$)$_2$C$\underline{H}_2$), 1.50 (sex, J= 8.0 Hz, 6H, 3 × PCH$_2$C$\underline{H}_2$), 1.58 (s, 3H, CH$_3$COO), 1.88 (d, J= 14.1 Hz, 3H, PCH$_3$), 2.22- 2.39 (unresolved, 6H, 3 × PCH$_2$).

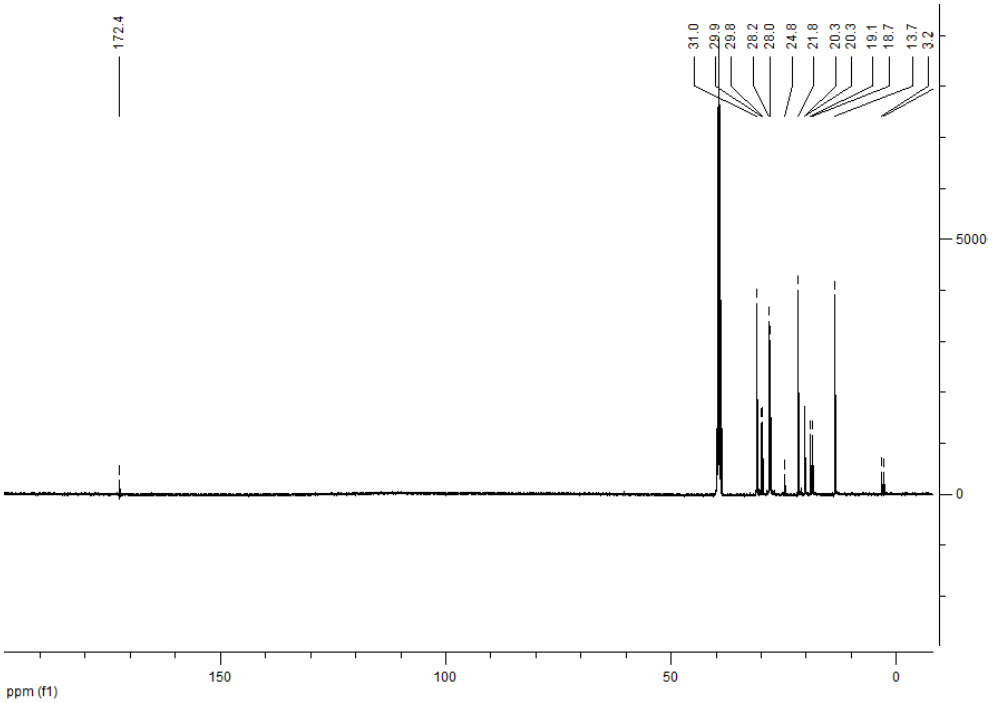

Figure A.18. ^{13}C NMR spectrum of $[P_{8\,8\,8\,1}][OAc]$. δ_C (DMSO-d_6, 75.4 MHz): 3.0 (d, $J_{C\text{-}P}$ = 51.3 Hz, 3 × P$\underline{C}H_2$), 13.7 (s, 3 × $P(CH_2)_7\underline{C}H_3$), 18-31 (unresolved, P$\underline{C}H_3$ and 3 × $PCH_2(\underline{C}H_2)_6$ and $\underline{C}H_3COO$), 172.4 ($CH_3\underline{C}OO$).

Tetrabutylphosphonium acetate ([P4444][OAc])

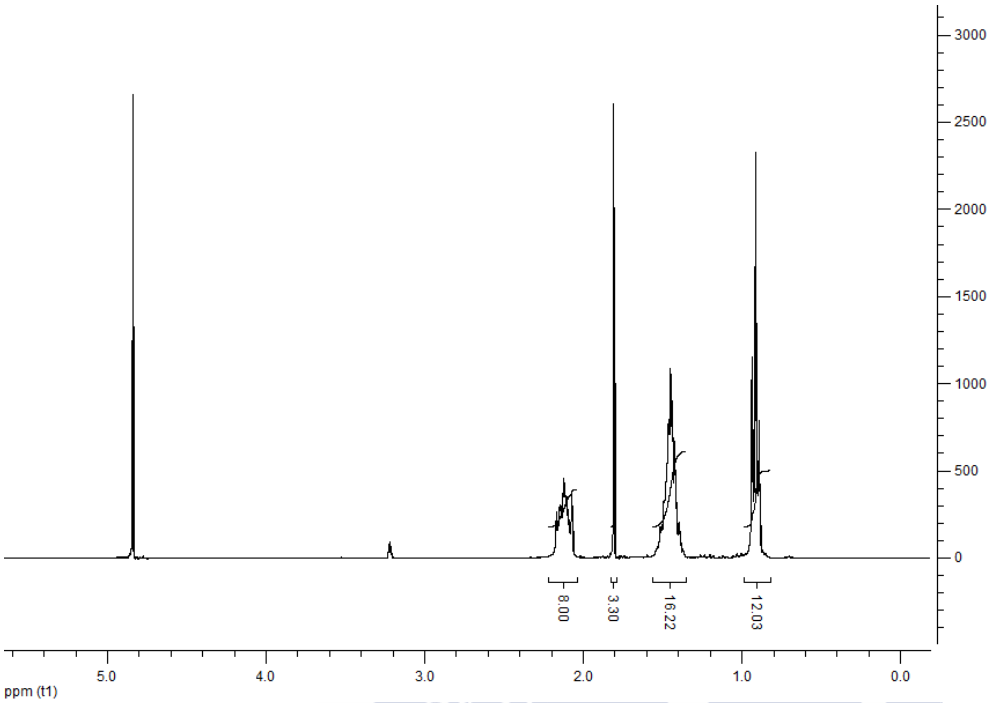

Figure A.19. ^{1}H NMR spectrum of [P4444][OAc]. δ_H (CD_3OD, 300 MHz): 0.91 (t, J= 7.0 Hz, 12H, 4 × $P(CH_2)_3C\underline{H}_3$), 1.35-1.56 (unresolved, 16H, 4 × $PCH_2(C\underline{H}_2)_2$), 1.81 (s, 3H, CH_3COO), 2.03- 2.22 (unresolved, 8H, 4 × PCH_2).

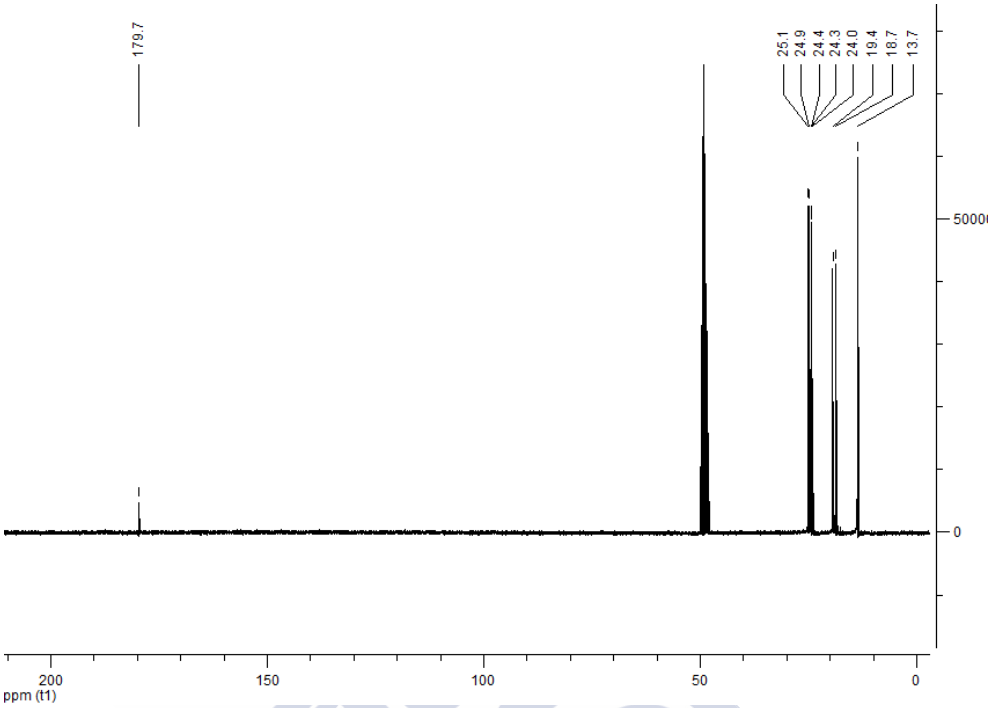

Figure A.20. ^{13}C NMR spectrum of $[P_{4444}][OAc]$. δ_C (CD_3OD, 75.4 MHz): 13.7 (s, 4 × $P(CH_2)_3\underline{C}H_3$), 19.0 (d, $J_{C\text{-}P}$ = 48.2 Hz, 4 × $P\underline{C}H_2$), 24.0 (s, $\underline{C}H_3COO$), 24.4 (d, J = 4.6 Hz, 4 × $PCH_2\underline{C}H_2$), 25.0 (d, J = 15.6 Hz, 4 × $P(CH_2)_2\underline{C}H_2$), 179.7 ($CH_3\underline{C}OO$).

Trihexyl(tetradecyl)phosphonium acetate ([$P_{6\,6\,6\,14}$][OAc])

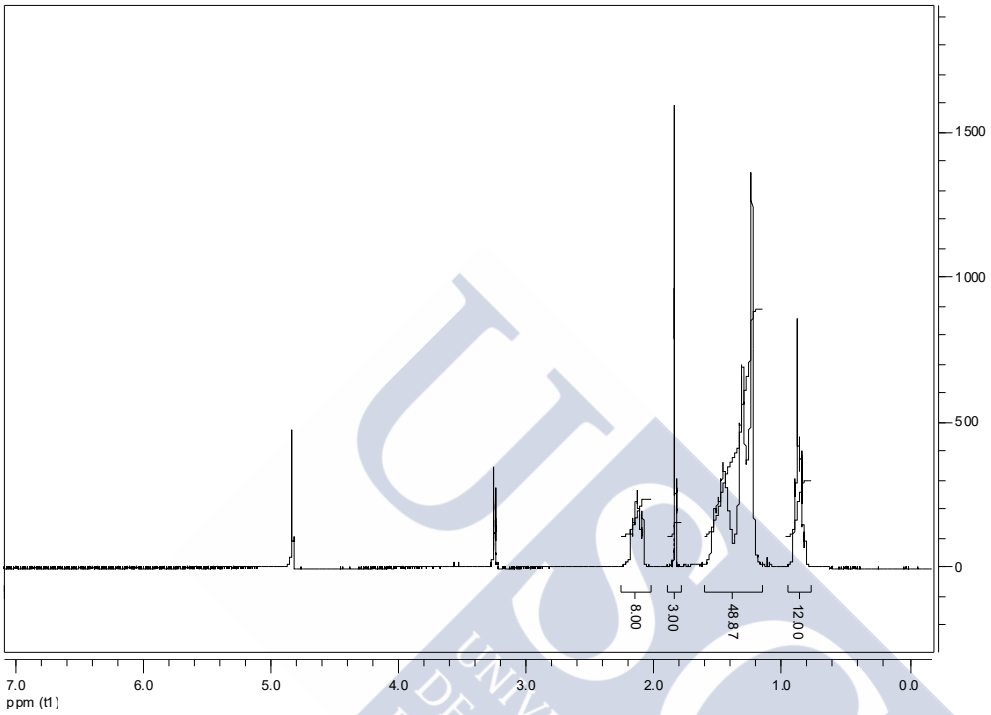

Figure A.21. ^{1}H NMR spectrum of [$P_{6\,6\,6\,14}$][OAc]. δ_H (CD_3OD, 300 MHz): 0.77-0.96 (unresolved, 12H, 4 × $P(CH_2)_nC\underline{H}_3$), 1.15-1.61 (unresolved, 48H, $PCH_2(C\underline{H}_2)_{12}CH_3$ and 3 × $PCH_2(C\underline{H}_2)_4CH_3$), 1.84 (s, 3H, CH_3COO), 2.03- 2.26 (unresolved, 8H, 4 × PCH_2). Subscript *n* takes the values 5 or 13.

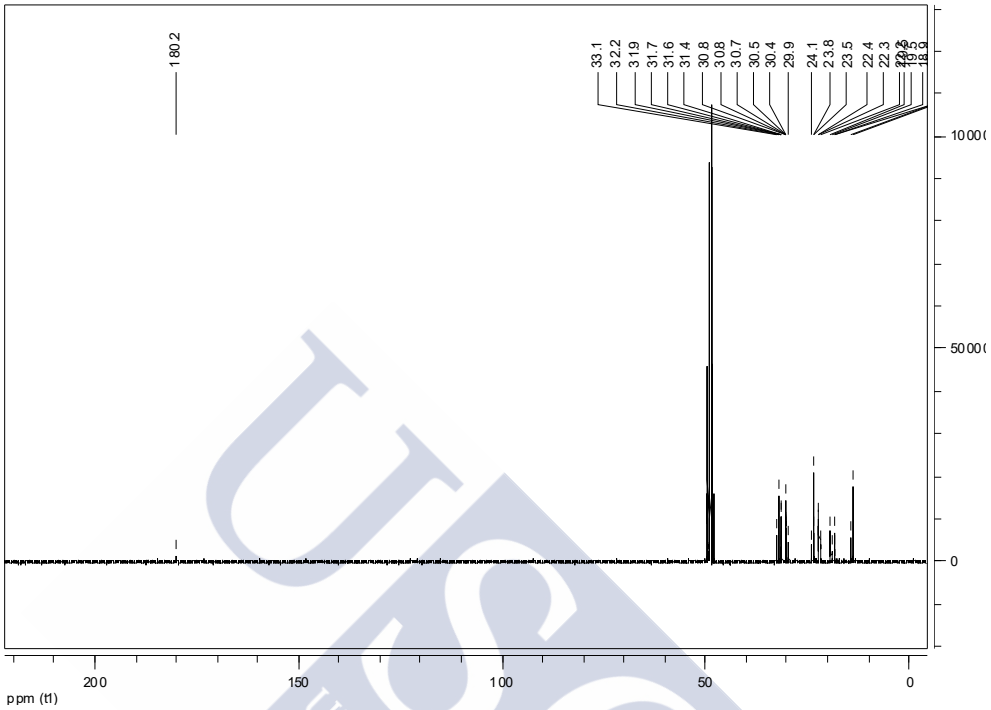

Figure A.22. ^{13}C NMR spectrum of $[P_{6\,6\,6\,14}][OAc]$. δ_C (CD_3OD, 75.4 MHz): 14-33 (unresolved, $P(\underline{C}H_2)_{13}\underline{C}H_3$ and $3 \times P(\underline{C}H_2)_5\underline{C}H_3$ and $\underline{C}H_3COO$), 180.2 ($CH_3\underline{C}OO$).

Trihexyl(tetradecyl)phosphonium chloride ([$P_{6\,6\,6\,14}$]Cl)

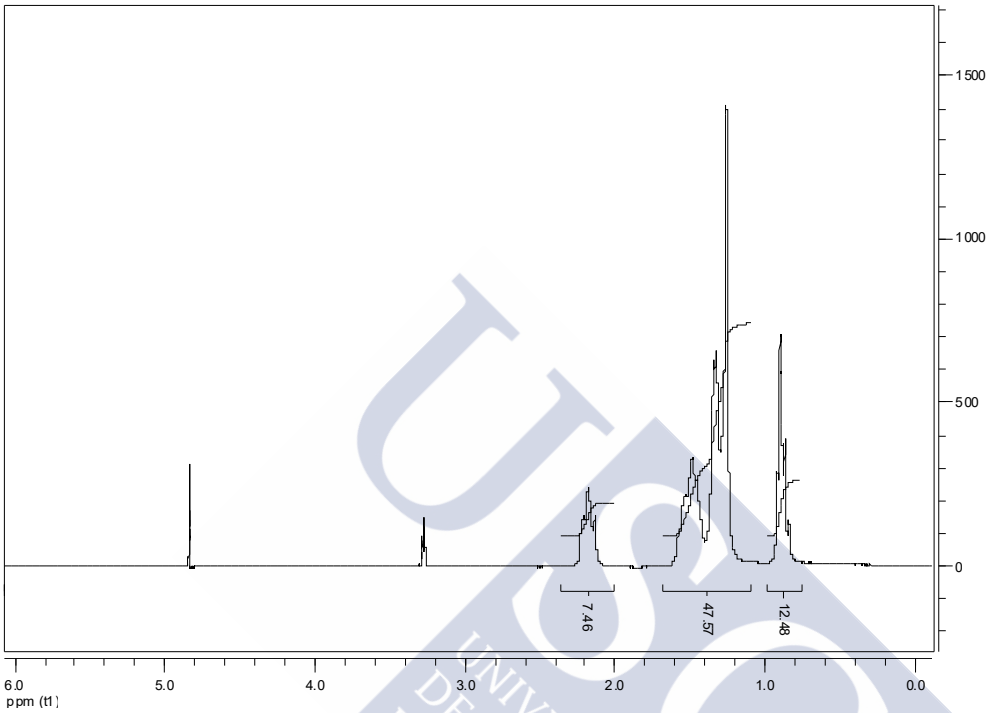

Figure A.23. ^{1}H NMR spectrum of [$P_{6\,6\,6\,14}$]Cl. δ_H (CD_3OD, 300 MHz): 0.77-0.99 (unresolved, 12H, 4 × $P(CH_2)_n\underline{CH_3}$), 1.10-1.68 (unresolved, 48H, $PCH_2(C\underline{H_2})_{12}CH_3$ and 3 × $PCH_2(C\underline{H_2})_4CH_3$), 2.01- 2.35 (unresolved, 8H, 4 × PCH_2). Subscript *n* takes values 5 or 13.

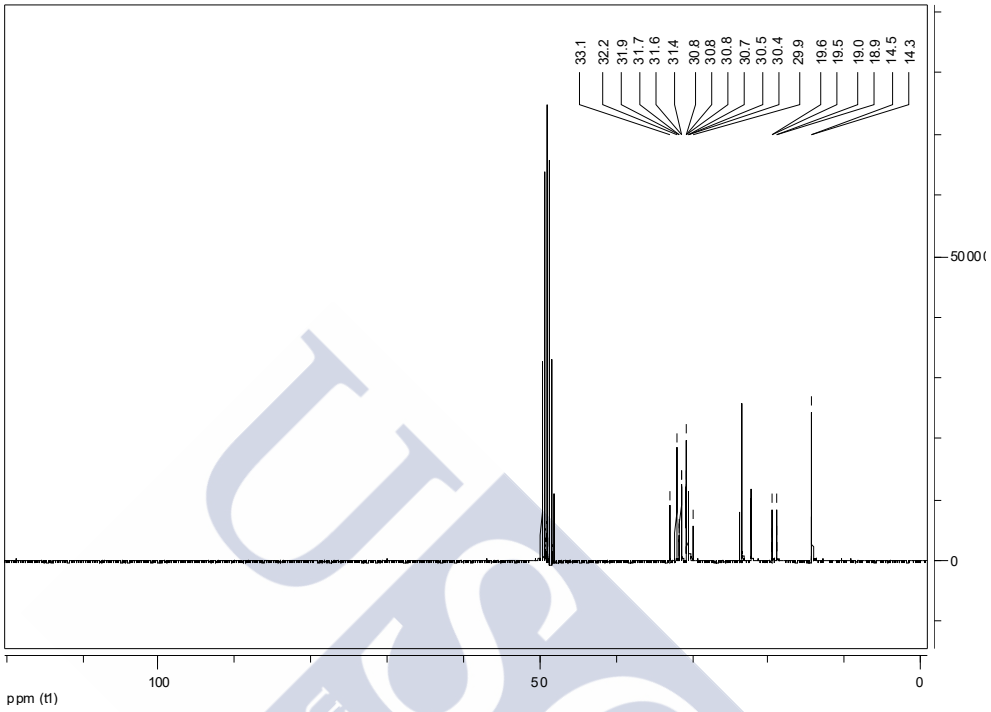

Figure A.24. ^{13}C NMR spectrum of $[P_{6\,6\,6\,14}]Cl$. δ_C (CD_3OD, 75.4 MHz): 14-33 (unresolved, $P(\underline{C}H_2)_{13}\underline{C}H_3$ and 3 × $P(\underline{C}H_2)_5\underline{C}H_3$).

USC
UNIVERSIDADE
DE SANTIAGO
DE COMPOSTELA

Appendix B:

DSC and TGA thermograms of ionic liquids

USC
UNIVERSIDADE
DE SANTIAGO
DE COMPOSTELA

Appendix B:

DSC and TGA thermograms of ionic liquids

The heating ramps of the last cycle of the DSC thermograms for all pure ionic liquids used in Chapter 3 are reported in the first part of this Appendix. After them, the corresponding TGA thermograms are also presented. To facilitate the visualisation of the TGA thermograms, solid lines are used to plot the weight percentage as a function of temperature, whereas dashed lines are used to plot its derivative.

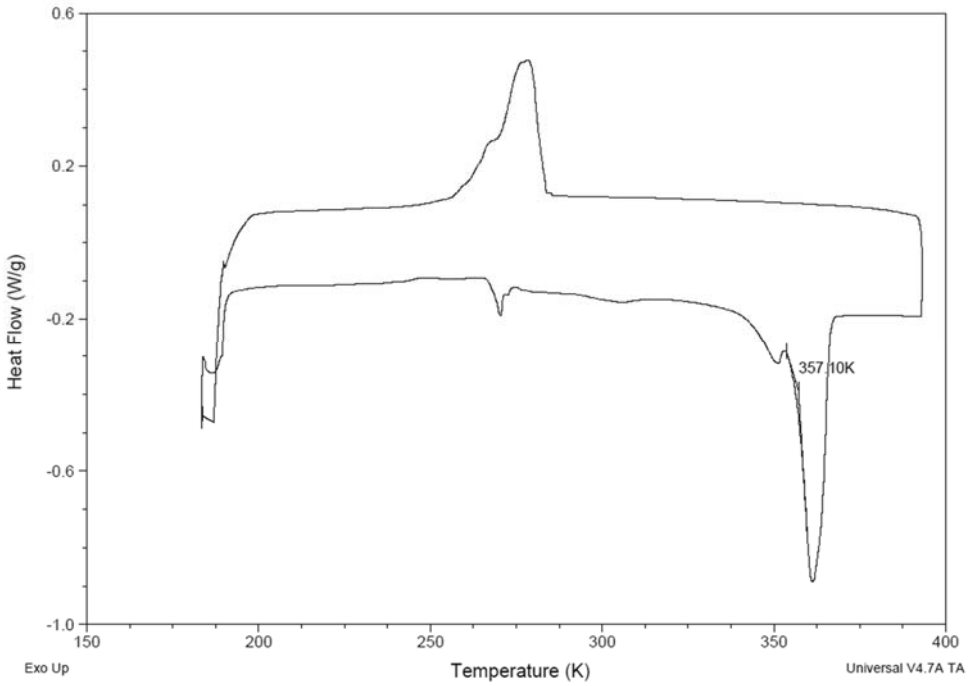

Figure B.1. DSC thermogram of [C_2mim]Cl. (The endothermic peak observed in the heating ramp in the range 250-300 K is assumed to correspond to a small melting event associated with the water inherently present in this hygroscopic ionic liquid, which also causes a partial pre-melting at temperatures near the actual onset of the melting temperature of the pure substance.)

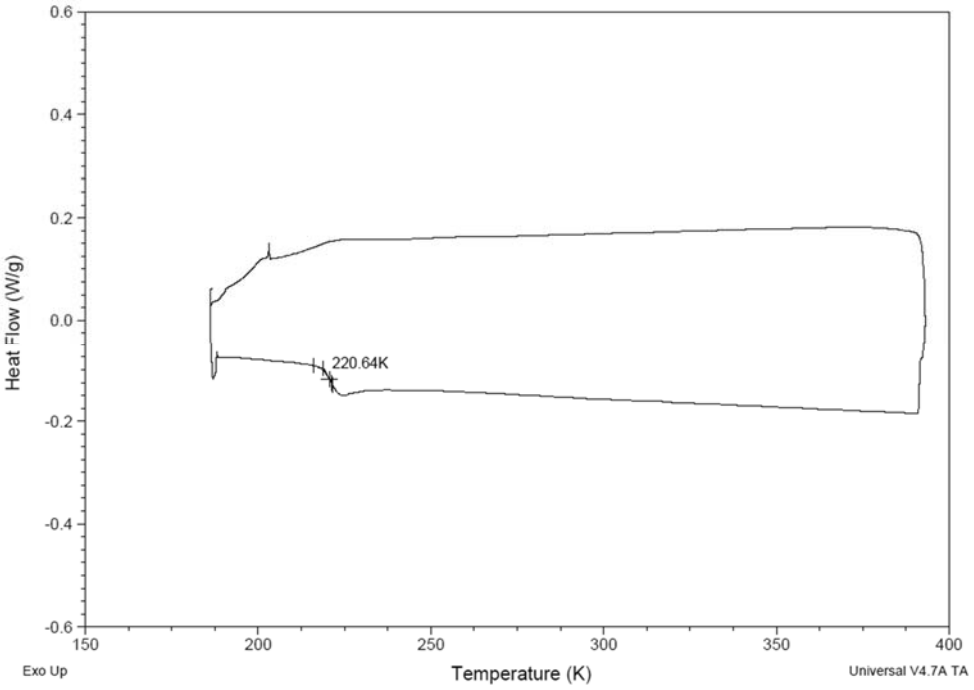

Figure B.2. DSC thermogram of [C_4mim]Cl.

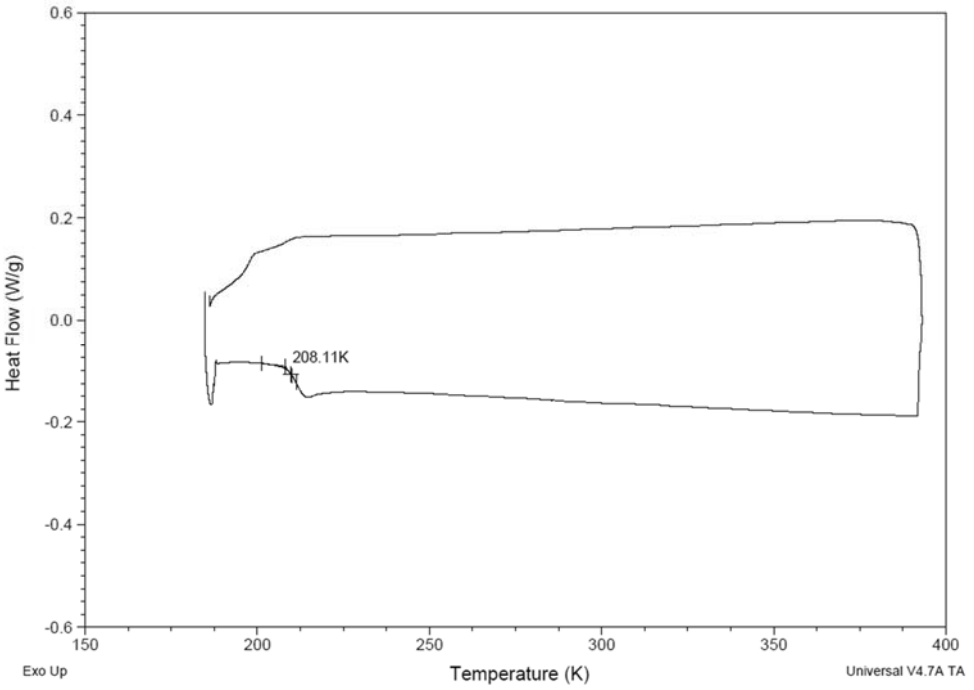

Figure B.3. DSC thermogram of [C_6mim]Cl.

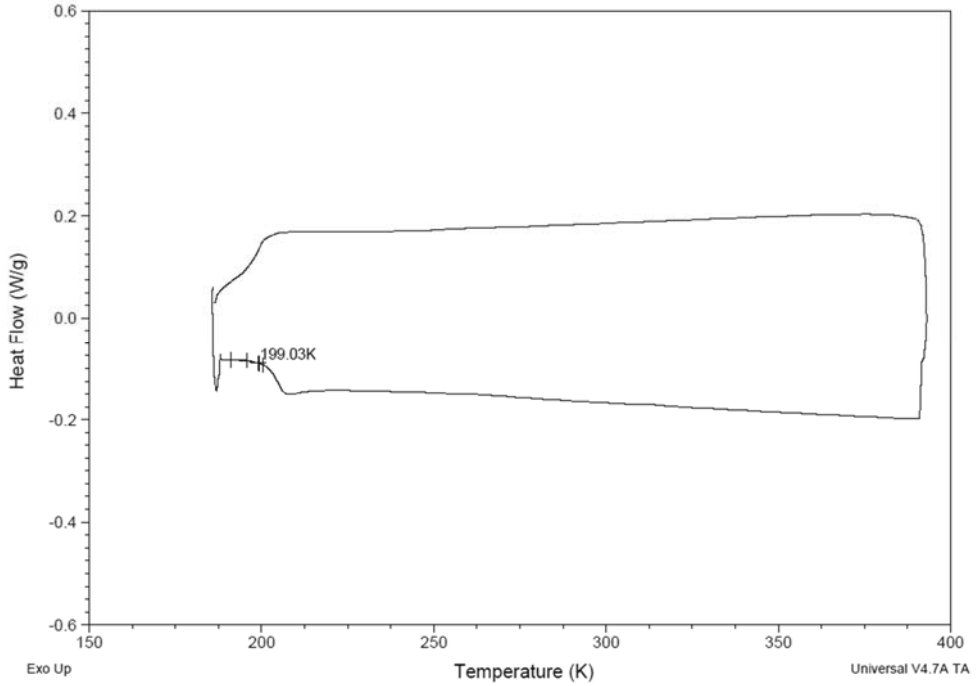

Figure B.4. DSC thermogram of [C_8mim]Cl.

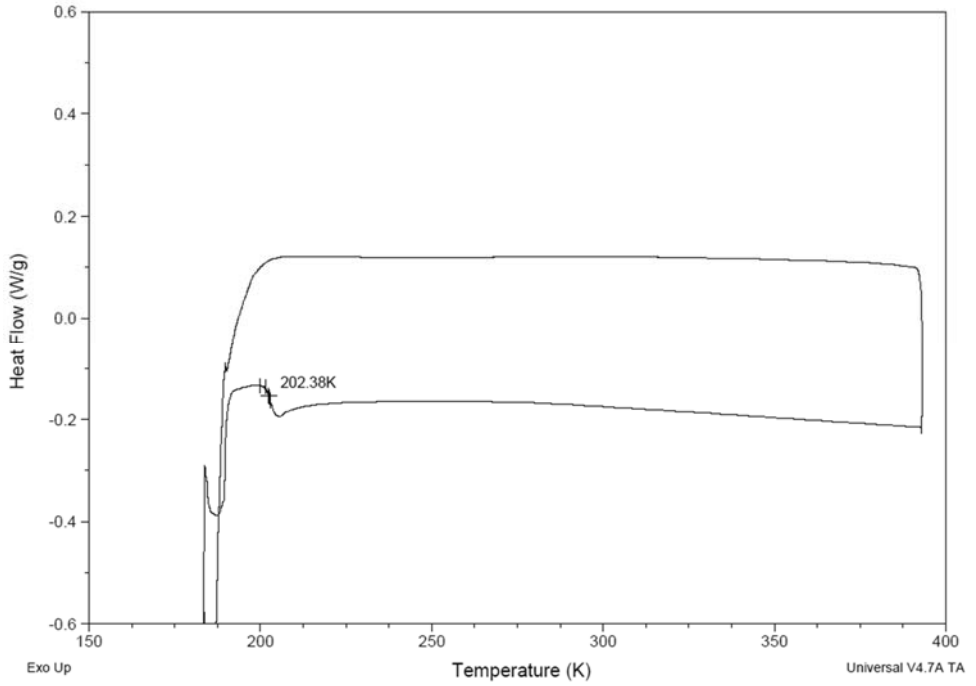

Figure B.5. DSC thermogram of [C_2mim][OAc].

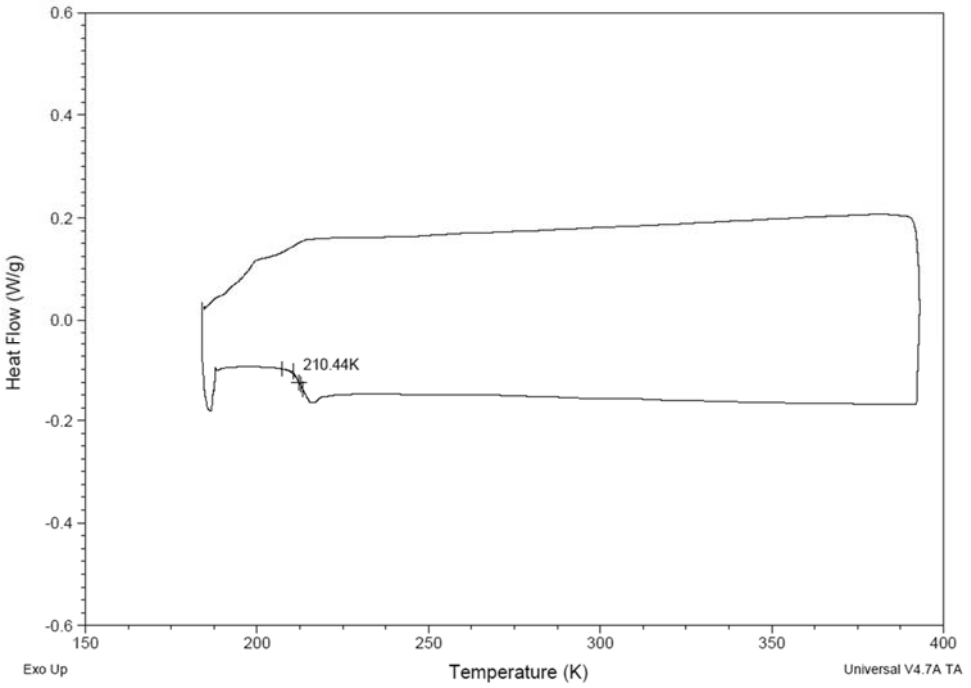

Figure B.6. DSC thermogram of [C_4mim][OAc].

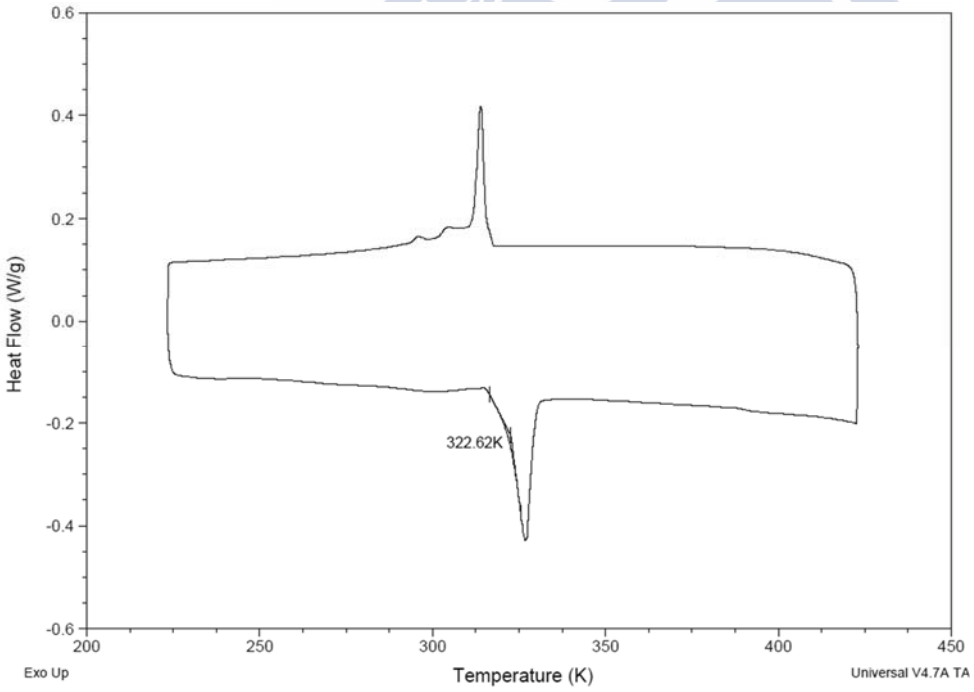

Figure B.7. DSC thermogram of [Aliquat]Cl.

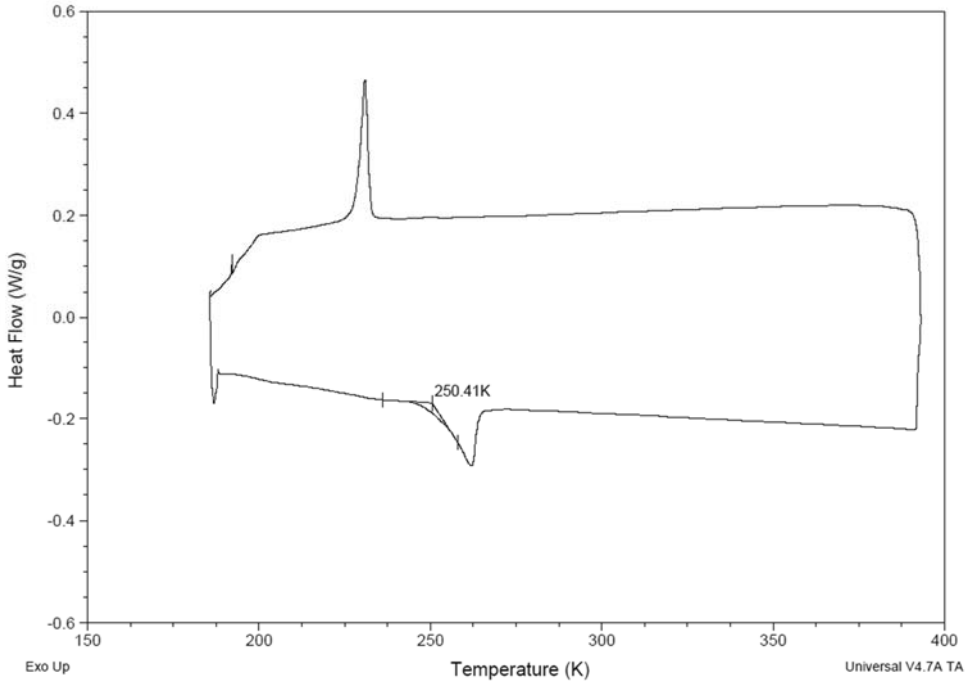

Figure B.8. DSC thermogram of [Aliquat][OAc].

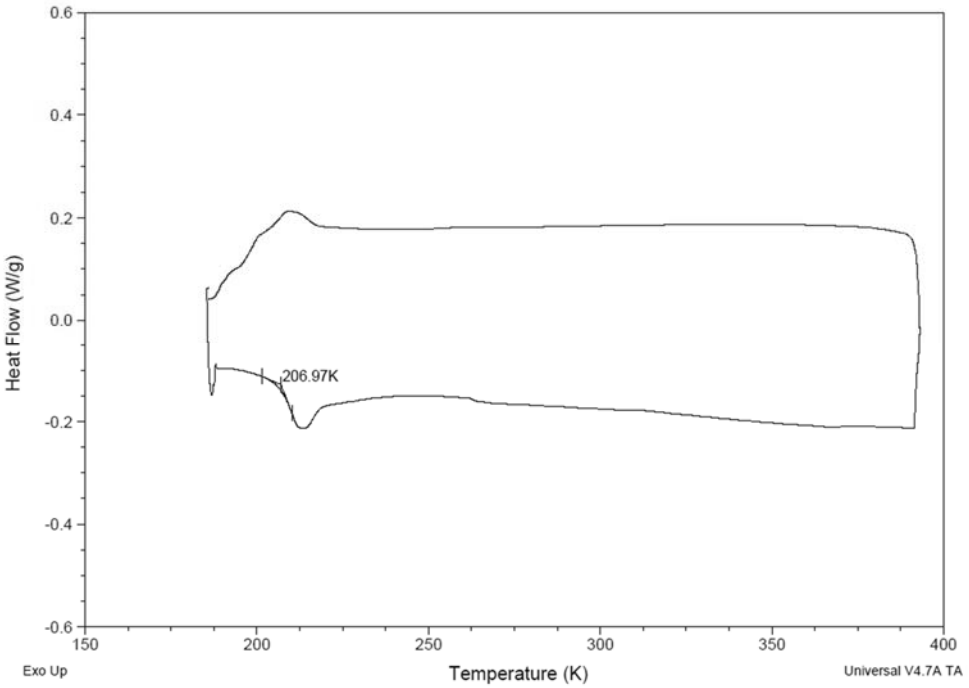

Figure B.9. DSC thermogram of $[P_{6\,6\,6\,14}]Cl$.

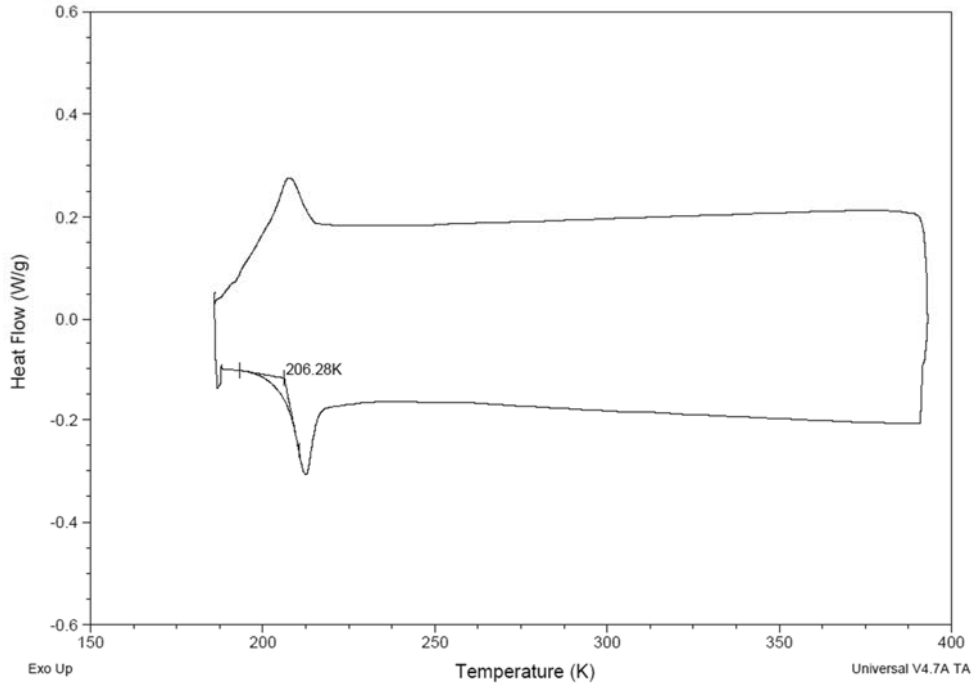

Figure B.10. DSC thermogram of $[P_{6\,6\,6\,14}][OAc]$.

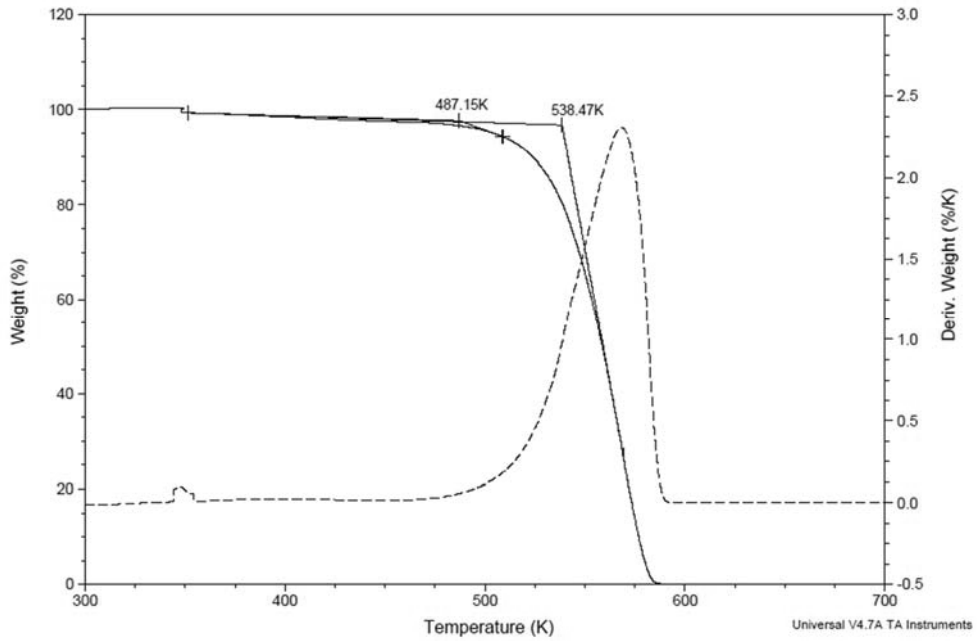

Figure B.11. TGA thermogram of $[C_2mim]Cl$.

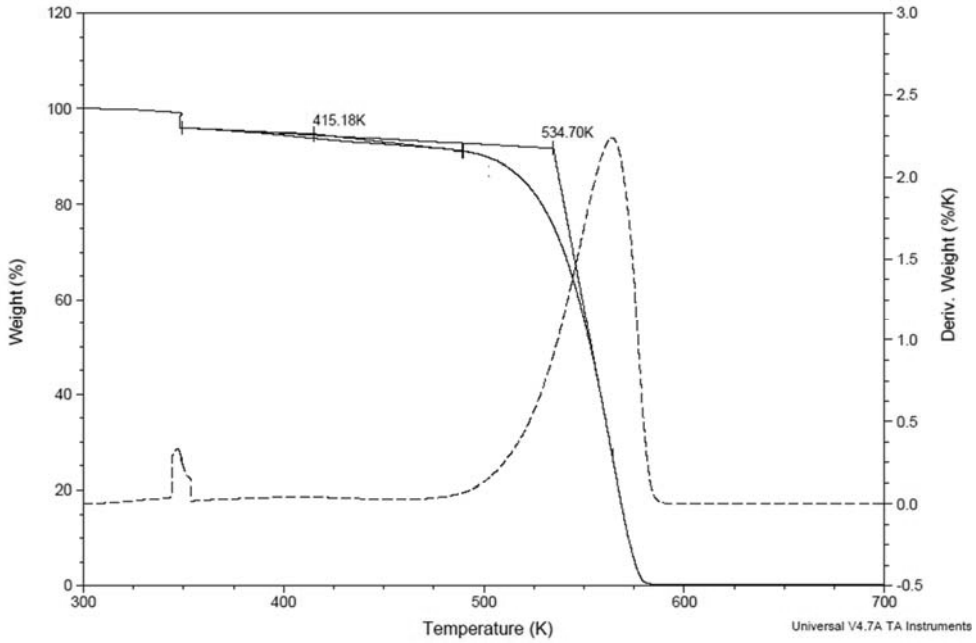

Figure B.12. TGA thermogram of [C_4mim]Cl.

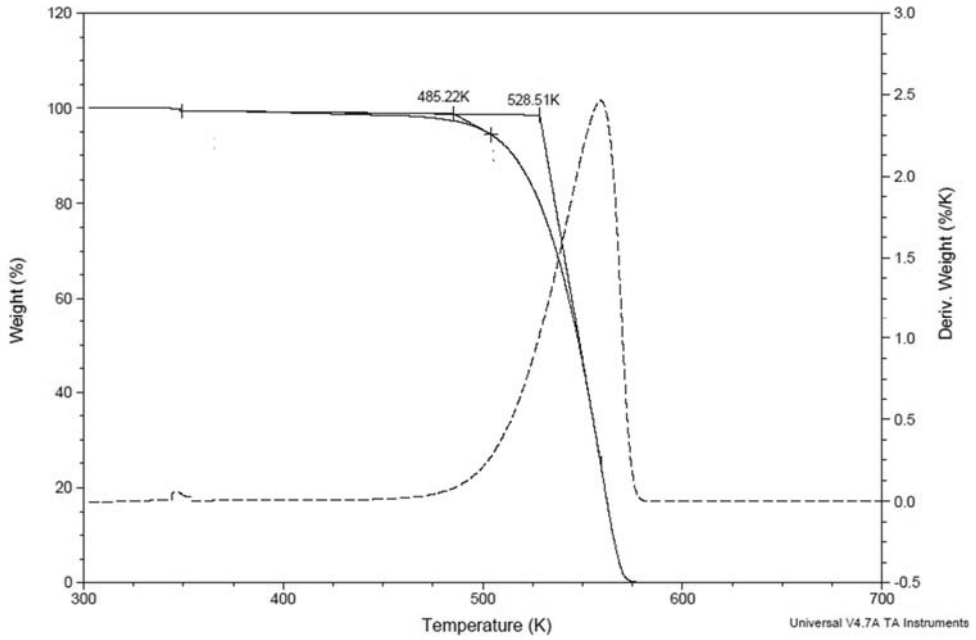

Figure B.13. TGA thermogram of [C_6mim]Cl.

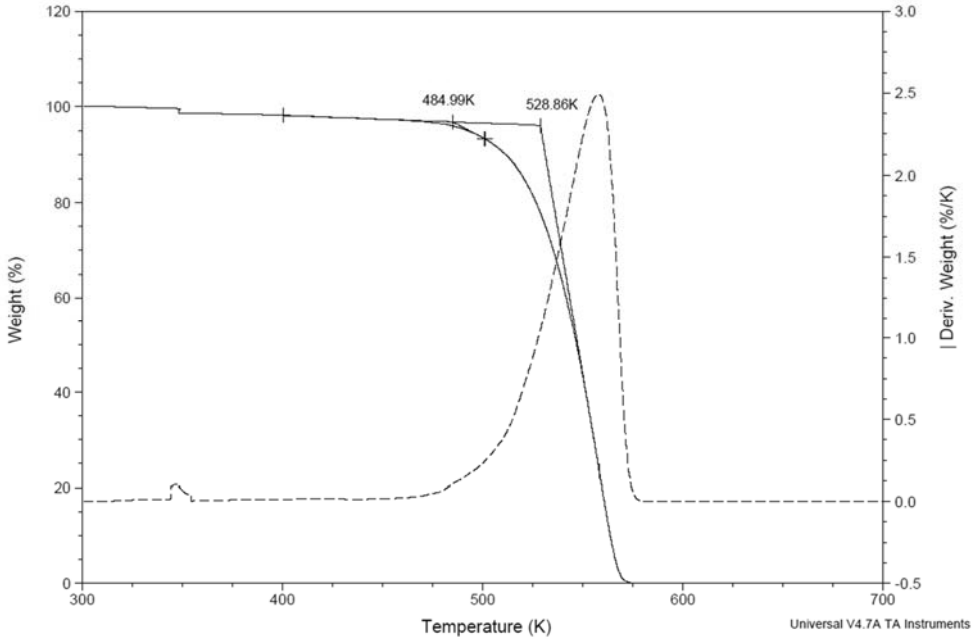

Figure B.14. TGA thermogram of [C_8mim]Cl.

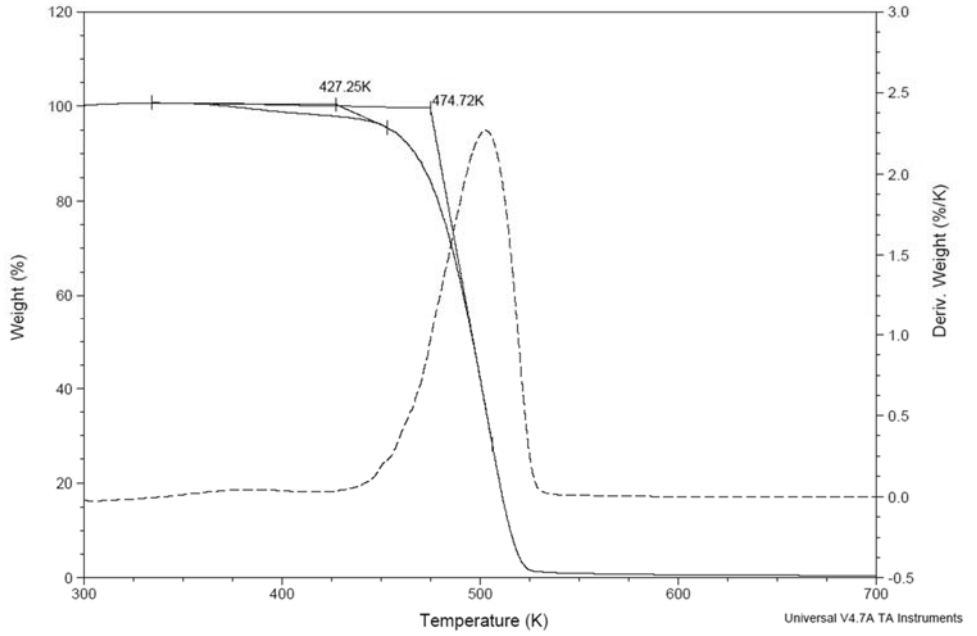

Figure B.15. TGA thermogram of [C_2mim][OAc].

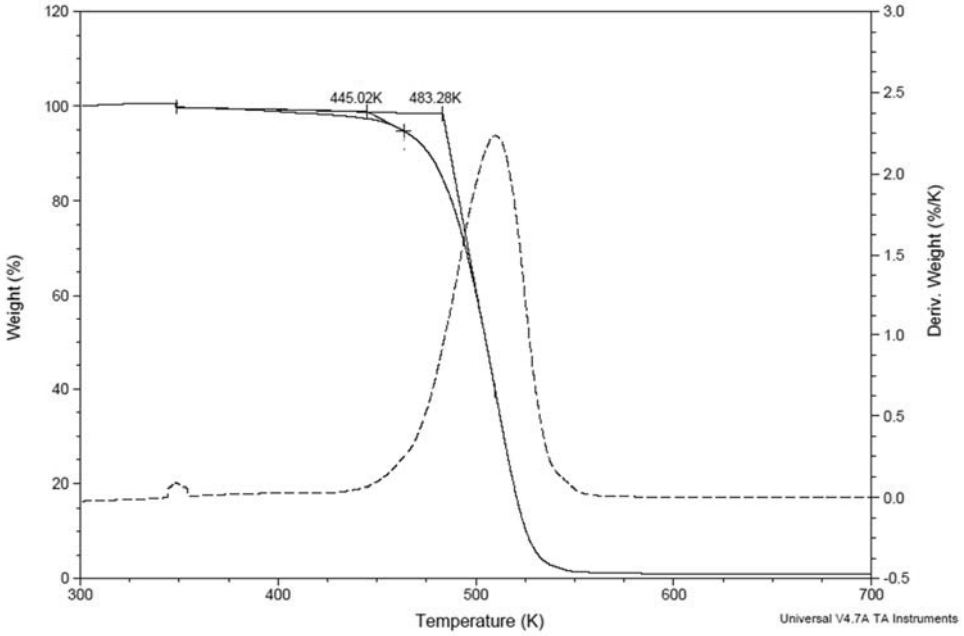

Figure B.16. TGA thermogram of [C_4mim][OAc].

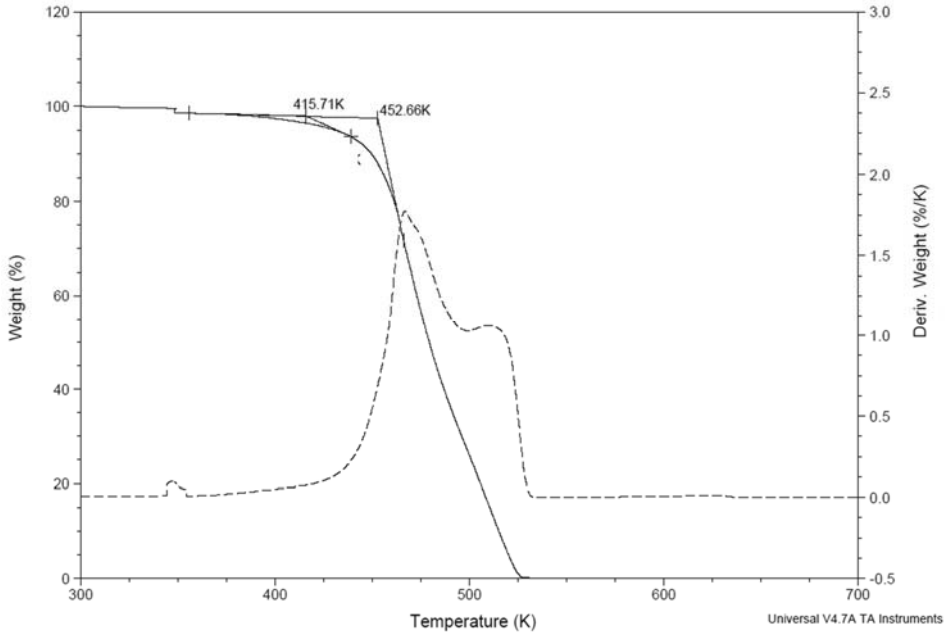

Figure B.17. TGA thermogram of [Aliquat]Cl.

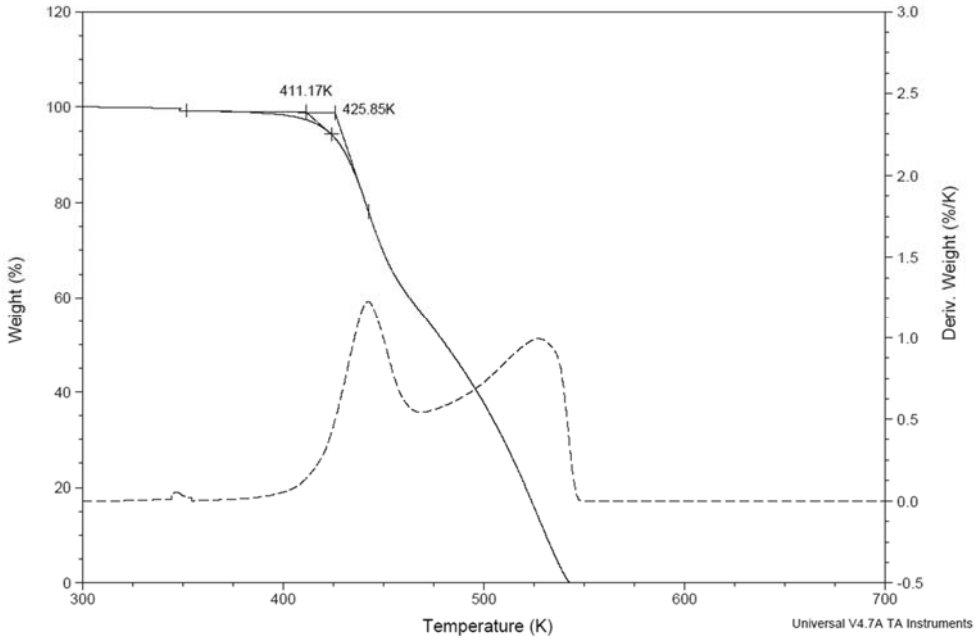

Figure B.18. TGA thermogram of [Aliquat][OAc].

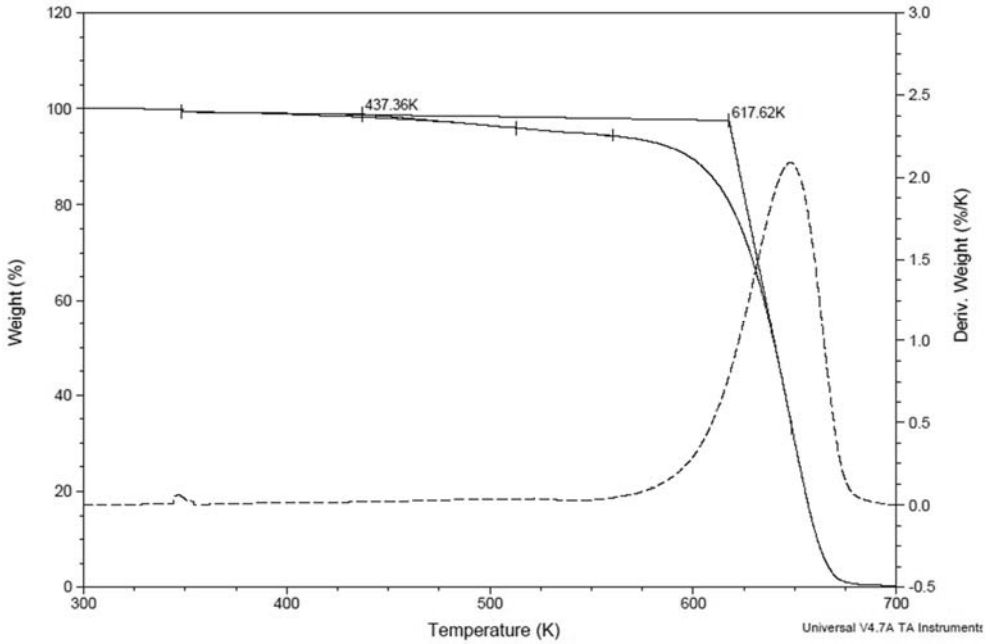

Figure B.19. TGA thermogram of $[P_{6\,6\,6\,14}]Cl$.

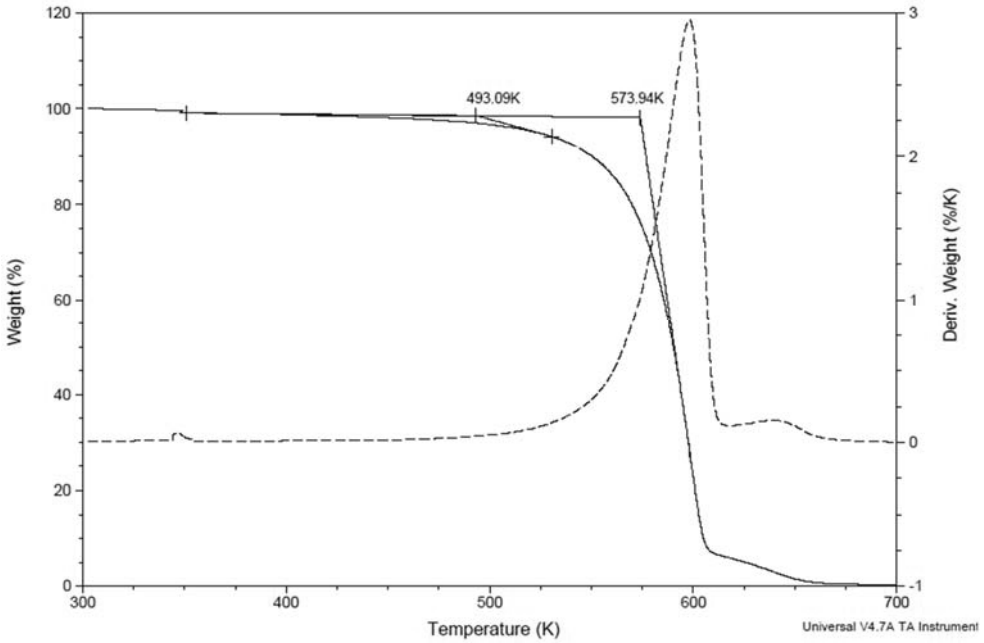

Figure B.20. TGA thermogram of $[P_{6\,6\,6\,14}][OAc]$.

USC
UNIVERSIDADE
DE SANTIAGO
DE COMPOSTELA

Appendix C:

Publications

USC
UNIVERSIDADE
DE SANTIAGO
DE COMPOSTELA

Appendix C:

Publications

The work contained in this thesis has produced, to date, the following research articles published in internationally reputed scientific journals:

- Castro, C. M.; Rodríguez, H.; Arce, A.; Soto, A. **2014**. "Mixtures of Ethanol and the Ionic Liquid 1-Ethyl-3-methylimidazolium Acetate for the Fractionated Solubility of Biopolymers of Lignocellulosic Biomass", *Ind. Eng. Chem. Res.*, 53, 11850–11861.
- Castro, C. M.; Arce, A.; Rodríguez, H.; Soto, A. **2015**. "Influence of Methanol on the Dissolution of Lignocellulose Biopolymers with the Ionic Liquid 1-Ethyl-3-methylimidazolium Acetate", *Ind. Eng. Chem. Res.*, 54, 9605–9614.
- Castro, C. M.; Arce, A.; Soto, A.; Rodríguez, H. **2016**. "Thermophysical Characterization of the Mixtures of the Ionic Liquid 1-Ethyl-3-Methylimidazolium Acetate with 1-Propanol or 2-Propanol", *J. Chem. Eng. Data*, 61, 2299–2310.
- Castro, C. M.; Arce, A.; Soto, A.; Rodríguez, H. **2016**. "Liquid-liquid equilibria of mutually immiscible ionic liquids with a common anion of basic character", *J. Chem. Thermodyn.*, 102, 12–21.

Two more manuscripts are in preparation at the moment of submitting this thesis, involving the work presented in Chapters 5 and 6. They will be submitted for publication in internationally renowned journals in the next months.

Additionally, the following patent application, in part considering work included in this thesis, has been filed:

- Holding, A. J.; Castro Valiña, M. C.; Parviainen, A.; Kilpeläinen, I.; Rodríguez Martínez, H.; King, A. W. T. **2018**. "Method for pre-treating cellulosic material", Finnish Patent Application Number 201805501.

USC
UNIVERSIDADE
DE SANTIAGO
DE COMPOSTELA

Appendix D:

"Resumen" (Summary, in Spanish)

USC
UNIVERSIDADE
DE SANTIAGO
DE COMPOSTELA

Appendix D:

"Resumen" (Summary, in Spanish)

La búsqueda de procesos más sostenibles, menos contaminantes y con un impacto ambiental reducido es una tendencia de actualidad en el sector industrial. En este contexto, el reemplazo de materias primas no renovables (en las que aún se fundamenta en gran medida el tejido industrial actual) por recursos de carácter renovable podría ser la base sobre la que desarrollar una nueva plataforma química industrial realmente sostenible para la producción de substancias químicas y materiales. Dentro de las opciones de recursos biorrenovables, la biomasa lignocelulósica se produce naturalmente en cantidades suficientes como para poder erigirse en la materia prima de referencia de esa nueva plataforma, dando cobertura a los grandes volúmenes actuales de producción industrial que se encargan de satisfacer nuestras necesidades. Además, la biomasa lignocelulósica presenta la ventaja añadida de estar geodistribuida de manera más homogénea que los recursos primarios no renovables sobre los que se basa la producción industrial hoy en día.

Las paredes celulares de las plantas están compuestas mayormente (otras sustancias suelen representar un pequeño porcentaje) por tres biopolímeros: celulosa, hemicelulosa y lignina, de características y naturaleza química dispares, que ofrecen una idea de la riqueza que las lignocelulosas atesoran para su potencial utilización en un marco de biorrefinería. No obstante, los biopolímeros mencionados se organizan en la pared celular de un modo complejo y de fuerte carácter recalcitrante (como consecuencia de la propia evolución de las plantas dirigida a resistir la acción de agentes degradantes). Por esta razón, para el adecuado aprovechamiento industrial de los biopolímeros presentes en el material lignocelulósico se hace necesario realizar lo que se denomina etapa de pretratamiento. Esta etapa tiene por objeto la modificación de la estructura lignocelulósica y la alteración de su tamaño de poro, por ejemplo a través de la reducción de la cristalinidad que presenta la fracción de celulosa en la planta en su estado natural.

Como la explotación industrial de la biomasa lignocelulósica como recurso para la industria química se ha centrado históricamente en la producción de celulosa, no

resulta extraño que los procesos industriales más desarrollados en la actualidad para el tratamiento de este recurso biorrenovable sean los de producción de pasta de celulosa y papel. En estos procesos la etapa de pretratamiento constituye en realidad la esencia del tratamiento, aplicando métodos agresivos que degradan/eliminan la hemicelulosa y la lignina en condiciones de operación severas, y con un importante impacto ambiental. Más allá del sector de pasta de celulosa y papel, se han desarrollado múltiples métodos de pretratamiento de biomasa lignocelulósica de diversa naturaleza: pretratamiento mecánico, hidrólisis con ácido diluido, hidrólisis alcalina, *steam explosion*, AFEX (a partir de sus siglas del inglés: *ammonia fibre explosion*), métodos organosolv, pretratamiento biológico, etc. A pesar de esta variedad, todos estos tipos de pretratamiento presentan inconvenientes significativos, que se traducen en que el coste de pretratamiento en procesos para el aprovechamiento de lignocelulosas suponga un porcentaje muy relevante del coste total. Así, es clara la necesidad de desarrollar mejores procesos de pretratamiento.

El concepto de biorrefinería ha emergido con fuerza en los últimos años, tratando de superar el foco en la producción de celulosa que se ha mencionado anteriormente, de manera que se aproveche también el potencial ofrecido por la hemicelulosa y la lignina en la materia prima. A día de hoy está ampliamente aceptado que el desarrollo de una biorrefinería viable pasa por la consideración de la valorización de los tres biopolímeros. En este contexto, se acentúa la necesidad de desarrollo de métodos de pretratamiento alternativos, que sean capaces de alterar la biomasa lignocelulósica, sin degradación de sus biopolímeros constituyentes, de manera que estos mismos se puedan aprovechar óptimamente en etapas de proceso posteriores.

Los líquidos iónicos son un tipo de sustancias constituidas íntegramente por iones y que presentan un punto de fusión (o de transición vítrea) relativamente bajo – inferior a 373 K. Estas sales han captado una importante atención del mundo académico e industrial durante los últimos años, fundamentalmente a causa de un interesante conjunto de propiedades que muchos líquidos iónicos poseen: presión de vapor despreciable, relativamente buenas estabilidades térmica y química, carácter no inflamable, gran capacidad para la disolución de compuestos muy variados, etc. Además, sus propiedades son ajustables a una determinada aplicación hasta un cierto punto mediante la apropiada selección de la combinación catión-anión y el diseño de sus estructuras químicas. Las aplicaciones para las que se han propuesto son

tremendamente variadas, con algunas aplicaciones ya convertidas en realidad a nivel industrial.

Entre las aplicaciones de líquidos iónicos que ofrecen gran potencial cabe destacar su uso en procesos para el tratamiento de materiales (ligno)celulósicos en un marco de biorrefinería. Dada la capacidad de algunos líquidos iónicos para disolver celulosa e incluso lignocelulosas como madera, estos líquidos iónicos pueden constituir la base de nueva tecnología para, por ejemplo, el pretratamiento efectivo de la biomasa lignocelulósica para una mejor valorización de sus biopolímeros constituyentes.

Objetivos

El objetivo general de esta tesis doctoral es el avance en el conocimiento sobre las posibilidades y el potencial de sistemas de fluidos basados en líquidos iónicos para la configuración de mejores esquemas de proceso para el pretratamiento de biomasa lignocelulósica. Este objetivo general incluye objetivos específicos con diferentes sistemas fluidos y esquemas de proceso, desde un enfoque en la ciencia fundamental que rige los sistemas investigados hasta su utilización en enfoques más aplicados. Así, un primer sistema fluido de interés es el constituido por dos líquidos iónicos mutuamente inmiscibles, uno con capacidad para disolver lignocelulosas y el otro no, y cuya miscibilidad mutua sea variable con un cambio en la temperatura. También es un objetivo la investigación del potencial de alcoholes ligeros como codisolventes o antidisolventes del más paradigmático líquido iónico para disolver biomasa hasta la fecha: acetato de 1-etil-3-metilimidazolio; así como la caracterización térmica y física de estos sistemas binarios. En un plano más aplicado, se busca que un sistema fluido de este último tipo pretrate satisfactoriamente madera (*Eucalyptus globulus*) en condiciones de baja temperatura (sin que se produzca disolución, con especial atención a la posible reducción en el grado de cristalinidad de la madera). En una línea similar, esta tesis también pretende explorar el uso de líquidos iónicos con otro tipo de catión (concretamente tetraalquilfosfonio) para el pretratamiento directo de madera (*Picea abies*, i.e. abeto noruego), con o sin codisolventes, así como diferentes variables de proceso y su influencia en el grado de fibrilación de las partículas y la composición de la madera pretratada resultante.

Líquidos iónicos mutuamente inmiscibles con un anión común de carácter básico

Los líquidos iónicos objeto de estudio fueron los siguientes: cloruro de 1-etil-3-metilimidazolio ([C_2mim]Cl), cloruro de 1-butil-3-metilimidazolio ([C_4mim]Cl), cloruro de 1-hexyl-3-metilimidazolio ([C_6mim]Cl), cloruro de 1-metil-3-octylimidazolio ([C_8mim]Cl), acetato de 1-etil-3-metilimidazolio acetato ([C_2mim][OAc]), acetato de 1-butil-3-metilimidazolio ([C_4mim][OAc]), Aliquat 336® ([Aliquat]Cl) y su correspondiente acetato ([Aliquat][OAc]), cloruro de trihexil(tetradecil)fosfonio ([$P_{6\,6\,6\,14}$]Cl) y acetato de trihexil(tetradecil)fosfonio ([$P_{6\,6\,6\,14}$][OAc]).

En primer lugar, se determinaron sus rangos de temperatura como líquidos estables, entre su temperatura de fusión o transición vítrea y su temperatura de descomposición, medidas mediante calorimetría diferencial de barrido y análisis termogravimétrico. Una vez identificados estos rangos se identificaron unas parejas de líquidos iónicos totalmente miscibles en el rango de temperatura investigado y sobre todo el rango de composición ([C_6mim]Cl + [Aliquat]Cl, [C_8mim]Cl + [Aliquat]Cl, [C_4mim][OAc] + [Aliquat][OAc] y [C_4mim][OAc] + [$P_{6\,6\,6\,14}$][OAc]), así como otras parejas que resultaban en algún tipo de inmiscibilidad mutua ([C_2mim]Cl + [Aliquat]Cl, [C_4mim]Cl + [Aliquat]Cl, [C_2mim][OAc] + [Aliquat][OAc] y [C_2mim][OAc] + [$P_{6\,6\,6\,14}$][OAc]). Así, en general un aumento en la longitud del sustituyente alquilo del líquido iónico de imidazolio conduce a la desaparición del dominio bifásico líquido-líquido en los sistemas; si bien en el caso de las mezclas de los acetatos tal desaparición se produce con un sustituyente alquilo de cadena más corta.

Se determinaron entonces los equilibrios líquido-líquido en función de la temperatura para las mezclas de líquidos iónicos que habían mostrado inmiscibilidad. Se elaboraron los correspondientes diagramas temperatura-composición, analizando la influencia de diferentes características estructurales de los iones constitutivos de los líquidos iónicos en la inmiscibilidad generada. Además, se identificaron comportamientos de temperatura superior/inferior de solución crítica (UCST/LCST, por las siglas en inglés de *upper/lower critical solution temperature*). Estos variados comportamientos son indicativos de la enorme versatilidad que pueden ofrecer los líquidos iónicos mutuamente inmiscibles. Se observó además que, en general, el líquido iónico de amonio/fosfonio apenas tiene presencia en la fase rica en imidazolio, mientras que la solubilidad del líquido iónico de imidazolio en la fase rica en amonio/fosfonio es

muy significativa. Esto permitió realizar un análisis termodinámico de estos sistemas líquido-líquido desde la perspectiva de la disolución del líquido iónico de imidazolio en el líquido iónico de amonio/fosfonio, calculando propiedades termodinámicas de la mezcla para obtener una comprensión más profunda de los fundamentos de estos sistemas líquido-líquido. Se vio que la solubilidad de los líquidos iónicos de imidazolio en los de fosfonio investigados estaba regida por la entropía en el sistema, mientras que en los líquidos iónicos con catión Aliquat estaba regida por la entalpía a temperaturas bajas y pasaba a estar regida por la entropía a temperaturas elevadas.

En ninguno de los sistemas líquido-líquido estudiados se alcanzó una temperatura de solución crítica (ni superior ni inferior).

Sistemas líquido iónico + alcohol. Solubilidad de biopolímeros

Se investigaron en este apartado las mezclas líquidas binarias formadas por el líquido iónico acetato de 1-etil-3-metilimidazolio ([C_2mim][OAc]), paradigmático en el contexto de disolución de (ligno)celulosa con líquidos iónicos, y un alcohol ligero: metanol, etanol, 1-propanol o 2-propanol.

Se realizó en primera instancia una caracterización térmica de estas mezclas, cubriendo el rango de composición desde el líquido iónico puro hasta una mezcla con fracción molar de líquido iónico de 0,10 (no se llevó a cabo para el alcohol puro debido a su carácter totalmente volátil). Mediante análisis termogravimétrico se evidenció que el alcohol se puede retirar de su mezcla con el líquido iónico (y por tanto recuperar éste en estado aproximadamente puro) por simple vaporización a temperaturas inferiores a la de descomposición del líquido iónico. Todos los termogramas presentaron una tendencia similar con el incremento de temperatura: se produce una pérdida de peso inicial como resultado de la volatilidad inherente del alcohol; a continuación se produce un punto de inflexión horizontal en la curva (transición de convexo a cóncavo) a una temperatura dada; y la pérdida de peso continúa después de manera similar a la observada para la descomposición del líquido iónico puro. A excepción del sistema con 2-propanol, los resultados obtenidos apuntaron claramente a la posibilidad de lograr una vaporización prácticamente total del alcohol (metanol, etanol o 1-propanol) en sus mezclas con el líquido iónico mediante el calentamiento a una temperatura por encima de la temperatura de ebullición del alcohol y por debajo de la temperatura de descomposición del líquido iónico, sin causar degradación térmica de éste. La

comparación de los cuatro sistemas binarios para una composición dada permitió observar una tendencia en los sistemas con alcoholes primarios (metanol, etanol y 1-propanol) para los cuales la pérdida de masa por calentamiento aumenta con un aumento de la longitud de la cadena de alquilo, resultado probablemente del peso molecular de los alcoholes. Sin embargo, se observó un comportamiento algo diferente para el sistema con 2-propanol, que exhibe una estabilidad térmica relativamente mejorada. Esto sugiere la presencia de formas alternativas/adicionales de interacción de las moléculas de 2-propanol con los iones del líquido iónico. Los estudios realizados por calorimetría diferencial de barrido permitieron confirmar complementariamente que las mezclas estudiadas permanecen en estado líquido incluso a temperaturas muy inferiores a la ambiental, por lo que no habría riesgo de precipitaciones indeseadas en su utilización en procesos industriales operados en condiciones de temperatura habituales.

Con respecto al estudio de propiedades físicas, se seleccionaron la densidad, la viscosidad, el índice de refracción y la tensión superficial, y se determinaron experimentalmente para los cuatro sistemas binarios a presión atmosférica, cubriendo todo el rango de composición y sobre amplios rangos de temperatura. Se observó que todas las propiedades disminuyen al aumentar la temperatura y al aumentar la concentración de alcohol en la mezcla. Si bien la densidad, el índice de refracción y la tensión superficial disminuyen de forma lineal o casi lineal al aumentar la temperatura, la evolución de la viscosidad con la temperatura fue adecuadamente correlacionada por la ecuación exponencial de Vogel-Fulcher-Tammann. Para el análisis del efecto de la composición sobre las propiedades, los valores experimentales de éstas se utilizaron para calcular las correspondientes propiedades de exceso o cambios de propiedad por efecto de mezcla. La correlación satisfactoria del volumen molar de exceso, cambio de logaritmo de viscosidad por efecto de mezcla y cambio de tensión superficial por efecto de mezcla, en función de la composición para las distintas isotermas, se logró mediante polinomios de Redlich-Kister. Para el exceso de volumen molar y el cambio de logaritmo de viscosidad por efecto de mezcla se observó una disminución en valor absoluto, a una temperatura dada, con el aumento de la longitud de la cadena del alcohol.

Teniendo en cuenta los resultados obtenidos en la determinación de las propiedades térmicas y físicas, junto con las características intrínsecas de los cuatro alcoholes explorados, se decidió seleccionar metanol y etanol como los candidatos más

interesantes para su uso como codisolventes o antidisolventes del líquido iónico [C_2mim][OAc] en el pretratamiento (con posible disolución y fraccionamiento parcial) de la biomasa lignocelulósica. Se investigó la solubilidad de celulosa microcristalina, xilano e Indulin AT (sustancias tomadas como estándares representativos de los tres biopolímeros principales de la biomasa lignocelulósica) en mezclas de [C_2mim][OAc] + (metanol o etanol), en función de la composición relativa de la mezcla. Los resultados mostraron claramente que ninguno de los estándares de biopolímeros era apreciablemente soluble en alcohol puro. Por contra, en [C_2mim][OAc] puro la solubilidad de celulosa microcristalina es elevada, en comparación con la solubilidad de la celulosa en otros disolventes (incluidos otros líquidos iónicos). Esta solubilidad mostró una tendencia similar para ambos sistemas: su valor disminuyó moderadamente con un aumento moderado en el porcentaje de alcohol en la composición del disolvente. La solubilidad en el sistema con etanol fue significativamente más baja que en el sistema con metanol para una concentración molar dada. Para xilano, su solubilidad en el líquido iónico puro disminuyó mucho más rápidamente en el sistema con metanol en comparación al sistema con etanol. En relación a la solubilidad de Indulin AT, se encontró que es muy elevada incluso con una concentración molar tan alta como 80 % en el disolvente. Se identificó una transición abrupta de la solubilidad de este biopolímero en los sistemas fluidos estudiados a concentraciones molares de 0,08 en el sistema con metanol y 0,14 en el sistema con etanol. En un contexto de fraccionamiento de biomasa, estos resultados sugieren la posibilidad de utilizar el sistema de [C_2mim] [OAc] + alcohol para separar, mediante disolución selectiva, una mezcla de los principales biopolímeros de lignocelulosa.

Sobre la base de los resultados de solubilidad obtenidos, se realizaron tests de precipitación para evaluar la capacidad del metanol como antidisolvente, añadido en cantidades controladas (tolerables desde una perspectiva de proceso industrial) para la reconstitución de fracciones de lignocelulosa disueltas en [C_2mim][OAc]. A pesar de los valores de solubilidad anteriormente obtenidos, en estos tests no se observó una precipitación limpia de sólidos en las pruebas. En su lugar se observó la formación de fases emulsionadas o de tipo gel. Este hecho dificulta la utilización de metanol en cantidades moderadas como un antidisolvente directo para la regeneración de fracciones de lignocelulosa antes disueltas en [C_2mim][OAc].

Pretratamiento de madera de eucalipto con una mezcla de líquido iónico + alcohol

Se utilizó la mezcla de [C_2mim][OAc] y etanol para realizar el pretratamiento de partículas de madera de *Eucalyptus globulus*, en condiciones a las que la capacidad del líquido iónico para disolver madera es muy baja, para beneficiarse de las ventajas de un pretratamiento sin disolución que implica un requerimiento energético menor (e.g. recuperación de la madera pretratada por simple filtración). Se investigaron [C_2mim][OAc] puro y su mezcla 95:5 en masa con etanol como disolventes, a dos temperaturas (318 K y 338 K) y con dos tamaños de partícula de eucalipto (en los rangos 125-250 μm y 250-500 μm). La realización de los experimentos de pretratamiento se llevó a cabo con una carga de biomasa de 5 g por cada 100 g de disolvente, por un período de 16 h con agitación, recuperando la biomasa pretratada mediante filtración.

Fotografías tomadas con microscopio óptico permitieron apreciar los efectos del pretratamiento de la madera en diferentes condiciones, en comparación con la madera no tratada. Se observó que los pretratamientos a 318 K tienen poco efecto sobre la morfología de las partículas de madera, mientras que, por el contrario, a 338 K se produce una importante fibrilación de la biomasa. Este efecto de fibrilación resultó más fuerte cuando se usó la mezcla [C_2mim][OAc] + etanol en vez del líquido iónico puro, posiblemente por causa de un mejor contacto entre partículas y líquido como consecuencia de la reducción de la viscosidad resultante de la adición del alcohol. Tratando de relacionar la fibrilación observada con los cambios potenciales inducidos en la matriz biopolimérica de las partículas de madera mediante el pretratamiento, se llevaron a cabo análisis de difracción de rayos X con cálculo del índice de cristalinidad mediante el "método de sustracción amorfa". Al comparar los difractogramas de las partículas de madera no tratadas y los de las partículas sometidas al pretratamiento, se observó una importante reducción de la cristalinidad de la celulosa de la madera, correspondiéndose los casos de mayor reducción con aquellas muestras que presentaban mayor grado de fibrilación. Con respecto a la influencia del tamaño de partícula, la reducción del grado de cristalinidad fue mayor con el tamaño de partícula más pequeño de los dos probados, especialmente en aquellas condiciones de pretratamiento en las que se experimentó en general una reducción notablemente de la cristalinidad.

Se determinó (mediante un método desarrollado por el Laboratorio Nacional de Energía Renovable del Departamento de Energía de los EE.UU.) la composición porcentual de celulosa, hemicelulosa y lignina de la madera no tratada y de la sometida a pretratamiento a diferentes condiciones de operación. Se observó que las condiciones en las que se llevó a cabo el pretratamiento no afectaron de manera relevante la concentración relativa de los principales biopolímeros en la madera. La variación más significativa correspondió a la lignina, con todos los pretratamientos conduciendo a una cierta disminución del porcentaje de lignina en la madera con respecto al material original. Sin embargo, esta reducción en el contenido de lignina fue mucho menor que la que se obtiene típicamente en los pretratamientos convencionales, que se centran principalmente en la deslignificación para mejorar el acceso a los carbohidratos en tratamientos posteriores. Respecto al efecto de las diferentes variables analizadas en el pretratamiento, un primer aspecto notable fue que el tamaño de partícula, dentro del rango estudiado, parece tener generalmente poca influencia en la composición de la madera pretratada obtenida. Sin embargo, esto debe considerarse en combinación con el hecho comentado anteriormente de que un tamaño de partícula más pequeño favorecerá la disminución de la cristalinidad de la celulosa (y supuestamente su reactividad posterior). Con respecto al efecto de la temperatura, se observó una menor contribución de los tres biopolímeros a la composición total en el caso de las muestras pretratadas a alta temperatura (338 K), probablemente debido a un pequeño grado de degradación polimérica; pero, como se comentó anteriormente, la temperatura de 318 K conduce a pretratamientos menos eficaces. Finalmente, la introducción del etanol como disolvente previo al tratamiento no afectó de manera relevante la composición resultante del eucalipto pretratado, mientras que es beneficiosa desde el punto de vista de la reducción de la cristalinidad, así como en términos de la ingeniería del proceso como resultado de su capacidad para disminuir la viscosidad del líquido iónico puro.

Se confirmó la estabilidad química del líquido iónico tras el proceso de pretratamiento, así como la ausencia en su seno de fracciones lignocelulósicas no volátiles residuales en niveles relevantes.

Pretratamiento de madera de pícea con líquidos iónicos de fosfonio

Se estudió el pretratamiento de fragmentos de astilla de *Picea abies*, así como de serrín industrial de la misma especie, mediante contacto con dos líquidos iónicos de acetato de tetraalquilfosfonio con cadenas sustituyentes de alquilo de diferentes longitudes: acetato de tetrabutilfosfonio ([P_{4444}][OAc]) y acetato de metiltrioctilfosfonio ([P_{8881}][OAc]). Ninguno de estos líquidos iónicos presenta capacidad para la disolución de madera en estado puro, si bien se sabe que pueden disolver celulosa en combinación con algún disolvente polar aprótico como el dimetilsulfóxido.

En un conjunto inicial de experimentos, se exploraron como disolventes de pretratamiento [P_{4444}][OAc], dimetilsulfóxido y γ-valerolactona (otro disolvente polar aprótico, y además de origen biorrenovable) en estado puro, así como las mezclas a un 50 % en peso del líquido iónico con cada uno de los disolventes moleculares. Se combinaron estos disolventes con las astillas en una relación de 5 g de biomasa por cada 100 g de disolvente, y se efectuaron los pretratamientos por un período de ca. 16 h a diferentes temperaturas en el rango 353-413 K. Los resultados arrojaron poco efecto o degradación térmica evidente en los casos en los que el dimetilsulfóxido o la γ-valerolactona participaban en el disolvente pretratante. En el caso del [P_{4444}][OAc] puro, a las temperaturas más elevadas se observó claramente fibrilación en la madera pretratada.

En vista del efecto negativo de la presencia de los disolventes moleculares en los experimentos precedentes, en el caso del [P_{8881}][OAc] se realizaron experimentos únicamente con el líquido iónico puro. También se observó fibrilación, aunque más incipiente y prácticamente sólo a la temperatura de 413 K, la más alta de las exploradas.

Analizando la fase líquida tras el tratamiento, se pudieron identificar pequeñas trazas asociables a los tres biopolímeros principales de la biomasa, quizás en mayor medida de fracciones hemicelulósicas; pero en cualquier caso cantidades muy pequeñas, confirmando el carácter de no-disolución del pretratamiento propuesto. El análisis composicional de la madera pretratada indicó una disminución relativa de la composición de hemicelulosa, siendo justamente esta disminución más relevante en el caso de pretratamiento con [P_{4444}][OAc], que es el que condujo a un pretratamiento más eficaz.

Conclusiones

A continuación se enumeran una serie de conclusiones que se derivan de los resultados originales presentados en esta tesis para diferentes aproximaciones de proceso utilizando sistemas fluidos basados en líquidos iónicos para el pretratamiento de biomasa lignocelulósica:

- Los equilibrios líquido-líquido de líquidos iónicos mutuamente inmiscibles desarrollados en esta tesis vienen a ampliar el corpus de conocimiento de este tipo de sistemas, muy limitado en la bibliografía científica. En el contexto de su potencial utilización como sistemas fluidos integrados disolvente-antidisolvente en el pretratamiento de materiales lignocelulósicos, desafortunadamente no se alcanzan puntos UCST o LCST dentro del rango de temperaturas en el que estas mezclas se comportan como líquidos estables. No obstante, dado el carácter no-volátil de los líquidos iónicos y su buena estabilidad térmica, estos sistemas bifásicos líquido-líquido pueden ser de particular interés en extracciones a alta temperatura.
- La densidad, viscosidad, índice de refracción y tensión superficial de las mezclas binarias [C_2mim][OAc] + (metanol, etanol, 1-propanol o 2-propanol) disminuyen con un aumento de la temperatura o un aumento de la concentración de alcohol. La viscosidad es correlacionable con la temperatura, para una composición dada, mediante la ecuación de Vogel-Fulcher-Tamman (excepto en el caso de los alcoholes puros, para los que funciona mejor la ecuación de Andrade); mientras que el resto de propiedades pueden ser correlacionadas adecuadamente mediante líneas rectas o, a lo sumo, un polinomio de segundo grado (para el caso de la densidad). El volumen molar de exceso en estas muestras evidencia la predominancia de fuerzas atractivas entre el líquido iónico y el alcohol. No obstante, el [C_2mim][OAc] es recuperable de sus mezclas con alcohol mediante la vaporización de este último a temperaturas inferiores a la de degradación del líquido iónico. La capacidad de disolución de biopolímeros por parte de estos sistemas fluidos se puede regular mediante la concentración. No obstante, la precipitación fraccionada de biopolímeros disueltos en [C_2mim][OAc] mediante adición de alcohol puede presentar complicaciones debido a la formación de emulsiones y geles.

- El pretratamiento de partículas de *Eucaliptus globulus* con [C_2mim][OAc] o con su mezcla con etanol (5 % en peso de este último) a una temperatura de 338 K conduce a un alto grado de fibrilación y una importante reducción de la cristalinidad de la madera en condiciones de no-disolución. Este resultado debería facilitar el procesamiento y transformación de los biopolímeros de la madera en siguientes etapas de proceso.
- El pretratamiento de astillas de *Picea abies* con [P_{4444}][OAc] a 413 K resulta en una fibrilación sustancial de la madera. No obstante, la utilización de dimetilsulfóxido o γ-valerolactona como co-disolventes del líquido iónico conduce a malos resultados de pretratamiento. Algo de fibrilación también se consigue en el pretratamiento con [P_{8881}][OAc], pero en menor medida que con [P_{4444}][OAc]. La madera pretratada presenta una concentración relativamente menor de hemicelulosa en comparación a la madera original.